THE UNIVERSITY
of EDINBURGH

Disilenes, Silylenes and Silyl Anions

Fundamentals and Catalysis

Martin W. Stanford

A Thesis Submitted for the Degree of Doctor of Philosophy

School of Chemistry

College of Science and Engineering

University of Edinburgh

2019

Declaration

I hereby certify:

a) That the thesis has been composed by me under the supervision of Dr Michael J. Cowley.

b) Either that the work is my own, or, where I have been a member of a research group, that I have made a substantial contribution to the work, such contribution being clearly indicated.

c) That the work has not been submitted for any other degree or professional qualification.

Martin Stanford

Lay Summary

In the 21st century we rely heavily on modern chemicals, such as pharmaceuticals, plastics, and dyes. However, many of these chemicals include specific chemical bonds that can only be formed using expensive, rare, and toxic metals, for example platinum, palladium, and iridium. These metals are not very abundant, they only exist in tiny quantities in the earth's crust. Furthermore, their high toxicity means they must be thoroughly removed from final products, which is often costly and time consuming.

In contrast, silicon is the second most abundant element in the earth's crust, after oxygen. All of our beaches, ocean floors, and many common rocks are actually made largely of silicon oxides, and it comes with absolutely no inherent health risks.

Most of this thesis focuses heavily on improving our fundamental understanding of silicon chemistry. How does the chemistry of silicon change when we modify the elements and chemicals that surround it? How can we force it to mimic expensive metals, like platinum or palladium?

The final chapter of this thesis actually proves that silicon might be able to replace such expensive metals. The method used is simple, and somewhat unexpected, but highly effective. Instead of trying to copy the metals, I have used a completely different, yet complimentary method with some interesting results.

Abstract

Disilenes, silylenes and silyl anions are examples of compounds with silicon in oxidation state +II. They are fundamentally interesting due to their analogy with common, reactive organic compounds and intermediates, such as alkenes and carbanions. Equally, low-valent main-group compounds, including disilenes and silylenes, are often able to mimic the reactivity of expensive and rare transition metals. Chapter 1 provides a background and introduction to the history and chemistry of low-oxidation state silicon in relation to this thesis.

Chapter 2 studies the equilibrium between disilenes and silylsilylenes. The equilibrium between disilenes ($R_2Si=SiR_2$) and their silylsilylene ($R_3Si\text{-}SiR$) isomers has been previously inferred but not directly observed, except in the case of the parent system ($H_2Si=SiH_2$). Chapter 2 reports a new method to prepare base-coordinated disilenes with hydride substituents. By varying the steric bulk of the coordinating base and other substituents, I have been able to control the rearrangement of disilene adducts to their silylsilylene tautomers. Remarkably, 1,2-migration of a trimethylsilyl group is preferred over hydride migration. A DFT investigation of the reaction mechanism provides a rationale for the observed reactivity

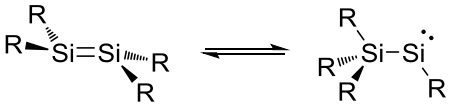

Disilene **Silylsilylene**

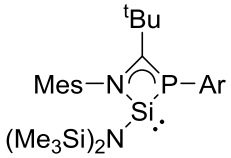

Ar = Mes
Tipp

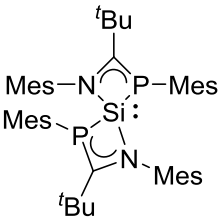

Phospha-Amidinato Silylenes

Chapter 3 focuses on synthesising phospha-amidinato silylenes. Recent studies have shown that phosphorus substituents may reduce the singlet-triplet gap of silylenes relative to more common nitrogen substituents, and therefore enhance their reactivity. Four phospha-amidinato silanes have been prepared from three novel phospha-amidinate ligands. Six silylenes were generated by reduction or reductive dehydrochlorination. A four coordinate phospha-amidinato silylene was isolated and fully characterised.

Chapter 4 investigates the use of silicon based initiators for the hydroboration of carbonyls and alkynes. A silyl anion was found to be the most effective initiator for both aldehydes and ketones. The mechanism was studied through stoichiometric reactions and found to proceed through coordination of the silyl anion to pinacolborane (HBpin), generating a reactive borohydride. Furthermore, the silyl anion was shown to decompose HBpin to BH_3 under certain conditions which can catalyse the hydroboration of alkynes.

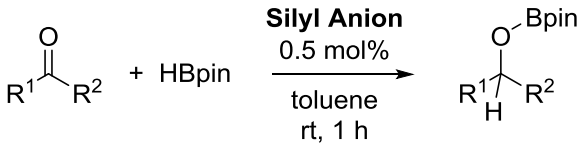

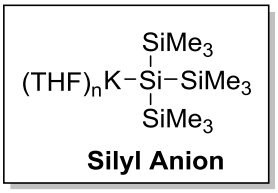

Publication

Parts of this thesis have been published in:

"Intercepting the Disilene-Silylsilylene Equilibrium"

M. W. Stanford, J. I. Schweizer, M. Menche, G. S. Nichol, M. C. Holthausen, M. J. Cowley

Angew. Chem. Int. Ed. **2019**, *58*, 1329–1333.

Conference Contributions

Parts of this thesis have been presented at:

Oral presentations:

IRIS-15, Kyoto, Japan (2018)
RSC Chemical Science Prize

Joseph Black Conference, Edinburgh (2018)
2nd Prize in Synthesis and Catalysis

Dalton Meeting, Warwick (2018)

ISOS-XVIII, Ji'nan, China (flash talk & poster) (2017)
3rd Place Silicon Youth Spring Prize

Poster presentations:

RSC Main Group Interest Meeting, London (2017)

Joseph Black Conference, Edinburgh (2017)

50th USIC, Strathclyde (2016)

Dalton Meeting, Warwick (2016)

Acknowledgments

First and foremost, I would like to thank my supervisor, Dr Michael Cowley, for his support and guidance during my studies. Thank you for teaching me everything I know about silicon chemistry and thank you for your encouragement, both when the results have been forthcoming and when they have not.

Thank you to all the members of the Cowley group, past and present. To Dr Amy Price, Dr Stephanie Urwin, Dr Clément Millet, Dr Lena Albers, Daniel De Rosa, Abigail Levy, Dr Rosalyn Falconer, Dr Andryj Borys and Ella Rice. Thank you for keeping me sane, happy and well fed over the last four years and thank you for making the lab such an enjoyable place to be. An extra thank you to Alessandro for your help with Chapter 4 and for all the time we spent together away from the lab.

I owe a lot to our computational collaborators, Julia I. Schweizer, Maximillian Menche and Prof. Dr Max C. Holthausen. Also to Dr Gary Nichol for your ridiculous patience with my “single” crystals and to Juraj Bella and Dr Lorna Murray for all your help with NMR.

Thank you to Dr Murray Low for your support in my teaching activities and thank you to Dr Euan Doidge for everything you have done and for your friendship outside of the teaching lab.

No doubt that my PhD would have been much more difficult without such good friends at Primal Gym, Edinburgh OCR, MudRun and at climbing.

Last, but most certainly not least, thank you to my family and to Jianzhu. Thank you for looking after me while I write this thesis and thank you for all your support, patience and care.

Abbreviations

4-PPy	4-Pyrrolidinopyridine
9-BBN	9-Borabicyclo(3.3.1)nonane
Ad	1-Adamantyl
Ar*	2,6-Bis(2,4,6-trimethylphenyl)phenyl
Cp*	Pentamethylcyclopentadienyl
DABCO	1,4-diazabicyclo[2.2.2]octane
DFT	Density functional theory
Dip	2,6-di*iso*propylphenyl
DMAP	4-Dimethylaminopyridine
DME	Dimethoxyethane
ee	Enantiomeric excess
HBcat	Catecholborane
HBpin	Pinacolborane
IDipp	1,3-(2,6-di*iso*propylphenyl)imidazol-2-ylidene
I^{t}Bu	1,3-Di*tert*butylimidazol-2-ylidene
KO^{t}Bu	Potassium *tert*butoxide
LiNp	Lithium naphthalenide
^{Me}I^{i}Pr	1,3-Di*iso*propyl-4,5-dimethylimidazol-2-ylidene
^{Me}IMe	1,3,4,5-tetramethylimidazol-2-ylidene
Mes	2,4,6-trimethylphenyl, mesityl
Mes*	2,4,6-tri*tert*butylphenyl
NaNp	Sodium naphthalenide
NaO^{t}Bu	Sodium *tert*butoxide
NHC	*N*-Heterocyclic carbene
NHSi	*N*-Heterocyclic silylene
NMR	Nuclear magnetic resonance
THF	Tetrahydrofuran
Tip	2,4,6-tri*iso*propylphenyl
$\nu_{½}$	Full width at half height maximum

Table of Contents

Chapter 1
Introduction

Chapter 1 Introduction

1.1 Silicon

Silicon is the second most abundant element in the earth's crust, after oxygen, making up approximately 28% by weight. Like carbon, silicon is found in group 14 of the periodic table and therefore naturally exists in oxidation state +IV, almost exclusively as oxygen containing compounds called silicates. More recently, silicon has found fame for its use in the semiconductor industry, both for its use in microchips and as thin films in solar cells. In these applications, silicon is found in its elemental state, often in an ultrapure and crystalline form.

In contrast, this thesis deals with organosilicon compounds in the unusual oxidation state of +II. Chapters 2 and 3 focus on disilenes and silylenes, which are the silicon analogues of alkenes and carbenes, and Chapter 4, makes use of a silyl anion which is the silicon analogue of a carbanion.

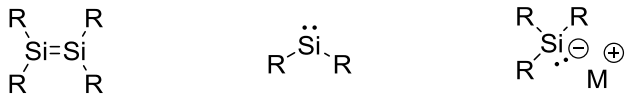

Scheme 1-1 *– Disilenes, silylenes and silyl anions are examples of silicon in oxidation state +II.*

This introduction provides an overview of the chemistry of such compounds, including their early history and some modern and relevant examples.

1.2 Disilenes

Disilenes are compounds containing a silicon-silicon double bond and are the heavier analogues of alkenes. The first attempted synthesis of a disilene was reported by Kipping and co-workers in 1921.[1] They treated diphenyldichlorosilane (Ph_2SiCl_2) with sodium metal and obtained evidence of a structure with the general formula $[Ph_4Si_2]$.[1] However, in the same paper they were able to conclusively prove that the product was actually Ph_8Si_4, a tetrasilabutane (Scheme 1-2). It was several decades later that the first real evidence of disilenes was presented. In 1969, tetramethyldisilene, $Me_2Si{=}SiMe_2$, was generated by

thermolysis of disilane bridged naphthalene **1.1** and trapped by anthracene in the reaction mixture to give disilene **1.2**(Scheme 1-2).[2,3] Although the disilene was not isolable, this was early evidence that disilenes may be synthetically accessible.

It was in 1981 when West, Fink and Michl reported the seminal, stable disilene tetra(2,4,6-trimethylphenyl)disilene ($Mes_2Si{=}SiMes_2$) **1.3**.[4] Their elegant synthesis involved the photolysis of a trisilane with bulky substituents, 2,4,6-trimethylphenyl (mesityl, Mes) to prevent oligomerisation and therefore generate the dimer, disilene **1.3**, as the most stable product.

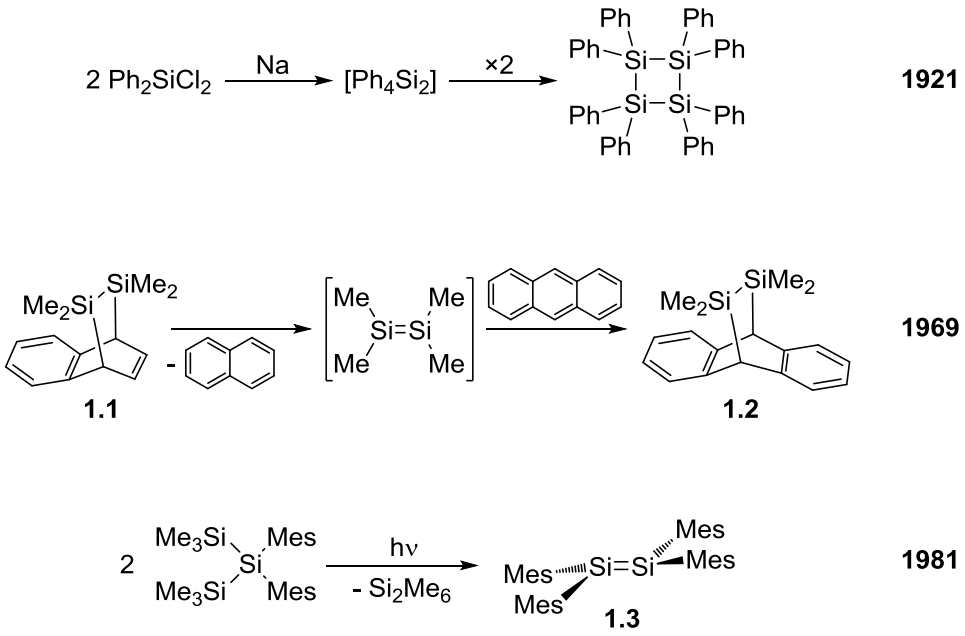

***Scheme 1-2** – Top to bottom: the earliest reported attempt to synthesise a disilene,[1] the first significant evidence of a transient disilene,[2] and the first isolable disilene.[4] Mes = 2,4,6-trimethylphenyl.*

Disilene **1.3** marked the beginning of a long line of isolable disilenes. Their properties and reactivity were studied extensively in the following years, particularly in regard to their analogy with alkenes. They were found to be similar to alkenes in many respects but with some important differences. For example, the π-bond energy of disilenes is usually 14-24 kcal·mol^{-1}, significantly smaller than that for alkenes which usually have π-bond energies above 45 kcal·mol^{-1}.[5] Correspondingly, the π-π* gap is also significantly smaller in disilenes. For example, tetramethyldisilene trapped in an argon matrix has λ_{max}(π-π*) = 344 nm,[6] while for ethene it is 165 nm.

The smaller π-bond energies of disilenes are a result of the differences in orbital overlap between carbon and silicon. The bonding situation in ethene is usually described as one σ bond and one π bond, formed from sp^2 and p orbitals, respectively (Scheme 1-3). However, the π orbital overlap in disilenes is substantially reduced. Disilenes, therefore, adopt a *trans*-bent structure which can be represented by the molecular orbitals shown in Scheme 1-3.[7,8] The weak "π-bond" leads to other potential isomers of disilene which are not usually observed but are discussed in more detail in Chapter 2 of this thesis.[9–12]

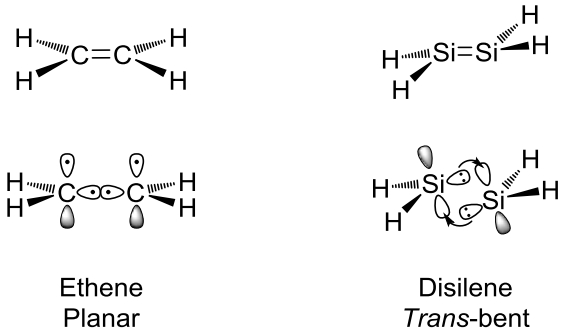

***Scheme 1-3** – A representation of the bonding situation in ethene and disilene which explains why disilenes are often* trans *bent.*

These results show some of the differences between alkenes and disilenes. There have been a large number of disilenes reported to date and multiple review articles.[5,7,13] Here I will highlight some of the most common synthetic routes to disilenes, as well as the reactivity of some of these compounds.

1.2.1 Common Synthetic Routes to Disilenes

As mentioned, the first isolable disilene, **1.3**, was prepared by the photolysis of a trisilane and this method was found to be somewhat general.[14] In a similar manner, the photolysis of cyclic trisilanes was also shown to be an effective route to simple disilenes. For example, the irradiation of cyclic trisilane **1.5** afforded the first tetrasilyl disilene **1.6**.[15]

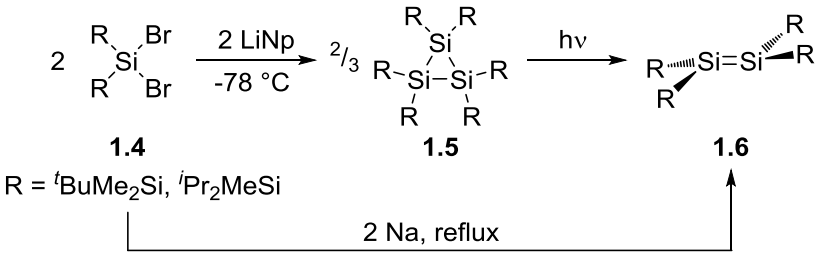

***Scheme 1-4** – Reudction of dibromo silane **1.4** with lithium naphalenide (LiNp) gives cyclotrisilane **1.5** which can be irridiated to afford disilene **1.6**. Reduction of dibromo silane **1.4** with sodium metal yields disilene **1.6** in one step.*

However, perhaps a more common method is the alkali metal reduction initially investigated by Kipping and co-workers. In fact, the preparation of cyclic trisilane **1.5** was actually achieved by the reduction of dibromo silane **1.4** using lithium naphthalenide (LiNp). Interestingly, when the same diboromosilane, **1.4**, was reduced with sodium metal instead, disilene **1.6** was isolated in one step.[16]

Using the same technique, tetra(2,4,6,-tri*iso*propylphenyl)disilene **1.7** ($Tip_2Si{=}SiTip_2$) was first synthesised in 1987 by the reduction of Tip_2SiCl_2, although this time lithium naphthalenide was found to be a suitable reductant.[17] Interesting, disilene **1.7** was found to be planar, in contrast to most other disilenes reported to date, reportedly due to the excessive steric bulk from the Tip substituents.[17]

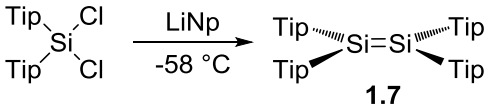

***Scheme 1-5** – Planar disilene **1.7** was first prepared by the reduction of Tip_2SiCl_2 with lithium napthalenide. Tip = 2,4,6-tri*isopropylphenyl.

Silyl anions were also found to be suitable reducing agents for the synthesis of disilenes. In these instances, the by-products are halosilanes and simple salts. For example, the first halogenated disilene, **1.8**, was prepared by the reduction of trihalo silanes with tri*tert*butylsilyl anion, as shown in Scheme 1-6.[18] This method was more recently used to prepare a landmark disilene, **1.9**, which is able to react with dihydrogen under extremely mild conditions.[19]

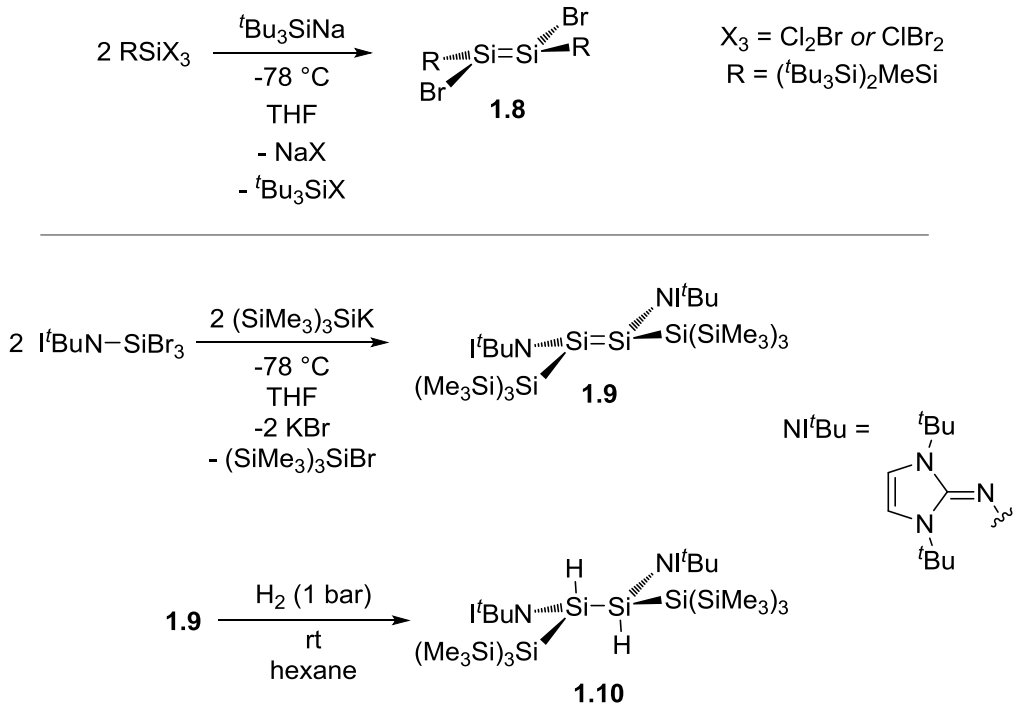

Scheme 1-6 *– Disilenes* ***1.8*** *and* ***1.9*** *were prepared by reduction using silylanions as reducing agents. Disilene* ***1.8*** *was the first isolable disilene with halogen substituents and* ***1.9*** *was the first disilene reported to react with dihydrogen to give disilane* ***1.10****.*

1.2.2 Disilenes with Interesting Functional Groups

Disilene **1.8** with halogen substituents represents one of several disilenes with interesting functionalities.[13] Another class of functionalised disilene is disilenides. Disilenides are disilenes with metallo functionalities and are analogous to metalo vinyl compounds. They were first reported by the Scheschkewitz (**1.11**) and Sekiguchi (**1.12**) groups separately in 2004,[20,21] although disilenide **1.11** had been proposed as a reactive intermediate several years earlier.[22] Disilenide **1.11** is very slightly *trans* bent while disilenide **1.12** is planar, as shown in Scheme 1-7. Disilenide **1.11** was prepared by the reaction of disilene **1.7** with lithium metal and is an excellent example of a reaction in the periphery of a disilene with preservation of the Si=Si double bond.

Disilenides act as versatile starting materials for the synthesis of a range of disilenes with interesting substituents. The reactivity of disilenide **1.11** has been particularly well explored. It has led to the preparation of a tetrasila-butadiene,[22] an iododisilene,[23] a trisila cyclopropylidene,[24] and phosphino-disilenes.[23]

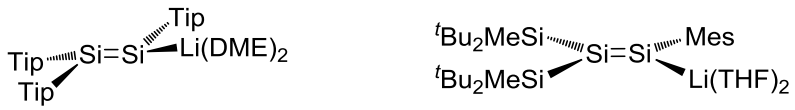

1.11 **1.12**

Scheme 1-7 *– Seminal disilenides reported by Scheschkewitz[21] and Sekiguchi.[20] Tip = 2,4,6-triisopropylphenyl, DME = 1,2-dimethoxyethane, Mes = 2,4,6-trimethylphenyl.*

A later example of a disilenide, **1.14**, was prepared directly by the reduction of trihalo-disilane **1.13**, as shown in Scheme 1-8. Disilenide **1.14** is important because its reaction with a chloro borane afforded the push-pull disilene **1.15**.[25] This example of a disilene with two functional substituents is another example of a silicon compound which is able to react with dihydrogen, as shown in Scheme 1-8.[25,26]

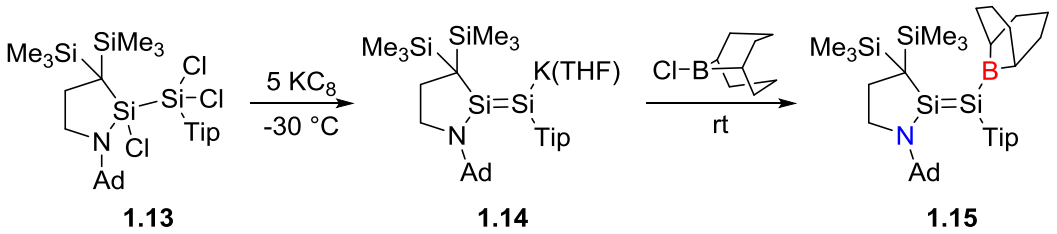

1.13 **1.14** **1.15**

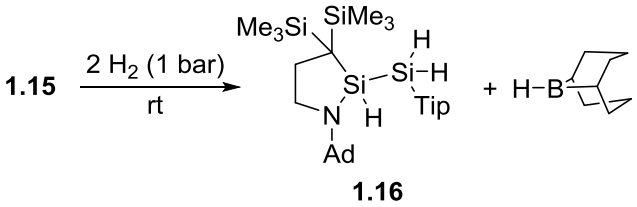

1.16

Scheme 1-8 *– The preparation of push-pull disilene **1.15** in two steps from disilane **1.13**.[25] Ad = 1-adamantyl, Tip = 2,4,6-triisopropylphenyl.*

The authors were able to show that both the nitrogen and boron substituents were necessary for the reactivity of disilene **1.15** with dihydrogen.[26] Scheme 1-9 shows a series of disilenes with boron, nitrogen and carbon substituents. While boryl disilene **1.17** does react with dihydrogen, the reaction is six times slower than that with push-pull disilene **1.15**.[26] Disilenes **1.18** and **1.19** did not react with dihydrogen, even at elevated temperature.[26]

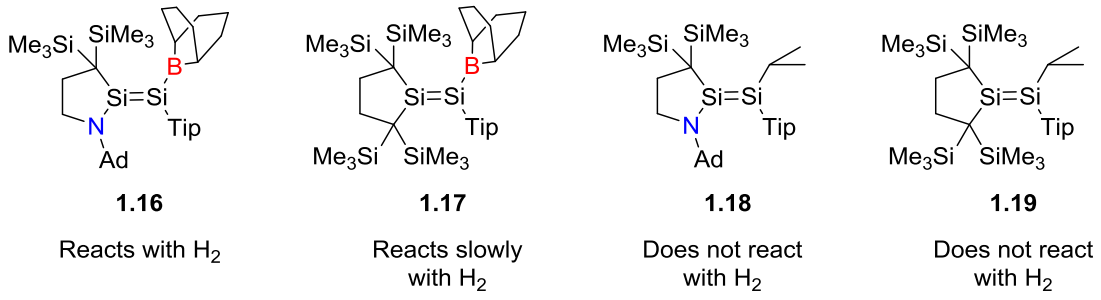

Scheme 1-9 *– Variations of disilene* ***1.15*** *with the boron, nitrogen, or both substiuents replaced with carbon.*[25,26] *Tip = 2,4,6-triisopropylphenyl.*

Other disilenes with boron and nitrogen substituents have been prepared by the hydroboration or hydroamination of disilynes, compounds with an Si-Si triple bond.[27–29] This is an interesting route because the disilene products also have hydride substituents which are also reactive functional groups. Furthermore, the hydroboration and hydroamination of alkynes often requires a catalyst while these reactions were performed catalyst free, again highlighting the differences between carbon and silicon.

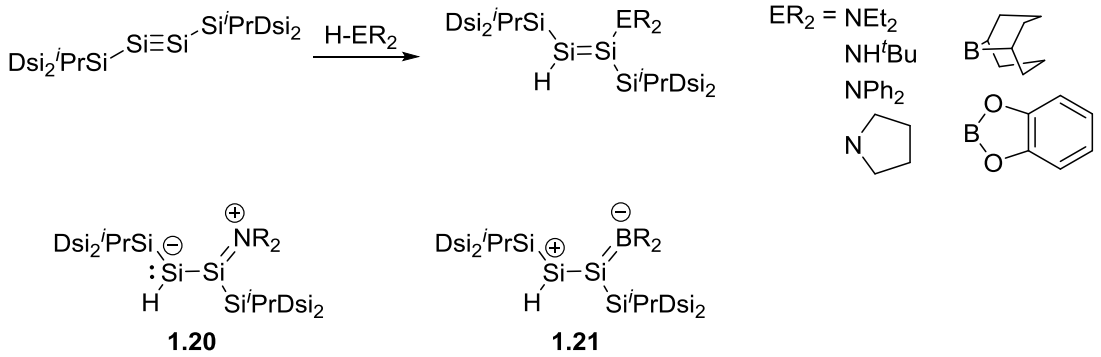

Scheme 1-10 *– The synthesis of boron and nitrogen substituted disilenes through hydroelementation reactions of disilyne.*[27–29] *Dsi = CH(SiMe₃)₃.*

In some instances, the resultant amino and boryl disilenes were shown to have significant contributions from resonance forms **1.20** or **1.21** whereby the nitrogen lone pair or empty p orbital on boron is involved in π-delocalisation. This only occurred in specific examples but was evident in the solid-state geometries as well as the chemical shifts in the ^{29}Si NMR spectra. The *Si*-H resonance of a conjugated boryl disilene was found at δ 123.4, indicating cationic character, while the *Si*-H resonances of the conjugated amino disilenes were found between δ −34.1 and δ −47.2, indicating anionic character.

1.2.3 Base-Coordinated Disilenes

The disilenes presented thus far have usually been protected by large, sterically encumbering substituents such as bulky aryl or silyl groups. However, disilenes that would otherwise be very reactive can be stabilised by coordination of a Lewis base.

One excellent example, while not strictly a disilene, is the disilicon complex **1.22** reported by Robinson and co-workers. The formal oxidation state of silicon in **1.22** is zero, therefore it is referred to as a disilicon(0) complex stabilised by two N-heterocyclic carbenes (NHCs). It was prepared by the reduction of the corresponding NHC-$SiCl_4$ adduct, as shown in Scheme 1-11.

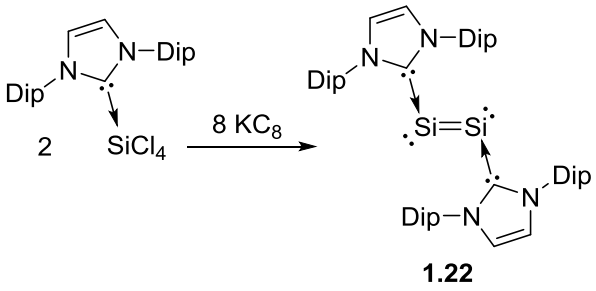

Scheme 1-11 *– Disilicon(0) compound* ***1.22*** *prepared by reduction.[30] Dip = 2,6-di*isopropylphenyl.

Another example of an NHC supported disilene compound is disilenyl cation **1.24**.[31] Cation **1.24** was prepared by the addition of methyl triflate to NHC coordinated disilyne **1.23**. The solid-state structure showed no significant interactions between the triflate anion and the Si_4 skeleton or the NHC. Cation **1.23** is a good example of a compound that would be highly reactive and therefore not isolable without a coordinating base.

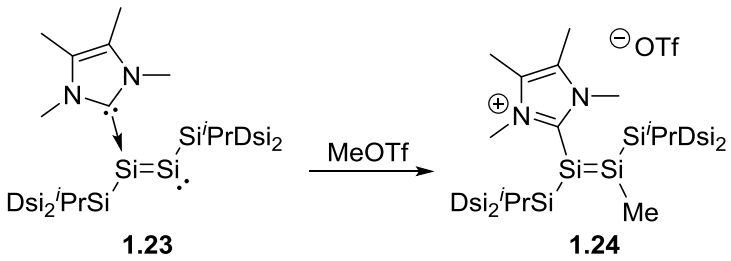

Scheme 1-12 *– The preparation of NHC stabilised disilenyl cation* ***1.24*** *from NHC coodinated disilyne* ***1.23****.[31] Dsi = CH(SiMe3)3, OTf = CF3SO3.*

In 2012, Scheschkewitz and co-workers showed that coordination of NHCs to disilenes could be reversible.[32] They reported the simple 1:1 NHC disilene adduct **1.26** which is in

equilibrium with the free disilene **1.25**. NMR spectroscopy showed that both **1.25** and **1.26** are present at room temperature. Cooling the mixture increases the concentration of adduct **1.26** with consistent changes in the concentration of free disilene **1.25** and free NHC.[32] Heating the sample gives the opposite effect.

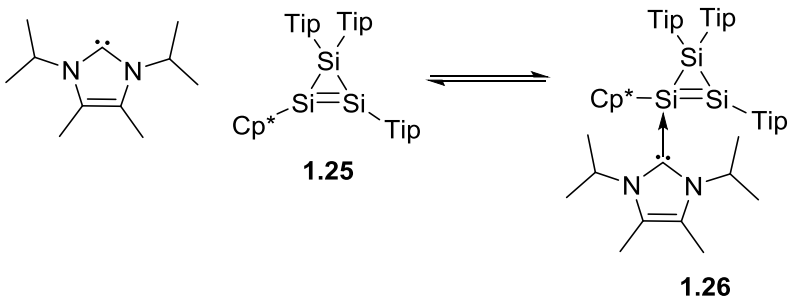

Scheme 1-13 *– Disilene **1.25** forms a simple 1:1 adduct **1.26** with an NHC which is reversible upon heating.[32] Cp* = pentamethylcyclopentadienyl, Tip = 2,4,6-tri*iso*propylphenyl.*

Another interesting example of a disilene adduct is amine stabilised perchlorodisilene **1.27**.[33] It was prepared by the disproportionation reaction of hexachlorodislane, Si_2Cl_6, in the presence of one equivalent of the amine base NMe_2Et. Disilene **1.27** was shown to be most accurately represented as having a dative Si-Si bond, as shown in **1.27a**, supported by the solid-state structure and extensive calculations. The bonding situation in the theoretical, base-free disilene can be explained by the simple molecular orbital representation shown in Scheme 1-14, which is similar to that for simple *trans* bent disilenes shown in Scheme 1-3.

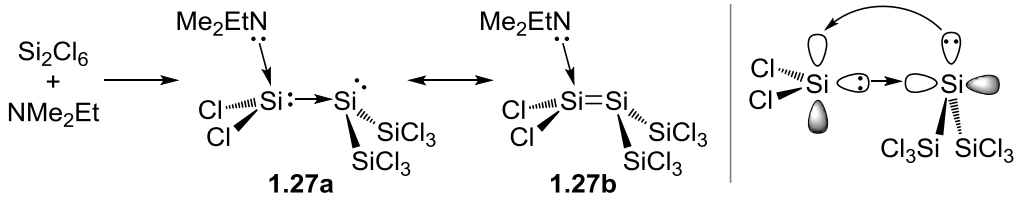

Scheme 1-14 *– The formation of disilene adduct **1.27** from hexachlorodisilane and its two signifcant resonance forms, **1.27a** with a dative Si-Si bond and **1.27b** with an Si=Si double bond.[33]*

In some instances, the reaction of disilenes with coordinating bases affords products other than the 1:1 adduct such as a trapped silylene isomer[34,35] or the silylene monomer of the disilene.[36] For example, when disilene **1.28** was treated with the coordinating pyridine base, 4-pyrollidinopyridine (4-PPy), base-stabilised silylene **1.29** was isolated as the major product (Scheme 1-15).[36]

This equilibrium between disilenes and silylenes is analogous to the proposed Wanzlick equilibrium, which was originally suggested for NHCs [37–41] but is also proposed for silicon.[7,42] Notably, when parent silylene was produced in an argon matrix it could not be converted to parent disilene.[10]

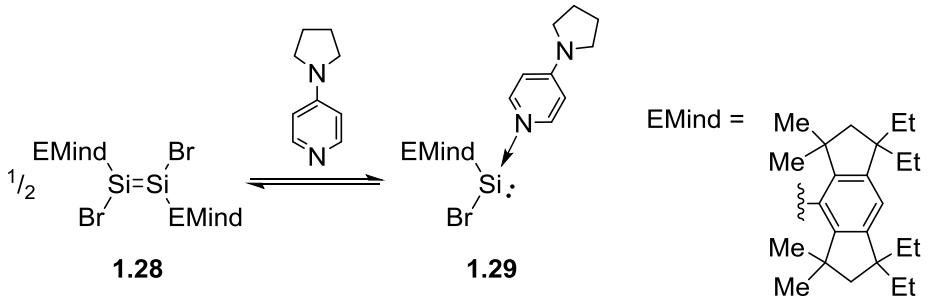

***Scheme 1-15** – The proposed Wanzlick equilibrium between disilene **1.28** and silylene **1.29**.[36]*

1.3 Silylenes

1.3.1 Early Silylenes

Silylenes, such as **1.29**, are the silicon analogues of carbenes. Like disilenes, they have been studied extensively as both transient and isolable species. The earliest significant evidence of a transient silylene was published in 1964.[43] By reacting dichlorodimethylsilane with sodium-potassium vapour, transient dimethylsilylene (**1.30**) was generated which could then be trapped by its reaction with trimethylsilane, as shown in Scheme 1-16.

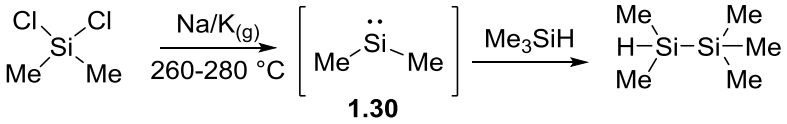

***Scheme 1-16** – The production of dimethylsilylene **1.30** and its trapping reaciton with trimethylsilane.[43]*

Similarly dimesitylsilylene **1.32** was produced by the irradiation of trisilane **1.31** and trapped by its reaction with triethyl silane, as shown in Scheme 1-17.[4] Formation of **1.33** is evidence of the formation of silylene **1.32** as an intermediate in the synthesis of disilene **1.3**.

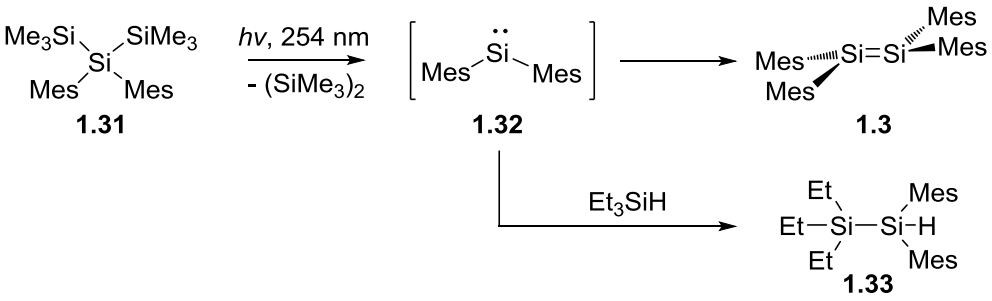

Scheme 1-17 *– Irradiation of trisilane **1.31** yields **1.3** as the final product. However, if the reaction is carried out in the presence of triethylsilane, disilane **1.33** is observed as the final product, evidence of dimesitylsilylene **1.32** as an intermediate.[4] Mes = 2,4,6-trimethylphenyl.*

A number of oligosilanes, including **1.31**, were studied as precursors to transient silylenes from the early 1970s.[4,44–50] Some of these compounds were tested for interesting reactivity with small molecules and functional groups including alkenes and alkynes, such as the cycloaddition reaction between trimethylsilylphenylsilylene **1.34** and 1-hexyne shown in Scheme 1-18.[44] This interest in the reactivity of silylenes has persisted and forms the basis for Chapter 3 of this thesis. Here I will introduce a range of historically and scientifically relevant silylenes, as well as their reactivity.

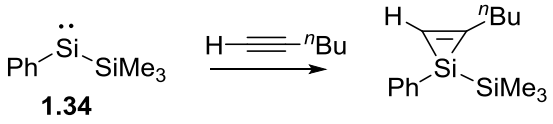

Scheme 1-18 *– The cycloaddition reaction of a simple silylene, **1.34**, with 1-hexyne.*

1.3.2 Isolable Silylenes

So far, I have discussed some transient silylenes. The first isolable silylene was reported in 1986 by Jutzi and co-workers.[51] Decamethylsilicocene **1.36** was prepared by the reaction of precursor **1.35** with sodium naphthalenide (NaNp) in just 15% yield. The ^{29}Si chemical shift of **1.36**, at δ −577, is at higher field than that of any other reported silicon compounds, a record still held to this day. The crystal structure of **1.36** showed two independent molecules with slightly different geometries, one of which clearly indicated the presence of a stereoactive lone pair. Lewis structures of both geometries are shown Scheme 1-19. The observation of only one ^{29}Si NMR resonance suggests that the two isomers are in rapid equilibrium in solution.

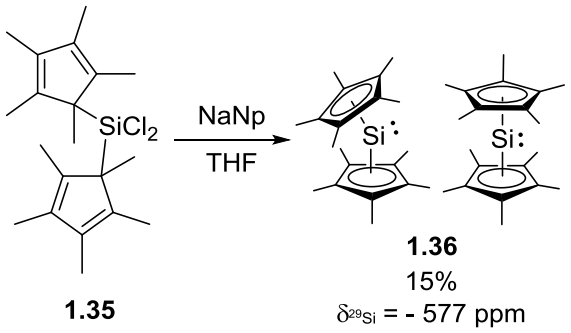

Scheme 1-19 *– The preparation of the first isolable silylene* ***1.36*** *from silane* ***1.35****. NaNp = sodium naphthalenide.*[51]

The first two-coordinate silylene, N-heterocylic silylene (NHSi) **1.37**, was reported by West and Denk in 1994.[52] NHSi **1.37** was also prepared by the reduction of a silicon(IV) precursor. The reduction of silicon halides has since become the most common method of synthesising silylenes. A range of N-heterocyclic silylenes were reported in the following years with structures based on **1.37**.[53–59] Their reactivity was thoroughly investigated and they were found to commonly insert into O-H, C-I, C-Li and Si-Li bonds.[53,57,59–61] However, they did not react with less reactive substrates such as silanes in the same way as earlier, transient silylenes. This is due to the stabilisation afforded by the adjacent nitrogen atoms. The nitrogen lone pairs are able to donate into the empty p-orbital of the silylene, raising the energy of the LUMO, while the electronegative nitrogen nucleus draws electron density from the silylene HOMO, lowering its energy, as shown in Scheme 1-20.

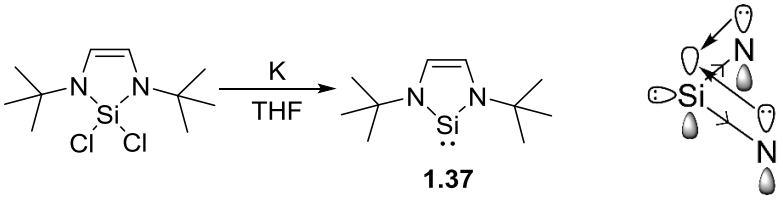

Scheme 1-20 *– Left: the preparation of the first two-coordinate silylene* ***1.37****.*[52] *Right:* ***1.37*** *is stabilised by the adjacent nitrogen atoms.*

1.3.3 Substituent Effects on Silylene Reactivity

Two interesting variations on silylene **1.37** have been published which allow for a pleasing systemic study on the impact of the nitrogen substituents. In 1999, Kira and coworkers published the cyclic dialkyl silylene **1.39**,[62] and more recently, the group of Iwamoto

reported cyclic alkyl-amino silylene **1.38**.[63] Both **1.38** and **1.39** were prepared by the reduction of silicon(IV) halide precursors with alkali metal reducing agents. Interestingly, dialkyl silylene **1.39** has a ^{29}Si NMR chemical shift for the silylene silicon at δ 567.4, the lowest field chemical shift for silicon reported to date.[62] The ^{29}Si chemical shifts of silylenes **1.37** and **1.38** are δ 78.3 and δ 274.7, respectively. This trend in chemical shift is replicated in the reactivity and properties of the three compounds.

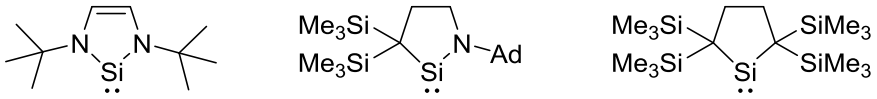

1.37 $\delta_{^{29}Si}$ 78.3 **1.38** $\delta_{^{29}Si}$ 274.7 **1.39** $\delta_{^{29}Si}$ 567.4

Scheme 1-21 *– A series of dicoordinate cyclic silylenes with two, one or zero stabilising nitrogen substituents.[62,63] Ad = 1-adamantyl.*

Diamino silylene **1.37** is extremely thermally stable and remains unchanged after heating to 150 °C for four months.[52] Equally, silylene **1.38** is unchanged after two days at 150 °C.[63] In contrast, dialkyl silylene **1.39** undergoes a slow isomerisation to silene **1.40** even at room temperature, shown in Scheme 1-22.[62] This shows that the presence of amino substituents can dramatically stabilise low-valent silicon centres.

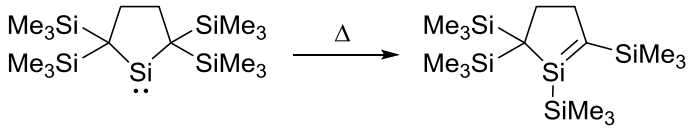

1.39 **1.40**

Scheme 1-22 *– The isomerisation of silylene **1.39** to silene **1.40** at room temperature.[62]*

The influence of amino substituents is also reflected in the reactivity of silylenes **1.37**, **1.38** and **1.39**. As mentioned, diamino silylene **1.37** does not react with Si-H bonds, even at 110 °C no reaction was observed between **1.37** and triethylsilane (Et_3SiH). In contrast, dialkyl silylene **1.39** inserts into the Si-H of Et_3SiH at room temperature. Alkyl amino silylene **1.38** offers a satisfying middle ground, reacting with Et_3SiH at 100 °C but not at room temperature.

Another interesting case study is the reactivity of silylenes **1.37**, **1.38** and **1.39** with aromatic substituents. Diamino silylene **1.37** showed no thermal or photochemical reaction when treated with benzene, toluene or mesitylene. In contrast, alkyl silylenes **1.38** and **1.39** gave

some interesting products. Both **1.38** and **1.39** react photochemically with benzene to form silepin structure **1.41**, as shown in Scheme 1-23.[63,64] Dialkyl silylene **1.39** also formed analogous products with 1,4-substituted benzenes, such as *para*-xylene to form product **1.42**.[64] However, when using a bulkier aromatic, mesitylene, the silylene inserted into the benzylic C-H position to form product **1.43**.

The most interesting result is that the middle ground silylene **1.38** is able to perform the C-H insertion in a thermal reaction, in this case using toluene as the substrate to afford **1.44**.[63] This reaction cannot happen thermally for silylene **1.39** due to its low stability, and cannot happen photochemically because of the preferable formation of a silepin such as **1.42**.

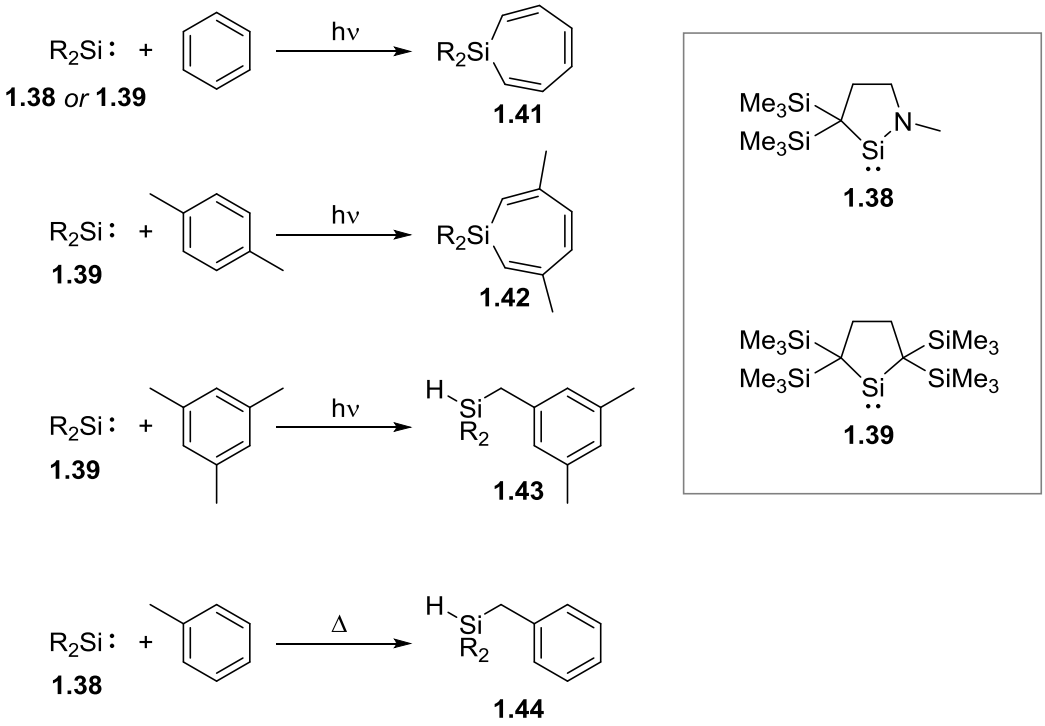

Scheme 1-23 *– Photochemical and thermal reactions of silylenes* ***1.38*** *and* ***1.39*** *with benzene,* para*-xylene, mesitylene and toluene.*[63,64]

1.3.4 Three Coordinate *N*-Heterocyclic Silylenes – Amidinato Silylenes

Amidinato silylenes are a class of *N*-heterocyclic silylenes where the silylene is three coordinate, coordinated by an additional Lewis base. Amidinate ligands had previously been used to stabilise the heavier analogues of silylenes: germylenes,[65] stannylenes and

plumbylenes.[66] Amidinato silylenes were first prepared in 2006 by the group of Roesky by the reduction of trichlorosilane **1.45** to give silylene **1.47** in just 10% yield.[67] The yield was dramatically improved through a reductive dehydrochlorination route from silane **1.46** which Roesky published four years later.[68] When the NHC 1,3-di-*tert*butylimadazol-2-ylidene was used as a strong base, **1.47** was isolated in 35% yield. However, using the amide base lithium bistrimethylsilyl amide, shown in Scheme 1-24, led to a 90% yield which enabled a vast range of reactivity studies on amidinato silylenes.[68]

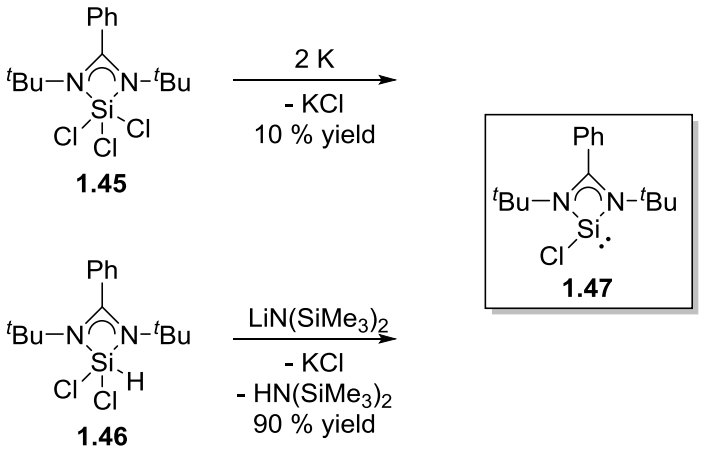

Scheme 1-24 *– The original and improved syntheses of silylene* ***1.47*** *by reduction or reductive dehydrochlorination.*

A whole range of amidinato silylenes could be prepared by simple substitution reactions with **1.47**, including silylenes with alkyl, amino, phosphino and alkoxy substituents (Scheme 1-25), as well as bis-amidinato silylenes and bis-silylenes.[69–71] These reactions are rare examples of reactivity of silylenes with no change in oxidation state at silicon.

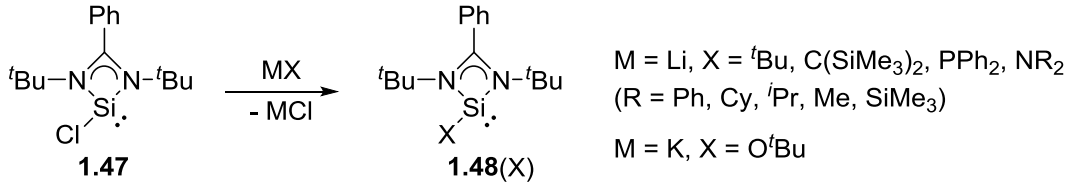

Scheme 1-25 *– The reaction of* ***1.47*** *with alkyl lithiums, lithium diphenylphosphanide, lithium amides or potassium* tert*butoxide gives substitution products* ***1.48****(X).*

The reactivity of amidinato silylenes has been widely explored, particularly by the Roesky group. In general, their reactivity is similar to that of five-membered NHSi's. Importantly, they

are also unable to perform fundamentally important E-H and E-E bond insertions typical of the early, short-lived silylenes.

Amidinato silylenes do readily undergo cyclisations with multiple bonds including C=N,[72] C=O,[73] and C=S[74] to form 3-membered C-Si-E rings (E = N, O, S). They also readily react with azo compounds. In this case the substituent at silicon can have a significant impact on the reactivity of the silylene. For example, three different types of polycyclic silane are afforded in the reaction of **1.48**(X) with azobenzene, PhN=NPh, depending on the substituent X. When X = ^{t}Bu, a simple cyclisation reaction occurs to afford product **1.49**.[75] When X = NPh_2, an [$_s$2+$_\pi$4] cycloaddition occurs involving the phenyl group. This is followed by a rapid [1,3]-hydride shift to restore aromaticity and form product **1.50**, shown at the bottom of Scheme 1-26.[72] In the case where X = Cl, the final product involves an additional molecule of silylene to give product **1.51** and silane **1.46** as a by-product.[76] In each case the reaction was carried out in toluene, at room temperature, and stirred for more than five hours.

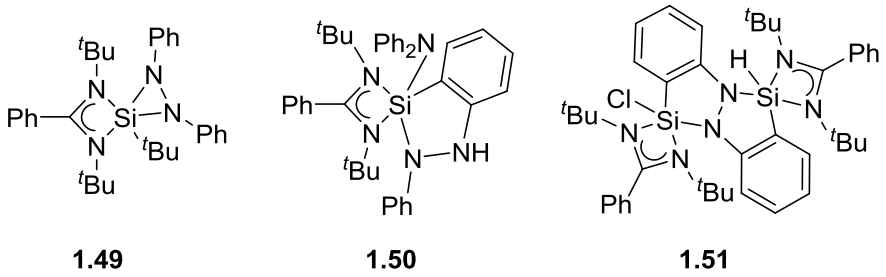

1.49 **1.50** **1.51**

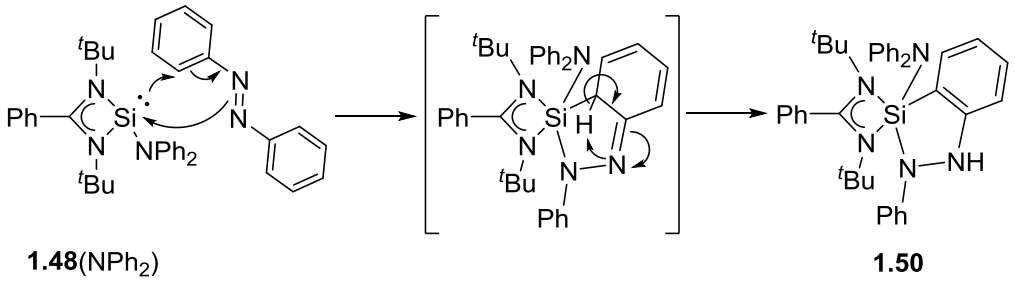

1.48(NPh_2) **1.50**

Scheme 1-26 *– Top: the reactions of **1.48**(X) with azobenzene with different X substituents, ^{t}Bu, $NPh_2$and Cl. Bottom: the mechansim of formation of product **1.50** from siylene **1.48**(NPh_2) with azobenzene.*[72,75,76]

Equally, the X substituent can impact the reactivity of amidinato silylenes **1.48**(X) with diphenyl acetylene.

When X = NPh_2 the final product is cycloaddition product **1.52**.[77] However, if X = Cl, a second molecule of silylene inserts into the C-Si bond to give cyclobutene analogue **1.53**.[68]

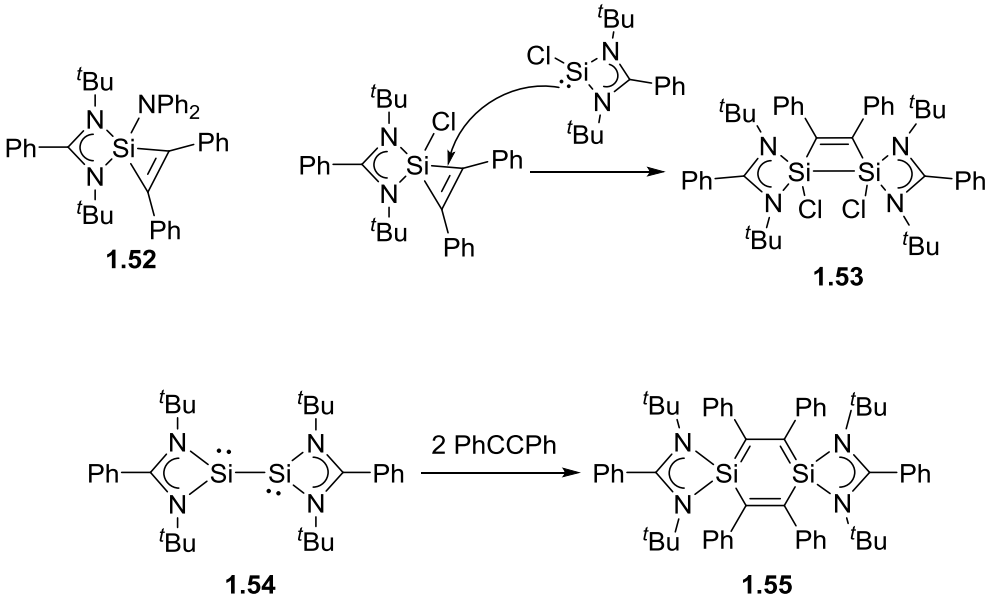

Scheme 1-27 *– The reactions of **1.48**(X) with diphenylacetylene when X = NPh_2, Cl or a second silylene.* [68,77,78]

Another notable reaction is that of bis-silylene **1.54** with two molecules of phenylacetylene. The cycloaddition product, 1,4-disilabenzene **1.55**, was a previously elusive aromatic structure.[78]

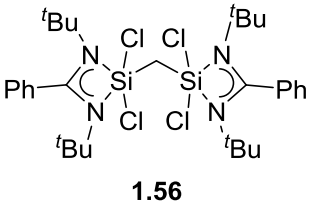

Scheme 1-28 *– Compound **1.56** formed by the insertion of silylene **1.48**(Cl) into the C-Cl bonds of dichloromethane.*[79]

The reaction of silylene **1.48**(Cl) with phenyl acetylene to give product **1.53** is evidence that amidinato silylenes may be able to insert into E-E' bonds. Another reaction that suggests this may be possible is the reaction of two equivalents of silylene **1.48**(Cl) with dichloromethane to give product **1.56**.[79] This reaction proceeds through C-Cl insertion. Although these

reactions involve breaking highly reactive bonds, they show that even base stabilised silylenes may have potential in small molecule activations.

1.3.5 More Reactive Isolable Silylenes

In recent years, several highly reactive silylenes have been isolated which are able to carry out reactions more typical of the early transient silylenes. In particular, oxidative addition reactions of unreactive E-E' or E-H bonds have been a significant target, as well as more challenging reductive elimination reactions, reactivity that has never been reported for amidinato silylenes. One example has even been shown to perform a migratory insertion reaction which is much more typical of transition metals. These results are discussed in the following pages.

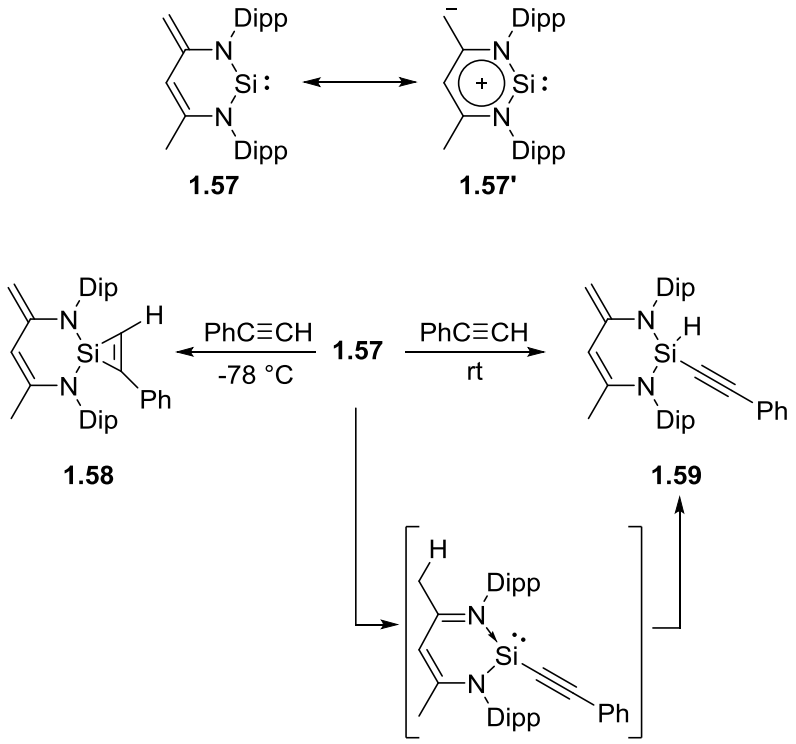

***Scheme 1-29** – Six-membered NHSi **1.57**, its zwitterionic resonance form, and its reactions with phenylactylene at −78 °C or room temperature.[80,81] Dip = 2,6-diisopropylphenyl.*

Six-membered NHSi **1.57**[80] is able to react with a variety of small molecules in a similar way to isolable silylenes already discussed.[82] Importantly, silylene **1.57** has a zwitterionic form which was shown to have a notable impact on its reactivity (Scheme 1-29). When **1.57** is subjected to phenylacetylene at −78 °C, the cycloaddition product **1.58** is observed, as for

amidinato and other silylenes.[81] However, when the reaction is carried out at ambient temperature, the thermodynamic product **1.59** is observed. Although this appears to be oxidative addition of the C-H bond, density functional theory (DFT) calculations showed that the mechanism proceeds through deprotonation of the alkyne by resonance form **1.57'** followed by a 1,4-hydride shift to final product **1.59**. This route is 17.2 kcal·mol^{-1} more favourable than direct C-H insertion. Compounds **1.58** and **1.59** cannot be interconverted.

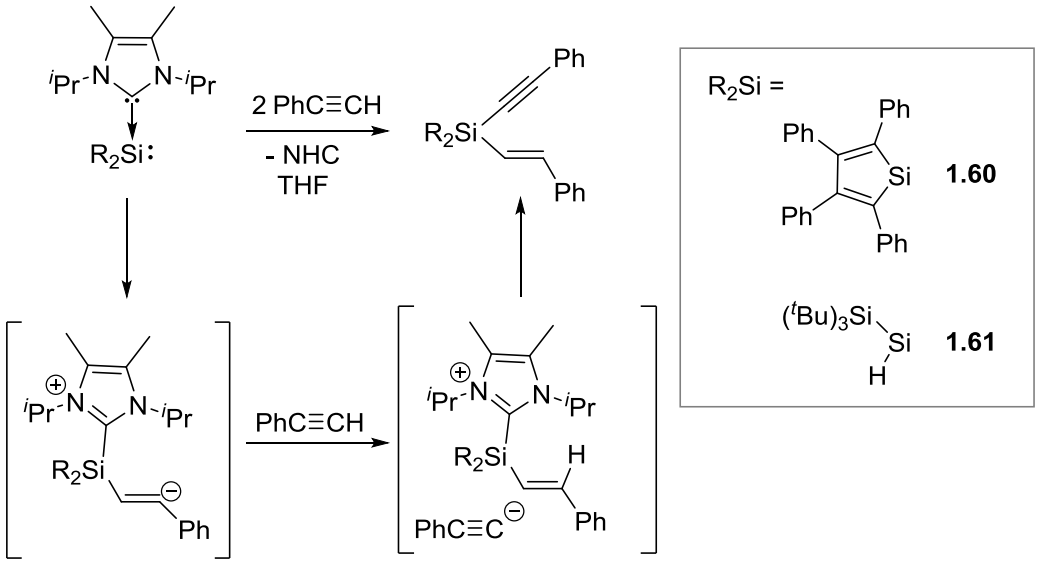

***Scheme 1-30** – The reactions of base-coordinted silylenes **1.60** and **1.61** with two equivalents of phenylacetylene.[83,84]*

Base-stabilised silylenes **1.60** and **1.61** (Scheme 1-30) were also shown to undergo insertion reactions with the C-H bond of phenylacetylene.[83–85] In these cases, insertion was coupled with simultaneous hydrosilylation, as shown in Scheme 1-30.[83–85] These reactions were also shown to use a mechanism other than direct insertion. The mechanism is shown in Scheme 1-30 which was computed for **1.61** but is assumed to be similar for **1.60**.[83] The first step is a nucleophilic attack by the silylene on the C-C triple bond. Subsequent deprotonation of a second equivalent of phenyl acetylene gives the hydrosilylation product plus an acetylide anion, which proceeds to displace the NHC.

1.3.6 Two-Coordinate, Acyclic Silylenes

Two-coordinate, acyclic silylenes have been suggested to be more reactive than their cyclic counterparts due to wider R-Si-R angles which act to decrease the HOMO-LUMO gap.[86] The first isolable two-coordinate, acyclic silylenes were published in 2012,[87,88] with a range of derivatives published in the following four years, some of which are shown in Scheme 1-31.[89–92]

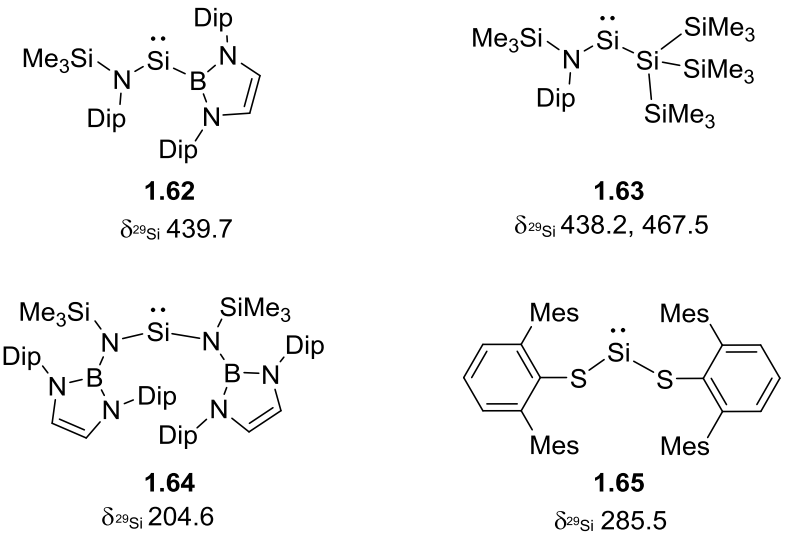

1.62
$\delta_{^{29}Si}$ 439.7

1.63
$\delta_{^{29}Si}$ 438.2, 467.5

1.64
$\delta_{^{29}Si}$ 204.6

1.65
$\delta_{^{29}Si}$ 285.5

Scheme 1-31 *– Some examples of acyclic two-coordinate silylenes.*[87–90]

Silylenes **1.62** and **1.63** showed unprecedented reactivity with dihydrogen, an example of a simple oxidative addition reaction.[87,90] In a similar manner, they both also underwent intramolecular rearrangements *via* insertion into the benzylic C-H bond of the Dip groups, as shown in Scheme 1-32.[87,90] Importantly, this reactivity was not observed for the diamino silylene **1.64**[89] or for dithiolatosilylene **1.65**.[88] This observation further highlights the detrimental effect that stabilising substituents can have on the reactivity of low-oxidation state silicon compounds.

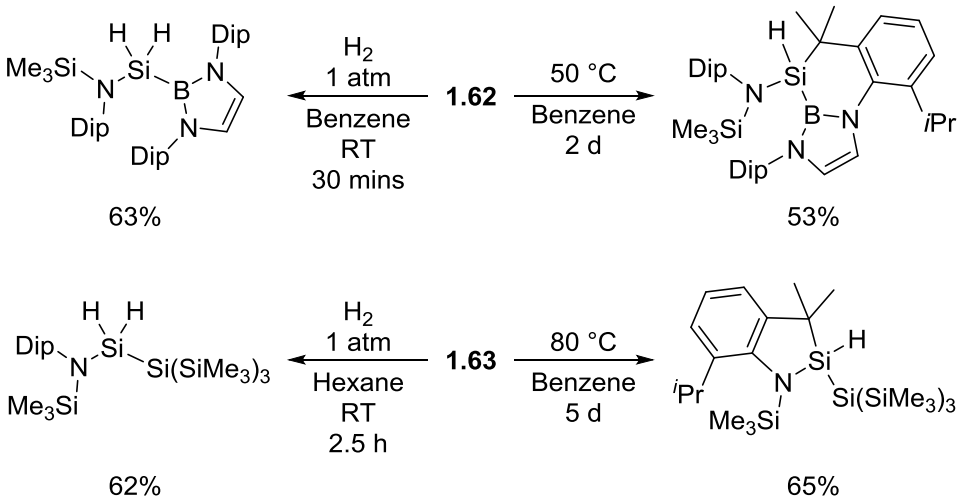

Scheme 1-32 *– The reactions of silylenes* ***1.62*** *and* ***1.63*** *with dihydrogen and their thermal rearrangments which show intramolecular C-H insertion.*

The boryl and silyl groups in **1.62** and **1.63** are σ-donating and are not π-donating, in contrast to amino substituents (see Scheme 1-20). This was further investigated by the Aldridge group in 2016, where they found that phosphino substituents are similar to boryl and silyl substituents,[93] a finding that contributed to the research in Chapter 3 of this thesis and is discussed fully in the introduction to that chapter.

Interestingly, the ^{29}Si NMR chemical shifts of silylenes **1.62** and **1.63** are highly deshielded at δ 438.2 and δ 467.5 for two isomers of **1.63** and δ 439.7 for **1.62**. These shifts are similar to cyclic dialkyl silylene **1.39** at δ 567.4 and close to the calculated value for parent silylene, :SiH_2, of δ 817 (calculated at MP2/tz2p level of theory). In contrast, stabilised silylenes **1.64** and **1.65** are found at δ 285.5 and δ 204.6, respectively, although these are still downfield shifted relative to the vast majority of isolable silylenes.

The reactions of acyclic silylenes with H_2 and C-H bonds represent challenging oxidative addition reactions which are usually more typical for transition metals or heavier main group elements and demonstrates the potential of silicon in important fundamental reactions.

1.3.7 Reactive Silylenes and Ethene

Another interesting story is the way in which some silylenes react with ethene. While the reactive silylene **1.63** is able to react with ethene in a cyclisation reaction, as shown in

Scheme 1-33, the reaction is irreversible.[94] This is not surprising as the reduction of silicon(IV) to silicon(II) usually requires harsh reducing conditions.

However, the reactions of dithiolato silylene **1.65**[92] and phosphine coordinated **1.66**[95,96] with ethene were shown to be fully reversible.

For example, when silylene **1.66** is subjected to ethene at 10 bar, the ethene bound product **1.67** is observed in 80% yield. At 8 bar the yield is 50% and at 3 bar it is 20%. In solution, silylene **1.66** is reproduced from **1.67** when the ethene pressure is reduced and the sample is kept above −30 °C. However, ethene bound product **1.67** was shown to be stable in the solid state for many weeks and in the solution state below −30 °C. Interestingly, when the phosphine substituent in **1.66** was replaced with PPh_2, the silylene was still able to bind ethene but the reaction was no longer reversible.

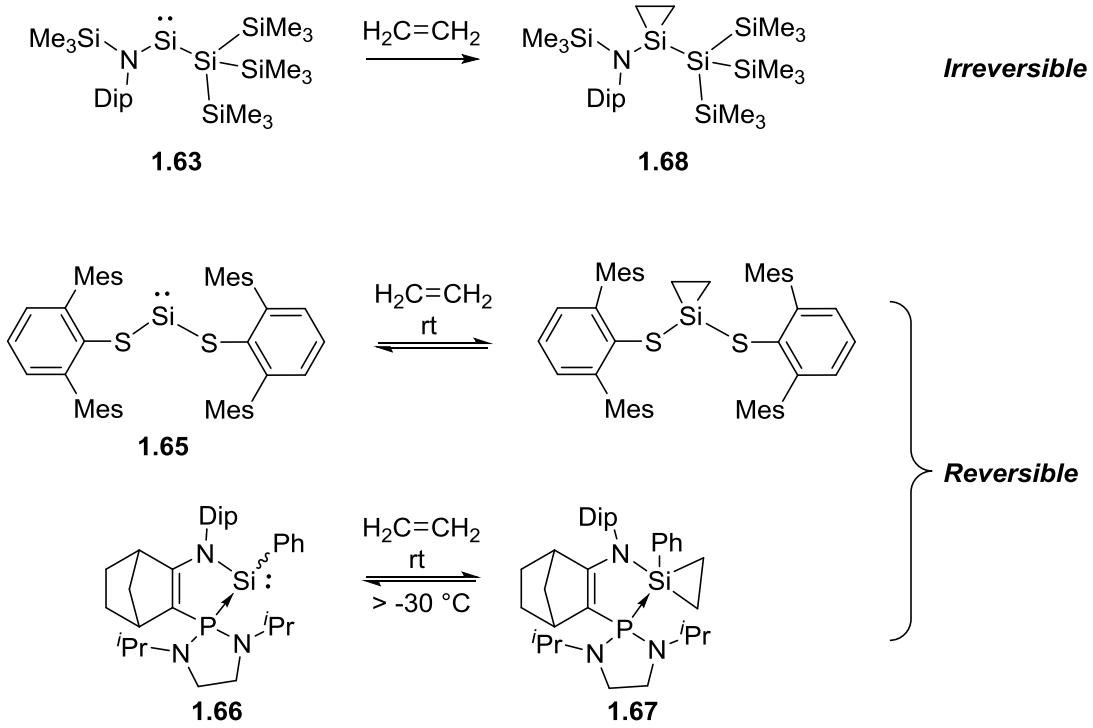

***Scheme 1-33** – The cycloaddition reactions of silylenes **1.63**, **1.65** and **1.66** with ethene, two of which are reversible.*[92,94–96]

The reversible binding of ethene to silylenes **1.65** and **1.66** demonstrates the potential for reductive elimination from silicon but also show that this fundamental reaction is dependent on the silylene being in a very specific environment. In particular, the Si(II) compound must

be stabilised relative to the Si(IV) product. This shows that a balance of stabilising and destabilising substituents is required in order to achieve any given desired result. In order to enable E-E' oxidative addition, destabilising B, Si or P substituents are required. In order to enable reductive elimination, stabilising S or N substituents are required and base-stabilisation can be employed.

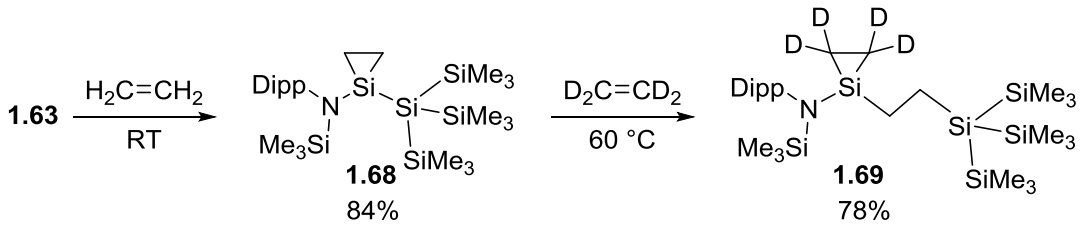

Scheme 1-34 *– The reaction of **1.63** with one equivalent of ethene selectively furnishes cycloaddition product **1.68**. Reaction with a further equivalent of deuterium labelled ethene gives migratory insertion product **1.69**.*[94]

Another interesting reaction is the reaction of ethene bound **1.68** with a further equivalent of ethene (Scheme 1-34).[94] Deuterium labelling showed that **1.69** is formed by migratory insertion of the first ethene into the Si-Si bond. This is an important example of the potential for low-valent silicon compounds to mimic transition-metal like reactivity.

1.3.8 Silylenes as Ligands for Transition Metals

So far, I have discussed the synthesis and fundamental reactivity of disilenes and silylenes. In some instances, the reactivity of silylenes is comparable to that of transition metals or heavier p-block elements. However, as analogues of carbenes, silylenes are suitable ligands for transition metals and some interesting compounds have been reported using silylene ligands.

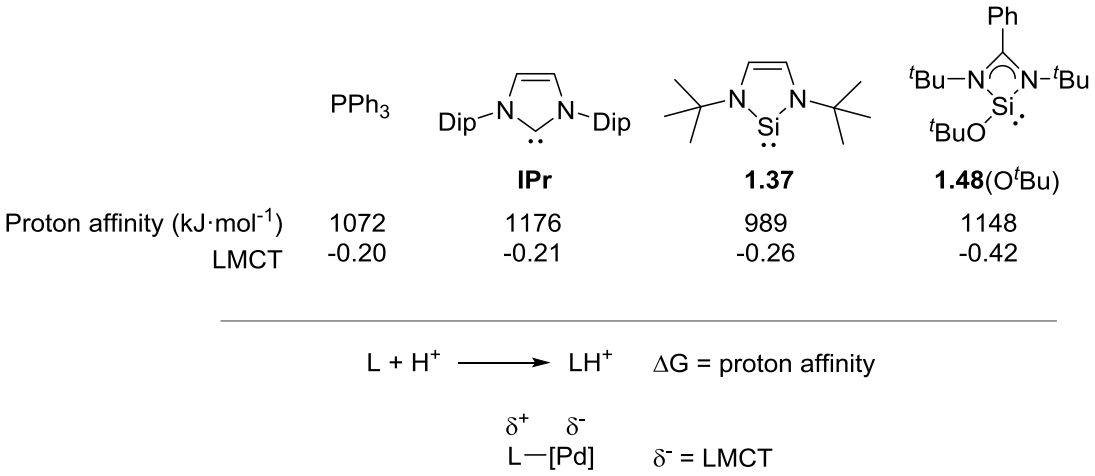

***Scheme 1-35** – Some properties of silylenes **1.37** and **1.48**(O^{t}Bu) and how they compare to a common phosphine and NHC.*

A recent paper analysed the σ-donor strengths of a range of silylenes by calculating their proton affinities.[97] Their findings suggested that simple silylenes, such as five membered NHSi's, should be weaker σ-donors than NHCs and even simple phosphines. For example, they calculated the proton affinity of silylene **1.37** to be 989 kJ·mol^{-1}, while IPr and triphenylphosphine (PPh_3) had proton affinities of 1176 kJ·mol^{-1} and 1072 kJ·mol^{-1}, respectively (see Scheme 1-35). Although some specific silylenes, such as **1.48**(O^{t}Bu) did have proton affinities similar to IPr.

Contrastingly, the same report studied the NBO charges of palladium in silylene-palladium complexes to investigate the ligand-to-metal charge transfer of different silylenes. The vast majority of silylenes transfer more charge to palladium than either NHCs or phosphines. For example, for **1.37** the transferred charge was found to be −0.26, while for IPr and PPh_3 it was found to be −0.21 and −0.20, respectively. For some silylenes, the charge transfer was found to be significantly stronger, for example −0.42 for **1.48**(O^{t}Bu). This suggests that the charge transfer does not only depend on the σ-donor strength but also depends on the π-accepting ability and the electronegativity of the donor atom.

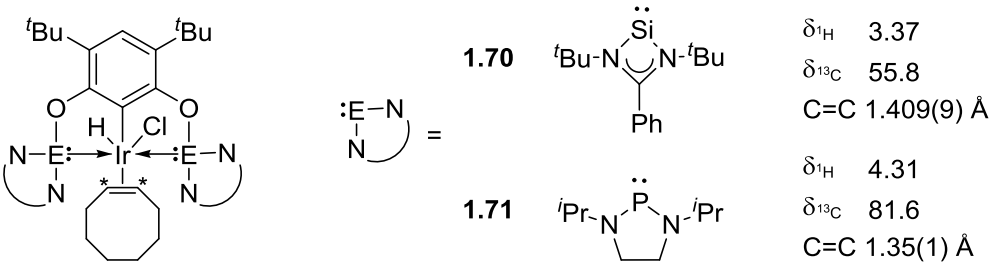

Scheme 1-36 *– Some properties of two iridium pincer complexes,* ***1.70*** *with silylene ligands and* ***1.71*** *with phosphine ligands.*[98]

A relatively large number of isolable silylene-metal complexes have now been reported, particularly with NHSi ligands.[99,100] An interesting pair of iridium complex, **1.70** and **1.71**, were examined in 2012.[98] Comparing the ^{1}H and ^{13}C NMR chemical shifts and the C=C bond distances of the cyclooctene ligand provided some valuable information on the nature of the silylene ligand when compared with phosphines.

The ^{1}H chemical shift of the alkene protons in **1.70** was found to be shifted upfield by δ 0.94 compared with phosphine complex **1.71**, while the ^{13}C resonance is δ 25.8 more upfield. This suggests greater electron density on iridium in **1.70** due to the silylene ligands. Furthermore, the C=C bond distance was found to be lengthened by 0.059(19) Å in **1.70**, again indicating greater electron density on iridium and therefore more π-back-donation. In fact, the C=C bond distance in **1.70** is one of the longest distance reported for a C=C bond in a cyclooctadiene complex.[See 98 especially reference 11] Both iridium complexes **1.70** and **1.71** were shown to catalyse the borylation of benzene with **1.70** giving a slightly higher yield after 24 h at 100 °C.

The related nickel(II) complex, **1.72** (Scheme 1-37), has been reported for the Ni-catalysed Sonogashira reaction.[101] Interestingly, using complex **1.72** allowed isolation of intermediate **1.73**. Compound **1.73** was confirmed as an intermediate through its stoichiometric reaction with a vinyl iodide to give the final product. This suggests that Sonogashira reactions catalysed by electron rich nickel complexes proceed by a mechanism in which transmetalation precedes oxidative addition, contrary to what is widely accepted for palladium catalysed reactions. The analogous intermediate could not be isolated using less electron rich ligands such as a phosphine pincer ligand.

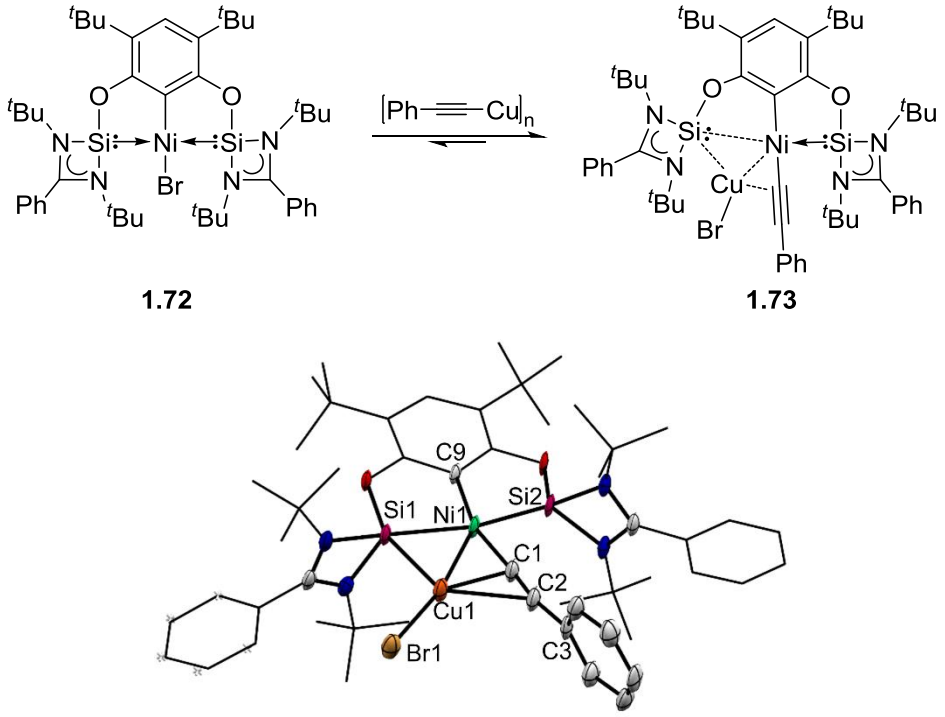

Scheme 1-37 *– The reaction of nickel complex* ***1.72*** *with an organocuprate to give the interesting Sonogashira reaction intermediate* ***1.73*** *and the solid-state structure of* ***1.73****. Thermal ellipsoids drawn at 50% probability, hydrogen atoms and solvent molecules omitted for clarity. Selected bond lengths (Å) and angles (°): Ni1–Si1 2.296(1), Ni1–Si2 2.137(1), Ni1–C9 1.940(4), Ni1–C1 1.860(4), Ni1–Cu1 2.4628(9), Si1–Cu1 2.508(1),C1–Cu1 1.976(4), C2–Cu1 2.420(4), C1–C2 1.213(6), C2–C3 1.451(6), Cu1–Br1 2.2855(7), Si1–Ni1–Si2 160.93(5), C1–Ni1–C9 162.9(2), Ni1–Si1–Cu1 61.49(3), C10–O1–Si1 115.4(2), C14–O2–Si2 110.4(2), Σ∢ Ni1 360.1(1).*[101]

Multiple other examples of silylene-transition metal complexes exist and can be used in catalysis.[99–103] Some of these complexes have been shown to give higher yields than their carbene or phosphine counterparts. These results show that the reactivity of silylene-transition metal complexes may be complementary to other metal complexes and, in some instances, may be superior.

1.4 Silyl Anions

Silyl anions are anionic silicon compounds with a lone pair of electrons at the silicon atom. In Chapter 4 of this thesis I describe the use of a silyl anion as a hydroboration initiator. As this is largely unrelated to the general chemistry of silyl anions I will only very briefly introduce silyl anions in this section. I will give a very brief overview of some of the synthetic methods

used to prepare silyl anions, some of their structural characteristics, and some of their common reactions.

1.4.1 Synthesis and Reactivity

Silyl anions were first described in the early 1930s by Kraus and co-workers.[104,105] Since then, the synthesis of silyl anions has been improved and they are now relatively common reagents in organosilicon synthesis.[106,107]

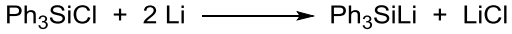

Scheme 1-38 *– The reaction of triphenylsilyl chloride with lithium metal to give silyl anion triphenylsilyl lithium.*[108]

Silyl lithium compounds, for example, triphenylsilyl lithium, can be prepared by the reaction of silyl chlorides with lithium metal, which was reported as early as 1960.[108]

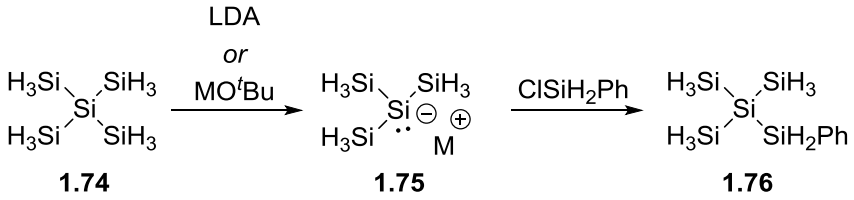

Scheme 1-39 *– The reaction of neopentasilane **1.74** with LDA or MO^{t}Bu to give anion **1.75** which can be quenched with chlorophenylsulane to give **1.76**. LDA = lithium di*isopropyl amide (LiN^{i}Pr$_2$). *M = Li, Na, or K.*

Equally, they can be prepared by the cleavage of Si-Si bonds or Si-H bonds by alkali metal alkoxides, lithium amides or alkyl lithiums. For example, neopentasilane **1.74** reacts with lithium, sodium or potassium *tert*butoxide to give silyl anion **1.75**.[109] Anion **1.75** was reacted with chlorophenylsilane to give silane **1.76** in a nucleophilic substitution reaction typical of silyl anions.

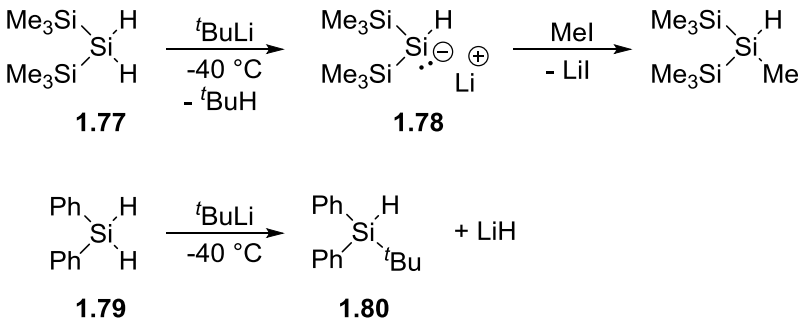

Scheme 1-40 *– The deprotonation of silane **1.77** by ^{t}BuLi to give anion **1.78** and its subsequent reaction with methyl iodide and the substitution reaction of **1.79** with ^{t}BuLi.*[110,111]

Silanes can also undergo deprotonation reactions, for example the reaction of bis(trimethyl)silane **1.77** with ^{t}BuLi gives silyl anion hydride **1.78**, which can be quenched in a nucleophilic substitution reaction with methyl iodide.[110,111] However, if the steric bulk is somewhat smaller, the alkyl lithium prefers a nucleophilic substitution as for the reaction of diphenyl silane **1.79** with ^{t}BuLi to give **1.80**.[110,111]

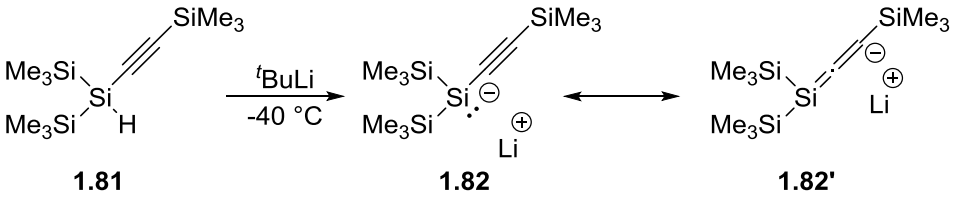

Scheme 1-41 *– Deprotonation of ethynylsilane **1.81** to give silyl anion **1.82** which has two resonance forms.*[112]

Deprotonation can also be favoured if the Si-H polarity is reversed using electron withdrawing substituents on silicon. For example, alkynyl silane **1.81** is readily deprotonated by ^{t}BuLi thanks to the electron withdrawing effect of the alkynyl group, as shown in Scheme 1-41.[112]

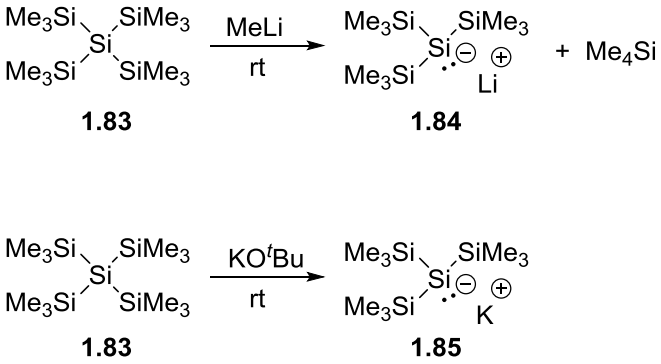

Scheme 1-42 *– The prepartion of lithium or potassium hypersilyl anion using MeLi or KO*^{t}*Bu.*[113–115]

A relatively common silyl anion is the hypersilyl anion used in Chapter 4 and shown in Scheme 1-42. Hypersilyl lithium **1.84** was first prepared in the 1960s by the lithiation of tetrakis(trimethylsilyl)silane **1.83**, as shown in Scheme 1-42.[113,114] It has since found use in the generation of silicon-transition metal complexes,[116,117] the formation of silenes,[118–123] and a range of other applications.[124–127] The potassium compound **1.85** was reported some time later in 1993[128] but the synthesis involved transmetalation from zinc, cadmium or mercury. In 1998, Marschner reported a straightforward synthesis from silane **1.83** and potassium *tert*butoxide with liberation of the volatile silyl ether, Me_3SiO^tBu, shown in Scheme 1-42.[115]

1.4.2 Some Synthetic Applications of Silyl Anions

This method of preparing polylsilyl anions is now common in the literature and has been used to prepare a range of interesting complexes. For example, cyclic oligosilanes, such as **1.88**, can be prepared by the reaction of polysilyldianions, such as **1.86**, with dihalosilanes, such as **1.87**.[129–131] In turn, these can be reacted with potassium *tert*butoxide to give cyclic anions, such as **1.89**. In this way, oligosilanes with varied and complex structures can by synthesised in a stepwise and logical fashion.

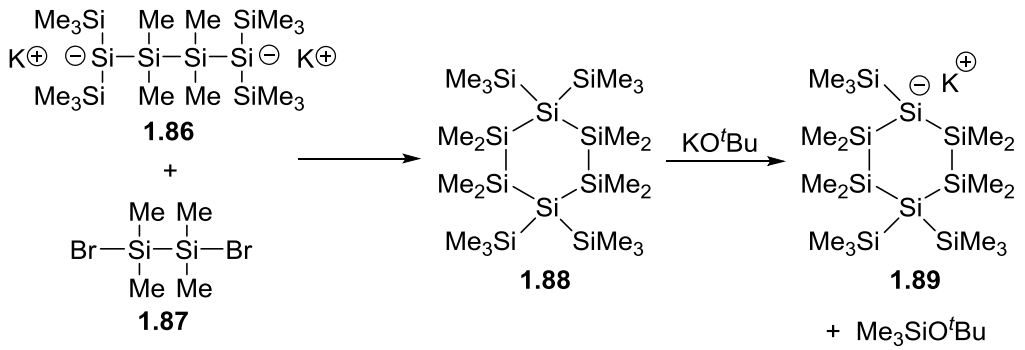

***Scheme 1-43** – The reaction of polysilyldianion **1.86** with dibromodisilane **1.87** to give cyclic oligosilane **1.88**. Oligosilane **1.88** can be converted to the silyl anion by its reaction with KO^tBu.*

One other notable use of silyl anions is the preparation of asymmetric disilenes. For example, the tetrasilabutdiene **1.92** can be prepared by the reaction of silyl dianion **1.90** with tetrachlorodislane **1.91**.[20]

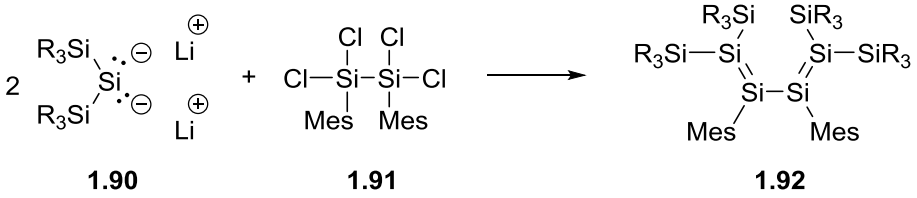

***Scheme 1-44** – The preparation of tetrasilabutadiene **1.92** by the reaction of a silyl dianion **1.90** with tetrachlorodisilane **1.91**.[20] $R_3 = Me^tBu_2$.*

1.5 Outlook and Aims

The previous work explored in this chapter demonstrates the extraordinary range of low-oxidation state organosilicon chemistry reported to date. Much of the early research focused on a fundamental comparison between silicon and carbon. More recently, focus has shifted to the reactivity of such compounds and how they can be related to transition metals.

This thesis aims to explore novel synthetic routes to low-oxidation state silicon and the fundamental behaviour of minimally substituted compounds. The reactivity of some species will also be examined. In the final chapter, a new method is explored in which a silicon(II) compound, a silyl anion, is able to mimic the reactivity of transition metals but using an orthogonal and complimentary method.

1.6 References

[1] F. S. Kipping, J. E. Sands, *J. Chem. Soc. Trans.* **1921**, *119*, 830–847.

[2] G. J. D. Peddle, D. N. Roark, A. M. Good, S. G. McGeachin, *J. Am. Chem. Soc.* **1969**, *91*, 2807–2808.

[3] D. N. Roark, G. J. D. Peddle, *J. Am. Chem. Soc.* **1972**, *94*, 5837–5841.

[4] R. West, M. J. Fink, J. Michl, *Science* **1981**, *214*, 1343–1344.

[5] T. Iwamoto, S. Ishida, in *Functional Molecular Silicon Compounds II* (Ed.: D. Scheschkewitz), Springer International Publishing, **2013**, pp. 125–202.

[6] A. Sekiguchi, I. Maruki, K. Ebata, C. Kabuto, H. Sakurai, *J. Chem. Soc. Chem. Commun.* **1991**, *0*, 341–343.

[7] M. Kira, T. Iwamoto, in *Adv. Organomet. Chem.* (Eds.: R. West, A.F. Hill), Academic Press, **2006**, pp. 73–148.

[8] G. Trinquier, J. P. Malrieu, P. Riviere, *J. Am. Chem. Soc.* **1982**, *104*, 4529–4533.

[9] G. Dolgonos, *Chem. Phys. Lett.* **2008**, *466*, 11–15.

[10] G. Maier, H. P. Reisenauer, J. Glatthaar, *Chem. – Eur. J.* **2002**, *8*, 4383–4391.

[11] W. D. Wulff, W. F. Goure, T. J. Barton, *J. Am. Chem. Soc.* **1978**, *100*, 6236–6238.

[12] L. C. Snyder, Z. R. Wasserman, *J. Am. Chem. Soc.* **1979**, *101*, 5222–5223.

[13] C. Präsang, D. Scheschkewitz, *Chem. Soc. Rev.* **2016**, *45*, 900–921.

[14] R. West, *Science* **1984**, *225*, 1109–1114.

[15] M. Kira, T. Maruyama, C. Kabuto, K. Ebata, H. Sakurai, *Angew. Chem. Int. Ed. Engl.* **1994**, *33*, 1489–1491.

[16] M. Kira, *Proc. Jpn. Acad. Ser. B* **2012**, *88*, 167–191.

[17] H. Watanabe, K. Takeuchi, N. Fukawa, M. Kato, M. Goto, Y. Nagai, *Chem. Lett.* **1987**, *16*, 1341–1344.

[18] N. Wiberg, W. Niedermayer, G. Fischer, H. Nöth, M. Suter, *Eur. J. Inorg. Chem.* **2002**, *2002*, 1066–1070.

[19] D. Wendel, T. Szilvási, C. Jandl, S. Inoue, B. Rieger, *J. Am. Chem. Soc.* **2017**, *139*, 9156–9159.

[20] M. Ichinohe, K. Sanuki, S. Inoue, A. Sekiguchi, *Organometallics* **2004**, *23*, 3088–3090.

[21] D. Scheschkewitz, *Angew. Chem. Int. Ed.* **2004**, *43*, 2965–2967.

[22] M. Weidenbruch, S. Willms, W. Saak, G. Henkel, *Angew. Chem. Int. Ed. Engl.* **1997**, *36*, 2503–2504.

[23] M. Hartmann, A. Haji-Abdi, K. Abersfelder, P. R. Haycock, A. J. P. White, D. Scheschkewitz, *Dalton Trans.* **2010**, *39*, 9288–9295.

[24] A. Jana, I. Omlor, V. Huch, H. S. Rzepa, D. Scheschkewitz, *Angew. Chem. Int. Ed.* **2014**, *53*, 9953–9956.

[25] T. Kosai, T. Iwamoto, *J. Am. Chem. Soc.* **2017**, *139*, 18146–18149.

[26] T. Kosai, T. Iwamoto, *Chem. – Eur. J.* **2018**, *24*, 7774 – 7780.

[27] K. Takeuchi, M. Ikoshi, M. Ichinohe, A. Sekiguchi, *J. Am. Chem. Soc.* **2010**, *132*, 930–931.

[28] K. Takeuchi, M. Ikoshi, M. Ichinohe, A. Sekiguchi, *J. Organomet. Chem.* **2011**, *696*, 1156–1162.

[29] K. Takeuchi, M. Ichinohe, A. Sekiguchi, *Organometallics* **2011**, *30*, 2044–2050.

[30] Y. Wang, Y. Xie, P. Wei, R. B. King, H. F. Schaefer, P. von R. Schleyer, G. H. Robinson, *Science* **2008**, *321*, 1069–1071.

[31] T. Yamaguchi, M. Asay, A. Sekiguchi, *J. Am. Chem. Soc.* **2012**, *134*, 886–889.

[32] K. Leszczyńska, K. Abersfelder, A. Mix, B. Neumann, H. Stammler, M. J. Cowley, P. Jutzi, D. Scheschkewitz, *Angew. Chem. Int. Ed.* **2012**, *51*, 6785–6788.

[33] J. I. Schweizer, M. G. Scheibel, M. Diefenbach, F. Neumeyer, C. Würtele, N. Kulminskaya, R. Linser, N. Auner, S. Schneider, M. C. Holthausen, *Angew. Chem. Int. Ed.* **2016**, *55*, 1782–1786.

[34] M. J. Cowley, V. Huch, H. S. Rzepa, D. Scheschkewitz, *Nat. Chem.* **2013**, *5*, 876–879.

[35] M. W. Stanford, J. I. Schweizer, M. Menche, G. S. Nichol, M. C. Holthausen, M. J. Cowley, *Angew. Chem. Int. Ed.* **2019**, *58*, 1329–1333.

[36] K. Suzuki, T. Matsuo, D. Hashizume, K. Tamao, *J. Am. Chem. Soc.* **2011**, *133*, 19710–19713.

[37] Y. Liu, D. M. Lemal, *Tetrahedron Lett.* **2000**, *41*, 599–602.

[38] M. K. Denk, K. Hatano, M. Ma, *Tetrahedron Lett.* **1999**, *40*, 2057–2060.

[39] H. E. Winberg, J. E. Carnahan, D. D. Coffman, M. Brown, *J. Am. Chem. Soc.* **1965**, *87*, 2055–2056.

[40] H.-W. Wanzlick, E. Schikora, *Chem. Ber.* **1961**, *94*, 2389–2393.

[41] H.-W. Wanzlick, E. Schikora, *Angew. Chem.* **1960**, *72*, 494–494.

[42] O. Renji, R. West, in *Adv. Organomet. Chem.* (Eds.: F. Gordon, A. Stone, R. West), Academic Press, **1996**, pp. 231–273.

[43] P. S. Skell, E. J. Goldstein, *J. Am. Chem. Soc.* **1964**, *86*, 1442–1443.

[44] M. Ishika, K. Nakagawa, M. Kumada, *J. Organomet. Chem.* **1977**, *131*, C15–C20.

[45] M. Ishikawa, K.-I. Nakagawa, M. Kumada, *J. Organomet. Chem.* **1979**, *178*, 105–118.

[46] V. J. Tortorelli, M. Jones, *J. Am. Chem. Soc.* **1980**, *102*, 1425–1426.

[47] V. J. Tortorelli, M. Jones, S. Wu, Z. Li, *Organometallics* **1983**, *2*, 759–764.

[48] D. Seyferth, D. C. Annarelli, D. P. Duncan, *Organometallics* **1982**, *1*, 1288–1294.

[49] M. Ishikawa, M. Kumada, *J. Chem. Soc. Chem. Commun.* **1971**, 489–489.

[50] M. Ishikawa, M. Kumada, *J. Chem. Soc. Chem. Commun.* **1970**, 612a–612a.

[51] P. Jutzi, D. Kanne, C. Krüger, *Angew. Chem. Int. Ed. Engl.* **1986**, *25*, 164–164.

[52] M. Denk, R. Lennon, R. Hayashi, R. West, A. V. Belyakov, H. P. Verne, A. Haaland, M. Wagner, N. Metzler, *J. Am. Chem. Soc.* **1994**, *116*, 2691–2692.

[53] B. Gehrhus, M. F. Lappert, J. Heinicke, R. Boese, D. Bläser, *J. Chem. Soc. Chem. Commun.* **1995**, 1931–1932.

[54] J. Heinicke, A. Oprea, M. K. Kindermann, T. Karpati, L. Nyulászi, T. Veszprémi, *Chem. – Eur. J.* **1998**, *4*, 541–545.

[55] T. A. Schmedake, M. Haaf, Y. Apeloig, T. Müller, S. Bukalov, R. West, *J. Am. Chem. Soc.* **1999**, *121*, 9479–9480.

[56] B. Gehrhus, P. B. Hitchcock, M. F. Lappert, *Z. Für Anorg. Allg. Chem.* **2005**, *631*, 1383–1386.

[57] W. Li, N. J. Hill, A. C. Tomasik, G. Bikzhanova, R. West, *Organometallics* **2006**, *25*, 3802–3805.

[58] L. Kong, J. Zhang, H. Song, C. Cui, *Dalton Trans.* **2009**, 5444–5446.

[59] A. C. Tomasik, A. Mitra, R. West, *Organometallics* **2009**, *28*, 378–381.

[60] M. Haaf, A. Schmiedl, T. A. Schmedake, D. R. Powell, A. J. Millevolte, M. Denk, R. West, *J. Am. Chem. Soc.* **1998**, *120*, 12714–12719.

[61] X. Cai, B. Gehrhus, P. B. Hitchcock, M. F. Lappert, J. C. Slootweg, *J. Organomet. Chem.* **2002**, *651*, 150–156.

[62] M. Kira, S. Ishida, T. Iwamoto, C. Kabuto, *J. Am. Chem. Soc.* **1999**, *121*, 9722–9723.

[63] T. Kosai, S. Ishida, T. Iwamoto, *Angew. Chem. Int. Ed.* **2016**, n/a-n/a.

[64] M. Kira, S. Ishida, T. Iwamoto, C. Kabuto, *J. Am. Chem. Soc.* **2002**, *124*, 3830–3831.

[65] S. R. Foley, C. Bensimon, D. S. Richeson, *J. Am. Chem. Soc.* **1997**, *119*, 10359–10363.

[66] U. Kilimann, M. Noltemeyer, F. T. Edelmann, *J. Organomet. Chem.* **1993**, *443*, 35–42.

[67] C.-W. So, H. W. Roesky, J. Magull, R. B. Oswald, *Angew. Chem. Int. Ed.* **2006**, *45*, 3948–3950.

[68] S. S. Sen, H. W. Roesky, D. Stern, J. Henn, D. Stalke, *J. Am. Chem. Soc.* **2010**, *132*, 1123–1126.

[69] R. Azhakar, R. S. Ghadwal, H. W. Roesky, H. Wolf, D. Stalke, *Organometallics* **2012**, *31*, 4588–4592.

[70] S. S. Sen, A. Jana, H. W. Roesky, C. Schulzke, *Angew. Chem. Int. Ed.* **2009**, *48*, 8536–8538.

[71] R. Azhakar, R. S. Ghadwal, H. W. Roesky, H. Wolf, D. Stalke, *Chem. Commun.* **2012**, *48*, 4561–4563.

[72] R. Azhakar, H. W. Roesky, H. Wolf, D. Stalke, *Organometallics* **2012**, *31*, 8608–8612.

[73] R. Azhakar, R. S. Ghadwal, H. W. Roesky, J. Hey, D. Stalke, *Organometallics* **2011**, *30*, 3853–3858.

[74] R. Azhakar, H. W. Roesky, J. J. Holstein, B. Dittrich, *Eur. J. Inorg. Chem.* **2013**, *2013*, 2777–2781.

[75] R. Azhakar, H. W. Roesky, R. S. Ghadwal, J. J. Holstein, B. Dittrich, *Dalton Trans.* **2012**, *41*, 9601–9603.

[76] S. Khan, S. S. Sen, R. Michel, D. Kratzert, H. W. Roesky, D. Stalke, *Organometallics* **2011**, *30*, 2643–2645.

[77] R. Azhakar, H. W. Roesky, H. Wolf, D. Stalke, *Z. Für Anorg. Allg. Chem.* **2013**, *639*, 934–938.

[78] S. S. Sen, H. W. Roesky, K. Meindl, D. Stern, J. Henn, A. C. Stückl, D. Stalke, *Chem. Commun.* **2010**, *46*, 5873–5875.

[79] S. S. Sen, J. Hey, D. Kratzert, H. W. Roesky, D. Stalke, *Organometallics* **2012**, *31*, 435–439.

[80] M. Driess, S. Yao, M. Brym, C. van Wüllen, D. Lentz, *J. Am. Chem. Soc.* **2006**, *128*, 9628–9629.

[81] S. Yao, C. van Wüllen, X.-Y. Sun, M. Driess, *Angew. Chem. Int. Ed.* **2008**, *47*, 3250–3253.

[82] B. Blom, M. Driess, in *Functional Molecular Silicon Compounds II* (Ed.: D. Scheschkewitz), Springer International Publishing, Cham, **2014**.

[83] C. Eisenhut, T. Szilvási, N. C. Breit, S. Inoue, *Chem. – Eur. J.* **2015**, *21*, 1949–1954.

[84] Y. Gao, J. Zhang, H. Hu, C. Cui, *Organometallics* **2010**, *29*, 3063–3065.

[85] S. Inoue, C. Eisenhut, *J. Am. Chem. Soc.* **2013**, *135*, 18315–18318.

[86] Y. Wang, J. Ma, *J. Organomet. Chem.* **2009**, *694*, 2567–2575.

[87] A. V. Protchenko, K. H. Birjkumar, D. Dange, A. D. Schwarz, D. Vidovic, C. Jones, N. Kaltsoyannis, P. Mountford, S. Aldridge, *J. Am. Chem. Soc.* **2012**, *134*, 6500–6503.

[88] B. D. Rekken, T. M. Brown, J. C. Fettinger, H. M. Tuononen, P. P. Power, *J. Am. Chem. Soc.* **2012**, *134*, 6504–6507.

[89] T. J. Hadlington, J. A. B. Abdalla, R. Tirfoin, S. Aldridge, C. Jones, *Chem. Commun.* **2016**, *52*, 1717–1720.

[90] A. V. Protchenko, A. D. Schwarz, M. P. Blake, C. Jones, N. Kaltsoyannis, P. Mountford, S. Aldridge, *Angew. Chem. Int. Ed.* **2013**, *52*, 568–571.

[91] B. D. Rekken, T. M. Brown, J. C. Fettinger, F. Lips, H. M. Tuononen, R. H. Herber, P. P. Power, *J. Am. Chem. Soc.* **2013**, *135*, 10134–10148.

[92] F. Lips, J. C. Fettinger, A. Mansikkamäki, H. M. Tuononen, P. P. Power, *J. Am. Chem. Soc.* **2014**, *136*, 634–637.

[93] A. V. Protchenko, J. I. Bates, L. M. A. Saleh, M. P. Blake, A. D. Schwarz, E. L. Kolychev, A. L. Thompson, C. Jones, P. Mountford, S. Aldridge, *J. Am. Chem. Soc.* **2016**, *138*, 4555–4564.

[94] D. Wendel, W. Eisenreich, C. Jandl, A. Pöthig, B. Rieger, *Organometallics* **2016**, *35*, 1–4.

[95] R. Rodriguez, D. Gau, T. Kato, N. Saffon-Merceron, A. De Cózar, F. P. Cossío, A. Baceiredo, *Angew. Chem. Int. Ed.* **2011**, *50*, 10414–10416.

[96] D. Gau, T. Kato, N. Saffon-Merceron, F. P. Cossío, A. Baceiredo, *J. Am. Chem. Soc.* **2009**, *131*, 8762–8763.

[97] Z. Benedek, T. Szilvási, *RSC Adv.* **2015**, *5*, 5077–5086.

[98] A. Brück, D. Gallego, W. Wang, E. Irran, M. Driess, J. F. Hartwig, *Angew. Chem. Int. Ed.* **2012**, *51*, 11478–11482.

[99] B. Blom, M. Stoelzel, M. Driess, *Chem. – Eur. J.* **2013**, *19*, 40–62.

[100] B. Blom, D. Gallego, M. Driess, *Inorg. Chem. Front.* **2014**, *1*, 134–148.

[101] D. Gallego, A. Brück, E. Irran, F. Meier, M. Kaupp, M. Driess, J. F. Hartwig, *J. Am. Chem. Soc.* **2013**, *135*, 15617–15626.

[102] W. Wang, S. Inoue, S. Enthaler, M. Driess, *Angew. Chem. Int. Ed.* **2012**, *51*, 6167–6171.

[103] M. Zhang, X. Liu, C. Shi, C. Ren, Y. Ding, H. W. Roesky, *Z. Für Anorg. Allg. Chem.* **2008**, *634*, 1755–1758.

[104] C. A. Kraus, H. Eatough, *J. Am. Chem. Soc.* **1933**, *55*, 5008–5014.

[105] C. A. Kraus, W. K. Nelson, *J. Am. Chem. Soc.* **1934**, *56*, 195–202.

[106] C. Präsang, D. Scheschkewitz, in *Functional Molecular Silicon Compounds II* (Ed.: D. Scheschkewitz), Springer International Publishing, **2013**, pp. 1–47.

[107] K. Tamao, A. Kawachi, in *Adv. Organomet. Chem.* (Ed.: F. Gordon, A. Stone, and R. West), Academic Press, **1995**, pp. 1–58.

[108] M. V. George, D. J. Peterson, H. Gilman, *J. Am. Chem. Soc.* **1960**, *82*, 403–406.

[109] H. Stueger, T. Mitterfellner, R. Fischer, C. Walkner, M. Patz, S. Wieber, *Chem. – Eur. J.* **2012**, *18*, 7662–7664.

[110] T. Iwamoto, J. Okita, C. Kabuto, M. Kira, *J. Am. Chem. Soc.* **2002**, *124*, 11604–11605.

[111] T. Iwamoto, J. Okita, C. Kabuto, M. Kira, *J. Organomet. Chem.* **2003**, *686*, 105–111.

[112] M. Kira, T. Kadowaki, D. Yin, K. Sakamoto, T. Iwamoto, C. Kabuto, *Organometallics* **2007**, *26*, 4890–4895.

[113] H. Gilman, J. M. Holmes, C. L. Smith, *Chem. Ind. Lond.* **1965**, 848.

[114] G. Gutekunst, A. G. Brook, *J. Organomet. Chem.* **1982**, *225*, 1–3.

[115] C. Marschner, *Eur. J. Inorg. Chem.* **1998**, *1998*, 221–226.

[116] T. D. Tilley, in *Chem. Org. Silicon Compd. Eds Patai Z Rappoport*, Wiley, Chichester, **1989**.

[117] T. D. Tilley, in *Silicon Heteroat. Bond Eds Patai Z Rappoport*, Wiley, Chichester, **1991**.

[118] F. Luderer, H. Reinke, H. Oehme, *J. Organomet. Chem.* **1996**, *510*, 181–188.

[119] C. Wendler, H. Oehme, *Z. Für Anorg. Allg. Chem.* **1996**, *622*, 801–806.

[120] F. Luderer, H. Reinke, H. Oehme, *Chem. Ber.* **1996**, *129*, 15–20.

[121] C. Krempner, H. Reinke, H. Oehme, *Chem. Ber.* **1995**, *128*, 1083–1088.

[122] C. Krempner, H. Reinke, H. Oehme, *Chem. Ber.* **1995**, *128*, 143–149.

[123] D. Bravo-Zhivotovskii, V. Braude, A. Stanger, M. Kapon, Y. Apeloig, *Organometallics* **1992**, *11*, 2326–2328.

[124] E. Jeschke, T. Gross, H. Reinke, H. Oehme, *Chem. Ber.* **1996**, *129*, 841–844.

[125] Y. Apeloig, I. Zharov, D. Bravo-Zhivotovskii, Y. Ovchinnikov, Y. Struchkov, *J. Organomet. Chem.* **1995**, *499*, 73–82.

[126] H. Oehme, R. Wustrack, A. Heine, G. M. Sheldrick, D. Stalke, *J. Organomet. Chem.* **1993**, *452*, 33–39.

[127] D. Bravo-Zhivotovskii, Y. Apeloig, Y. Ovchinnikov, V. Igonin, Y. T. Struchkov, *J. Organomet. Chem.* **1993**, *446*, 123–129.

[128] K. W. Klinkhammer, W. Schwarz, *Z. Für Anorg. Allg. Chem.* **1993**, *619*, 1777–1789.

[129] R. Fischer, T. Konopa, S. Ully, J. Baumgartner, C. Marschner, *J. Organomet. Chem.* **2003**, *685*, 79–92.

[130] M. Zirngast, J. Baumgartner, C. Marschner, *Organometallics* **2008**, *27*, 6472–6478.

[131] A. Wallner, J. Hlina, T. Konopa, H. Wagner, J. Baumgartner, C. Marschner, U. Flörke, *Organometallics* **2010**, *29*, 2660–2675.

Chapter 2

Intercepting the Disilene-Silylsilylene Equilibrium

Chapter 2 Intercepting the Disilene-Silylsilylene Equilibrium

Unless otherwise stated, all computations in this chapter were carried out by Julia I. Schweizer, Maximillian Menche and Max C. Holthausen at the Institut für Anorganische Chemie, Goethe-Universität, Max-von-Laue-Straße 7, 60438 Frankfurt/Main, Germany.

2.1 Introduction

Unlike ethene, Si_2H_4 has several accessible structural isomers.[1–8] The relative energy of the five major isomers have been determined computationally and are shown in Figure 2-1. Disilene **A** is the lowest energy isomer and is analogous to ethene with an Si=Si double bond. Silylsilylene **B** and monobridged isomer **C** are 6-8 kcal·mol^{-1} higher in energy than disilene **A** and are practically isoenergetic.[1–8] The dibridged isomers **D** and **E** are around 20 kcal·mol^{-1} higher in energy than disilene **A**. Isomers **A**, **B** and **D** were also observed experimentally in an argon matrix and could be interconverted upon irradiation with ultraviolet light.[9]

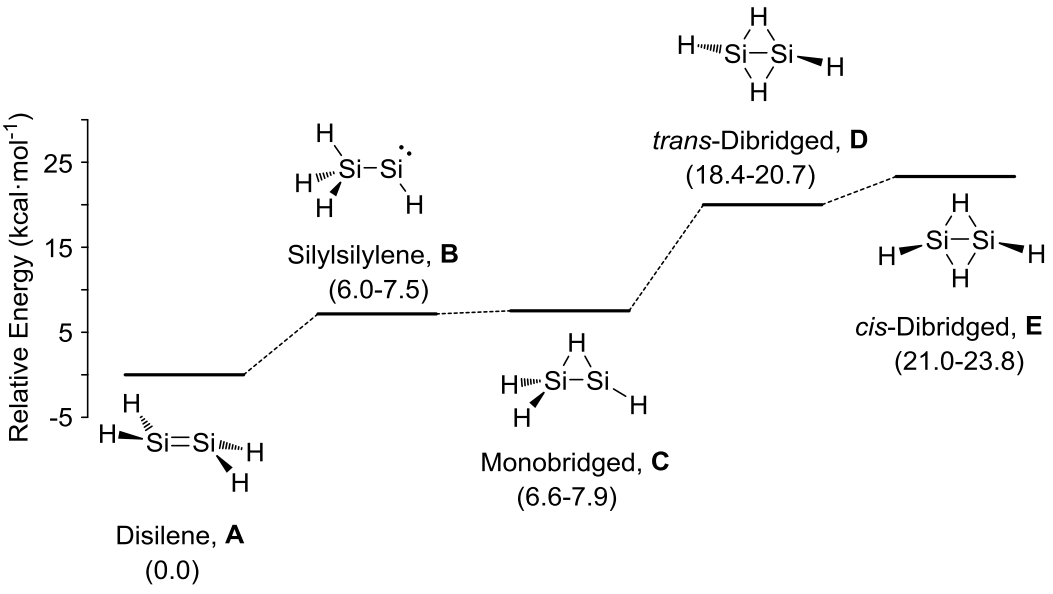

***Figure 2-1** – The potential energy surface of Si_2H_4. Relative energies are given in brackets as ranges and are taken from multiple references.[1–8]*

Si_2H_4 is important because it is a key intermediate in the chemical vapour deposition of polysilicon (Scheme 2-1).[10] Silylsilylene **B**, in particular, can form new Si-Si bonds through

insertion of the silylene into Si-H bonds.[11] There have been a number of theoretical studies on the disilene-silylsilylene isomerisation.[9–14] The isomerisation has also been inferred in the gas phase for the smallest organo disilene, Si_2Me_4,[15] and other transient disilenes.[16]

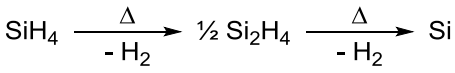

Scheme 2-1 *– Si_2H_4 is the key intermediate in the chemical vapour deposition of polysilicon from silane gas.*[10]

The disilene-silylsilylene isomerisation has been computed and observed under extreme conditions but there are limited examples reported for isolable compounds. Persistent disilenes with bulky substituents have been widely studied and are thoroughly introduced in Chapter 1 of this thesis. In contrast, silylsilylenes are far less common with only five examples reported to date, some of which are shown in Scheme 2-2.[17–20] Of the five reported examples, four are base-stabilised, for example by a bidentate amidinate ligand, in **2.1** (X = H or Cl),[19] or by an NHC in **2.2**.[18] The only reported base-free silylsilylene is **2.3** which is a rare example of a two-coordinate, acyclic silylene.[17] The reactivity of silylsilylene **2.3** offers an explanation for the lack of silylsilylenes reported to date. The strongly σ-donating and poorly π-accepting silyl group decreases the singlet triplet gap of **2.3** and increases its reactivity. Indeed, silylene **2.3** reacts with both dihydrogen and C-H bonds, as discussed in Chapter 1.

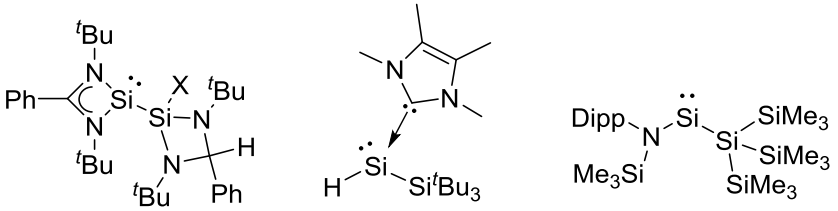

2.1
X = H, Cl

2.2

2.3

Scheme 2-2 *– Some reported examples of silylsilylenes.*[17–19]

Although rare, the disilene-silylsilylene isomerisation has also been inferred from the reactivity of some isolable compounds. For example, the reduction of dibromosilane **2.4** was expected to give silylene **2.5** (or the corresponding disilene dimer).[21] However, the isolated product was found to be disilene **2.6**. The formation of disilene **2.6** proceeds by the migration of a silyl group in a silylsilylene-disilene isomerisation, as shown in Scheme 2-3.

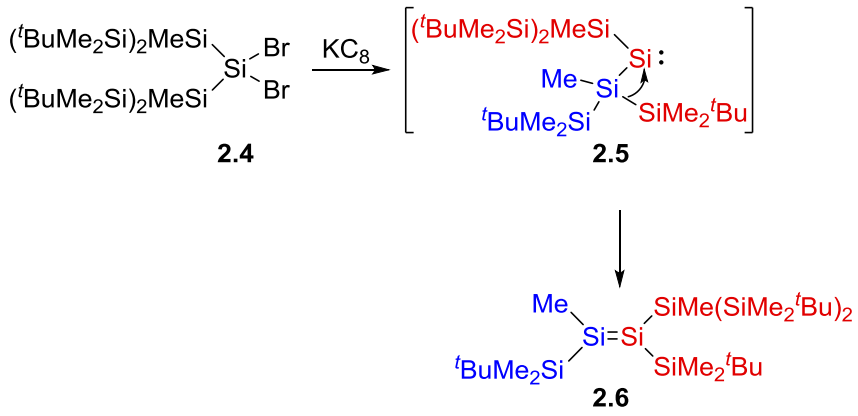

Scheme 2-3 *– The reaction of dibromosilane **2.4** forms intermediate silylsilylene **2.5** which rearranges to give methyl disilene **2.6** as the final product.*[21]

Other examples invoke the reverse reaction: isomerisation from disilene to silylsilylene. Usually the isomerisation can be inferred from intramolecular bond insertions that must proceed *via* a rearrangement.

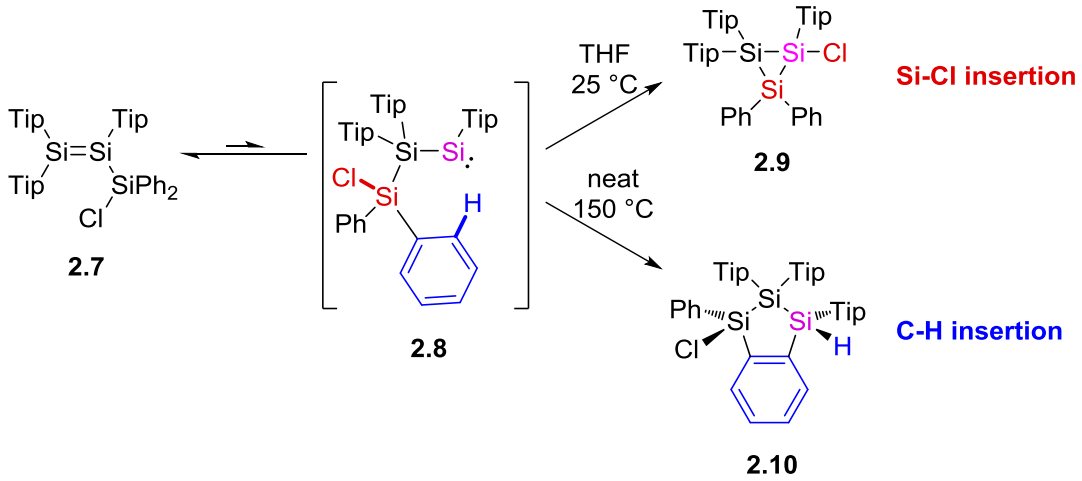

Scheme 2-4 *– Upon heating, **2.7** rearranges to products **2.9** or **2.10** depending on the conditions, presumably through silylsilylene **2.8** as an intermediate.*[22]

For example, when disilene **2.7** is left at room temperature in THF, the cyclotrisilane **2.9** is observed.[22] Similarly, if it is heated in the absence of solvent, trisilaindane **2.10** is the final product. Both of these products suggest silylsilylene **2.8** as a key intermediate, formed by a 1,2-silyl migration. The silylsilylene **2.8** is highly reactive and therefore rapidly undergoes Si-Cl or C-H insertion to give the final products **2.9** and **2.10**.

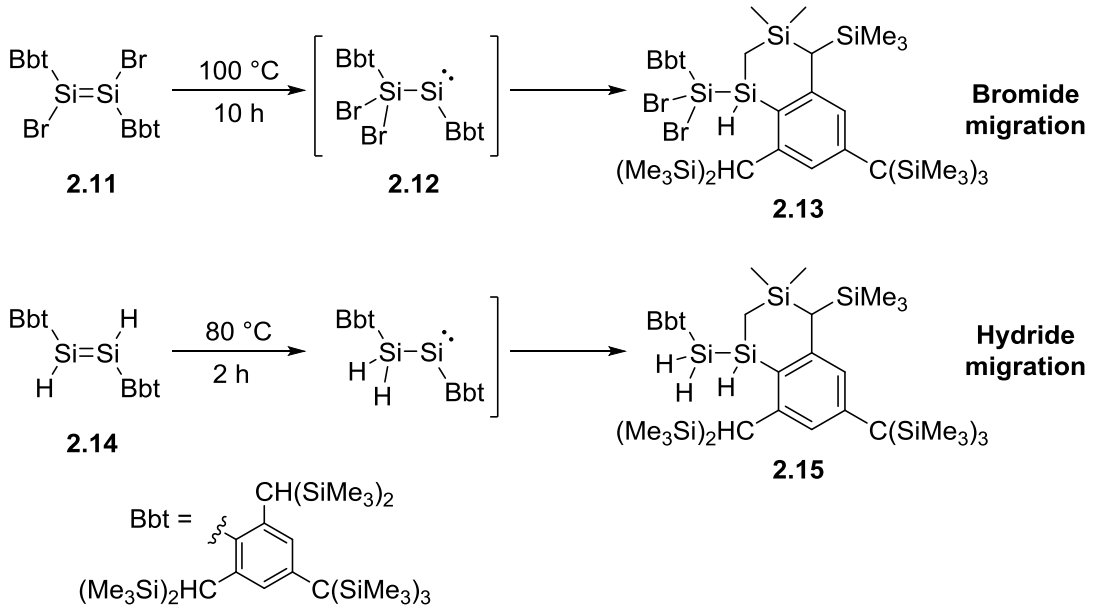

Scheme 2-5 *– Dibromo and dihydrido disilenes **2.11** and **2.14** undergo analogous rearrangements to give cyclic products **2.13** and **2.15**.*[23,24]

A similar route was proposed for the rearrangement of disilene **2.11** to cyclic silane **2.13**.[23] Again, a thermal reaction was proposed to yield a silylsilylene intermediate, **2.12**. The analogous reaction was also reported using dihydrodisilene **2.14** to give **2.15**.[24] In this instance the starting disilene **2.14** was difficult to isolate with **2.15** being the favoured product. The silylsilylene was found computationally to be 13.2 kcal·mol^{-1} higher in energy than the disilene, while the final product **2.15** was found to be favourable by −23 kcal·mol^{-1} relative to disilene **2.14**.

All four intramolecular insertion products, **2.9**, **2.10**, **2.13** and **2.15**, were formed as the major reaction products in greater than 65% yield. They each serve as evidence of the highly reactive nature of silylsilylenes.

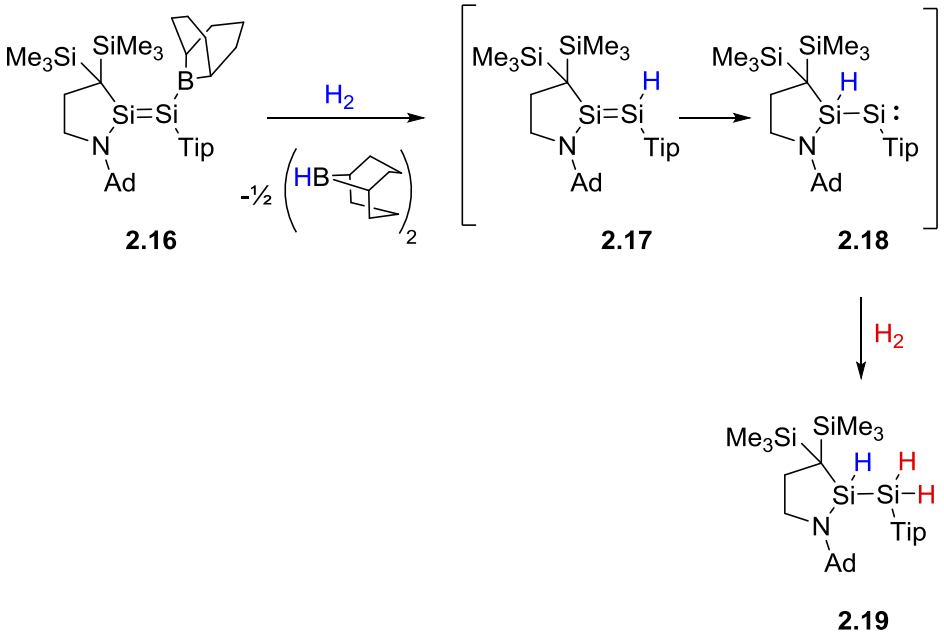

Scheme 2-6 *– Disilene* ***2.16*** *reacts with two molecules of H_2 to give disilane* ***2.19*** *as the final product. The mechanism of addition invokes a disilene-silylsilylene rearrangement.*[25,26]

Evidence for the disilene to silylsilylene isomerisation is also observed in intermolecular reactions. The highly reactive boryl disilene **2.16**, shown in Scheme 2-6, reacts with two equivalents of dihydrogen to give final product **2.19** and liberate 9-borabicyclo(3.3.1)nonane (9-BBN).[25,26] Calculations suggest that the first molecule of H_2 (blue) is cleaved by the B-Si bond to form hydridodisilene **2.17** as an intermediate and liberate 9-BBN. Disilene **2.17** rapidly isomerises to silylsilylene **2.18** with barrier of only 12.7 kcal·mol^{-1}. The final product is formed by insertion of the silylene into a second molecule of H_2 (red).

An additional, highly relevant example is the unexpected reaction of disilyne **2.20** with 4-dimethylaminopyridine (DMAP), shown in Scheme 2-7.[27] The disilyne performs a C-H insertion reaction into the *ortho* C-H bond of DMAP to give unstable silylsilylene **2.21**. Silylsilylene **2.21** is unstable at ambient temperatures and rearranges over time to afford disilene **2.22**. This is the only reported example where both the disilene and silylsilylene isomers are isolable, albeit in low yields.

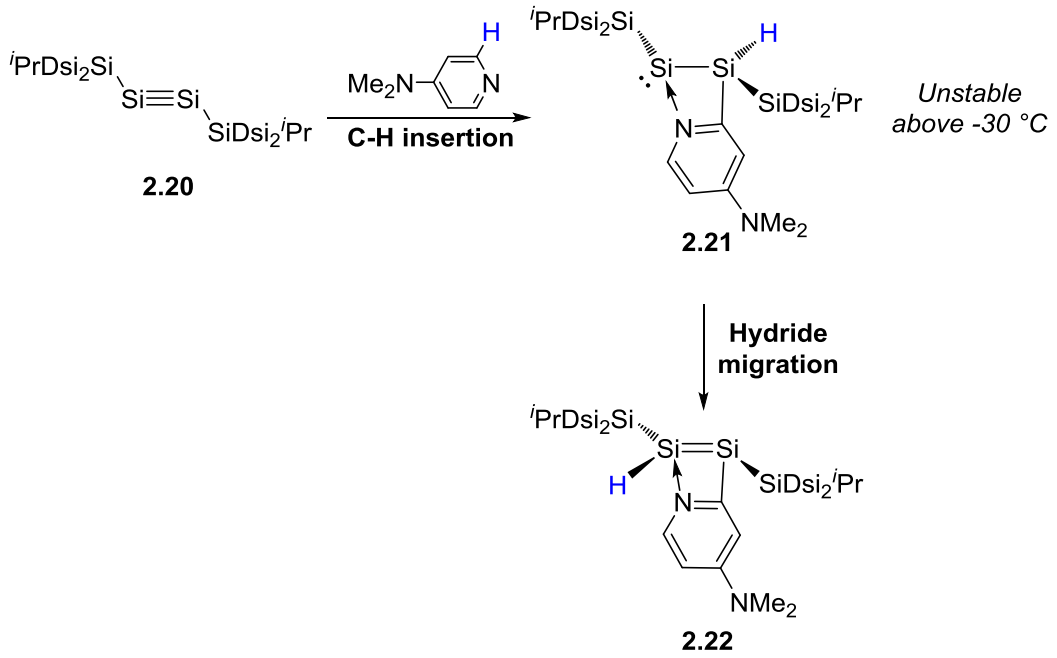

Scheme 2-7 *– The unusual reactivity of disilyne* ***2.20*** *with DMAP to initially give silylsilylene* ***2.21*** *which rapidly rearranges to disilene* ***2.22****.*[27]

Other reactions related to the disilene-silylsilylene isomerisation have also been reported including the ring opening of a cyclic trisilene,[28,29] the rearrangement of a homocylic silylene,[30] silylene insertion into a P-C bond,[31] and the formation of a molecular model for a silicon surface.[32]

Each of the examples reported thus far serves as strong evidence of the equilibrium and these are well supported by theoretical investigations. The rearrangement of **2.20** to **2.22**, in particular, is the only example where both disilene and silylsilylene have been isolated. However, there has been no reports of both disilene and silylsilylene observed under the same conditions and no control of the isomerisation has been reported.

2.2 Aims and Objectives

The aim of this project is to observe and control the disilene-silylsilylene isomerisation in isolable compounds.

Disilenes will be prepared with hydride and small silyl substituents which may be able to perform a 1,2-migration. They will be prepared by extracting trimethylsilyl and chloride substituents using a strong base, a method previously reported for the synthesis of other

main group double bonds.[33–36] Disilenes with small substituents are expected to be highly reactive, therefore a base coordination strategy will be employed in order to intercept transient species for characterisation.

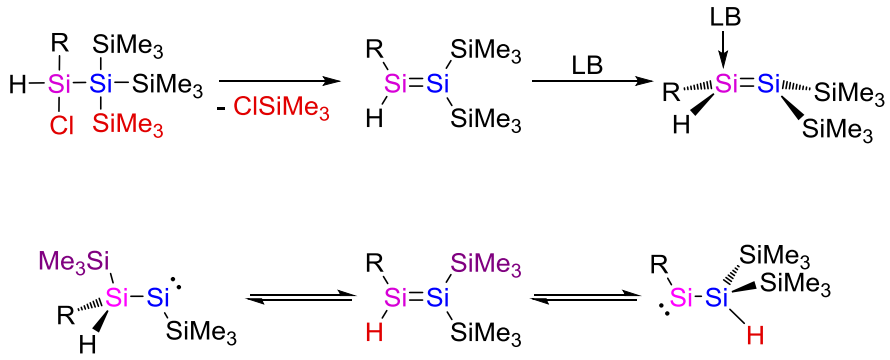

2.3 Synthesis of Disilene 2.28

2.3.1 Preparation of the Silane Starting Material 2.23

In order to achieve formal elimination of trimethylsilyl chloride across a silicon-silicon bond, silicon(IV) compounds were prepared bearing hypersilyl and chloro substituents.

The pentamethylcyclopentadienyl (Cp*) group was initially chosen as a suitable group to provide some steric protection. Additionally, the Cp* group is able to act as a π-donor and therefore provide an element of electronic stabilisation to Si(II).[37–40]

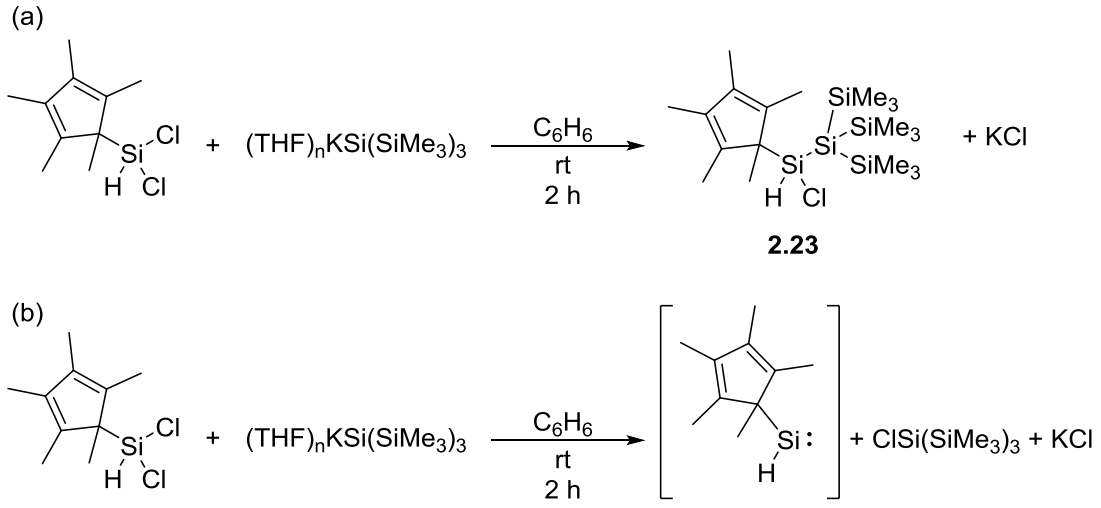

Scheme 2-8 *– (a) Synthesis of silane* ***2.23****. (b) Potential formation of silylene to explain the red colour observed during the synthesis of* ***2.23****.*

Silane **2.23** was prepared in 62% yield by the reaction of (pentamethylcyclopentadienyl)dicholorosilane (Cp^*SiHCl_2)[41] with hypersilyl anion $(THF)_nKSi(SiMe_3)_3$[42] in benzene at room temperature. During the reaction, an orange/red colour is observed, however the product crystallises as large, colourless blocks. This could suggest some amount of reduction to the corresponding silylene, as the silyl anion is a known reducing agent,[17,43] although no evidence for this was observed by ^1H or ^{29}Si NMR spectroscopy.

The ^1H NMR spectrum of **2.23** shows a broad singlet resonance for the Cp* methyl protons at δ 1.79. This is consistent with the Cp* group underdoing a haptotropic shift on the NMR timescale, slowed down by the large steric bulk of the hypersilyl group. The signal corresponding to Si-*H* is observed at δ 5.43 with a $^1J_{H\text{-}Si}$ coupling constant of 200 Hz.

The ^{29}Si NMR spectrum shows three resonances at δ 20.2, −8.8 and –126.1, corresponding to the *Si*-H, $Si(\underline{Si}Me_3)_3$ and $\underline{Si}(SiMe_3)_3$, respectively. The upfield signal is typical for a quaternary silane due to the σ-donating effects of four silicon substituents (e.g. δ −135 for $Si(SiMe_3)_4$).

Colourless, block-shaped crystals of **2.23** suitable for X-ray diffraction were readily grown from hexane at room temperature. The solid-state structure of **2.23** is shown in Figure 2-2. All Si-Si bond lengths and angles are in the expected range for four single Si-Si bonds. The Cp* group is bound η^1 through C1. The C-C bond lengths indicate the presence of two double bonds and three single bonds: C1-C2 1.527(16), C2-C3 1.323(18), C3-C4 1.466(17), C4-C5 1.352(17) and C5-C1 1.486(17).

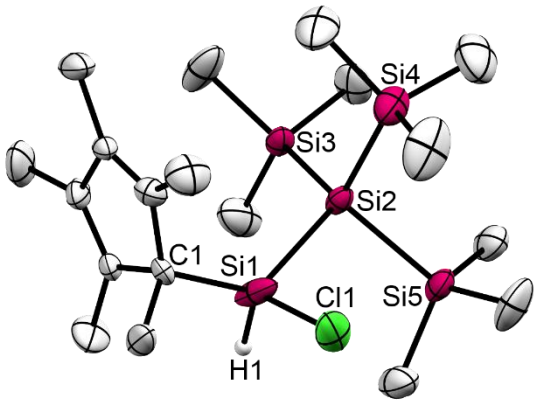

***Figure 2-2** – Solid-state structure of **2.23**. Disorder, second independent molecule, and hydrogen atoms, with the exception of H1, omitted for clarity. Thermal ellipsoids set to 50% probability. Selected bond lengths (Å) and angles (°): Cl1-Si1 2.272(5), Si1-Si2 2.331(3), Si1-C1 1.82(2).*

2.3.2 Trimethylsilyl Chloride Elimination by NHCs and KO^{t}Bu

2.3.2.1 ^{Me}IMe

The reaction of **2.23** with the small NHC 1,3,4,5-tetraimethylimidazol-2-ylidene (^{Me}IMe) in C_6D_6 or THF led to a bright orange solution with only 50% consumption of the starting material (Scheme 2-9). The reaction with two equivalents led to complete consumption of **2.23** and formation of base-stabilised disilene **2.24** along with the by-product NHC·$SiMe_3Cl$ adduct, as shown in Scheme 2-9. The ^{29}Si NMR spectrum of disilene **2.24** showed new resonances at δ −5.3, −10.3 and −216.5, the latter of which is indicative of a silyl anion.[42,44,45] The ^{1}H NMR showed downfield shifted and desymmetrised resonances corresponding to coordinated ^{Me}IMe (δ 3.93, 3.70, 2.21 and 2.15) and the loss of one $SiMe_3$ group, determined by integration. The presence of an Si-H functionality was confirmed by a ^{1}H resonance at δ 5.54 with a $^1J_{HSi}$ coupling of 166 Hz to the ^{29}Si resonance at δ −10.3, revealed by ^{1}H-^{29}Si HMQC and ^{1}H-^{29}Si HMBC correlation spectroscopy.

The disilene ^{29}Si resonances in **2.24** at δ −10.3 and δ −216.5 are significantly more shielded than the vast majority of disilenes, even other base-stabilised disilenes and amino disilenes, both of which show increased localised charges on one silicon centre (see Chapter 1).[28,46–49]

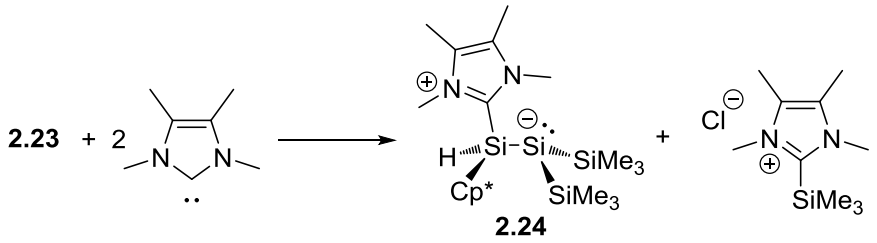

***Scheme 2-9** – The reaction of **2.23** with two equivalents of ^{Me}IMe to give proposed product **2.24**.*

It is known that NHCs are able to promote reduction elimination of $SiMe_3Cl$ to give multiply bonded main group species.[33–36] Equally, the π* orbital of silicon-silicon multiple bonds is Lewis acidic and is able to accept electrons from a suitable base, including NHCs, as discussed in Chapter 1.[28,50,51] Together, this evidence supports formation of base-stabilised disilene **2.24** by elimination of $SiMe_3Cl$ across the silicon-silicon bond. However, it proved impossible to separate **2.24** from the reaction by-product, ^{Me}IMe·$SiMe_3Cl$.

2.3.2.2 Larger NHCs

No reaction was observed between **2.23** and the larger NHCs 1,3-bis(2,6-di*iso*propylphenyl)-4,5-dimethylimidazol-2-ylidene (IDipp) and 1,3-di*iso*propyl-4,5-dimethylimidazol-2-ylidene ($^{Me}I^{i}Pr$). This is consistent with results concerning phosphorus-boron systems in which larger NHCs react considerably slower.[33] In fact, in the case of IDipp the intermediate borylphosphide anion **2.26** was found to be isolable due to the slow rate of reaction.

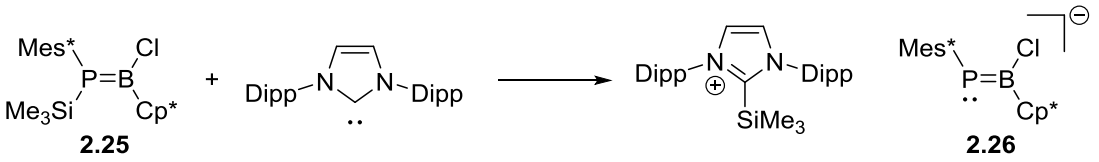

***Scheme 2-10** – The reaction of phosphino borane **2.25** with IDipp. Dipp = 2,6-diisopropylphenyl.[33]*

2.3.2.3 KO^{t}Bu

Potassium *tert*butoxide (KO^{t}Bu) is a known reagent for extracting trimethylsilyl groups from polysilanes in the form of the volatile silyl ether $Me_3SiO^{t}Bu$.[44] This method is usually used to synthesise silyl anions, for example the synthesis of the hypersilyl anion $(THF)_nKSi(SiMe_3)_3$.[42] It was anticipated that the extraction of one trimethylsilyl group from **2.23** would lead to an anion which could eliminate chloride across the Si-Si bond to afford **2.27** with a new Si=Si double bond, as shown in Scheme 2-11.

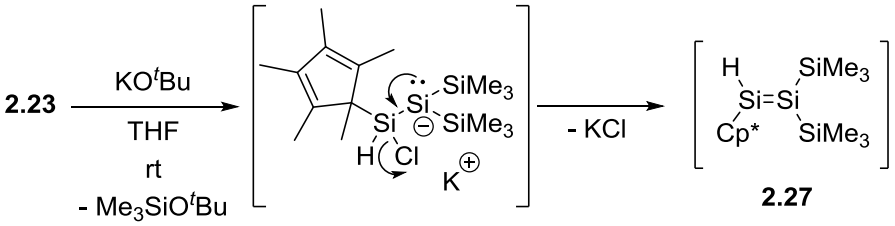

*Scheme 2-11 – Extraction of $SiMe_3Cl$ from 2.23 to give proposed disilene **2.27**.*

Indeed, the reaction of **2.23** with KO^{t}Bu in THF-d_8 gives the silyl ether $Me_3SiO^{t}Bu$, as evidenced by the characteristic ^{1}H NMR signals at δ 0.12 for the $SiMe_3$ protons and δ 1.27 for the ^{t}Bu protons. The reaction mixture turns deep red, however ^{1}H and ^{29}Si NMR spectroscopy reveal a complex mixture of products with no clear evidence for formation of **2.27**. Furthermore, the mixture rapidly turns colourless above 5 °C. This is unsurprising as the expected product, **2.27**, lacks the stabilisation from bulky substituents that are usually

required to isolate disilenes. The steric stabilisation is required to prevent the formation of dimers and oligomers of small low-valent silicon compounds, both of which could be present in solution alongside **2.27**. Equally, the hydride and trimethylsilyl substituents can easily undergo migration to afford the silylsilylene isomer, or even bridged species such as those proposed for the parent compound.[1,9,12–15] Figure 2-3 shows some of the potential species, however no spectroscopic evidence is observed for any particular compound.

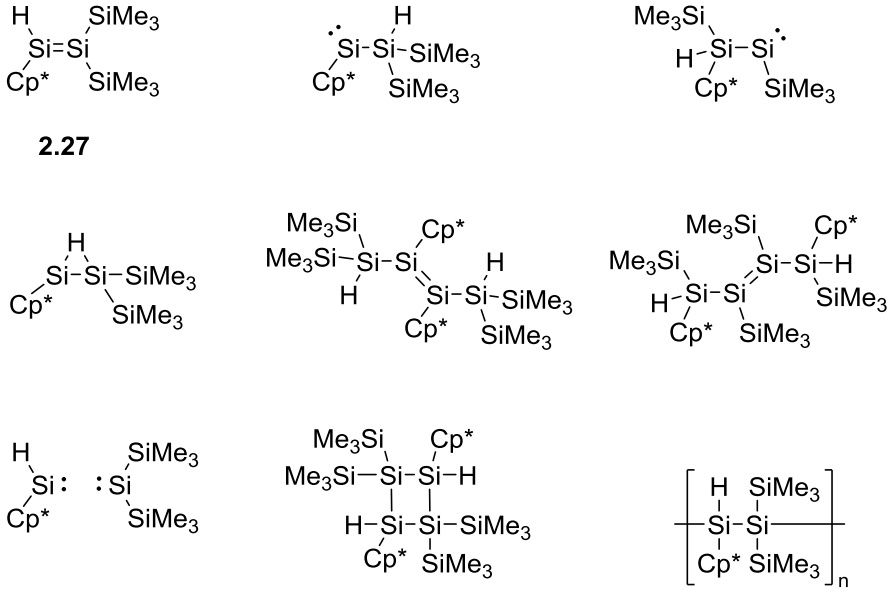

2.27

Figure 2-3 *– A selection of potential species in equilibrium with* ***2.27****. Left to right, top to bottom:* ***2.27****, hydride migration, silyl group migration, monobdridged isomer, hydride migration followed by dimerisation, silyl group migration followed by dimerisation, Wanzlick equilibrium, disilene dimerasation, disilene oligomerisation/polymerisation. Cp* = pentamethylcyclopentadienyl.*

2.3.2.4 KO^{t}Bu + ^{Me}I^{i}Pr

As stated in section 2.3.2.2, no reaction is observed between **2.23** and ^{Me}I^{i}Pr in the absence of KO^{t}Bu. However, given the proposed base-stabilised disilene **2.24**, the reaction of **2.23** with KO^{t}Bu was performed in the presence of ^{Me}I^{i}Pr. The ^{1}H NMR showed the formation of the silyl ether Me$_3$SiO^{t}Bu with clear formation of a new product which is spectroscopically similar to **2.24** and is therefore identified as disilene **2.28**.

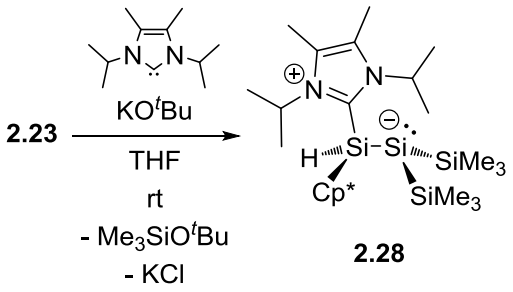

***Scheme 2-12** – The reaction of **2.23** with KO^{t}Bu and ^{Me}I^{i}Pr to give base-coordinated disilene **2.28**. Cp* = pentamethylcyclopentadienyl.*

The ^{1}H NMR spectrum of **2.28** shows two septet signals at δ 5.83 and 5.06 which are indicative of coordinated ^{Me}I^{i}Pr.[52–54] Coordination was further confirmed by the ^{13}C carbene resonance at δ 156.1. Loss of one $SiMe_3$ group was confirmed by integration of the ^{1}H NMR spectrum. Signals in the ^{29}Si NMR spectrum at δ –5.1, −13.0 and −202.2 are assigned to the two $\underline{Si}Me_3$ groups, the hydride-substituted silicon and the three-coordinate $\underline{Si}(SiMe_3)_2$ centre, respectively. The assignment of the $\underline{Si}$-H was confirmed by ^{1}H-^{29}Si correlation spectroscopy which showed clear coupling to the Si-$\underline{H}$ signal in the ^{1}H NMR at δ 5.71 ($^1J_{HSi}$ = 165 Hz). Together, the NMR data support the formation of **2.28** as the product, a base-coordinated disilene. Disilene **2.28** was isolated as a bright orange powder in 53% yield.

Bright orange single crystals of **2.28** were grown from diethyl ether. Single crystal X-ray diffraction revealed the solid-state structure shown in Figure 2-4. A single crystal was also grown from benzene at ambient temperature which showed a structure almost identical to that given in Figure 2-4.

The Si1-Si2 bond distance of 2.3575(8) Å indicates the presence of a single bond and is comparable to the other Si-Si bond distances in **2.28** (2.3569(9) Å and 2.3611(8) Å) and **2.23**. Furthermore, Si2 is significantly pyramidalised (Σ∢ = 296.15(5)°) which signifies the presence of a stereoactive lone pair at Si2. This is in agreement with the high field ^{29}Si resonance for Si2 at δ −202.2, which suggests anionic character[42,44,45] (although, in some instances, silyl anions can show significantly less shielded resonances[55]). The NHC C1-Si1 bond distance, 1.945(2) Å, is typical of NHC-silicon bonds.[20,29,56–60]

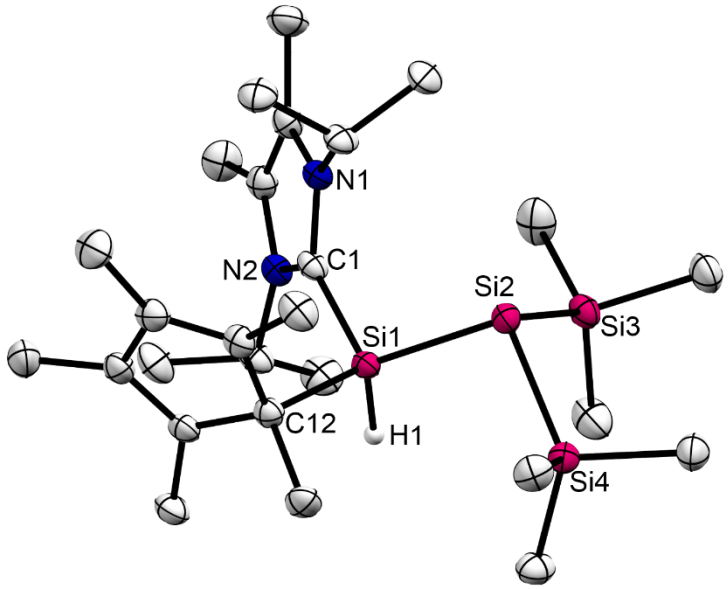

Figure 2-4 *– Solid-state structure of* ***2.28****. Hydrogen atoms, with the exception of H1, omitted for clarity. Thermal ellipsoids set to 50% probability. Selected bond lengths (Å) and angles (°):Si1-Si2 2.3575(8), Si1-C1 1.945(2), Si1-C12, 1.947(2), Si2-Si3 2.3569(9), Si2-Si4 2.3611(8); Si1-Si2-Si4 94.97(3), Si3-Si2-Si1 101.61(3), Si3-Si2-Si4 99.57(3).*

Combined, this data suggests that **2.28** can be represented as the zwitterion **2.28a** (Scheme 2-13), where Si2 carries a negative charge and the countering positive charge is carried by the two NHC nitrogen atoms. This is further supported by the short C-N bonds distances of 1.360(3) and 1.361(3) Å, although they are still lengthened with respect to uncoordinated NHC.[61]

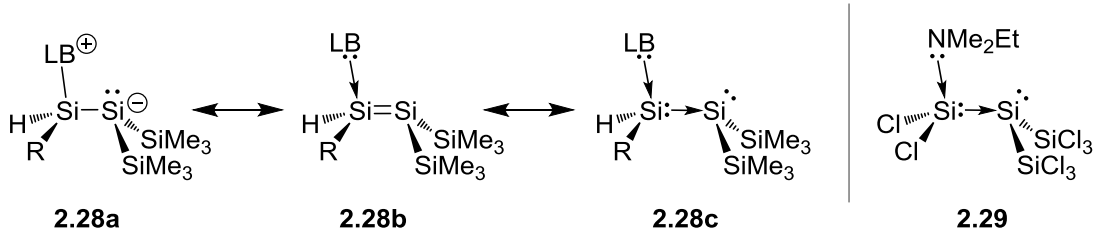

2.28a **2.28b** **2.28c** **2.29**

Scheme 2-13 *– Left: The three resonance forms of* ***2.28****,* ***a*** *a zwitterion,* ***b*** *a base-coordinate disilene,* ***c*** *a disilene with a dative Si-Si bond. LB =* ^{Me}*I*^{i}*Pr, R = Cp*. Right: A disilene with a dative Si-Si bond reported by Holthausen and co-workers.*[49]

In order to further investigate the bonding nature of **2.28**, density functional theory calculations were performed by Prof. Dr Max Holthausen and co-workers. Geometry optimisations were performed at the RI-M06-L/6-31+G(d,p) level and improved energies and

wave functions were obtained from M06-2X/6-311++G(2d,2p) single point calculations (with SMD model with THF as solvent for energies). The computed structural metrics were in good agreement with the experimental X-ray structure (≤ 2.2% different in bond distances, see experimental methods section 5.6).

A natural bond orbital (NBO) analysis shows a natural localised molecular orbital (NLMO) with s-character as a lone pair at Si2. The Si1-Si2 bond is represented by a NLMO 2c-2e single bond which is polarised towards Si1 (55%). The Wiberg Bond Index (WBI) 1.04 is in agreement with the experimental structure which shows a bond length typical for Si-Si single bonds.

The C1-Si1 bond is also represented by a polarised single 2e-2c bond ([76%]C1-Si1[22%]). This is similar to but less polarised than the N-Si bond in *per*-chlorinated disilene **2.29** ([86%]N1-Si1[12%]).[49]

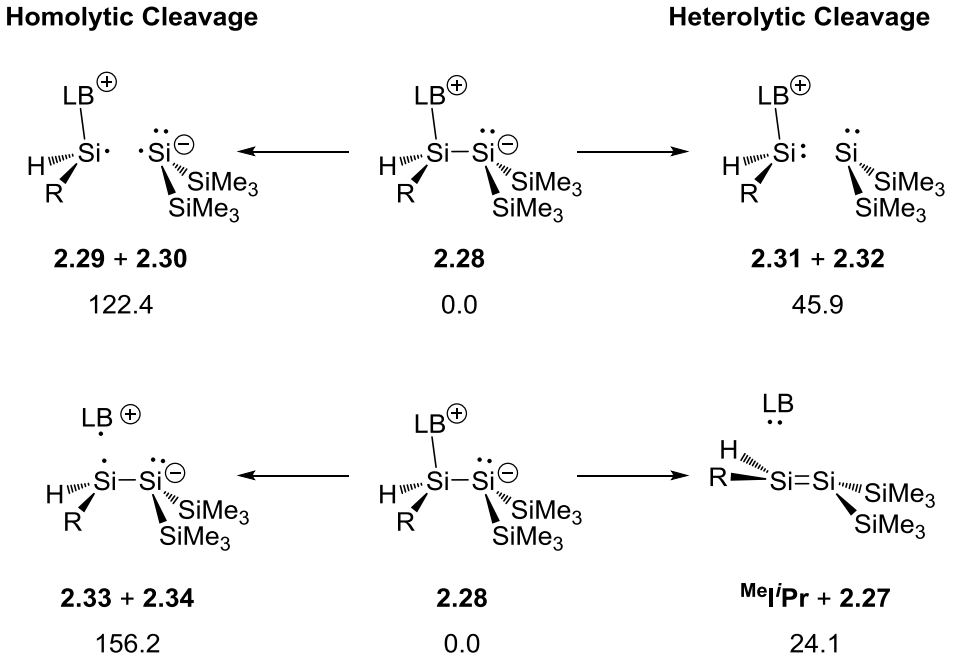

Scheme 2-14 *– Computed homolysis and heterolysis of bonds in* ***2.28.*** *ΔG^{298} in kcal mol^{-1} (M06-2X/6-311++G(2d,2p)//RI-M06-L/6-31+G(d,p)). LB = ^{Me}I^{i}Pr, R = Cp*.*

Haaland's definition of dative bonds states that if a bond is dative the minimum-energy rupture will proceed heterolytically, while if a bond is a normal covalent bond, the minimum-energy rupture will proceed homolytically.[62] Therefore, if the cleavage of the Si1-Si2 bond of **2.28** to give fragments **2.29** and **2.30** (homolytic) is preferred to **2.31** and **2.32** (heterolytic),

then the interaction is a normal covalent bond. If not, the interaction is better described as dative. The same description applies to the C1-Si1 interaction. It transpires that heterolytic cleavage is preferred in both instances, by 76.5 kcal mol^{-1} for Si1-Si2, and by 132.1 kcal mol^{-1} for C1-Si1 (Figure 2-13). Further computations support this definition but are outside the scope of this thesis.[63]

2.4 Reaction of a Terphenyl Silane with KO^{t}Bu

2.4.1 Preparation of the Silane Starting Material 2.35

The terphenyl substituent has been used extensively to stabilise low-valent main group compounds including a range of low-valent silicon species.[56,64–68] It is substantially more bulky than Cp*. Terphenyl chloro silane **2.35** can be readily synthesised from previously reported terphenyldichlorosilane (Ar*$SiHCl_2$),[69] as shown in Scheme 2-15. Crystallisation of the reaction mixture from hot diethyl ether afforded colourless crystals of pure silane **2.35** in 64% yield.

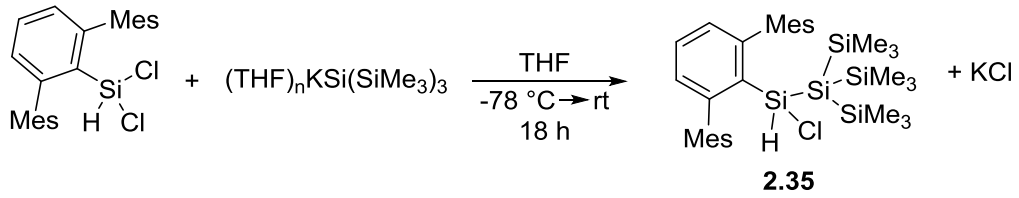

2.35

Scheme 2-15 *– Synthesis of silane* ***2.35****. Mes = 2,4,6-trimethylphenyl.*

The ^{1}H NMR spectrum of **2.35** shows an Si-*H* resonance at δ 5.39 ppm with $^1J_{HSi}$ and $^2J_{HSi}$ coupling constants of 215 and 13 Hz, respectively. The ^{29}Si NMR shows three singlet resonances at δ –7.53, −8.72, and –117.6 corresponding to *Si*-H, Si(*Si*$Me_3)_3$) and *Si*$(SiMe_3)_3$, respectively. The solid state structure of **2.35** is shown in Figure 2-5. All Si-Si bond lengths and angles are in the expected range for Si-Si single bonds.

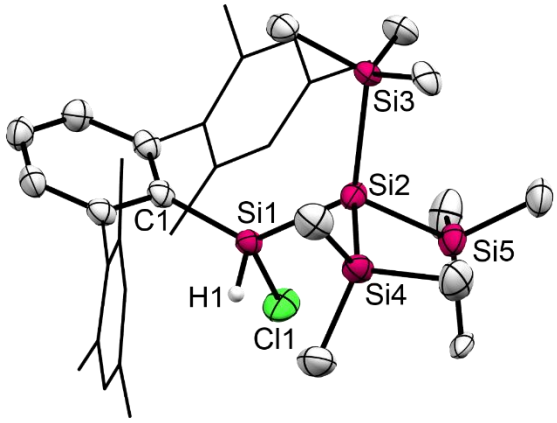

***Figure 2-5** – Solid-state structure of **2.35**. Disorder and hydrogen atoms, with the exception of H1, omitted for clarity. Thermal ellipsoids set to 50% probability. Selected bond lengths (Å) and angles (°): Cl1-Si1 2.080(3), Si1-Si2 2.327(3), Si1-C1 1.897(4).*

2.4.2 Reductive $SiMe_3Cl$ Elimination from 2.35

The reaction of **2.35** with KO^{t}Bu at 5 °C gave a deep red colour which disappeared upon warming to ambient temperature. Assuming a similar reaction to that of **2.23** with KO^{t}Bu there will be a number of species in solution alongside the expected disilene (see Figure 2-3).

The reaction of **2.23** with KO^{t}Bu was monitored at low temperature. No reaction was observed below −10 °C. Above −10 °C slow consumption of **2.23** and KO^{t}Bu was observed with concurrent formation of the silyl ether Me_3SiO^tBu. However, no significant new ^{29}Si or ^{1}H signals were observed by NMR spectroscopy. This suggests that the formation of any new species is significantly slower than their decomposition.

Interestingly, the reaction of **2.35** with KO^{t}Bu in the presence of $^{Me}I^iPr$ showed clean formation of two distinct products plus the silyl ether Me_3SiO^tBu. This is in contrast to the identical reaction with **2.23** which showed only one product, disilene **2.28**.

The ^{1}H NMR spectrum shows two new Si-*H* resonances at δ 5.49 ($^1J_{H\text{-}Si}$ = 178 Hz) and 3.91 ($^1J_{H\text{-}Si}$ = 155 Hz) in a ratio of approximately 1:1. The signal at δ 5.49 is similar in chemical shift to that observed for disilene **2.28** (δ 5.71). Furthermore, ^{1}H-^{29}Si correlation experiments revealed associated ^{29}Si signals at δ –4.8, −37.1 and −188.0, assigned to two *Si*Me$_3$ groups, *Si*-H and *Si*(SiMe$_3$)$_2$ centres, respectively, by ^{1}H-^{29}Si correlation spectroscopy. On the basis of

similarity with the spectrum of disilene adduct **2.28**, this species is identified as the NHC coordinated disilene **2.36**.

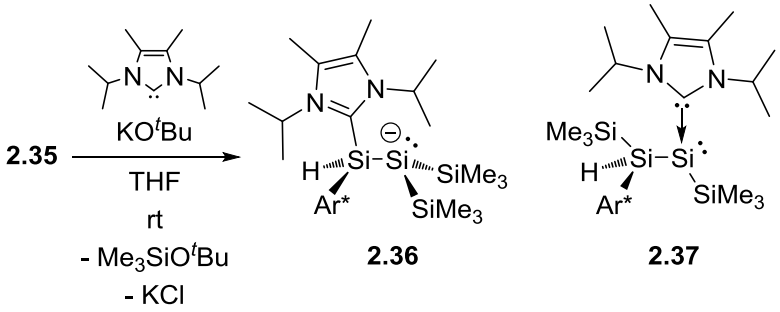

***Scheme 2-16** – The reaction of **2.35** with KO^{t}Bu in the presence of ^{Me}I^{i}Pr to give a roughly 1:1 mixture of disilene **2.36** and silylsilylene **2.37**. Ar* = 2,6-(2,4,6-trimethylphenyl)phenyl.*

The other product of the reaction shows an Si-*H* resonance at δ 3.91 with a $^1J_{HSi}$ coupling constant of 155 Hz, typical of four coordinate silanes (e.g., $^1J_{HSi}$ in $HSi(SiMe_3)_3$ = 156 Hz). Correlation spectroscopy revealed an associated *Si*-H resonance at δ −69.8. Interestingly, the product shows two distinct environments typical of $SiMe_3$ groups in the ^{1}H, ^{13}C and ^{29}Si NMR spectra. A further ^{29}Si NMR resonance at δ −121.4 corresponds to a silylsilylene centre. Crystallisation from pentane afford red single crystals which were identified as silylsilylene **2.37** by single crystal X-ray diffraction, in good agreement with the NMR data.

The ^{29}Si NMR resonance of silylsilylene **2.37** at δ −121.4 is comparable to that for the only other NHC coordinated silylsilylene, reported by Inoue and Eisenhut, **2.2**, found at δ −137.8 (Scheme 2-17).[18]

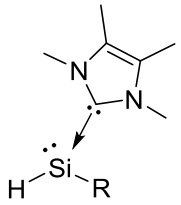

	δ(^{29}Si)	
R = Si^{t}Bu$_3$	-137.8	**2.2**
R = Ter	-87.6	**2.38**

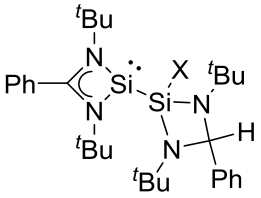

2.1

	δ(^{29}Si)
X = H	45.6
X = Cl	26.8

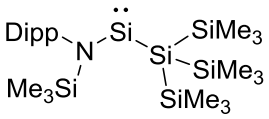

2.3

δ(^{29}Si)

498.5, 452.3
(two isomers)

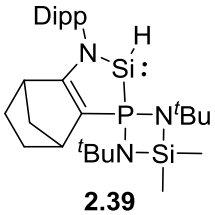

2.39

δ(^{29}Si)

-38.0, -44.8
(two isomers)

Scheme 2-17 *– NHC coordinated silyl- and hydridosilylenes* ***2.2****[18] and* ***2.38****,[56] three coordinate silylsilylenes* ***2.1****,[19] two coordinate silylsilylene* ***2.3****,[17] and hydrido silylene* ***2.39****.[70] Ter = 2,6-bis(2,4,6-trimethylphenyl)phenyl,, Dipp = 2,6-diisopropylphenyl.*

The ^{29}Si NMR resonances for **2.37** and **2.2** are found at higher field compared with most other three-coordinate silylenes and with other silylsilylenes.[18,19,56,71–73] In fact, three-coordinate amidinato silylsilylenes (**2.1**) show ^{29}Si resonances for the low-valent centre at δ 26.8 and 45.6.[19] Two coordinate silylsilylene **2.3** shows highly deshielded resonances at δ 498.5 and 452.3 for two different isomers.[17] However, three-coordinated hydridosilylenes **2.38** and **2.39** do have shielded resonances at δ −87.6 for **2.38**[56] and δ −38.0 and −44.8 for two isomers of **2.39**,[70] somewhat more similar to **2.37** and **2.2**.

Stirring the reaction mixture of **2.36** and **2.37** for 3 weeks at room temperature, or 3 hours at 55 °C, leads to complete consumption of disilene **2.36** leaving silylsilylene **2.37** as the sole observable product. Silylsilylene **2.37** is isolable in 41% yield by extraction with pentane.

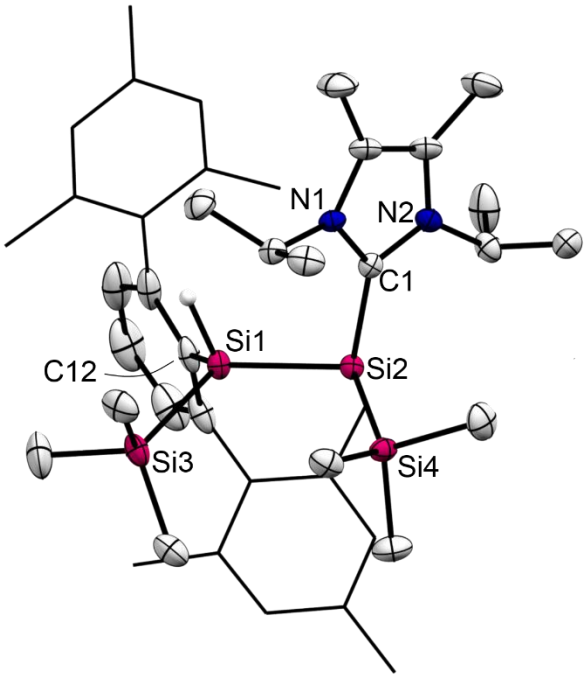

***Figure 2-6** – Solid-state structure of **2.37**. Hydrogen atoms, with the exception of H1, omitted for clarity. Thermal ellipsoids set to 50% probability. Selected bond lengths (Å) and angles (°): Si2-Si1 2.3674(9), Si2-Si3 2.3421(8), Si2-C1 1.960(2), Si1-Si4 2.3639(8), C1-N1 1.373(3), C1-N2 1.366(3), Si3-Si2-Si1 111.37(3), C1-Si2-Si1 102.35(7), C1-Si2-Si3 103.54(6).*

The solid-state structure of silylsilylene **2.37** is shown in Figure 2-6. The Si1-Si2 bond distance of 2.3674(9) Å is in the expected range for a Si-Si single bond. The C1-Si2 bond distance of 1.960(2) Å is marginally longer than the NHC C-Si bond in disilene adduct **2.28** (1.945(2) Å). Coupled with the less shielded resonance in the ^{13}C NMR for the carbene carbon (δ 172.2 for **2.37** versus δ 156.1 for **2.28**), this indicates slightly more dative character in the interaction between the NHC and the silicon containing fragment.

The bond angles at Si2 support the presence of a stereoactive lone pair with the sum of angles being 317.26(10)°. Furthermore, the NHC C-N bond distances are slightly longer than in disilene adduct **2.28** at 1.373(3) and 1.366(3) Å, compared with 1.360(3) and 1.361(3) Å for **2.28**. They are also longer than uncoordinated NHC at 1.356(2) Å.[61] This indicates stronger π back donation from the silicon centre in silylsilylene **2.37** which is consistent with the presence of a lone pair at Si2.

The presence and location of H1 in **2.37** was unambiguously confirmed by X-ray crystallography and NMR spectroscopy. Crystallographically, the silicon hydride was

identified from a Fourier map and freely refined. In the solution phase, a ^{1}H-^{29}Si HMQC correlation experiment showed ^{1}J coupling between the ^{1}H resonance at δ 3.91 and the ^{29}Si resonance at δ −69.8 (Figure 2-7a). A ^{1}H-^{29}Si HMBC experiment showed a cross peak between the two resonances with ^{1}J coupling of 155 Hz, confirming the single-bond correlation. The ^{1}H-^{29}Si HMBC also showed long range coupling between the silicon resonance at δ −69.8 and the aromatic C-*H* signals of the terphenyl ligand (Figure 2-7b). Together this confirms that the terphenyl ligand is bound to the same silicon as the hydride substituent.

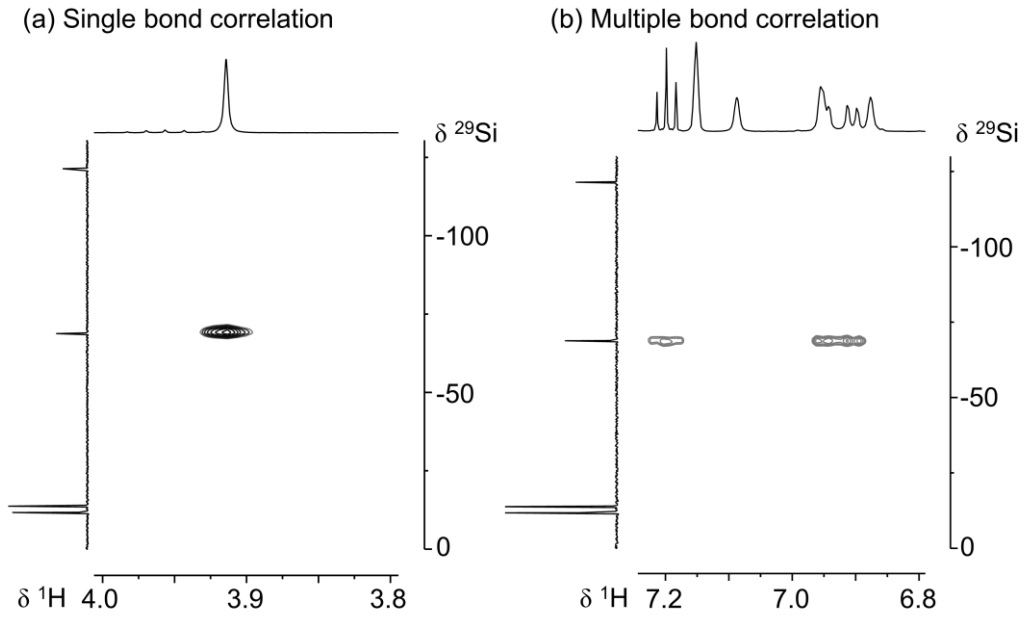

***Figure 2-7** – (a) ^{1}H-^{29}Si HMQC spectrum showing a single bond correlation between the Si-H resonance at δ 3.91 and the Si-H resonance at δ −69.8. (b) ^{1}H-^{29}Si HMBC spectrum showing long range correlation between the Si-H resonance and the aromatic signals of the terphenyl substituent.*

Silylsilylene adduct **2.37** shows broad ^{1}H resonances at δ 7.33 and δ 5.48 ($\nu_{½}$ = 40 Hz) for the C*H*Me$_2$ protons of the NHC *iso*propyl groups. It is known that the C*H*Me$_2$ resonances of ^{Me}I^{i}Pr become deshielded upon coordination,[52–54] however this level of deshielding is exceptional. The ^{1}H-^{1}H NOESY NMR shows no NOE interaction for the C*H*Me$_2$ protons other than with the NHC methyl groups. However, the two signals do show a strong exchange cross peak which could explain the broadness of the signals. Heating the sample to 60 °C significantly broadens the signals, while cooling to 10 °C somewhat sharpens them. There is no obvious reason for the extreme deshielding of the signals relative to other examples. In the solid-state structure, the hydrogen positions were determined geometrically. However, the *iso*propyl *C*HMe$_2$ is

4.720 Å from the nearest aromatic ring and 3.417 Å from the Si-Si bond. Equally, they are 3.549(2) Å and 3.249(2) Å from the silylene centre. These distances suggest no through-space interaction between the *iso*propyl hydrogens and any electronically significant part of **2.37**. This implies the level of deshielding is due to through-bond interactions or other factors.

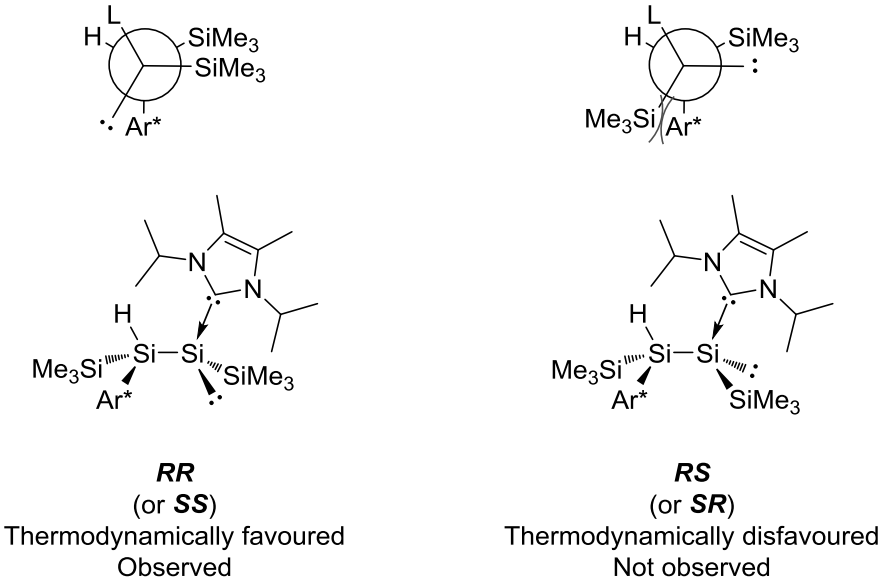

Scheme 2-18 *– Newman projections of the RR and RS diasteromers of silylsilylene* ***2.37****, highlighting the steric clash in the RS diastereomer.*

Notably, silylsilylene **2.37** has two stereocentres and therefore four stereoisomers. These can be divided into two enantiomeric pairs, *RR*/*SS* and *RS*/*SR*, which are theoretically interchangeable through base dissociation and coordination. Therefore, silylsilylene **2.37** should show two sets of signals by NMR spectroscopy, which is not the case. This can be explained by steric repulsion between the bulky terphenyl group and one trimethylsilyl group, as shown in Scheme 2-18. During the formation of adduct **2.37**, the *RS*/*SR* product is thermodynamically disfavoured due to the repulsion. Therefore, only the *RR* and *SS* diastereoisomers are observed in the final product, as confirmed by the solid-state structure shown in Figure 2-6.

2.4.3 Steric Control of the Disilene-Silylsilylene Ratio

The reactions of silanes **2.23** and **2.35** with KO^{t}Bu in the presence of an NHC gives disilene or silylsilylene products. The ratio of disilene to silylsilylene can be controlled by altering the combined steric bulk of the NHC and the R substituent (Cp* for **2.23** and terphenyl for **2.35**).

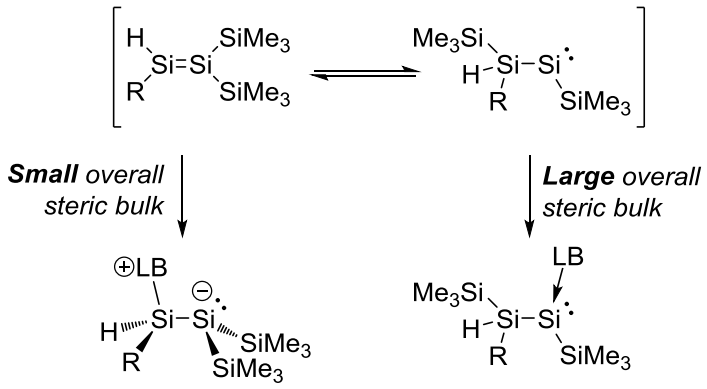

Scheme 2-19 *– An overall small steric bulk favours disilene as the thermodynamic product. An overall large steric bulk favours the silylsilylene isomer. R = Cp* or Ar*, LB = ^{Me}IMe or ^{Me}I^{i}Pr. Cp* = pentamethylcyclopentadienyl, Ar* = 2,6-bis(2,4,6-trimethylphenyl)phenyl.*

The reaction of silane **2.23** with KO^{t}Bu in the presence of ^{Me}I^{i}Pr only gives the disilene product, **2.28** (Table 2-1, entry 1). In this instance, the Cp* group is small and both the NHC and Cp* substituent are bonded to the same silicon atom in the final product.

Table 2-1 *– Increasing the overall steric bulk increases the amount of silylsilylene product when silanes **2.23** or **2.35** are reacted with KO^{t}Bu in the presence of NHCs. Cp* = pentamethylcyclopentadienyl, Ar* = 2,6-bis(2,4,6-trimethylphenyl)phenyl.*

Entry	Base	Substituent	Disilene (%)	Silylsilylene (%)	
1	^{Me}I^{i}Pr	Cp*	**2.28** (100)	(0)	Increasing overall steric bulk.
2	^{Me}IMe	Ar*	**2.40** (75)	**2.41** (25)	
3	^{Me}I^{i}Pr	Ar*	**2.36** (50)	**2.37** (50)	Increasing ratio of silylsilylene.

When the same reaction is carried out starting from terphenyl silane **2.35** in the presence of ^{Me}I^{i}Pr, the increased steric bulk makes the disilene product less thermodynamically favourable. This leads to observation of two products, disilene **2.36** and silylsilylene **2.37** in a 50:50 ratio (Table 2-1, entry 3).

This is substantiated by the reaction of terphenyl silane **2.35** with KO^{t}Bu in the presence of the slightly smaller NHC, ^{Me}IMe, as shown in Scheme 2-20. The products are disilene **2.40** and silylsilylene **2.41** in a 75:25 ratio (Table 2-1, entry 2). The products were easily identified by comparison with disilene **2.36** and silylsilylene **2.37**.

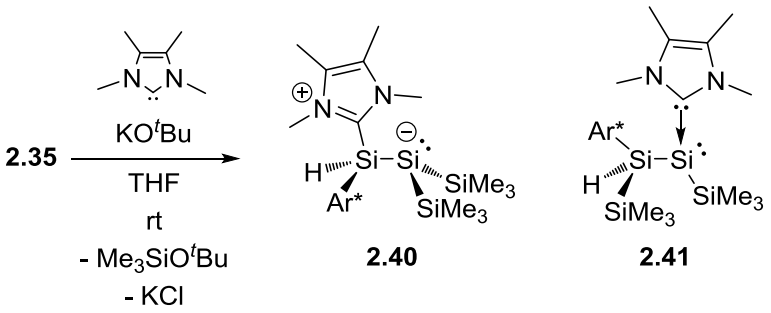

Scheme 2-20 *– The reaction of* ***2.35*** *with KO^{t}Bu in the presence of ^{Me}IMe gives a mixture of* ***2.40*** *and* ***2.41*** *in a ratio of roughly 3:1. Ar* = 2,6-bis(2,4,6-trimethylphenyl)phenyl.*

NMR spectroscopy reveals ^{29}Si resonances corresponding to disilene **2.40** at δ −200.6 for *Si*$(SiMe_3)_2$ and δ −41.6 for *Si*-H. Correlation spectroscopy reveals the corresponding ^{1}H signal of the Si-*H* at δ 5.28. These resonances are similar to those observed for **2.36** and are assigned to disilene adduct **2.40**. The other product, silylsilylene **2.41**, shows a similar spectrum to that for silylsilylene **2.37**. The silylene ^{29}Si resonance is found at δ −123.8 while the *Si*-H is found at δ −67.2. Again, heating the mixture of **2.40** and **2.41** led to complete consumption of disilene **2.40** and formation of silylsilylene **2.41** as the major product.

2.5 The Conversion of 2.36 to 2.37

When solutions of **2.36** and **2.37** or **2.40** and **2.41** are heated, complete consumption of the disilene adduct is observed within three hours at 55 °C, 16 hours at 50 °C (Figure 2-8), or three weeks at room temperature. This suggests isomerisation from the disilene to silylsilylene which would represent the first direct observation of this rearrangement. However, monitoring the reaction of **2.36** to **2.37** (Figure 2-9) showed that the rate of consumption of **2.36** far exceeds the rate of production of **2.37** and the vast majority of **2.36** simply decomposes to leave a large number of minor signals in the ^{1}H NMR.

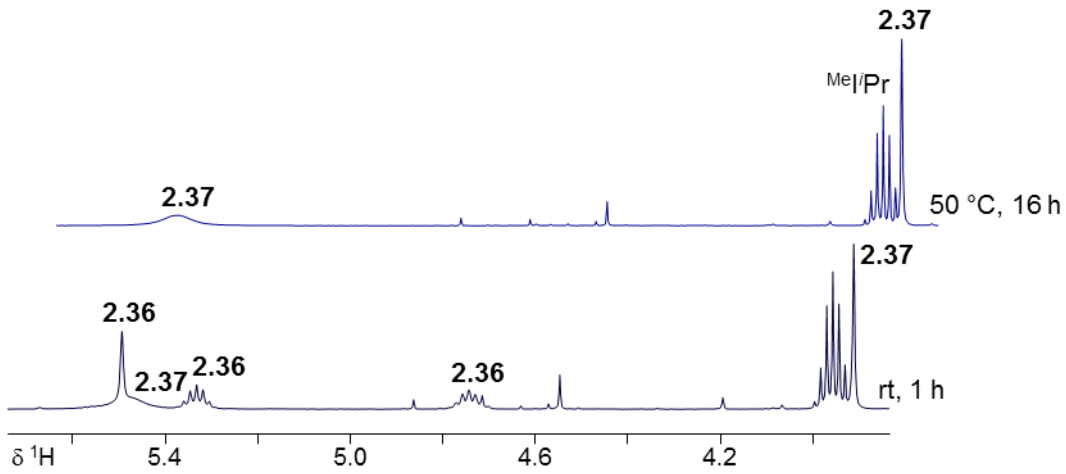

Figure 2-8 *- Expansion of ^{1}H NMR (500.2 MHz, C_6D_6, 300 K) showing the Si-H and some C<u>H</u>$(CH_3)_2$ resonances from a mixture of* ***2.36*** *and* ***2.37*** *after 1 hour at room temperature and after 16 hours at 50 °C.*

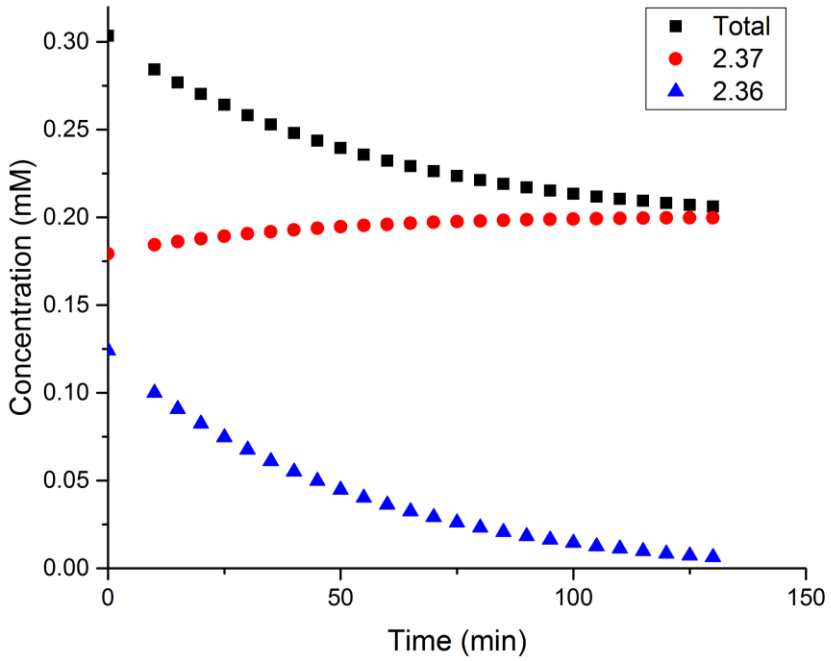

Figure 2-9 *– The concentration of* ***2.36*** *to* ***2.37*** *and the total concentration when a roughly 1:1 mixture is heated at 55 °C. The conversion of* ***2.36*** *to* ***2.37*** *is not quantitative and the total concentration decreases signifcantly over the course of the reaction.*

The reaction was carried out with varying amounts of excess NHC in order to gain an insight into the mechanism of conversion. In each case, the mixture was generated *in situ* by the reaction of **2.35** with KO^{t}Bu in the presence of ^{Me}I^{i}Pr which gave a roughly 1:1 mixture of **2.36**

and **2.37**. The reaction was heated in order to induce lability of the NHC and the reaction progress was monitored by integration of the $SiMe_3$ substituents in the ^1H NMR using mesitylene as an internal standard.

When one equivalent of NHC was used there was only an 11% increase in the concentration of **2.37** over two hours at 55 °C, while **2.36** was completely consumed in the same time (Table 2-2, entry 1).

When using three equivalents of NHC there was only a 12% increase in concentration of **2.37** in the time that **2.36** was completely consumed. However, in this instance the reaction took three hours to reach completion (the decreased rate is in agreement with NHC dissociation as the rate-limiting step). When ten equivalents of NHC were used the reaction took four hours and the concentration of **2.36** increased by 20%.

Table 2-2 *– The reaction of **2.35** with one equivalent of KO^tBu and a known amount of $^{Me}I^iPr$ gives a roughly 1:1 mixture of **2.36** and **2.37**. When the mixture is heated to 55 °C **2.36** is fully consumed but it does not quantitatively form **2.37**.*

Entry	Equivalents of $^{Me}I^iPr$	Time (min)	Consumption of 2.36 (%)	Formation of 2.37 (%)
1	1	130	100	11
2	3	185	100	12
3	10	235	100	20

The proposed mechanism of formation of **2.37** from **2.36** is shown in Scheme 2-20 (blue). It proceeds *via* dissociation of the NHC followed by silyl group migration and subsequent coordination of the NHC to the resultant silylsilylene. Computations show that the silyl group migration is accompanied by a barrier of 24.1 kcal·mol^{-1}, consistent with the reaction temperature of 55 °C. The overall reaction is favourable by −2.1 kcal·mol^{-1}.

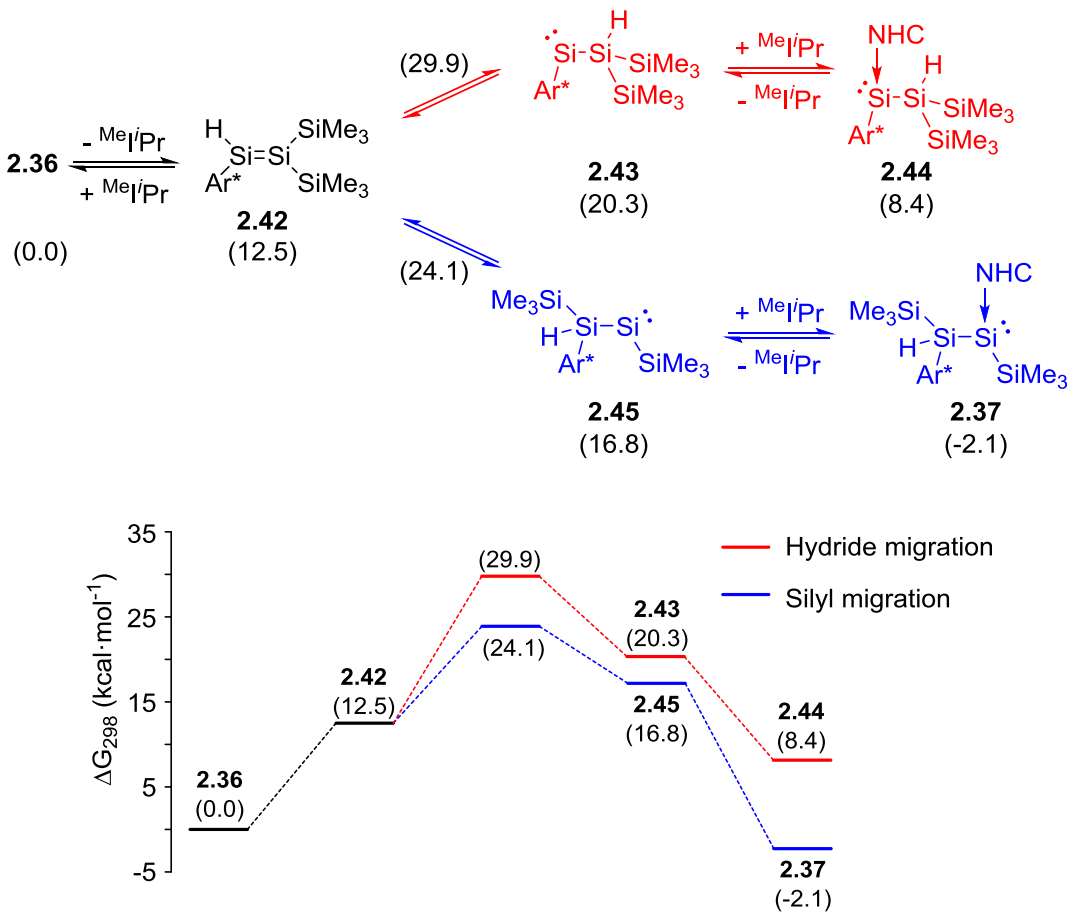

Figure 2-10 *– The computed reaction pathway for the rearrangement of* ***2.36*** *to* ***2.37*** *(blue) and the higher energy pathway to* ***2.14*** *(red), which is not observed.* ΔG_{298} *in kcal·mol^{-1} (SMD-M06-2X/6–311++G(2d,2p)//RI-M06L/6–31+G(d,p), solvent THF). NHC = $^{Me}I^{i}Pr$ = 1,3-diisopropyl-4,5-dimethylimidazol-2-ylidene, Ar* = 2,6-bis(2,4,6-trimethylphenyl)phenyl.*

The formation of **2.37** as the final product indicates that silyl group migration is preferred over hydride migration. Indeed, calculations showed that the transition state for hydride migration is 5.8 kcal·mol^{-1} higher in energy than that for silyl group migration (Figure 2-10). Furthermore, the resultant free silylsilylene **2.43** is 3.5 kcal·mol^{-1} higher in energy and the final product, NHC coordinated silylsilylene **2.44**, is 10.5 kcal·mol^{-1} higher in energy. Hydride migration without NHC dissociation would also lead to **2.44**, however the barrier to that reaction was found to be 42.5 kcal·mol^{-1}. Overall these energies explain why **2.44** is not observed in the reaction mixture at any point.

Note that the analogous mechanism for the conversion of NHC coordinated Cp* disilene **2.28** to the silylsilylene proceeds through a significantly higher barrier of 37.1 kcal·mol^{-1} for silyl

group migration (Figure 2-11) and the final product is 3.8 kcal·mol^{-1} higher in energy than disilene **2.28**. This is consistent with no observation of silylsilylene in the synthesis of **2.28**. The reduced steric bulk of disilene adduct **2.28** might explain the stronger binding and the relative stability of the disilene adduct.

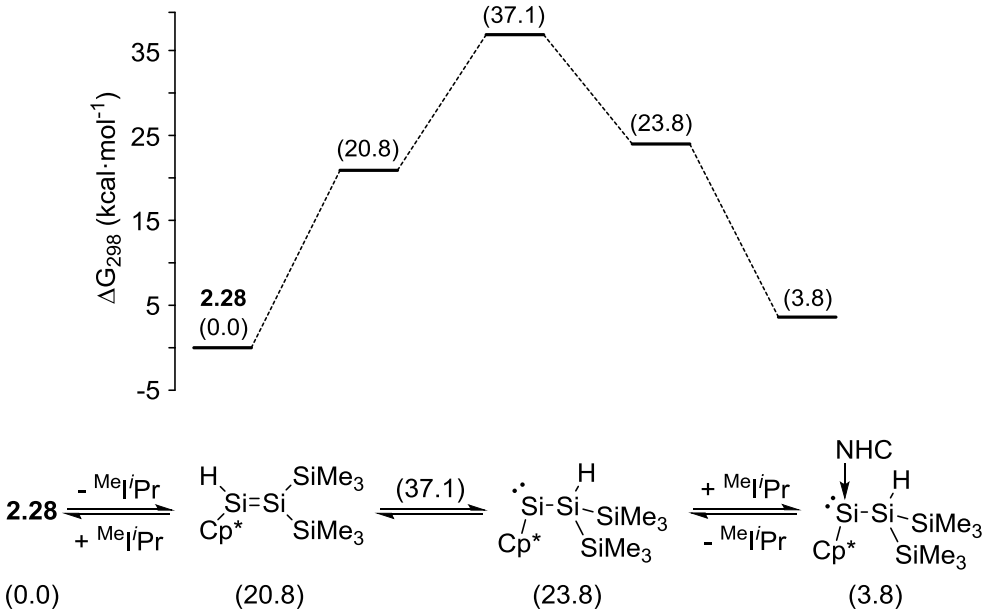

***Figure 2-11** – The computed reaction pathway for the unobserved rearrangement of **2.28** to the corresponding silylsilylene. ΔG_{298} in kcal·mol^{-1} (SMD-M06-2X/6–311+ +G(2d,2p)//RI-M06L/6–31+G(d,p), solvent THF). NHC = $^{Me}I^{i}Pr$ = 1,3-diisopropyl-4,5-dimethylimidazol-2-ylidene, Cp* = C_5Me_5.*

Other possible mechanisms for the transformation of disilene **2.36** to silylsilylene **2.37** were investigated in order to explain the poor conversions rates. In the presence of excess NHC, disilene **2.36** could dissociate into silylenes **2.46** and **2.47**. Insertion of silylene **2.46** into an Si-Si bond of **2.47** would give the silylsilylene product **2.37**. However, silylene **2.47** would be very reactive due to two strongly σ-donating silyl substituents and could lead to multiple side reactions.[17,74] Furthermore, silylene **2.46** should be relatively stable by comparison with related silylenes[18,68] but no **2.46** is observed by ^{1}H NMR spectroscopy. These observations, and the large reaction barrier of 47.5 kcal·mol^{-1} suggest this reaction is not significant.

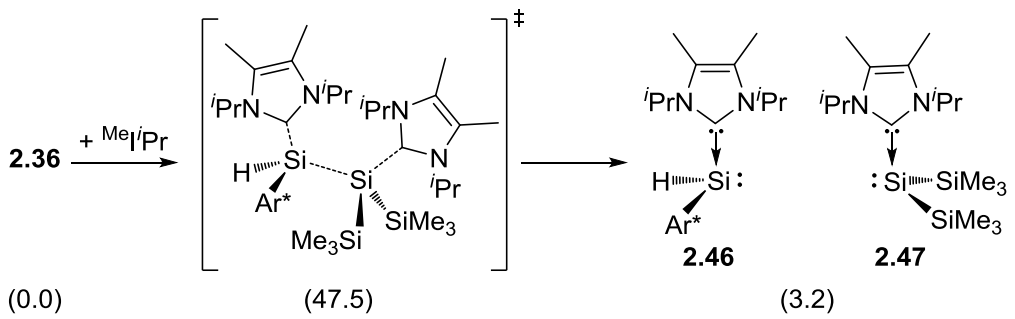

Scheme 2-21 *– Potential formation of silylenes **2.46** and **2.47** was ruled out by the high transition state of 47.5 kcal·mol^{-1}. ΔG_{298} in kcal·mol^{-1} (SMD-M06-2X/6-311++G(2d,2p)//RI-M06-L/6-31+G(d,p)).*

Although no competitive side reactions were found experimentally or computationally, general decomposition routes of **2.36** and **2.37** must explain the low rate of conversion. These side reactions could be exacerbated by the elevated temperatures required to dissociate the strongly coordinating NHC. The high overall transition state at 24.1 kcal·mol^{-1} could potentially be reduced by preparing a disilene coordinated by a more labile base.

2.6 Nitrogen-Coordinated Disilenes

The conversion of disilene **2.36** to silylsilylene **2.37** is evidence of the disilene-silylsilylene isomerisation. However, the reaction is low yielding and leads to an unidentified mixture of products. The poor conversion could be exasperated by the high barrier to NHC dissociation, therefore I sought to prepare a disilene stabilised by a more labile base.

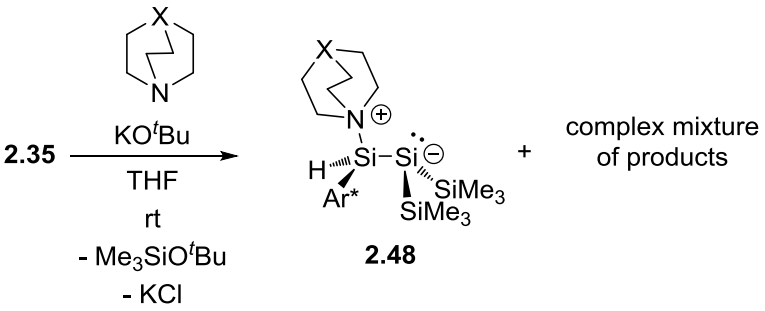

Scheme 2-22 *– The reaction of **2.35** with KO^{t}Bu in the presence of DABCO (X = N) or quinuclidine (X = CH) to give a complex mixxture of products containing a small amount of **2.48**.*

Silane **2.35** was reacted with KO^{t}Bu in the presence of two amine bases. Quinuclidine and 1,4-diazabicyclo[2.2.2]octane (DABCO) were selected as potential bases with reasonable steric bulk.

The reaction of **2.35** with KO^{t}Bu in the presence of DABCO afforded a complex mixture of products, most of which could not be identified. However, two new Si-H signals were observed in the ^{29}Si NMR at δ 21.6 and 22.4 which were found to correspond to ^{1}H signals at δ 5.14 and 5.17 using ^{1}H-^{29}Si correlation spectroscopy. Furthermore, the ^{1}H resonance at δ 5.17 showed long range correlation to a new ^{29}Si signal at δ −183.4. By comparison with and **2.28** and **2.36**, this data could support the formation of a DABCO-disilene adduct, **2.48**. However, the product is only a small fraction of the mixture and could not be separated from the side products.

Quinuclidine has almost identical steric properties to DABCO, however it is a slightly stronger base — the pK_a of the conjugate acid is 11.0 in H_2O compared with 8.8 for DABCO. Despite this, the reaction of **2.35** with KO^{t}Bu in the presence of quinuclidine gave a large number of new ^{29}Si signals with at least six new Si-H resonances observed in the ^{1}H-^{29}Si HMBC. Only a very weak ^{29}Si signal was observed in the region typical of silyl anions at δ −171.9 which could correspond to the base-coordinated disilene **2.48**. Other Si-H signals could correspond to the silylsilylene isomer or the silylene product of the Wanzlick equilibrium (L→Si(H)Ar*), as shown for **2.27** in Figure 2-3, bottom left.

2.6.1 Preparation of DMAP Coordinated Disilene 2.49

Aminopyridine ligands are more coordinating than simple amines like DABCO. 4-Dimethylaminopyridine (DMAP) offers a similar basicity to DABCO and quinuclidine, the pK_a of the conjugate acid is 9.2 in water. However, its coordinating ability is enhanced, as explained by a resonance form involving the NMe_2 substituent shown in Scheme 2-23.

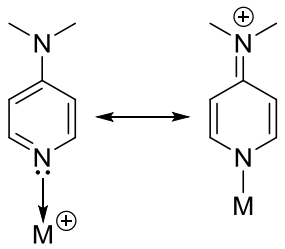

***Scheme 2-23** – The coordinating ability of DMAP is enhanced through a resonance form involving the NMe_2 substituent.*

The reaction of **2.35** with KO^{t}Bu in the presence of DMAP cleanly gave one new product with ^{29}Si NMR resonances at δ −187.7, −6.3 and 32.2. The ^{1}H and ^{29}Si NMR also showed formation

of the silyl ether Me_3SiO^tBu. The proposed product is DMAP coordinated disilene **2.49**, shown in Scheme 2-24.

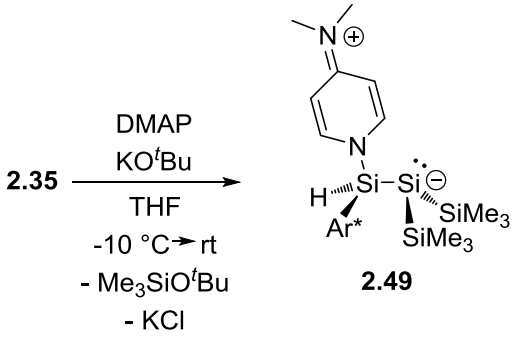

***Scheme 2-24** – The reaction of **2.35** with KO^tBu in the presence of DMAP to give proposed product **2.49**. DMAP = 4-dimethylaminopyridine, Ar* = 2,6-bis(2,4,6-trimethylphenyl)phenyl.*

The ^{29}Si resonance at δ −187.7 is assigned to the three-coordinate, anionic silicon centre, by comparison with disilenes **2.28** and **2.36**. The signal at δ −6.3 is consistent with the trimethylsilyl substituents and shows strong correlation to a ^1H resonance at δ −0.16 in the ^1H-^{29}Si HMBC. The resonance at δ 32.2 is assigned to the *Si*-H and shows strong one-bond correlation to a ^1H resonance at δ 5.44 with a $^1J_{HSi}$ coupling constant of 190 Hz. In the ^1H NMR, the integrals of the Si-H and $SiMe_3$ signals at δ 5.44 and δ −0.16 are in the ratio 1:18, further confirming the ^1H and ^{29}Si NMR assignment.

The resonance for the base-coordinated silicon centre is found at lower field than NHC-disilene adducts. For DMAP adduct **2.49** it is found at δ 32.2 while for the NHC adducts it is found at δ −13.0 for **2.28** and δ −37.1 **2.36**. This is consistent with weaker donation from the amine base when compared with the NHC $^{Me}I^iPr$. Furthermore, **2.49** is unstable in solution and rapidly decomposes, presumably through base-dissociation followed by polymerisation or E-H insertions of the transient, base-free disilene. This supports a weak N-Si dative interaction.

Despite repeated attempts, **2.49** could not be isolated as a pure compound and crystals suitable quality for single-crystal X-ray diffraction were not obtained.

2.6.2 Preparation of 4-PPy Stabilised Disilene 2.50

The related base, 4-pyrrolidinopyridine offers an alternative to DMAP with similar electronic and steric properties but different packing features in the solid-state. Therefore, the analogous reaction of silane **2.35** with KO^{t}Bu was carried out in the presence of 4-PPy.

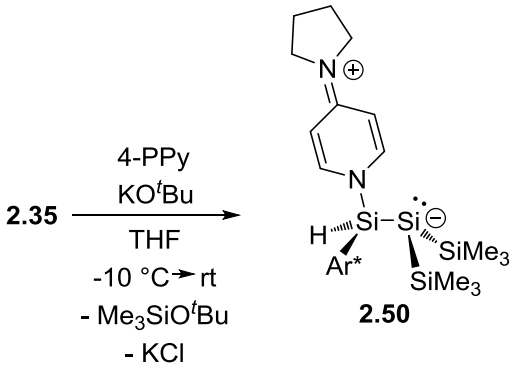

***Scheme 2-25** – The synthesis of 4-PPy stabilised disilene **2.50** from silane **2.35**. Ar* = 2,6-(2,4,6-trimethylphenyl)phenyl. 4-PPy = 4-Pyrrolidinopyridine*

Carrying out the reaction in THF, followed by crystallisation from toluene afforded disilene adduct **2.50** in 39% yield. Bulk samples of **2.50** could not be purified beyond *ca.* 90% due to the labile nature of 4-PPy, as discussed below. Indeed, multiple recrystallisations led to the release of uncoordinated 4-PPy and unidentified decomposition products. However, small quantities of analytically pure sample could be obtained as single crystals by careful recrystallisation from toluene at −20 °C.

The ^{29}Si NMR spectrum of disilene **2.50** shows a singlet resonance at δ −184.0 corresponding to the three-coordinate silicon centre. This is comparable to that for disilenes **2.36**, **2.28** and **2.49** which have upfield ^{29}Si resonances at δ −188.0, −202.2 and −187.7. The donor ability of 4-PPy is significantly weaker than that of NHCs. This is evident in the lower field chemical shift for the four coordinate *Si*-H centre of 4-PPy disilene **2.50** at δ 34.7, compared with δ −13.0 and −37.1 for NHC disilenes **2.28** and **2.36**, respectively. However, it is very similar to that of DMAP disilene adduct **2.49** which is found at δ 32.2. Abstraction of one $SiMe_3$ is confirmed by integration of the Si-*H* resonance to the single $SiMe_3$ resonance at δ 0.41. A single $SiMe_3$ environment is also observed in the ^{13}C and ^{29}Si NMR spectra at δ 6.28 and δ −5.92, respectively.

The solid-state structure of **2.50** is shown in Figure 2-12. The Si1-Si2 bond distance of 2.3224(7) Å is slightly shorter than in NHC disilene adduct **2.28** (2.3575(8) Å) and is still well within the range of a Si-Si single bond.

The presence of a lone pair and negative charge at Si2 is still evidenced in the highly shielded ^{29}Si chemical shift of δ −184.0, and in the pyramidalised nature of Si2 in the solid- structure (Σ∢ = 297.66(3)°, 296.15(5)° for **2.28**).

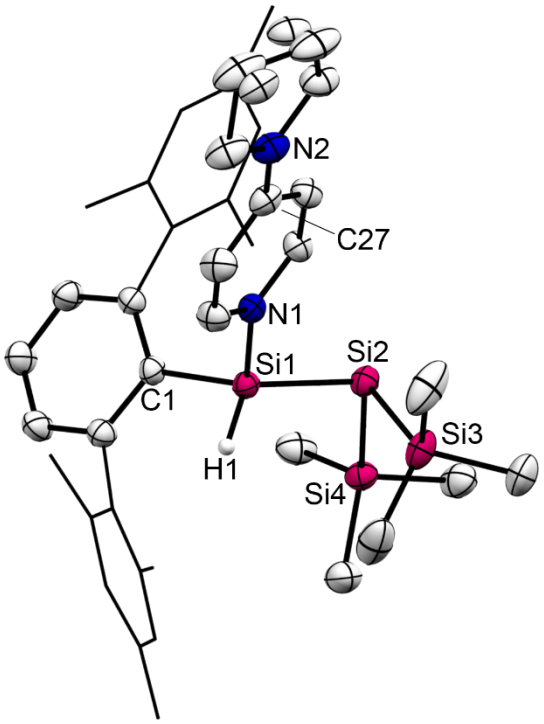

Figure 2-12 *– Solid-state structure of* ***2.50****. Hydrogen atoms, with the exception of H1 omitted for clarity. Thermal ellipsoids set to 50% probability. Selected bond lengths (Å) and angles (°): Si1-Si2 2.3224(7), Si2-Si3 2.3502(7), Si2-Si4 2.3594(6), Si1-C1 1.908(2), Si1-N1 1.884(1), N2-C27 1.336(2); N1-Si1-C1 106.92(7), N1-Si1-Si2 103.70(5), Si1-Si2-Si3 105.43(2), Si1-Si2-Si3 91.87(2).*

Only one other 4-PPy adduct of a silicon species has been reported, a base-stabilised bromosilylene **2.51**.[75] However, there have been multiple reports of DMAP coordinated low-valent silicon species, including base-coordinated silylene **2.52**,[76] a Si(II) cation,[77] and multiple acid-base stabilised silylenes.[78–83]

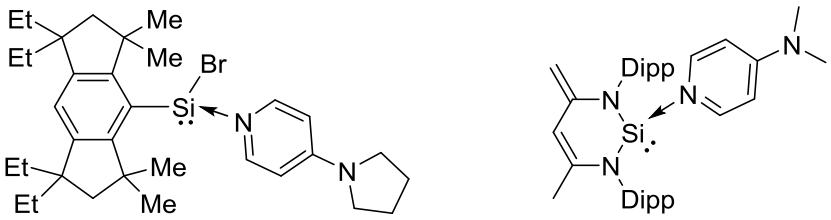

2.51 **2.52**

Scheme 2-26 *– 4-PPy coordinated bromosilylene* ***2.51***[75] *and DMAP coordinated silylene* ***2.52***.[76]

The N1-Si1 bond length in disilene **2.50** of 1.8839(14) Å is notably shorter than in silylenes **2.51** (1.939(2) Å) and **2.52** (2.005(2) Å). The N2-C27 bond length in **2.50** (1.336(2) Å) is the same (within error) as in **2.51** (1.339(3) Å) and both are considerably shorter than in uncoordinated 4-PPy (1.355(1) Å).[84]

Table 2-3 *– The amount of uncoordinated and coordinated 4-PPy in a solution of* ***2.50*** *in THF-d_8 upon heating from 278 K to 333 K and cooling again to 278 K. Concentrations were calculated by calibrating integrals against mesitylene as an internal standard.*

Temp (°C)	Uncoordinated 4-PPy (µmol)	Coordinated 4-PPy (µmol)	Uncoordinated 4-PPy (%)	Coordinated 4-PPy (%)	
278	1.28	3.61	26.1	73.9	
298	1.30	3.79	25.5	74.5	Heating
328	1.52	3.50	30.3	69.7	
333	1.61	3.11	34.0	66.0	
328	1.55	3.73	29.4	70.6	
298	1.29	3.81	25.3	74.7	Cooling
278	1.27	3.62	26.0	74.0	

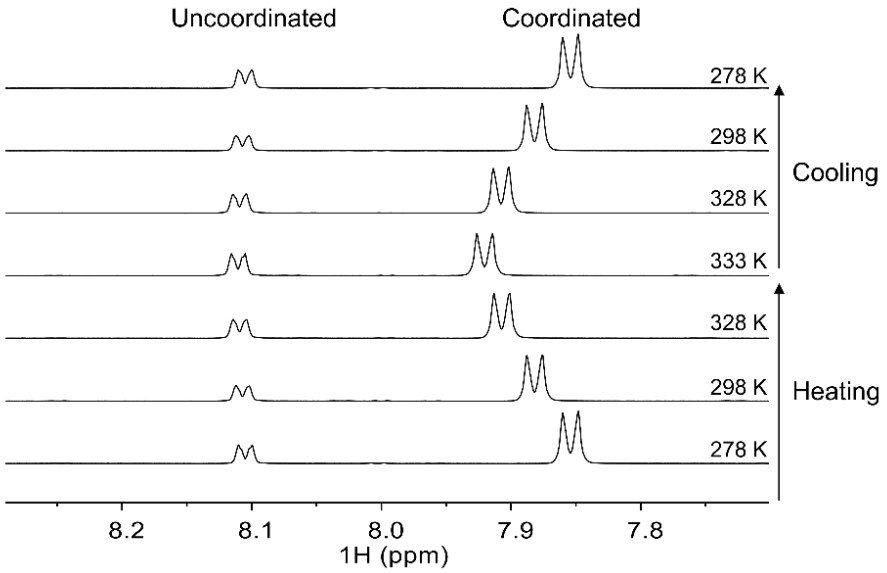

Figure 2-13 *– Expansion of the ^{1}H NMR of **2.50** in THF-d_8 upon heating from 278 K to 333 K and cooling again to 278 K. The region shows one of the C-H environments of the pyridine fragment.*

Similar to silylene **2.51**, the 4-PPy ligand of disilene **2.50** is labile. When a solution of **2.50** in THF-d_8 is heated to 60 °C, the concentration of uncoordinated 4-PPy increases; when it is cooled the concentration decreases. This lability leads to rapid decomposition of **2.50** in non-coordinating solvents. For example, its half-life in C_6D_6 at 60 °C is approximately 30 minutes. Table 2-3 shows the integration of coordinated and uncoordinated 4-PPy for a sample heated from 0 °C to 60 °C and then cooled again. Figure 2-13 shows an expansion of the ^{1}H NMR at each temperature showing one C-*H* environment of the pyridine fragment of both coordinated and uncoordinated 4-PPy.

2.7 Conversion of 2.50 to 2.36 and 2.37

The proposed mechanism for the conversion of NHC disilene adduct **2.36** to silylsilylene **2.37** (Figure 2-10) proceeds *via* initial dissociation of the coordinating NHC. Given the increased lability of the 4-PPy ligand, disilene adduct **2.50** was heated in the presence of excess NHC in an attempt to induce conversion of disilene **2.50** to silylsilylene **2.37**.

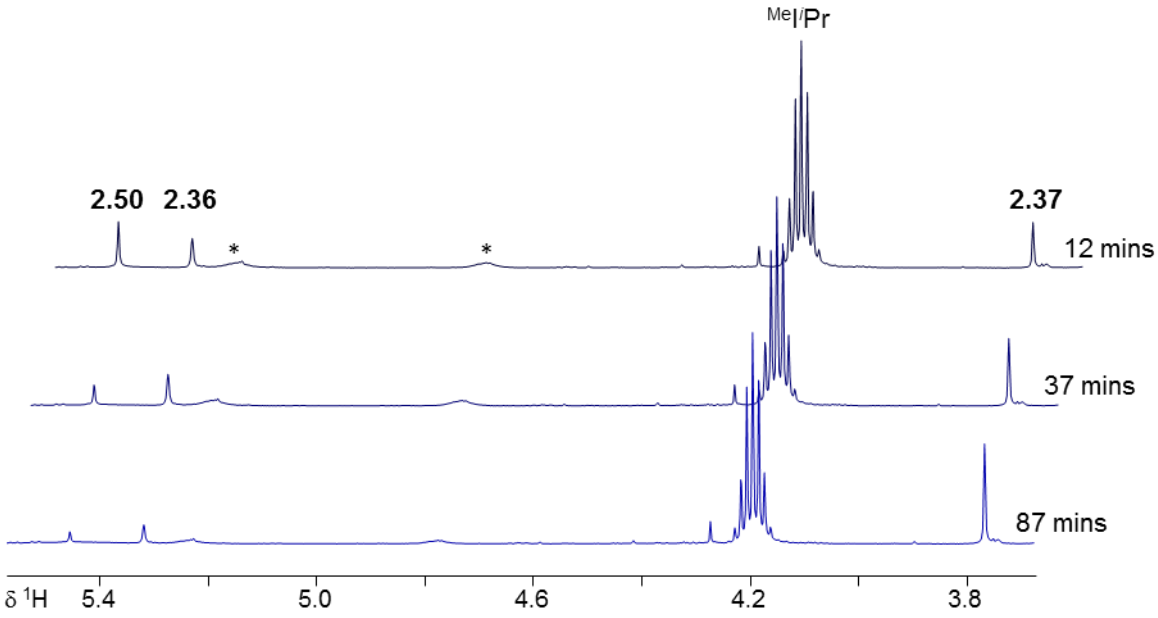

Figure 2-14 *– Expansion of $_1$H NMR (500.2 MHz, C_6D_6, 300 K) showing the Si-H and some $CH(CH_3)_2$ resonances when a sample of* ***2.50*** *is heated to 55 °C in the presence of excess $^{Me}I^iPr$. * = unidentified reaction products.*

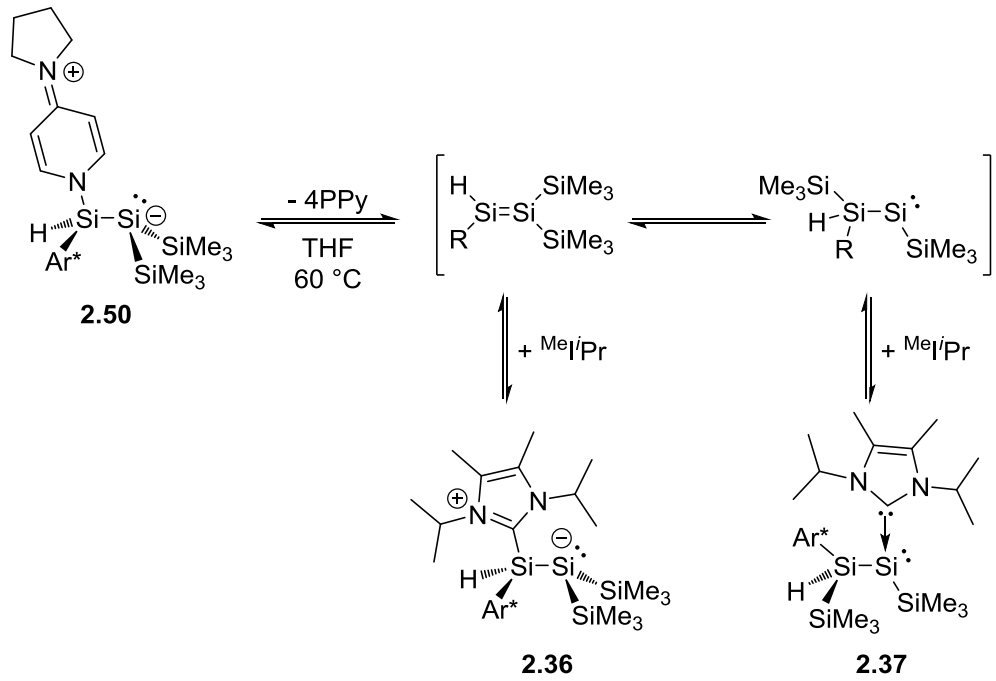

Scheme 2-27 *– The reaction of disilene adduct* ***2.50*** *with $^{Me}I^iPr$ at 60 °C initially gives a mixture of disilene adduct* ***2.36*** *and silylsilylene adduct* ***2.37*** *which converts fully to silylsilylene over time. Ar* = 2,6-bis(2,4,6-trimethylphenyl)phenyl, 4-PPy = 4-pyrollidinopyridine, $^{Me}I^iPr$ = 1,3-Diisopropyl-4,5-dimethylimidazol-2-ylidene.*

Indeed, when the reaction was monitored by ^{1}H NMR at 55 °C, consumption of disilene **2.50** was observed. Interestingly, the consumption of **2.50** was coupled with formation of both NHC coordinated disilene **2.36** and silylsilylene **2.37**, as shown in the ^{1}H NMR expansion in Figure 2-14. Over time, disilene **2.36** is completely consumed leaving silylsilylene **2.37** as the sole observable product.

Importantly, the overall conversion of 4-PPy stabilised disilene **2.50** to silylsilylene **2.37** is 80%, which is considerably higher than 20% for when disilene **2.36** is directly transformed to **2.37**. This observation suggests that the free silylsilylene is formed from 4-PPy disilene *via* two competing routes, one of which involves **2.36** as an intermediate.

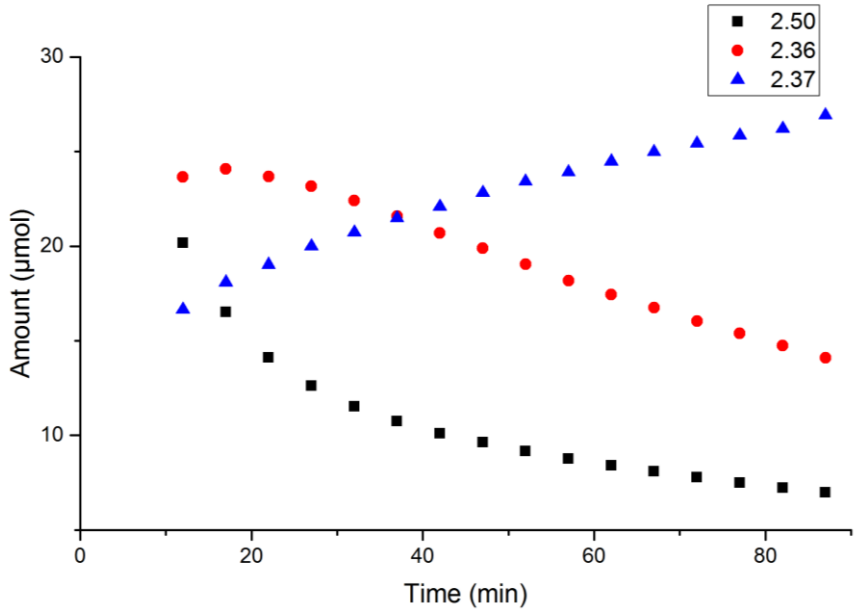

Figure 2-15 *– The amount of **2.50**, **2.36** and **2.37** over time when a sample of **2.50** is heated at 55 °C in the presence of excess $^{Me}{}^{i}$Pr. Concentrations measured against mesitylene as an internal standard.*

Indeed, calculations showed that **2.50** is only 1 kcal·mol^{-1} higher in energy than **2.36** (Figure 2-16). Dissociation of the 4-PPy base from **2.50** was computed to be barrierless. However, no NHC disilene adduct **2.36** is observed when 4-PPy disilene adduct **2.50** is stirred with excess NHC at room temperature. Conversion to **2.36** is only observed upon heating.

This reaction represents the first controllable and observable rearrangement of a disilene to a silylsilylene.

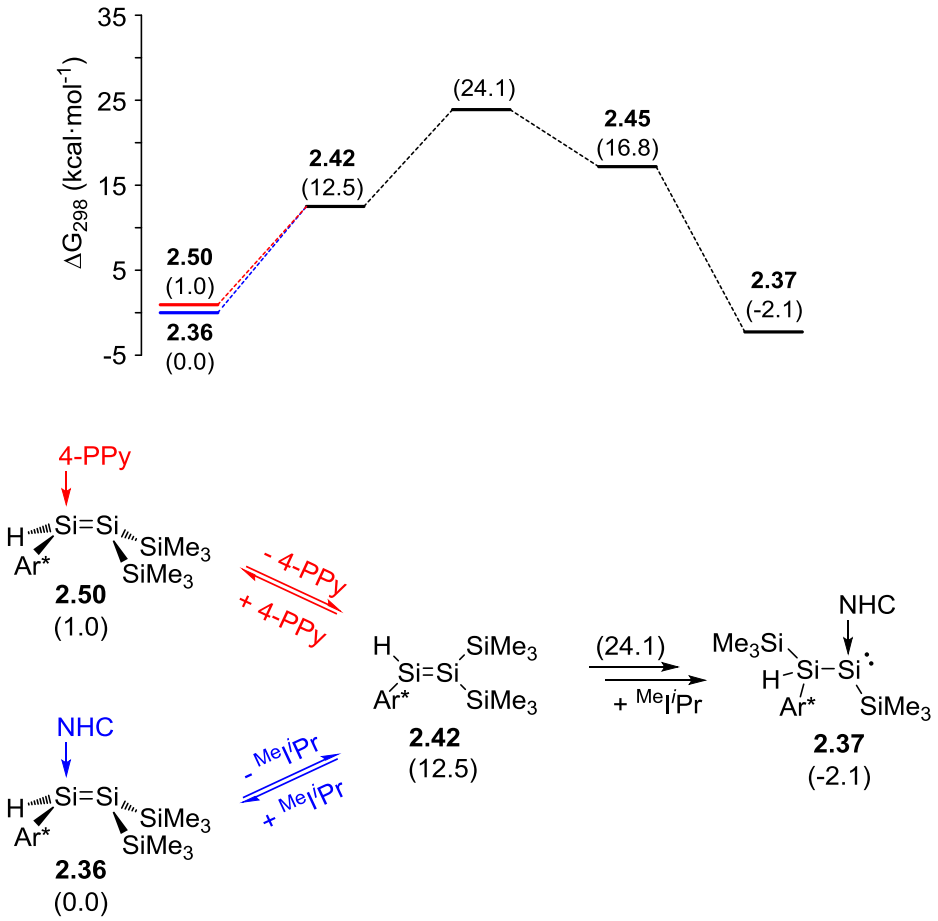

Figure 2-16 *– The computed reaction pathway for the rearrangement of* ***2.50*** *to* ***2.37*** *(red) and the accessible equilibrium with* ***2.36*** *(blue).* ΔG_{298} *in kcal·mol*$^{-1}$ *(SMD-M06-2X/6–311+ +G(2d,2p)//RI-M06L/6–31+G(d,p), solvent THF). NHC =* ^{Me}*I*^{i}*Pr = 1,3-diisopropyl-4,5-dimethylimidazol-2-ylidene, Ar* = 2,6-bis(2,4,6-trimethylphenyl)phenyl.*

2.8 Conclusions

In conclusion, a novel route for the preparation of low-oxidation state silicon compounds has been reported. This has enabled ready access to disilenes with small hydride and trimethylsilyl substituents as well as a rare example of a silylsilylene.

Transient species were coordinated by the use of NHC and pyridine bases and the resultant adducts were fully characterised by NMR spectroscopy and X-ray crystallography.

The observation of disilenes and silylsilylenes under the same conditions serves as evidence of the disilene-silylsilylene equilibrium in solution. Migration of the silyl group is preferred over the hydride. The base coordination strategy enabled control of the equilibrium and direct observation of the disilene to silylene isomerisation by NMR spectroscopy.

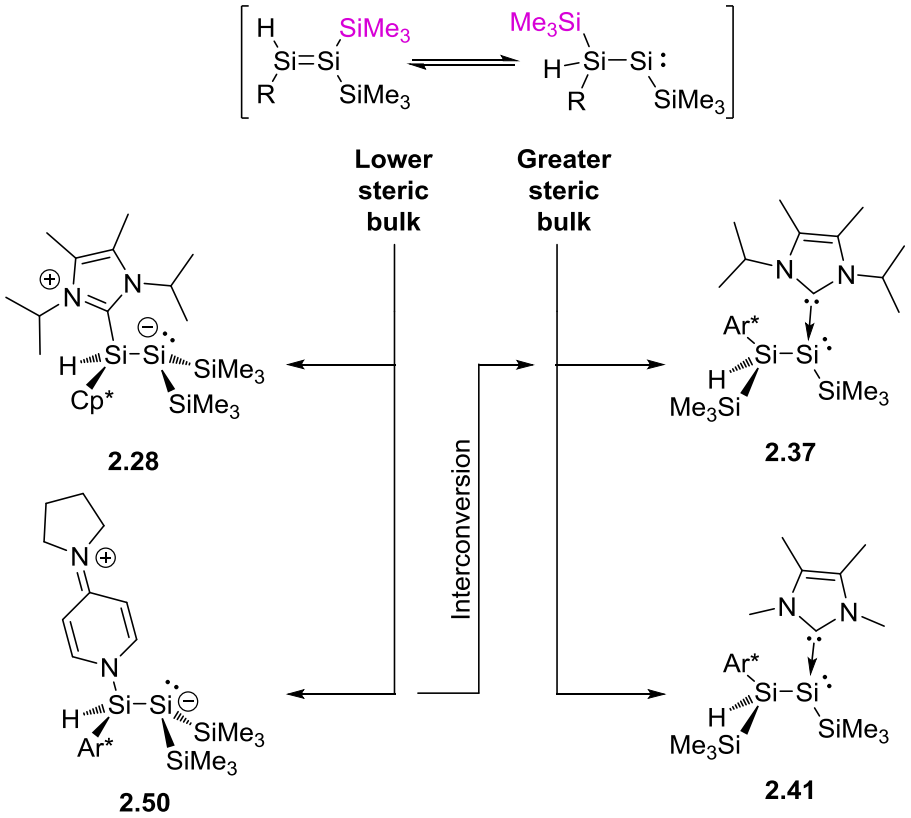

2.9 References

[1] G. Dolgonos, *Chem. Phys. Lett.* **2008**, *466*, 11–15.

[2] L. Sari, M. C. McCarthy, H. F. Schaefer, P. Thaddeus, *J. Am. Chem. Soc.* **2003**, *125*, 11409–11417.

[3] C. Pak, J. C. Rienstra-Kiracofe, H. F. Schaefer, *J. Phys. Chem. A* **2000**, *104*, 11232–11242.

[4] M. C. Ernst, A. F. Sax, J. Kalcher, *Chem. Phys. Lett.* **1993**, *216*, 189–193.

[5] L. A. Curtiss, K. Raghavachari, P. W. Deutsch, J. A. Pople, *J. Chem. Phys.* **1991**, *95*, 2433–2444.

[6] B. T. Luke, J. A. Pople, M. B. Krogh-Jespersen, Y. Apeloig, M. Karni, J. Chandrasekhar, P. v. R. Schleyer, *J. Am. Chem. Soc.* **1986**, *108*, 270–284.

[7] K. Krogh-Jespersen, *J. Phys. Chem.* **1982**, *86*, 1492–1495.

[8] R. A. Poirier, J. D. Goddard, *Chem. Phys. Lett.* **1981**, *80*, 37–41.

[9] G. Maier, H. P. Reisenauer, J. Glatthaar, *Chem. Eur. J.* **2002**, *8*, 4383–4391.

[10] *Ullmann's Encyclopedia of Industrial Chemistry*, Wiley-VCH, Weinheim, **2011**.

[11] F. Falk, G. Mollekopf, H. Stafast, *Appl Phys A* **1998**, *67*, 507–512.

[12] L. C. Snyder, Z. R. Wasserman, *J. Am. Chem. Soc.* **1979**, *101*, 5222–5223.

[13] H. Teramae, *J. Am. Chem. Soc.* **1987**, *109*, 4140–4142.

[14] H. Jacobsen, T. Ziegler, *J. Am. Chem. Soc.* **1994**, *116*, 3667–3679.

[15] W. D. Wulff, W. F. Goure, T. J. Barton, *J. Am. Chem. Soc.* **1978**, *100*, 6236–6238.

[16] H. Sakurai, Y. Nakadaira, H. Sakaba, *Organometallics* **1983**, *2*, 1484–1486.

[17] A. V. Protchenko, A. D. Schwarz, M. P. Blake, C. Jones, N. Kaltsoyannis, P. Mountford, S. Aldridge, *Angew. Chem. Int. Ed.* **2013**, *52*, 568–571.

[18] S. Inoue, C. Eisenhut, *J. Am. Chem. Soc.* **2013**, *135*, 18315–18318.

[19] S.-H. Zhang, H.-X. Yeong, H.-W. Xi, K. H. Lim, C.-W. So, *Chem. Eur. J.* **2010**, *16*, 10250–10254.

[20] P. Ghana, M. I. Arz, U. Das, G. Schnakenburg, A. C. Filippou, *Angew. Chem. Int. Ed.* **2015**, *54*, 9980–9985.

[21] M. Ichinohe, R. Kinjo, A. Sekiguchi, *Organometallics* **2003**, *22*, 4621–4623.

[22] K. Abersfelder, D. Scheschkewitz, *J. Am. Chem. Soc.* **2008**, *130*, 4114–4121.

[23] T. Sasamori, K. Hironaka, Y. Sugiyama, N. Takagi, S. Nagase, Y. Hosoi, Y. Furukawa, N. Tokitoh, *J. Am. Chem. Soc.* **2008**, *130*, 13856–13857.

[24] T. Agou, Y. Sugiyama, T. Sasamori, H. Sakai, Y. Furukawa, N. Takagi, J.-D. Guo, S. Nagase, D. Hashizume, N. Tokitoh, *J. Am. Chem. Soc.* **2012**, *134*, 4120–4123.

[25] T. Kosai, T. Iwamoto, *Chem. Eur. J.* **2018**, *24*, 7774–7780.

[26] T. Kosai, T. Iwamoto, *J. Am. Chem. Soc.* **2017**, *139*, 18146–18149.

[27] T. Yamaguchi, A. Sekiguchi, *J. Am. Chem. Soc.* **2011**, *133*, 7352–7354.

[28] K. Leszczyńska, K. Abersfelder, A. Mix, B. Neumann, H. Stammler, M. J. Cowley, P. Jutzi, D. Scheschkewitz, *Angew. Chem. Int. Ed.* **2012**, *51*, 6785–6788.

[29] M. J. Cowley, V. Huch, H. S. Rzepa, D. Scheschkewitz, *Nat. Chem.* **2013**, *5*, 876–879.

[30] X.-Q. Xiao, H. Zhao, Z. Xu, G. Lai, X.-L. He, Z. Li, *Chem. Commun.* **2013**, *49*, 2706–2708.

[31] M. Hartmann, A. Haji-Abdi, K. Abersfelder, P. R. Haycock, A. J. P. White, D. Scheschkewitz, *Dalton Trans.* **2010**, *39*, 9288–9295.

[32] H. Kobayashi, T. Iwamoto, M. Kira, *J. Am. Chem. Soc.* **2005**, *127*, 15376–15377.

[33] A. N. Price, M. J. Cowley, *Chem. Eur. J.* **2016**, *22*, 6248–6252.

[34] S. Inoue, D. Franz, T. Szilvási, A. Pöthig, *Chem. Eur. J.* DOI 10.1002/chem.201902877.

[35] R. Appel, F. Knoll, I. Ruppert, *Angew. Chem. Int. Ed. Engl.* **1981**, *20*, 731–744.

[36] P. Paetzold, C. von Plotho, *Chemische Berichte* **1982**, *115*, 2819–2825.

[37] P. Jutzi, D. Kanne, C. Krüger, *Angew. Chem. Int. Ed. Engl.* **1986**, *25*, 164–164.

[38] P. Jutzi, A. Mix, B. Rummel, W. W. Schoeller, B. Neumann, H.-G. Stammler, *Science* **2004**, *305*, 849–851.

[39] S. Inoue, K. Leszczyńska, *Angew. Chem. Int. Ed.* **2012**, *51*, 8589–8593.

[40] P. Jutzi, K. Leszczyńska, B. Neumann, W. W. Schoeller, H.-G. Stammler, *Angew. Chem. Int. Ed.* **2009**, *48*, 2596–2599.

[41] A. H. Cowley, E. a. V. Ebsworth, S. K. Mehrotra, D. W. H. Rankin, M. D. Walkinshaw, *J. Chem. Soc., Chem. Commun.* **1982**, 1099–1100.

[42] C. Marschner, *Eur. J. Inorg. Chem.* **1998**, *1998*, 221–226.

[43] D. Wendel, T. Szilvási, C. Jandl, S. Inoue, B. Rieger, *J. Am. Chem. Soc.* **2017**, *139*, 9156–9159.

[44] C. Marschner, *Organometallics* **2006**, *25*, 2110–2125.

[45] C. Präsang, D. Scheschkewitz, in *Functional Molecular Silicon Compounds II* (Ed.: D. Scheschkewitz), Springer International Publishing, **2013**, pp. 1–47.

[46] K. Takeuchi, M. Ikoshi, M. Ichinohe, A. Sekiguchi, *J. Am. Chem. Soc.* **2010**, *132*, 930–931.

[47] K. Takeuchi, M. Ikoshi, M. Ichinohe, A. Sekiguchi, *J. Organomet. Chem.* **2011**, *696*, 1156–1162.

[48] K. Takeuchi, M. Ichinohe, A. Sekiguchi, *Organometallics* **2011**, *30*, 2044–2050.

[49] J. I. Schweizer, M. G. Scheibel, M. Diefenbach, F. Neumeyer, C. Würtele, N. Kulminskaya, R. Linser, N. Auner, S. Schneider, M. C. Holthausen, *Angew. Chem. Int. Ed.* **2016**, *55*, 1782–1786.

[50] T. Yamaguchi, M. Asay, A. Sekiguchi, *J. Am. Chem. Soc.* **2012**, *134*, 886–889.

[51] M. Zirngast, M. Flock, J. Baumgartner, C. Marschner, *J. Am. Chem. Soc.* **2008**, *130*, 17460–17470.

[52] H. Schneider, A. Hock, R. Bertermann, U. Radius, *Chem. Eur. J.* **2017**, *23*, 12387–12398.

[53] M. D. Francis, D. E. Hibbs, M. B. Hursthouse, C. Jones, N. A. Smithies, *J. Chem. Soc., Dalton Trans.* **1998**, 3249–3254.

[54] H. Braunschweig, W. C. Ewing, K. Geetharani, M. Schäfer, *Angew. Chem. Int. Ed.* **2015**, *54*, 1662–1665.

[55] K. Tamao, A. Kawachi, in *Adv. Organomet. Chem.* (Eds.: F. Gordon, A. Stone, R. West), Academic Press, **1995**, pp. 1–58.

[56] D. Lutters, C. Severin, M. Schmidtmann, T. Müller, *J. Am. Chem. Soc.* **2016**, *138*, 6061–6067.

[57] A. C. Filippou, O. Chernov, G. Schnakenburg, *Angew. Chem.* **2009**, *121*, 5797–5800.

[58] A. C. Filippou, Y. N. Lebedev, O. Chernov, M. Straßmann, G. Schnakenburg, *Angew. Chem. Int. Ed.* **2013**, *52*, 6974–6978.

[59] Y. Xiong, S. Yao, M. Driess, *J. Am. Chem. Soc.* **2009**, *131*, 7562–7563.

[60] R. S. Ghadwal, H. W. Roesky, S. Merkel, J. Henn, D. Stalke, *Angew. Chem.* **2009**, *121*, 5793–5796.

[61] D. Bläser, R. Boese, M. Göhner, F. Herrmann, N. Kuhn, M. Ströbele, *Z. Naturforsch. Pt B* **2014**, *69*, 71–76.

[62] A. Haaland, *Angew. Chem. Int. Ed. Engl.* **1989**, *28*, 992–1007.

[63] M. W. Stanford, J. I. Schweizer, M. Menche, G. S. Nichol, M. C. Holthausen, M. J. Cowley, *Angew. Chem. Int. Ed.* **2019**, *58*, 1329–1333.

[64] K. Hansen, T. Szilvási, B. Blom, E. Irran, M. Driess, *Chem. Eur. J.* **2015**, *21*, 18930–18933.

[65] S. U. Ahmad, T. Szilvási, S. Inoue, *Chem. Commun.* **2014**, *50*, 12619–12622.

[66] A. C. Filippou, O. Chernov, G. Schnakenburg, *Angew. Chem. Int. Ed.* **2011**, *50*, 1122–1126.

[67] A. C. Filippou, O. Chernov, K. W. Stumpf, G. Schnakenburg, *Angew. Chem. Int. Ed.* **2010**, *49*, 3296–3300.

[68] A. C. Filippou, O. Chernov, B. Blom, K. W. Stumpf, G. Schnakenburg, *Chem. Eur. J.* **2010**, *16*, 2866–2872.

[69] C. Gerdes, W. Saak, D. Haase, T. Müller, *J. Am. Chem. Soc.* **2013**, *135*, 10353–10361.

[70] R. Rodriguez, D. Gau, Y. Contie, T. Kato, N. Saffon-Merceron, A. Baceiredo, *Angew. Chem. Int. Ed.* **2011**, *50*, 11492–11495.

[71] Y. Gao, J. Zhang, H. Hu, C. Cui, *Organometallics* **2010**, *29*, 3063–3065.

[72] R. Rodriguez, D. Gau, T. Kato, N. Saffon-Merceron, A. De Cózar, F. P. Cossío, A. Baceiredo, *Angew. Chem. Int. Ed.* **2011**, *50*, 10414–10416.

[73] R. Azhakar, R. S. Ghadwal, H. W. Roesky, H. Wolf, D. Stalke, *Organometallics* **2012**, *31*, 4588–4592.

[74] A. V. Protchenko, J. I. Bates, L. M. A. Saleh, M. P. Blake, A. D. Schwarz, E. L. Kolychev, A. L. Thompson, C. Jones, P. Mountford, S. Aldridge, *J. Am. Chem. Soc.* **2016**, *138*, 4555–4564.

[75] K. Suzuki, T. Matsuo, D. Hashizume, K. Tamao, *J. Am. Chem. Soc.* **2011**, *133*, 19710–19713.

[76] Y. Xiong, S. Yao, R. Müller, M. Kaupp, M. Driess, *J. Am. Chem. Soc.* **2010**, *132*, 6912–6913.

[77] H.-X. Yeong, H.-W. Xi, Y. Li, K. H. Lim, C.-W. So, *Chem. Eur. J.* **2013**, *19*, 11786–11790.

[78] E. Suzuki, T. Komuro, Y. Kanno, M. Okazaki, H. Tobita, *Organometallics* **2010**, *29*, 5296–5300.

[79] E. Suzuki, T. Komuro, M. Okazaki, H. Tobita, *Organometallics* **2009**, *28*, 1791–1799.

[80] R. Begum, T. Komuro, H. Tobita, *Chem. Lett.* **2007**, *36*, 650–651.

[81] T. Watanabe, H. Hashimoto, H. Tobita, *J. Am. Chem. Soc.* **2006**, *128*, 2176–2177.

[82] E. Suzuki, M. Okazaki, H. Tobita, *Chem. Lett.* **2005**, *34*, 1026–1027.

[83] M. Okazaki, K. A. Jung, K. Satoh, H. Okada, J. Naito, T. Akagi, H. Tobita, H. Ogino, *J. Am. Chem. Soc.* **2004**, *126*, 5060–5061.

[84] M. a. M. Abu-Youssef, S. M. Soliman, M. M. Sharaf, J. H. Albering, L. Öhrström, *CrystEngComm* **2016**, *18*, 1883–1886.

Chapter 3

Phospha-Amidinato Silylenes

Chapter 3 Phospha-Amidinato Silylenes

Unless otherwise stated, all computations in this chapter were carried out by Stephanie Urwin at the University of Edinburgh.

3.1 Introduction

3.1.1 Phosphorus Ligands for Silicon

In recent years there has been a growing interest in the synthesis of highly reactive silicon(II) compounds.[1] Particular attention has been given to silylenes that can react with small molecules such as CO_2, H_2, C-C multiple bonds and E-H or E-E' bonds (where E and E' are any element). These reactions are common fundamental steps in catalysis but are usually limited to transition metals. Replicating these reactions with silicon represents a significant step towards transition-metal-like catalysis.[1]

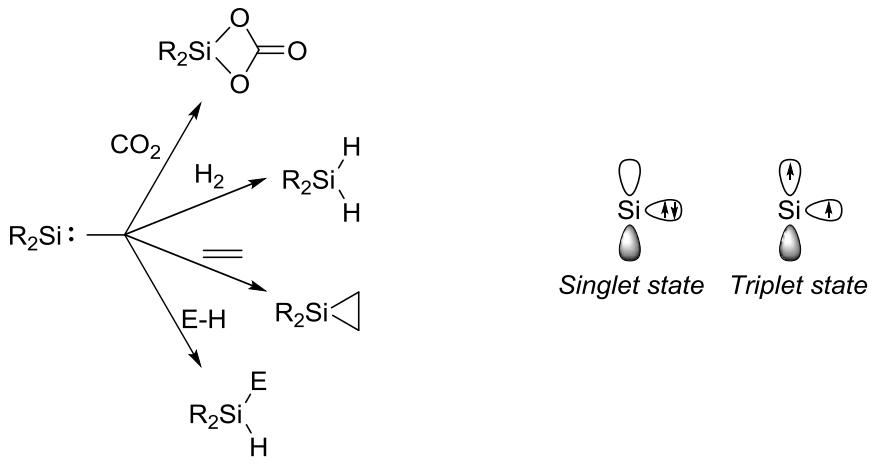

Scheme 3-1 *– Reactions of silylenes with small molecules are fundamentally interesting but the reactivity of silylenes strongly depends on the energy difference between the singlet and triple states: the singlet triple gap.*[1–6]

It has been known for some time that the HOMO-LUMO or singlet-triplet gap (which are inherently linked) of metallylenes correlates with their ability to react with such small molecules.[1–6] A higher lying HOMO and lower lying LUMO makes the triplet state metallylene more accessible and therefore increase the reactivity of the metallylene.

An important study published by Aldridge and co-workers in 2016 highlighted the ability of certain substituents to reduce the singlet-triplet gap of group(IV) metallylene compounds.[6] Their report showed that more electropositive substituent atoms, such as boron, silicon and phosphorus, were able to dramatically reduce the singlet-triplet gap of stannylene, germylene and silylene compounds, relative to more commonly used nitrogen substituents. For example, comparing entries 2 and 5 in Table 3-1, the singlet-triplet gap of the stannylene is reduced by 8.7 kcal·mol^{-1} (37%) upon substituting nitrogen for phosphorus. This is largely due to increased σ-donation from the electropositive substituent which has the effect of raising the energy of the HOMO and therefore decreasing the singlet-triplet gap. Furthermore, in contrast to amine substituents which are capable π-donors, phosphino, silyl and boryl substituents are not capable π-donors. Therefore, phosphino, silyl and boryl substituents give metallylenes with lower energy LUMOs and smaller singlet-triplet gaps.

Table 3-1 *– The calculated singlet triplet gap of theoretical and isolated metallylenes of the type [X][Y]M:, where M = Sn, Ge or Si. [N] = N(SiMe$_3$)(B{DAB}), [B] = B(NMeCH)$_2$, [N'] = N(SiMe$_3$)Me, [Si] = Si(SiH$_3$)$_3$, [P] = PMe$_2$, DAB = (XylNCH)$_2$, Xyl = 2,6-dimethylphenyl.*[6,7]

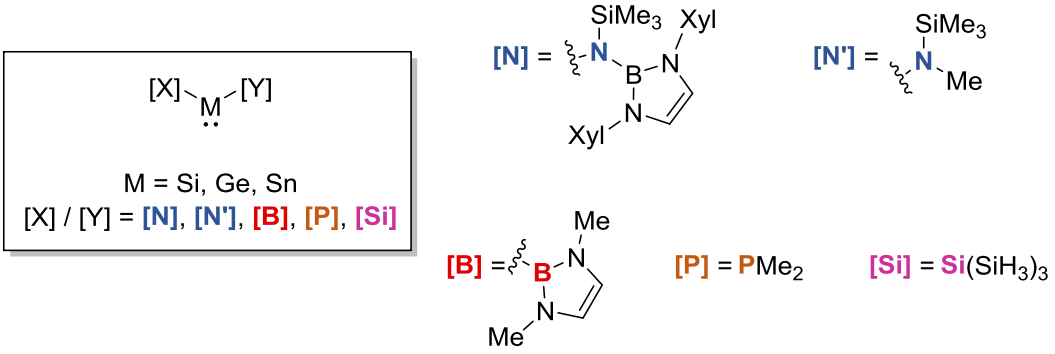

Entry	[X]	[Y]	ΔE_{st} (kcal·mol^{-1})		
			Sn	Ge	Si
1	[N]	[N]	-	-	37.8
2	[B]	[N']	23.5	24.2	21.4
3	[B]	[B]	12.8	10.5	7.8
4	[Si]	[N']	24.5	-	-
5	[Si]	[Si]	14.5	-	-
6	[B]	[P]	14.8	-	-

These results were supported experimentally by the publication of two-coordinate silylenes with silicon and boron substituents that were significantly more reactive than their predecessors, including towards H-H and C-H bonds.[2–4] Some examples are discussed in Chapter 1 of this thesis.

There have been some reports of silicon and boron substituted silylenes but there has been very few reports of phosphorus substituted examples, although some attention has been dedicated to phosphorus substituted disilenes, germylenes and stannylenes.[8–10]

That said, one of the earliest reported isolable silylenes, **3.1**, was coordinated by two phosphinomethanide ligands.[11] However, the reactivity of **3.1** was largely unexplored[12] and the four-coordinate nature of the silicon centre results in significant donation into to the LUMO and therefore raised energy of the LUMO, rendering small molecule activation less likely for this system.

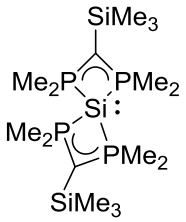

3.1

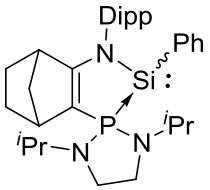

3.2

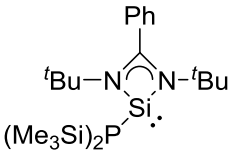

3.3

Scheme 3-2 *– Previously reported silylenes with phosphorus substituents or donors.[11,13,14]*

In 2009, Kato and Bacierado reported the sila-ylide **3.2**[13] which is a phosphine coordinated silylene. The onwards reactivity of **3.2** has led to a wealth of interesting compounds and reactivity, including a silicon(II) hydride,[15] a silanone[16] and reversible activation of ethene.[17] The reactivity of silylene **3.2** supports the hypothesis that phosphorus substituents can lead to interesting reactivity of low-oxidation state silicon, however in this instance the phosphorus acts as a coordinating ligand and not a substituent.

The only other reported example of a phosphorus substituted silylene is amidinato silylene **3.3** reported by Driess and Inoue in 2011.[14] Silylene **3.3** differs from sila-ylide **3.2** in that there is a covalent bond between phosphorus and silicon, as opposed to dative bond in **3.2**. However, the major focus of their study was the formation of an important Si-P analogue of cyclobutadiene and not its reactivity with small molecules.

The reactivity of silylene **3.2** strongly suggests that phosphorus substituents can allow access to silylenes with very interesting reactivity. Furthermore, the three-coordinate nature of **3.2** and lability of the donor atom provide extra stabilisation of the Si(II) species.[17] This could aid reductive elimination to silylene **3.2**, therefore, three-coordinate silylenes with phosphorus substituents and a labile donor ligand should be targeted.

3.1.2 Phospha-Amidinate Ligands

Amidinate and guanimidate ligands are well-known in main group and transition metal chemistry,[18] and amidinato silylenes are thoroughly discussed in the introduction to this thesis.

Phospha-amidinate ligands are analogous to amidinate ligands. Scheme 3-3 shows examples of amidinate, guanidinate and phospha-amidinate ligands. Phospha-amidinate coordination to silicon(II) could lead to silylenes with interesting reactivity but phospha-amidinates have not been widely explored, partly due to their more challenging synthesis. Only recently was a straightforward preparation of phospha-amidinates reported.[19]

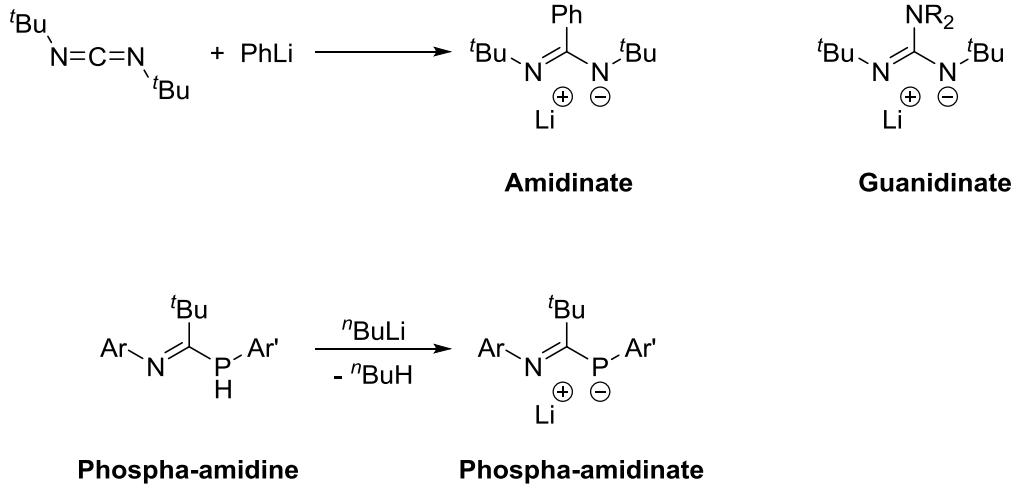

Scheme 3-3 *– Amidinate, guanidinate and phospha-amidinate ligands are structurally related. Amidinate ligands are often prepared directly while phospha-amidinates are usually prepared by deprotonation of phospha-amidines.*

The first phospha-amidine was reported by Schmidt over 40 years ago (Scheme 3-4).[20] He reacted a silylphosphine with an imidoyl chloride to prepare the phospha-amidine through $SiMe_3Cl$ elimination. However, the procedure was largely limited to tertiary phosphines.

In 2004, Boeré reported that a simple primary phosphine could react with an imidoyl chloride to directly synthesise the phospha-amidine but only after four days refluxing in xylenes.[21] Cui later reported that phospha-amidines could be prepared from a lithium phosphanide and an imidoyl chloride.[22]

However, the real breakthrough was the versatile synthesis reported by Slootweg and Lammertsma in 2014.[19] They showed that converting imidoyl chlorides to nitrilium triflates activated them for nucleophilic attack by phosphines (Scheme 3-4, bottom). This method is general for a range of phosphines and imidoyl chlorides substituents and therefore provides a simple method for fine-tuning the ligand.

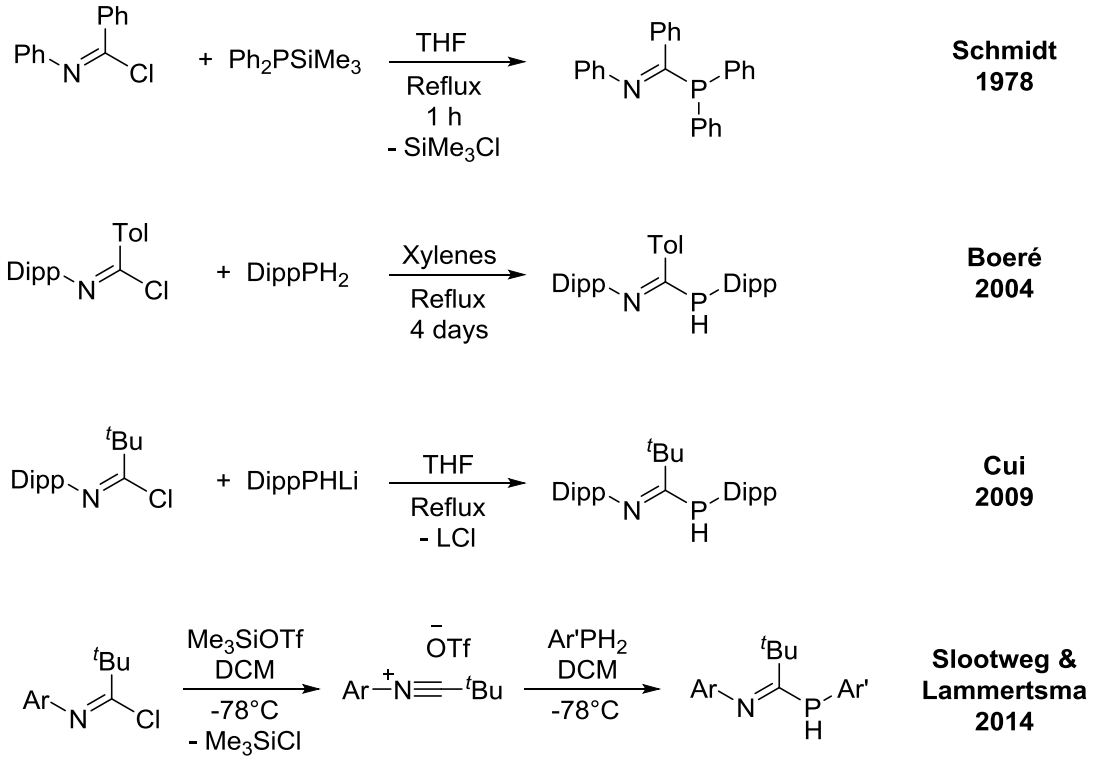

Scheme 3-4 *– Some reported methods for the preparation of phospha-amidines.[19–22]*

Phospha-amidinates are generated from phospha-amidines by simple deprotonation by ^{n}BuLi. This is in contrast to amidinate ligands which are often synthesised directly from an aryl lithium and a carbodiimide (see Scheme 3-3).[23]

3.2 Project Aims

The aims of this project are to investigate the use of phospha-amidinate ligands in silicon chemistry. A series of novel phospha-amidinate ligands will be synthesised and coordinated to silicon(IV) chlorides. Reductions and reductive dehydrochlorinations will be tested in order to generate new silicon(II) complexes.

Furthermore, the new phospha-amidinate ligands will be coordinated to other main group elements as a proof of concept of their general use.

3.3 Novel Phospha-Amidinate Ligands

Nitrilium triflate **3.4** was prepared according to literature procedures.[19] The reaction of pivaloyl chloride with 2,4,6-trimethylaniline ($MesNH_2$) affords the corresponding amide, which is converted to the imidoyl chloride through reflux in thianyl chloride ($SOCl_2$). The reaction with trimethylsilyl triflate (Me_3SiOTf) affords nitrilium **3.4** in an overall yield of 89% after three steps (Scheme 3-5).

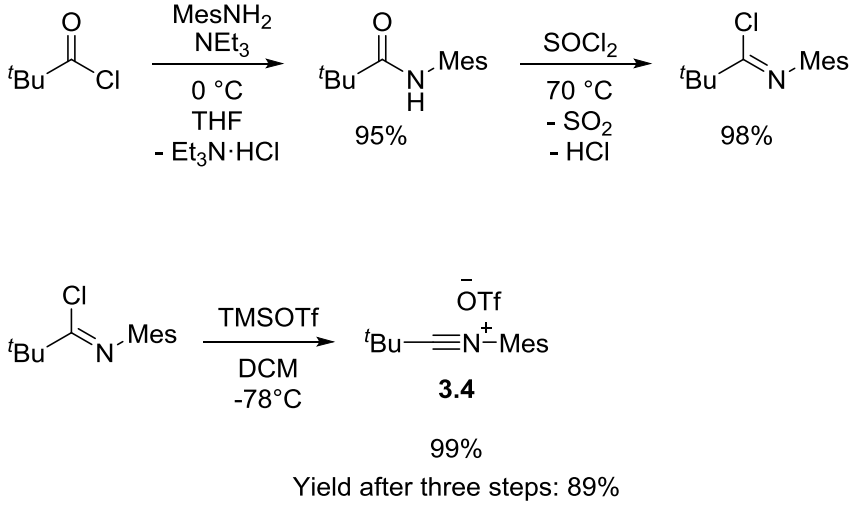

Scheme 3-5 *– The preparation of nitrilium* ***3.4*** *which can be used as an imine synthon in the synthesis of phospha-amidines. Mes = 2,4,6-trimethylphenyl.*[19]

Nitrilium triflate **3.4** was treated with three different primary phosphines with varying steric bulk to prepare a set of phospha-amidinate ligands. The primary phosphines were 2,4,6-trimethylphenylphosphine ($MesPH_2$), 2,4,6-tri*iso*propylphenylphosphine ($TippPH_2$) and

2,4,6-tri*tert*butylphosphine (Mes*PH_2), each of which were synthesised according to literature procedures in good yields.[24,25]

The reaction of $MesPH_2$ with nitrlium triflate **3.4** in the presence of triethyl amine (NEt_3) gave phospha-amidine **3.5** in 77% yield after crystallisation from pentane. The ^{31}P NMR spectrum of phospha-amidine **3.5** shows a doublet at δ −80.6 with a $^1J_{PH}$ coupling constant of 246 Hz. The ^1H revealed an associated P-*H* resonance at δ 4.91. The large coupling P-H coupling constant indicates phospha-amidine **3.5** adopts a phosphino-imine structure, as shown in Scheme 3-6.

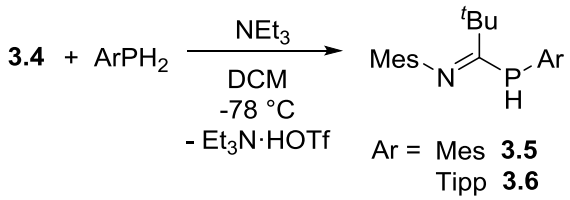

***Scheme 3-6** – The preparation of phospha-amidines **3.5** and **3.6** from **3.4** and primary phosphines. Mes = 2,4,6-trimethylphenyl, Tipp = 2,4,6-tri*isopropylphenyl.

Phospha-amidine **3.6** with the bulkier Tipp substituent was prepared by the same method in 57% yield. NMR spectroscopy reveals a doublet in the ^{31}P spectrum at δ −88.9 and a doublet in the ^1H spectrum at δ 5.03 with a $^1J_{HP}$ coupling constant of 251 Hz.

The reaction of nitrilium triflate **3.4** with Mes*PH_2 was somewhat less straightforward. Three new resonances were observed in the ^{31}P NMR (Figure 3-1), a doublet at δ 98.5 (J_{PH} = 18 Hz), a singlet at δ 80.1, and another doublet at δ −53.6 (J_{PH} = 253 Hz). The ^{31}P signals at δ 98.5 and δ 80.1 are in the region typical for phospha-alkenes while the signal at δ −53.6 is similar to that for **3.5** and **3.6** and is typical for a secondary phosphine.

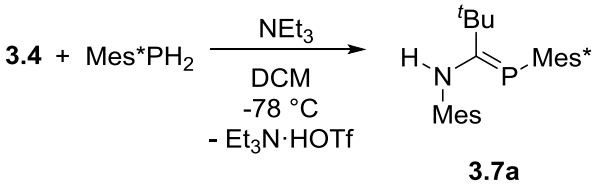

***Scheme 3-7** – The preparation of phospha-amidine **3.7** from nitrlium triflate **3.4** and Mes*PH_2. Mes* = 2,4,6-tritertbutylphenyl.*

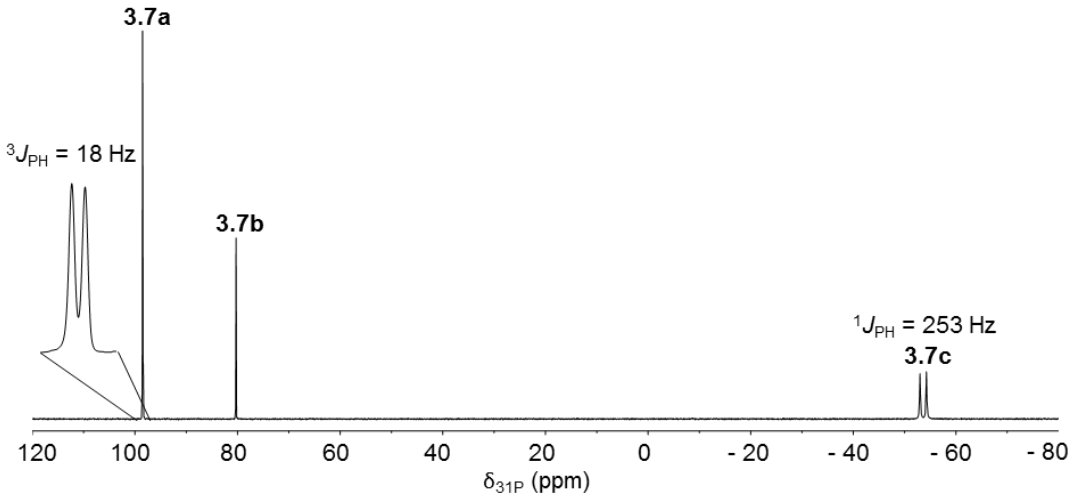

***Figure 3-1** – The ^{31}P NMR spectrum of the mixture of tautomers observed for phosph-amidine **3.7** when single crystals of **3.7a** are dissolved in C_6D_6..*

Crystallisation from pentane afforded pure crystals of phospha-amidine **3.7a** which has a different structure to phospha-amidines **3.5** and **3.6**. The solid-state structure of **3.7a** is shown in Figure 3-2 and indicates an amino phospha-alkene. The P=C bond distance of 1.738(2) Å is typical of a P=C double bond, while the C-N distance of 1.375(2) Å supports a single bond.

When single crystals of **3.7a** are dissolved in C_6D_6, ^{31}P NMR spectroscopy reveals the same three ^{31}P resonances shown in Figure 3-1.

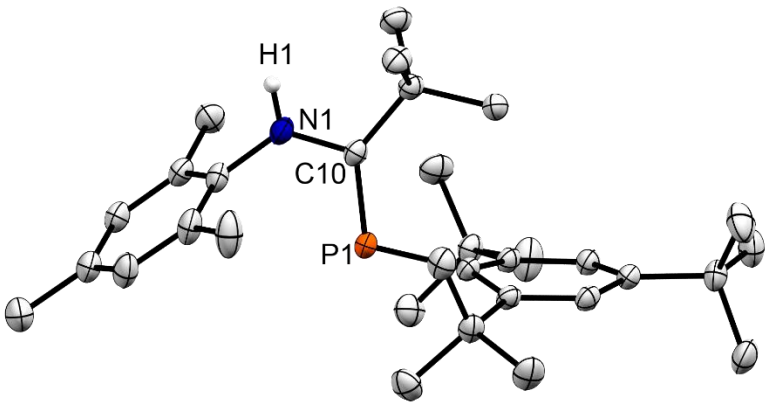

***Figure 3-2** – The solid state structure of **3.7a**. Hydrogen atoms other than H1 omitted for clarity. Thermal ellipsoids set to 50% probability. Selected bond distances (Å) and angles (°): P1-C19 1.738(2), N1-C19 1.375(2), P1-C19-N1 114.3(1), C19-P1-C1 109.50(7), C19-N1-C24 124.3(1).*

Calculations performed by Dr Stephanie Urwin showed there are four tautomers of **3.7** which lie close in energy.[26] A thorough computational investigation identified **3.7a**, **3.7b** and **3.7c** as the three tautomers present in solution, shown in Scheme 3-8. Furthermore, chemical shift and coupling constant calculations allowed assignment of the ^{31}P resonances as shown in Figure 3-1.

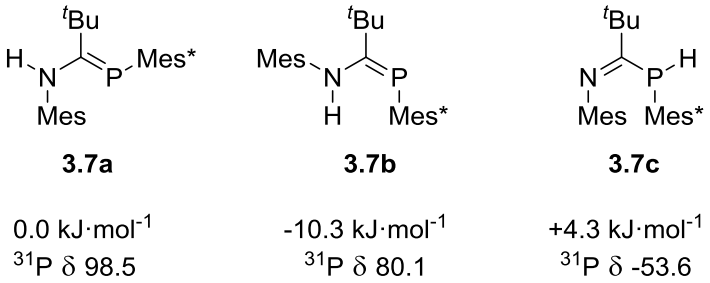

Scheme 3-8 *– The three tautomers of phospha-amidine* ***3.7*** *present in solution, as calculated by Urwin.[26] Only* ***3.7a*** *was observed in the solid state.*

When the mixture of tautomers is treated with ^{n}BuLi, a single broad resonance is observed in the ^{31}P NMR spectrum at δ 25.3 which is assigned to phospha-amidinate lithium complex **3.8**. This supports the hypothesis that the three resonances observed for **3.7** are interconvertible tautomers.

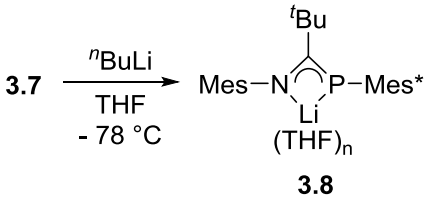

Scheme 3-9 *– Lithiation of a mixture of tautomers of* ***3.7*** *gives a single compound,* ***3.8****.*

3.4 Phospha-Amidinato Silanes

Amidinato silylenes are usually synthesised by reduction or dehydrochlorination of Si(IV) precursors. Therefore, phospha-amidines **3.5** – **3.7** were lithiated using ^{n}BuLi and reacted with trichlorosilane and tetrachlorosilane in order to generate silicon(IV) precursors for reduction.

3.4.1 Dichlorosilanes 3.10 and 3.13

Phospha-amidine **3.5** was reacted with ^{n}BuLi at −78 °C before warming to room temperature in order to ensure complete conversion to lithiate **3.9**. Addition of *in situ* generated **3.9** to a solution of trichlorosilane afforded dichlorosilane **3.10** which could be isolated in 82% yield by crystallisation from toluene.

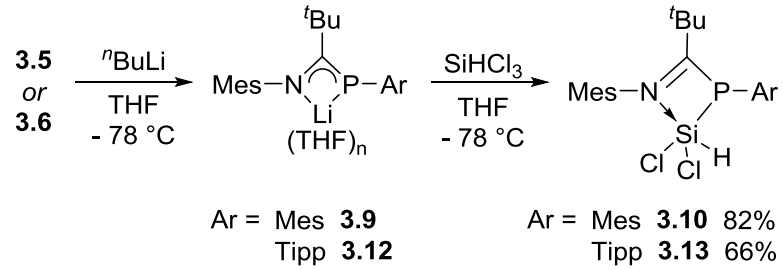

Scheme 3-10 *– The preparation of silicon(IV) complexes* ***3.10*** *and* ***3.13*** *starting from phospha-amidines* ***3.5*** *and* ***3.6****. Mes = 2,4,6-trimethylphenyl, Tipp = 2,4,6-triisopropylphenyl.*

The ^{31}P NMR spectrum of silane **3.10** showed a new resonance at δ −7.45 with $^{1}J_{PSi}$ coupling of 54 Hz. A corresponding doublet was observed in the ^{29}Si{^{1}H} spectrum at δ −67.6. The ^{1}H revealed a new Si-*H* resonance at δ 6.52 with $^{1}J_{HSi}$ coupling of 340 Hz. The ^{29}Si signal is comparable to that reported for the amidinato silane **3.11** at δ −96.8.[27]

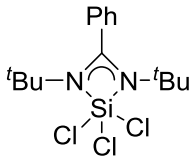

3.11

Scheme 3-11 *– Previously reported amidinato silane* ***3.11****.*

Samples of silane **3.10** were shown to be pure by elemental analysis, however ^{1}H and ^{31}P NMR consistently showed *ca*. 5-10% phospha-amidine **3.5** in the isolated product. This was a recurring issue during the project and is attributed to the weak P-Si bond being extremely susceptible to hydrolysis by trace water, even under Schlenk conditions.

The solid-state structure of silane **3.10** is shown in Figure 3-3. The C10-N1 bond distance of 1.306(3) Å is indicative of a relatively long double bond, while the C10-P1 distance of 1.833(3) Å indicates a single bond. The C1-N1 bond distance is similar to the shorter C-N

distance in amidinato silane **3.11** which has two C-N distances of 1.309(4) Å and 1.367(4) Å. The sum of the angles around N1 and P1 in **3.10** are 359.8(4)° and 313.0(2)°, respectively (in amidinato silane **3.11**, both nitrogen atoms are completely planar). This supports the proposed structure of **3.10** with a C=N double bond and a C-P single bond. Therefore **3.10** is best described as an imine coordinated phosphino silane. This is further supported in the solution state by the phosphorus chemical shift of δ –7.6 ppm, suggesting sp^3 hybridisation at phosphorus, and the small $^1J_{CP}$ coupling constant of 28.5 Hz indicating a C-P single bond.

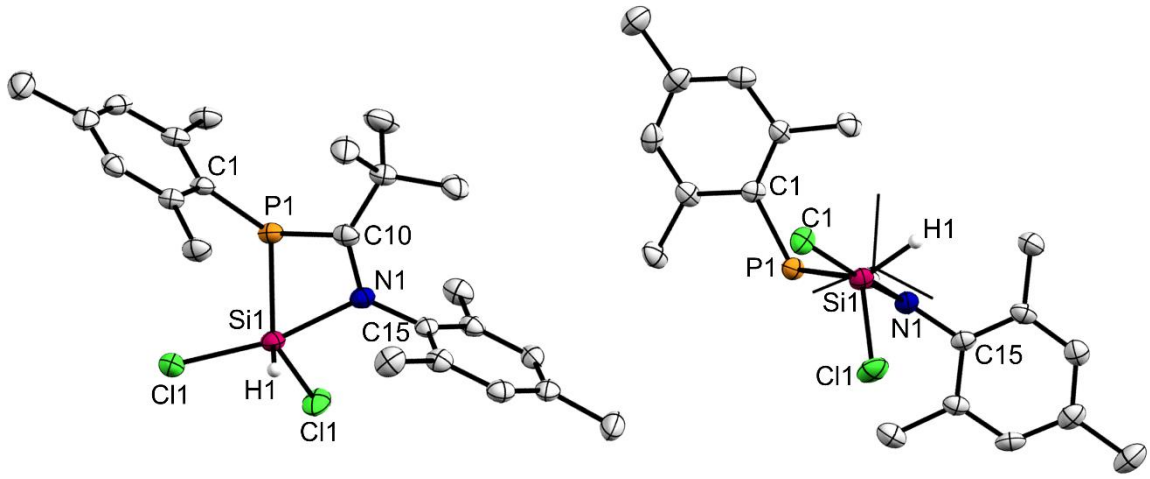

Figure 3-3 *– Two perspectives of the crystal structure of silane **3.10** showing the geometry around P1, N1 and Si1. Thermal ellipsoids drawn at 50% probability, all hydrogen atoms other than H1 omitted for clarity. Selected distances (Å) and angles (°): C10-P1 1.833(3), P1-Si1 2.2386(10), N1-C10 1.306(3), N1-Si1 2.086(2), Σ∠N1 359.8(4), Σ∠P1 313.0(2).*

Silane **3.13** was prepared by an identical method starting from Tipp phospha-amidine **3.6**. The ^{31}P and ^{29}Si NMR spectra reveal a similar structure to silane **3.10** with a new ^{31}P resonance at δ −13.2 and a new ^{29}Si resonance at δ −65.6, with $^1J_{PSi}$ coupling of 58 Hz. A new Si-H resonance is observed in the ^{1}H NMR at δ 6.34 with $^1J_{HSi}$ coupling of 336 Hz. Crystallisation from toluene afforded the product **3.13** in 66% yield which was pure according to elemental analysis and NMR.

Single bond coupling constants between ^{1}H and ^{29}Si are usually below 250 Hz, for example in silanes discussed in Chapter 2 of this thesis. The $^1J_{HSi}$ coupling constants in silanes **3.10** and **3.13** are unusually large at 340 Hz and 336 Hz, respectively. These values were confirmed by

^{1}H-^{29}Si correlation spectroscopy, as shown in Figure 3-4.The $^{1}J_{HSi}$ coupling of the analogous amidinato dichloro silane was not reported.

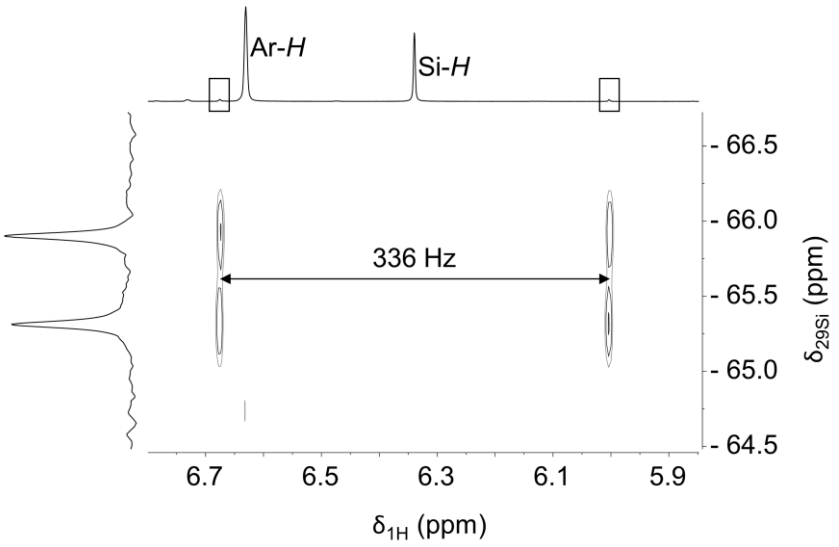

Figure 3-4 *– Expansion of the ^{1}H-^{29}Si HMBC of **3.13** showing large $^{1}J_{HSi}$ coupling of 336 Hz. Recorded on an 11.7 T, 500 MHz spectrometer.*

3.4.2 Trichlorosilanes 3.14 and 3.15

The reaction of lithiates **3.9** and **3.12** with silicon tetrachloride afforded trichlorosilanes **3.14** and **3.15**.

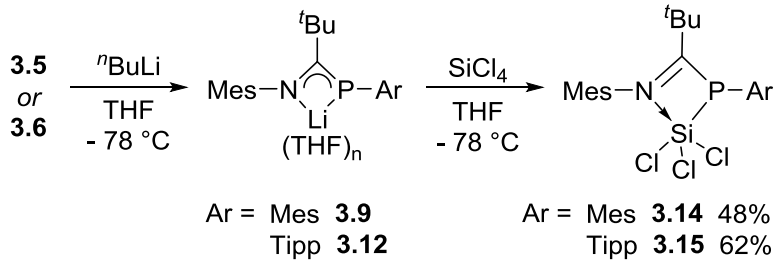

Scheme 3-12 *– The preparation of silicon(IV) complexes **3.14** and **3.15** starting from phospha-amidines **3.5** and **3.6**. Mes = 2,4,6-trimethylphenyl, Tipp = 2,4,6-triisopropylphenyl.*

Silane **3.14** was identified by ^{1}H, ^{29}Si and ^{31}P NMR spectroscopy. The ^{29}Si NMR reveals a new singlet at δ −37.2 while a new ^{31}P resonance is found at δ 8.78. The ^{29}Si signal is shifted downfield compared with dichlorosilane **3.10**, as would expected given the additional chloride substituent.[23,27] The $^{1}J_{PSi}$ coupling constant is 29 Hz which is somewhat smaller than

for **3.10** (54 Hz). This suggests a longer P-Si bond, consistent with reduced electron density due to an additional electron withdrawing chloride on silicon.

Similar trends are observed for trichlorosilane **3.15** which shows new ^{29}Si and ^{31}P resonances at δ −42.6 and δ 8.8. Again, the downfield shift relative to dichlorosilane **3.13** is attributed to the additional chloride on silicon. Equally, the $^{1}J_{PSi}$ coupling of 33 Hz is considerably smaller than that observed for **3.13** (58 Hz).

The structure of trichlorosilane **3.15** was confirmed by single crystal X-ray diffraction. The solid-state structure of **3.15** is shown in Figure 3-5. The bond distances and angles of **3.15** are very similar to dichlorosilane **3.10**. There is clearly a double bond between the nitrogen and carbon atoms in the phospha-amidinate ligand with an N1-C16 distance of 1.301(4) Å. The P1-C16 distance of 1.828(3) Å is typical of a P-C single bond. Again, this is further supported by the sum of the bonding angles around N1 and P1 which are 359.7(4)° and 315.8(2)°, respectively.

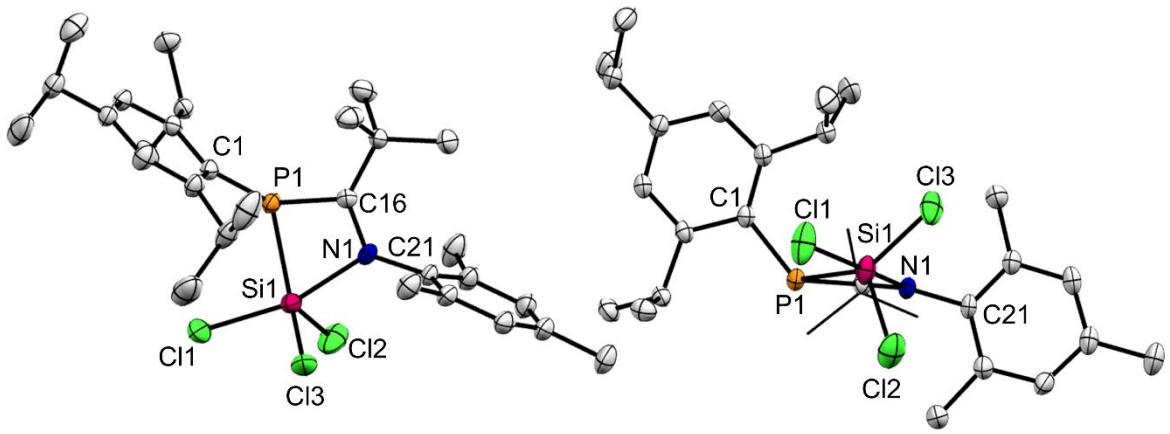

Figure 3-5 *– Two perspectives of the crystal structure of silane* ***3.15*** *showing the geometry around P1, N1 and Si1. Thermal ellipsoids drawn at 50% probability, hydrogen atoms omitted for clarity. Selected distances (Å) and angles (°): C16-P1 1.828(3), P1-Si1 2.2393(11), N1-C16 1.301(4), N1-Si1 2.073(3), Σ∠N1 359.7(4), Σ∠P1 315.78(19).*

3.5 Phospha-Amidinato Silylenes

With silanes **3.10** – **3.15** in hand, low-oxidation state silicon species were targeted by reduction and reductive dehydrochlorination.

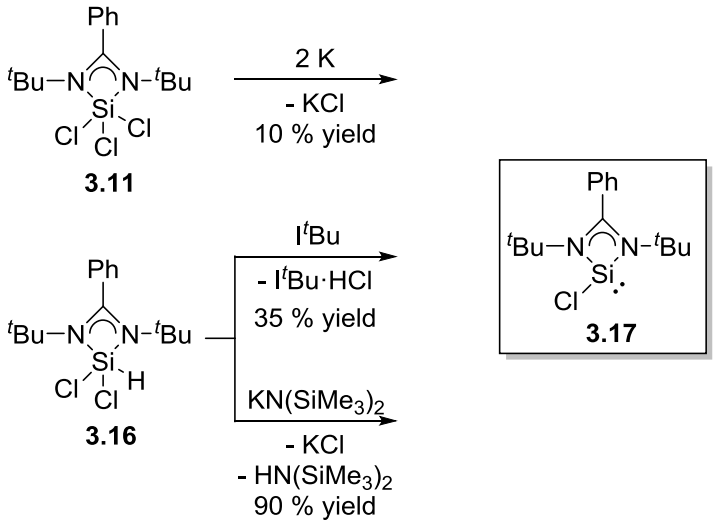

Scheme 3-13 *– The reductive dehydrochlorination from amidinato silanes* ***3.16*** *yields* ***3.17*** *in much higher yields than the reudction from trichlorosilane* ***3.11****. I*^{t}*Bu = 1,3-diterbutylimidazol-2-ylidene.*[23,27]

Although reduction by alkali metals is still the most common method of synthesising low oxidation state silicon, the reduction of amidinato silane **3.11** provided the silylene in only 10% yield (Scheme 3-13).[23] In contrast, the reductive dehydrochlorination by an NHC led to 35% yield and using the amide base $LiN(SiMe_3)_2$ gave an even higher yield of 90%.[27]

Dichlorosilanes **3.10** and **3.13** were treated with a variety of bases and trichlorosilanes **3.14** and **3.15** were treated with alkali metal reducing agents.

3.5.1 Reduction of 3.15

Initially, trichlorosilane **3.15** and two equivalents of potassium graphite (KC_8) were stirred In THF at −78 °C. The reaction was allowed to slowly warm to room temperature. The crude ^{31}P NMR spectrum showed a large amount of unreacted **3.15** and a significant amount of free phospha-amidine **3.6**. The only major new resonance appeared as a doublet at δ −114.6 with coupling of 7 Hz. This resonance accounted for 28% of the reaction mixture according to ^{31}P NMR integration. When using excess KC_8 the same signals were observed in a similar ratio.

The new resonance in the ^{31}P NMR at −114.6 has no observable silicon satellites and there was no corresponding resonance in the ^{29}Si NMR. The small coupling constant corresponds to a small ^{31}P-^{1}H coupling, as confirmed by the observation of the same signal as a singlet in the $^{31}P\{^{1}H\}$ NMR spectrum.

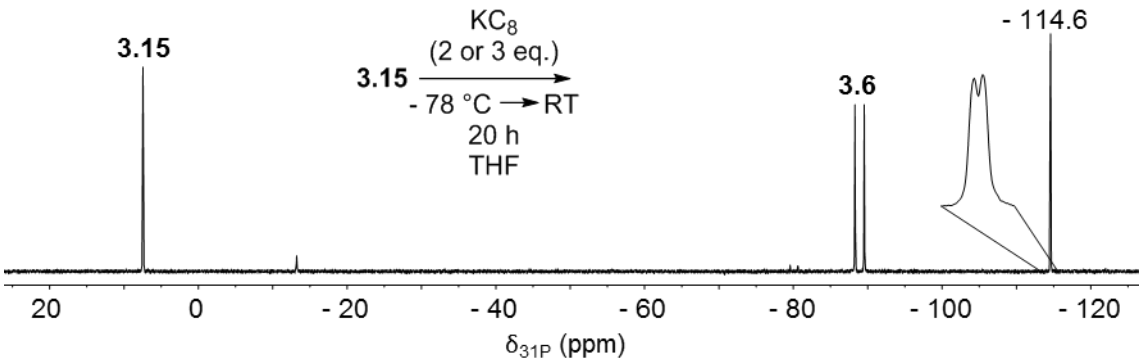

Figure 3-6 *– ^{31}P NMR of the reaction of **3.15** with 2 or 3 equivalents of KC_8*

The reduction was also attempted using lithium naphthalenide ($LiC_{10}H_8$). However, these reactions showed no new signals in the ^{31}P NMR, only silane **3.15** and phospha-amidine **3.6** were observed.

3.5.2 Reductive Dehydrochlorination of 3.10 and 3.13

The reaction of silane **3.10** with two equivalents of potassium hexamethyldisilazide ($KN(SiMe_3)_2$) or sodium hexamethyldisilazide ($NaN(SiMe_3)_2$) affords three-coordinate silylene **3.18** through a substitution reaction and reductive dehydrochlorination, not necessarily in that order. Amide bases are known to perform nucleophilic substitution reactions with silicon chlorides[28] and they are also known dehydrochlorinating reagents.[27]

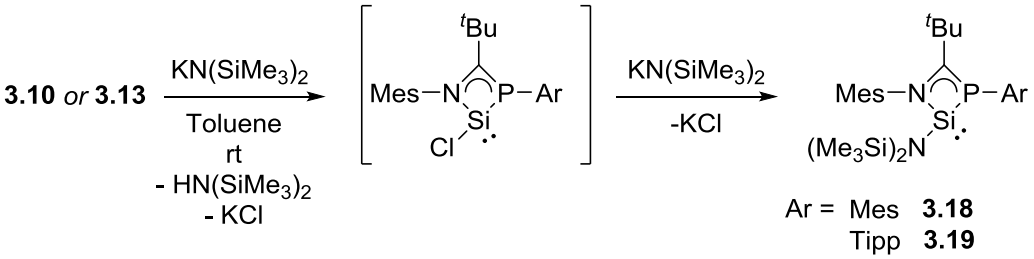

Scheme 3-14 *– The preparation of unisolable silylenes **3.18** and **3.19** from silanes **3.10** and **3.13**. Mes = 2,4,6-trimethylphenyl, Tipp = 2,4,6-triisopropylphenyl.*

When silane **3.10** was treated with just one equivalent of $KN(SiMe_3)_2$, **3.18** was produced in 50% yield while 50% of **3.10** remains unreacted. This indicates that the second step is much faster than first, whether it is dehydrochlorination or substitution.

Silylene **3.18** is evidenced by a new resonance in the ^{31}P NMR spectrum at δ −45.8 with a $^{1}J_{PSi}$ coupling constant of 69 Hz. The ^{1}H NMR spectrum shows a new singlet resonance for two $SiMe_3$ groups at δ 0.30 and a new singlet resonance for the ^{t}Bu protons at δ 0.95, which integrate in a ratio of 18:9. Five signals are observed for the aliphatic mesityl protons in a ratio of 6:3:3:3:3, indicating that one mesityl substitutent is unable to rotate freely on the NMR timescale, probably due to the increased steric bulk of the $N(SiMe_3)_2$ group.

Silylene **3.18** could be consistently generated in greater than 85% conversion. However, rapid decomposition led to formation of large quantities of phospha-amidine **3.5**, perhaps due to the weakness of the Si-P bond, as mentioned above. Silylene **3.18** was never isolated in greater than 90% purity and was only ever isolated as a viscous oil, presumably due to the impurity.

Increasing the steric bulk around the silicon-phosphorus bond could provide kinetic stabilisation. Therefore, Tipp silane **3.13** was subjected to the same conditions. A new ^{31}P resonance was observed at δ −47.2 which was assigned to silylene **3.19** by comparison with **3.18**. However the same issues were encountered and **3.19** could not be separated from *ca.* 10% phospha-amidine **3.6**.

3.5.3 A Four Coordinate Silylene

Silane **3.10** was reacted with an alternative amide base, lithium di*iso*propylamide ($LiN^{i}Pr_2$, LDA). The reaction of **3.10** with two equivalents of LDA gave two new signals in the ^{31}P NMR, a sharp singlet at δ −17.7 and an extremely broad singlet at δ −26.6. Monitoring of the reaction mixture showed slow disappearance of the signal at δ −17.7 with concomitant growth of the signal at δ −26.6 over a number of hours (Figure 3-7).

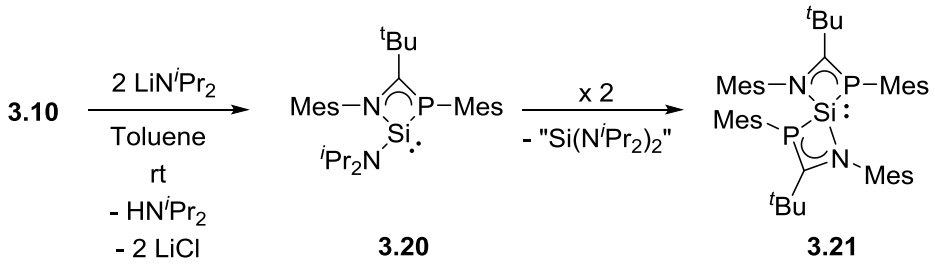

Scheme 3-15 *– The preparation of silylene* ***3.21*** *from* ***3.10*** *and LDA. Mes = 2,4,6-trimethylphenyl.*

The ^{31}P signal at δ −26.6 is assigned to silylene **3.21**. A corresponding broad singlet observed in the ^{1}H NMR spectrum at δ 1.03 is assigned to the ^{t}Bu protons. Six broad resonances are observed for the aliphatic mesityl protons between δ 2.95 and δ 2.10, indicating slow rotation on the NMR timescale, consistent with two sterically encumbering phospha-amidinate ligands.

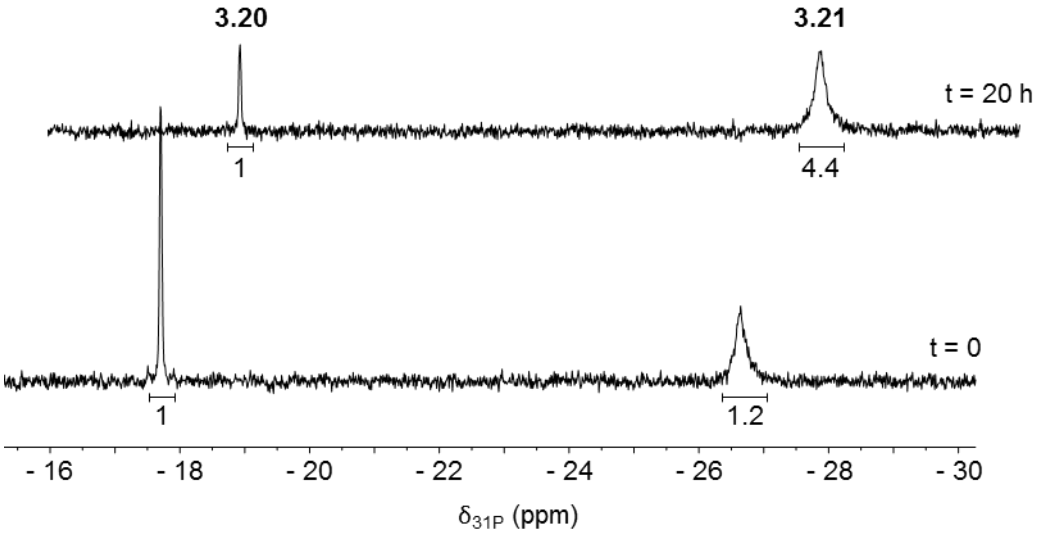

***Figure 3-7** – ^{31}P NMR initially and after 20 h of the reaction of **3.21** with LDA in toluene at room temperature. Numbers below resonances are relative intergrals.*

The signal at δ −17.7 is tentatively assigned to intermediate silylene **3.20** which could be formed in a similar way to silylene **3.18**, however silylene **3.20** was not isolated and was only ever observed as an intermediate in the formation of four-coordinate silylene **3.21**.

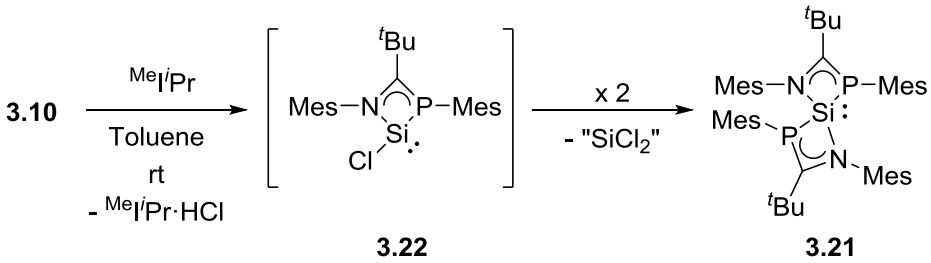

***Scheme 3-16** – The preparation of silylene **3.21** from **3.10** and ^{Me}I^{i}Pr. Mes = 2,4,6-trimethylphenyl.*

Four-coordinate silylene **3.21** was also observed as the major product in the reaction of silane **3.10** with the NHC 1,3-di*iso*propyl-4,5-dimethylimidazol-2-ylidene (^{Me}I^{i}Pr). Again, a short lived

intermediate was observed by ^{31}P NMR at δ −36.9. The intermediate could be silylene **3.22** or its dimer, however the potential by-product, dichlorosilylene, could not be trapped by the addition of excess NHC.[29]

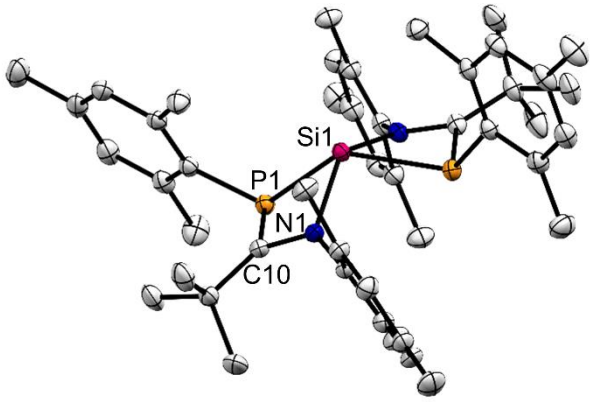

Figure 3-8 *– Solid-state structure structure of* ***3.21*** *showing the full independent molecule (left) and the asymmetric unit (right). Hydrogen atoms omitted for clarity, thermal ellipsoids drawn at 50% probability. Selected distances (Å) and angles (°): C10-P1 1.7772(15), P1-Si1 2.4202(4), N1-C10 1.3470(18), N1-Si1 1.9074(13), Σ∠N1 359.92(17), Σ∠P1 310.22(10), Σ∠Si1 321.90(8).*

Crystals of four coordinate silylene **3.21** suitable for X-ray diffraction were grown from cold toluene. The solid-state structure of **3.21** is shown in Figure 3-8. The silicon, Si1, adopts a distorted seesaw geometry. The stereoactive lone pair is clearly indicated by the sum of angles around silicon at 321.90(8)°. As for **3.10** and **3.15**, the short C-N bond length of 1.3470(18) suggests a C=N double bond which is further supported by the sum of angles around nitrogen at 359.92(17)° indicating almost complete planarity and sp^2 hybridisation. Accordingly, the C-P bond distance of 1.7772(15) is indicative of a single bond. The angles around phosphorus sum to 310.22° which suggests the presence of an uncoordinated lone pair. Therefore, **3.21** is best described as an imine coordinated phospha-silylene, similar to silanes **3.10** and **3.15**. However, the broad signals observed by NMR spectroscopy suggest the situation is more complex in solution.

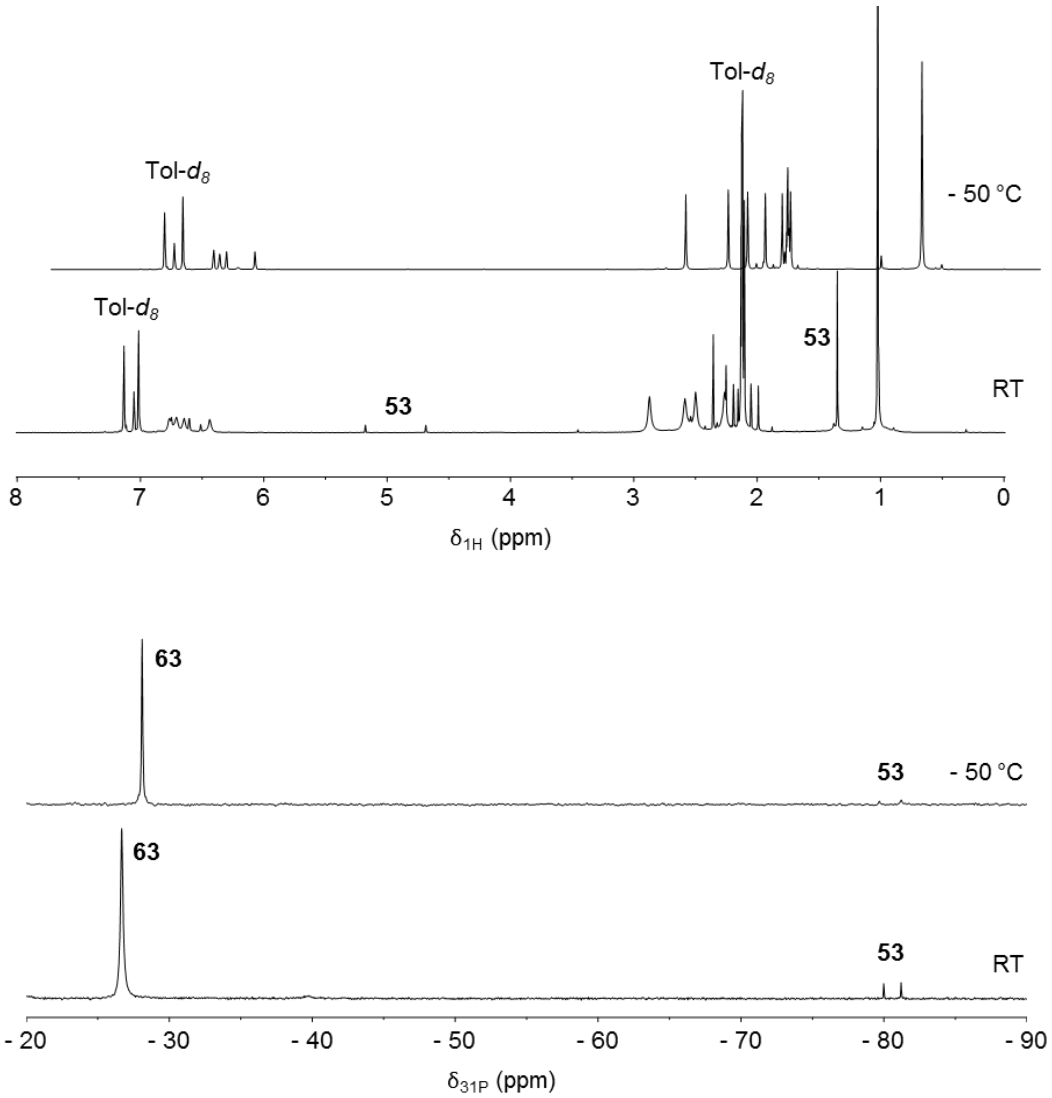

***Figure 3-9** – ^{1}H and ^{31}P NMR of **3.21** at RT and – 50 °C.*

As mentioned, the ^{1}H and ^{31}P NMR spectra of silylene **3.21** are extremely broad (Figure 3-9) and no ^{29}Si signal was observed. Cooling a sample of **3.21** decreases the line width to give sharper spectra, as shown in Figure 3-9.

The broad signals observed by NMR indicates slow exchange on the NMR timescale. The ^{1}H NMR spectrum recorded at −50 °C, shown in Figure 3-9, reveals six aliphatic methyl resonances with equal integrals. This indicates a four-coordinate symmetrical species, as observed in the solid state. At higher temperatures, the broad peaks suggest a different species becomes accessible. By comparison with bis(amidinato)silylene **3.23**, a three coordinate tautomer is one plausible explanation.

Bis(amidinato)silylene **3.23** was proven to be three-coordinate in the solid-state by X-ray crystallography, while a four-coordinate silylene was the favoured tautomer in solution.[30] This was supported by solid-state NMR and variable temperature solution-state NMR. This supports that the equivalent three-coordinate tautomer of **3.21** could be present in solution.

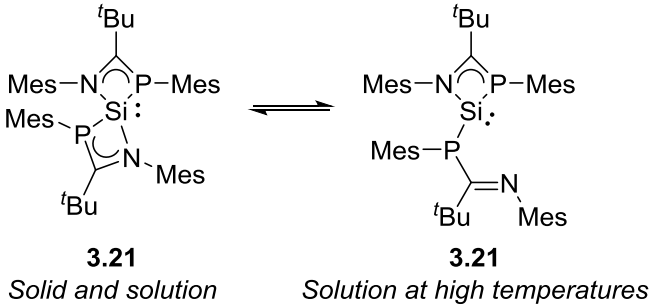

3.21 *Solid and solution* — **3.21** *Solution at high temperatures*

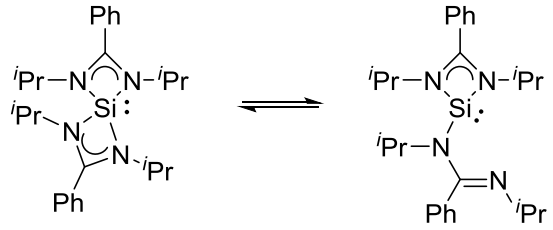

3.23 *Solution* — **3.23** *Solid*

Scheme 3-17 *– Tautomers of **3.21** and **3.23**[30] in solution and the solid state.*

3.5.4 Reactivity of Silylene 3.21

3.5.4.1 Small Molecules

Silylene **3.21** was treated with a range of small molecules in order to investigate its reactivity.

1-Hexene Phenylacetylene Triethylsilane Triphenylsilane

Scheme 3-18 *– Some common small molecules which can potentially react with silylenes. See Scheme 3-1.*

Amidinato silylenes are known to react with acetylenes,[27] however when **3.21** was treated with phenylacetylene no reaction was observed, even at 50 °C. Above 50 °C the

decomposition of **3.21** is rapid. Heating a sample of **3.21** with phenylacetylene gives a mixture of products very similar to when **3.21** is heated independently.

Some donor-coordinated silylenes are able to react with alkenes, including the phosphine stabilised silylene **3.2**, which reacts reversibly.[17,31] However, **3.21** did not react with 1-hexene at room temperature and only decomposition was observed at higher temperatures.

Early transient silylenes were often trapped by their reaction with E-H bonds such as the Si-H bond of triethylsilane.[32] The phosphino substituent of **3.21** should increase its reactivity towards such systems compared with amino silylenes however, no reaction occurred with triphenyl- or triethylsilane.

As discussed, the reactivity of silylenes has often been related to their singlet-triplet or HOMO-LUMO gaps.[1–6] The coordinating ligands on silylene **3.21** act to raise the energy of the LUMO and greatly increase the singlet triplet gap. This likely counters any effect of the phosphorus substituents and explains the low reactivity of **3.21**.

3.5.4.2 Transition Metal Complexes

The reactivity of silylene **3.21** with transition metals was also investigated. Cleavage of the weak Si-P bonds could lead to an N-Si(II)-N pincer complex which would be the first ligand of this type. Electron rich metals Pd(0), Ni(0) and Au(I) were investigated as π-back donation could act to stabilise the low-valent silylene centre, as shown in Figure 3-10.

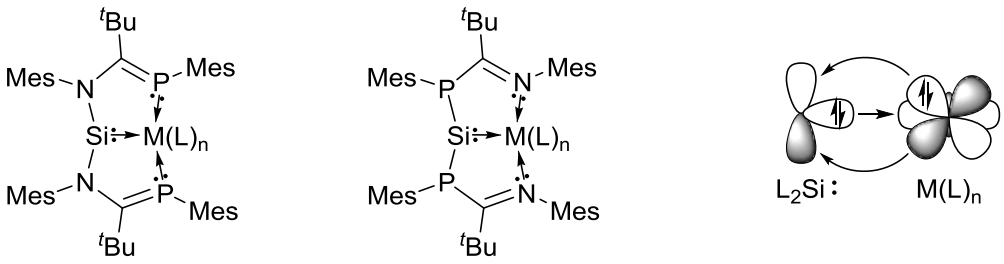

Figure 3-10 *– Potential complexes formed in the reactions of electron rich transition metals with* ***3.21****. Electron rich metal centres will be required to stabilise the singlet state of the silylene by π-back donating into the empty p orbital.*

Tetrakis(triphenylphosphine) palladium(0), $Pd(PPh_3)_4$, is a readily available source of palladium(0). The reaction of silylene **3.21** with $Pd(PPh_3)_4$ at room temperature gave one new

resonance in the ^{31}P NMR spectrum at δ 48.5. The ^{1}H NMR showed a new ^{t}Bu resonance at δ 0.92 and six mesityl resonances in the region δ 2.95 – δ 1.75. Heating the reaction mixture to 50 °C led to a further new species with a ^{31}P resonance at δ 34.1 and a new ^{t}Bu resonance in the ^{1}H NMR at δ 1.05. No triphenylphosphine was observed in the reaction mixture at room temperature or 50 °C.

Importantly, phospha-amidine **3.5** was observed as a small fraction of the reaction mixture, suggesting the new products are not formed by coordination of **3.5** to palladium.

The analogous reaction was carried out between silylene **3.21** and bis(tricyclohexylphosphine) palladium(0), $Pd(PCy_3)_2$. After 12 hours at room temperature a new species was observed with a ^{31}P resonance at δ 44.0 as just 10% of the reaction mixture. Heating the mixture to speed up the reaction led to an intractable mixture of products by ^{1}H and ^{31}P NMR. No products could be isolated from the reactions of silylene **3.21** with either palladium(0) complex.

Nickel(0) and gold(I) are both electron-rich, diamagnetic metals. Bis(cyclooctadiene)nickel(0), $Ni(cod)_2$, is a common source of Ni(0). The reaction of **3.21** with $Ni(cod)_2$ showed only consumption of free phospha-amidine impurity while **3.21** remained unchanged. The disappearance of phospha-amidine **3.5** was coupled with appearance of two new signals in the ^{31}P NMR spectrum at δ −43.9 and 121.9. These could be related to oxidative addition of the P-H of **3.5** to the nickel(0) centre as the ^{31}P resonances show no $^{1}J_{PH}$ coupling. Again, no products were isolated from the reaction of **3.21** with $Ni(cod)_2$.

Some silylenes insert into metal-halogen bonds, such as decamethylsilicocene **3.24** which inserts into the Au-Cl bond of chloro(triphenylphosphine)gold(I), $AuCl(PPh_3)$ (Scheme 3-19).[33] However, amidinato silylenes are known to coordinate without insertion in their reactions with chloro(dimethylsulfide)gold(I), $AuCl(SMe_2)$.[34,35]

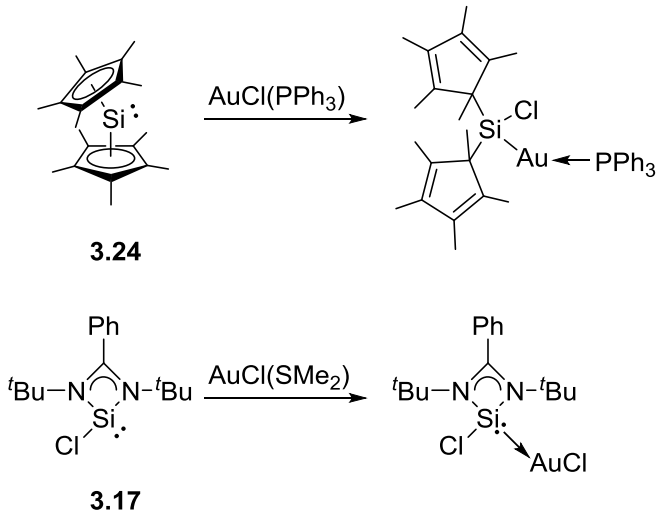

Scheme 3-19 *– When treated with gold(I) chloride, decamethylsilicocene* ***3.24*** *undergoes insertion into the Au-Cl bond to give a silicon(IV) complex. In contrast, the reaction of amidinato silylene* ***3.17*** *with gold(I) chloride forms a coordination compound.*

Therefore **3.21** was treated with $AuCl(SMe_2)$ at room temperature. Although a mixture of products was observed, only two well-defined peaks were identified as major products (>10% by ^{31}P signal integration) at δ −11.1 and δ −13.4, as well as a broad peak at δ –27. Crystallisation of the reaction mixture afforded a single crystal of gold-phosphorus macrocycle **3.25**. Gold macrocycle **3.25** is formed from four phospha-amidinate ligands and four gold(I) cations. The phospha-amidinates only bind through the phosphorus atoms and the resultant macrocycle has S_4 symmetry.

The formation of **3.25** proves that the Si-P bonds can be broken by coordination to a metal, however in this instance coordination of the phospha-amidinate is preferred to coordination of the silylene.

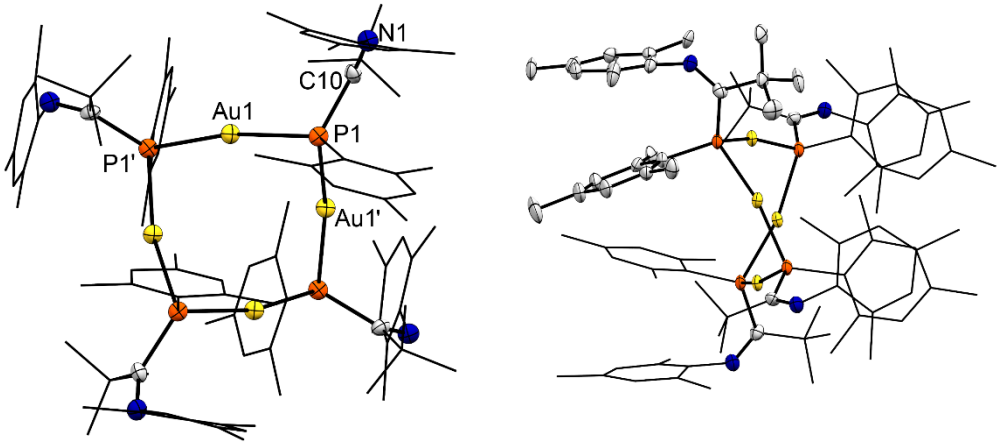

Figure 3-11 *– Two perspectives of the solid-state structure of* ***3.25****. Hydrogen atoms omitted for clarity. Thermal ellipsoids drawn at 50% probability. The left figure shows the overall cyclic structure and the right figure shows the intact phospha-amidinate and the geometry of the macrocycle. Selected bond lengths (Å) and angles (°):Au1-P1 2.322(2), Au1-P1' 2.327(2), P1-C10 1.892(2), C10-N1 1.277(12), N1-C10-P1 125.0(7), C10-P1-Au1 121.1(3), C10-P1'-Au1 114.2(3), Au1-P1-Au1' 89.95(9), Au1-P1-C1 120.6(3).*

Slootweg and Lammertsma prepared a similar macrocycle, **3.26**, by the reaction of a lithium phospha-amidinate with gold chloride thiophene complex (Scheme 3-20). The bond distances in **3.25** and **3.26** are broadly very similar, for example the P-C bond distance of the phospha-amidine suggests a single bond in both cases at 1.892(2) Å in **3.25** and 1.848(8) Å in **3.26**. Accordingly, the C-N bond distance is representative of a double bond in both cases at 1.277(12) Å in **3.25** and 1.309(3) Å in **3.26**. The P-Au distances are also similar with the two interactions in **3.25** at 2.322(2) Å and 2.327(2) Å and in **3.26** at 2.354(2) Å and 2.339(2) Å.

Given the large number of signals observed by ^{1}H and ^{31}P NMR, macrocycle **3.25** is probably formed alongside other sized macrocyles as part of the reaction mixture.

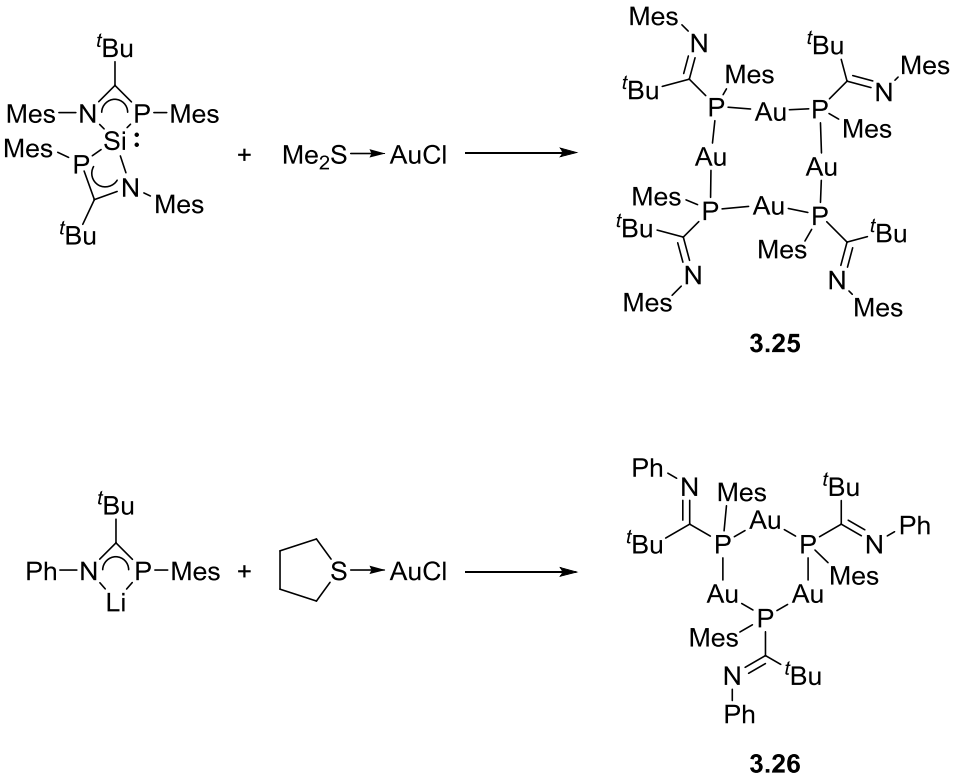

Scheme 3-20 *– The reaction of* ***3.21*** *with* $(Me_2S)AuCl$ *gave macrocycle* ***3.25****. Macrocycle* ***3.26*** *was previously reported.*[19]

3.6 Phospha-Amidinate Complexes of Other Main Group Elements

This section was carried out in collaboration with Dr Alessandro Bismuto and the results were later extended by Dr Stephanie Urwin who prepared and characterised a range of lithium, magnesium and aluminium phospha-amidinate complexes.

Phospha-amidinate ligands were also investigated for their potential to support other main group metals. Before the start of this project, the only main group phospha-amidinate complex was thallium complex **3.27**.[22] Interestingly, **3.27** does not coordinate through the imine and instead coordinates through an interaction with the aryl substituent.

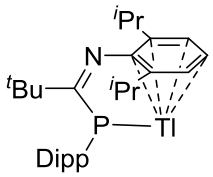

3.27

Scheme 3-21 *– Thallium complex* ***3.27*** *is the only previously reported main group phospha-amidinate complex. Dipp = 2,6-di*isopropylphenyl.

Phospha-amidine **3.5** was reacted with aluminium compounds as a proof of concept. The reaction of **3.5** with trimethylaluminium in hexane provided a new sharp resonance in the ^{31}P NMR spectrum at δ −32.7. Heating the reaction mixture to 60 °C for three hours gave full conversion to the new resonance. The observation of methane in the ^{1}H NMR supports formation of a new phospha-amidinate complex. Indeed, crystallisation of the reaction mixture cleanly provided phospha-amidinate aluminium complex **3.28**.

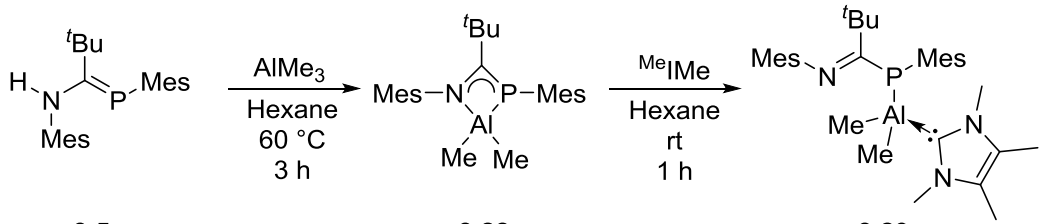

3.5 **3.28** **3.29**

Scheme 3-22 *– The syntheses of* ***3.28*** *and* ***3.29*** *from phospha-amidine* ***3.5****.*

The solid-state structure of **3.28** is shown in Figure 3-12. As for the silicon complexes, planarity at nitrogen (Σ∠N1 = 359.1(2)°) and not phosphorus (Σ∠P1 = 313.49(13)°), along with the short C12-N1 bond distance of 1.325(2) Å and the long C12-P1 distance of 1.816(2) suggest the best description of the structure is an imine coordinated phosphino alane, similar to silanes **3.10** and **3.15** and silylene **3.21**. However, the P1-Al1 bond distance of 2.4065(8) Å is longer than most other Al-P single bonds.[36–39]

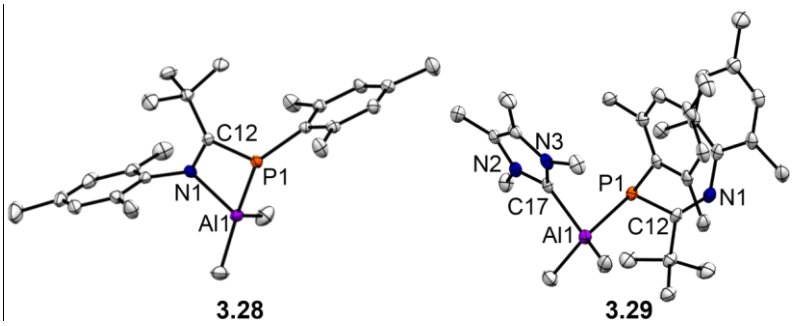

***Figure 3-12** – The solid-state structures of **3.28** and **3.29**. Hydrogen atoms omitted for clarity. Ellipsoids set to 50% probability. Selectred bond distances (Å) and angles (°): **3.28** C12-N1 1.325(2), C12-P1 1.816(2), P1-Al1 2.4065(8), Al1-N1 1.970(2), C17-N1-Al1 125.6(1), C17-N1-C12 128.5(2), C12-N1-Al1 105.0(1), Al1-P1-C12 76.08(6), C12-P1-C3 114.89(9), C3-P1-Al1 122.52(7); **3.29** P1-Al1 2.410(1), P1-C12 1.850(2), N1-C12 1.285(3), C26-Al1 2.064(3), Al1-C2 1.984(3), C1-Al1 1.989(3), C26-N2 1.357(3), C26-N3 1.356(3), Al1-P1-C12 123.18(8), C12-P1-C3 105.7(1), C26-Al1-P1 91.96(7), N2-C26-N3 103.9(2), P1-C12-N1 125.6(2).*

The imine coordination of **3.28** is readily displaced by coordination of the NHC ^{Me}IMe to give NHC coordinated dimethyl aluminium complex **3.29**. The P-Al bond length is slightly longer in **3.29** at 2.410(1) Å compared with 2.4065(8) Å in **3.28**. The central C12-P1 bond length remains largely unchanged at 1.850(2) Å in **3.29** compared with 1.816(2) Å in **3.28**.

Phospha-amidine **3.5** was also treated with $LiAlH_4$. Two new signals were observed in the ^{31}P NMR at δ −9.2 and δ −24.8, the latter of which was extremely broad. Prolonged heating led to complete conversion to the signal at δ −9.2. The ^{1}H spectrum showed formation of dihydrogen but no Al-H peaks, although this is not uncommon due to the large quadrapolar coupling exhibited by aluminium in an asymmetric environment. Removal of the volatiles and extraction into toluene, followed by crystallisation at −20 °C, afforded single crystals of aluminium hydride **3.30**. The solid-state structure of **3.30** is shown in Figure 3-13. Compound **3.30** is reminiscent of silylene **3.21**. The central aluminium is five-coordinate and is best described as a distorted trigonal bipyramid. As for other phospha-amidinate complexes, the ligand is planar around nitrogen (Σ∠N1 = 359.8(2)°) and trigonal pyramidal around phosphorus (Σ∠P1 = 315.94(12)°). Again, the N-C bond distance is indicative of a double bond at 1.338(2) Å, while the P-C distance of 1.787(2) suggests a single bond.

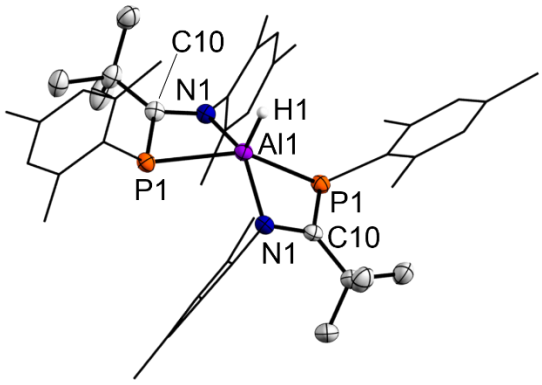

Figure 3-13 *– The solid-structure of* ***3.30****. Hydrogen atoms other than H1 omitted for clarity. Thermal ellipsoids set to 50%. Selected bond distances (Å) and angles (°):P1-C10 1.787(2), C10-N1 1.338(2), N1-Al1 1.9686(15), Al1-P1 2.4707(5), Al1-N1-C15 126.88(12), C15-N1-C10 126.71(15), C10-N1-Al1 106.17(12), Al1-P1-C10 75.81(6), C10-P1-C1 113.41(8), C1-P1 Al1 126.72(6), P1-Al1-N1 98.63(5), N1-Al1-P1 67.93(5).*

The reaction of **3.5** with $LiAlH_4$ was further investigated by Dr Stephanie Urwin. She also investigated the related sequential reaction of **3.5** with ^{n}BuLi followed by $AlH_3{\cdot}NMe_3$ which afforded the same product. It was found that dihydrides **3.31** and **3.32** were key intermediates, either of which could correspond to the ^{31}P signal at δ −24.8.

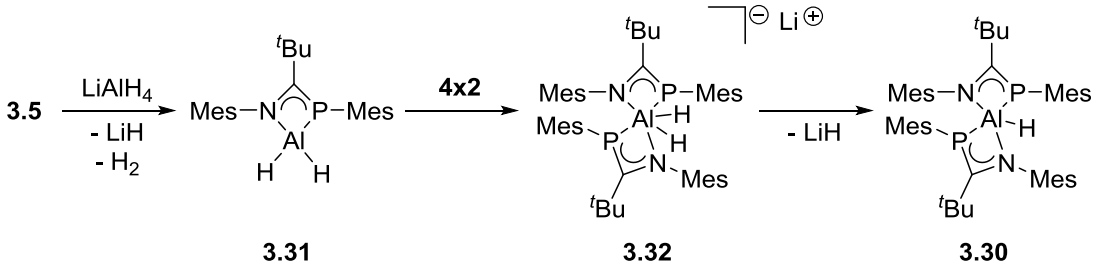

3.31 **3.32** **3.30**

Scheme 3-23 *– The reaction of* ***3.5*** *with $LiAlH_4$ to give* ***3.30****, presumably through intermediates* ***3.31*** *and* ***3.32****.*

Urwin also prepared and characterised a range of phospha-amidinate lithium and magnesium complexes, some of which are shown in Scheme 3-24.[26] She was also able to synthesise a range of new ligands with increased steric bulk on nitrogen. Interestingly, some phospha-amidinate magnesium complexes were shown to be catalytically active in the ring opening polymerisation of *rac*-lactide to isotactic polylactide.

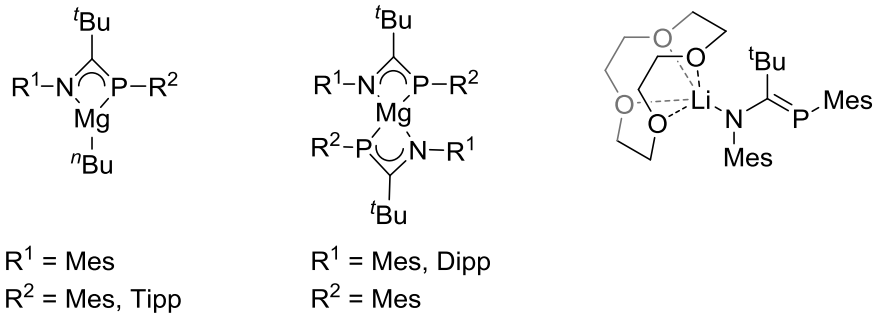

***Scheme 3-24** – Some examples of isolated magnesium and lithium complexes reported by Urwin.[26]*

3.7 Summary and Outlook

Novel phospha-amidinate ligands have been prepared and four phospha-amidinato silanes have been isolated. Their reactions with reducing and dehydrochlorinating agents have been investigated and three three-coordinate silylenes were observed.

A four-coordinate silylene, **3.21**, was isolated and fully characterised. Silylene **3.21** represents the first structurally characterised phospha-amidinato silylene and a rare example of phospha-amidinate ligand use in main group chemistry. However, the four-coordinate nature of **3.21** inhibits its reactivity with small molecules. The reaction of **3.21** with electron rich transition metals was also investigated but the weak Si-P bond led to degradation of the silylene.

Phospha-amidinate ligands were also demonstrated as viable ligands in aluminium chemistry and the preparation and characterisation of such compounds, as well as their magnesium and lithium counterparts, has since been thoroughly investigated by Dr Urwin.[26]

3.8 References

[1] B. Blom, M. Driess, in *Functional Molecular Silicon Compounds II* (Ed.: D. Scheschkewitz), Springer International Publishing, Cham, **2014**.

[2] A. V. Protchenko, K. H. Birjkumar, D. Dange, A. D. Schwarz, D. Vidovic, C. Jones, N. Kaltsoyannis, P. Mountford, S. Aldridge, *J. Am. Chem. Soc.* **2012**, *134*, 6500–6503.

[3] A. V. Protchenko, A. D. Schwarz, M. P. Blake, C. Jones, N. Kaltsoyannis, P. Mountford, S. Aldridge, *Angew. Chem. Int. Ed.* **2013**, *52*, 568–571.

[4] B. D. Rekken, T. M. Brown, J. C. Fettinger, H. M. Tuononen, P. P. Power, *J. Am. Chem. Soc.* **2012**, *134*, 6504–6507.

[5] P. P. Power, *Nature* **2010**, *463*, 171–177.

[6] A. V. Protchenko, J. I. Bates, L. M. A. Saleh, M. P. Blake, A. D. Schwarz, E. L. Kolychev, A. L. Thompson, C. Jones, P. Mountford, S. Aldridge, *J. Am. Chem. Soc.* **2016**, *138*, 4555–4564.

[7] T. J. Hadlington, J. A. B. Abdalla, R. Tirfoin, S. Aldridge, C. Jones, *Chem. Commun.* **2016**, *52*, 1717–1720.

[8] K. Izod, P. Evans, P. G. Waddell, *Angew. Chem. Int. Ed.* **2017**, *56*, 5593–5597.

[9] K. Izod, P. Evans, P. G. Waddell, M. R. Probert, *Inorg. Chem.* **2016**, *55*, 10510–10522.

[10] K. Izod, D. G. Rayner, S. M. El-Hamruni, R. W. Harrington, U. Baisch, *Angew. Chem. Int. Ed.* **2014**, *53*, 3636–3640.

[11] H. H. Karsch, U. Keller, S. Gamper, G. Müller, *Angew. Chem. Int. Ed. Engl.* **1990**, *29*, 295–296.

[12] H. H. Karsch, R. Richter, in *Organosilicon Chem. Set*, John Wiley & Sons, Ltd, **2008**, pp. 187–193.

[13] D. Gau, T. Kato, N. Saffon-Merceron, F. P. Cossío, A. Baceiredo, *J. Am. Chem. Soc.* **2009**, *131*, 8762–8763.

[14] S. Inoue, W. Wang, C. Präsang, M. Asay, E. Irran, M. Driess, *J. Am. Chem. Soc.* **2011**, *133*, 2868–2871.

[15] R. Rodriguez, D. Gau, Y. Contie, T. Kato, N. Saffon-Merceron, A. Baceiredo, *Angew. Chem. Int. Ed.* **2011**, *50*, 11492–11495.

[16] I. Alvarado-Beltran, A. Rosas-Sánchez, A. Baceiredo, N. Saffon-Merceron, V. Branchadell, T. Kato, *Angew. Chem. Int. Ed.* **2017**, *56*, 10481–10485.

[17] R. Rodriguez, D. Gau, T. Kato, N. Saffon-Merceron, A. De Cózar, F. P. Cossío, A. Baceiredo, *Angew. Chem. Int. Ed.* **2011**, *50*, 10414–10416.

[18] F. T. Edelmann, in *Adv. Organomet. Chem.* (Eds.: A.F. Hill, M.J. Fink), Academic Press, **2013**, pp. 55–374.

[19] T. van Dijk, S. Burck, M. K. Rong, A. J. Rosenthal, M. Nieger, J. C. Slootweg, K. Lammertsma, *Angew. Chem. Int. Ed.* **2014**, *53*, 9068–9071.

[20] K. Issleib, H. Schmidt, H. Meyer, *J. Organomet. Chem.* **1978**, *160*, 47–57.

[21] R. T. Boeré, M. L. Cole, P. C. Junk, J. D. Masuda, G. Wolmershäuser, *Chem. Commun.* **2004**, 2564–2565.

[22] X. Li, H. Song, C. Cui, *Dalton Trans.* **2009**, 9728–9730.

[23] C.-W. So, H. W. Roesky, J. Magull, R. B. Oswald, *Angew. Chem. Int. Ed.* **2006**, *45*, 3948–3950.

[24] Y. van den Winkel, H. M. M. Bastiaans, F. Bickelhaupt, *J. Organomet. Chem.* **1991**, *405*, 183–194.

[25] Y. Takeda, T. Nishida, S. Minakata, *Chem. – Eur. J.* **2014**, *20*, 10266–10270.

[26] S. Urwin, Rational Ligand Design to Support Reactive Main-Group Compounds, University of Edinburgh, **2018**.

[27] S. S. Sen, H. W. Roesky, D. Stern, J. Henn, D. Stalke, *J. Am. Chem. Soc.* **2010**, *132*, 1123–1126.

[28] R. Azhakar, R. S. Ghadwal, H. W. Roesky, H. Wolf, D. Stalke, *Organometallics* **2012**, *31*, 4588–4592.

[29] R. S. Ghadwal, H. W. Roesky, S. Merkel, J. Henn, D. Stalke, *Angew. Chem.* **2009**, *121*, 5793–5796.

[30] K. Junold, J. A. Baus, C. Burschka, R. Tacke, *Angew. Chem. Int. Ed.* **2012**, *51*, 7020–7023.

[31] F. Lips, J. C. Fettinger, A. Mansikkamäki, H. M. Tuononen, P. P. Power, *J. Am. Chem. Soc.* **2014**, *136*, 634–637.

[32] P. S. Skell, E. J. Goldstein, *J. Am. Chem. Soc.* **1964**, *86*, 1442–1443.

[33] M. Theil, P. Jutzi, B. Neumann, A. Stammler, H.-G. Stammler, *J. Organomet. Chem.* **2002**, *662*, 34–42.

[34] S. Khan, S. K. Ahirwar, S. Pal, N. Parvin, N. Kathewad, *Organometallics* **2015**, *34*, 5401–5406.

[35] S. Khan, S. Pal, N. Kathewad, I. Purushothaman, S. De, P. Parameswaran, *Chem. Commun.* **2016**, *52*, 3880–3882.

[36] T. Chu, I. Korobkov, G. I. Nikonov, *J. Am. Chem. Soc.* **2014**, *136*, 9195–9202.

[37] D. A. Atwood, L. Contreras, A. H. Cowley, R. A. Jones, M. A. Mardones, *Organometallics* **1993**, *12*, 17–18.

[38] K. Knabel, I. Krossing, H. Nöth, H. Schwenk-Kircher, M. Schmidt-Amelunxen, T. Seifert, *Eur. J. Inorg. Chem.* **1998**, *1998*, 1095–1114.

[39] T. Chu, Y. Boyko, I. Korobkov, L. G. Kuzmina, J. A. K. Howard, G. I. Nikonov, *Inorg. Chem.* **2016**, *55*, 9099–9104.

Chapter 4

Silyl Anion Initiated Hydroboration

Chapter 4 Silyl Anion Initiated Hydroboration

Parts of sections 4.3 and 4.7 were carried out in collaboration with Dr Alessandro Bismuto. Parts of section 4.4.1 were carried out by a BSc student, Callum Asplen, under my supervision.

4.1 Introduction

4.1.1 Organoboron Reagents and Hydroboration

Organoboron compounds are common and versatile reagents in organic chemistry. This is largely due to their use in Suzuki cross coupling reactions which has found far reaching popularity thanks to the mild reaction conditions and good functional group tolerance.[1] Suzuki initially reported the coupling between alkenyl boronic esters with alkenyl halides in 1979[2] and continued to extend his methodology to include aryl, alkynyl and alkyl systems (Scheme 4-1).[3,4] Since Suzuki's initial investigation, numerous protocols have been developed to build up complex molecular architectures.[3]

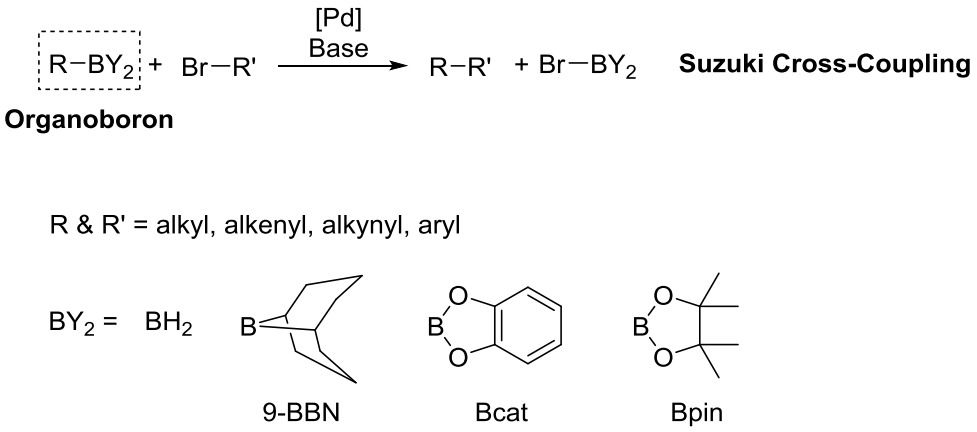

Scheme 4-1 *– General Suzuki cross coupling between an organoboron and an organobromide.*

Aryl and alkynyl boron species are usually synthesised by C-H borylation reactions or through nucleophilic substitution of boron halides by aryl lithium reagents. Alkyl and alkenyl compounds are synthesised through hydroboration reactions – the addition of a B-H bond to an unsaturated bond (Scheme 4-2).

Hydroboration was first developed by Herbert Brown. He initially reported the addition of BH_3 to carbonyls,[5] which he later extended to alkenes and alkynes to produce the alkyl or alkenyl organoboron (Scheme 4-2, left). Although his procedure was extremely efficient, the reactions were often unselective and BH_3 can be difficult to handle. Hydroboration using BH_3 can also give di- and tri-hydroborated products. Since Brown's work, a range of boranes and boronic esters have been used in hydroboration reactions. Some of these, such as 9-BBN (Scheme 4-1), are almost as reactive as BH_3 but are somewhat easier to handle. Boronic esters, such as pinacolborane (HBpin) and catacholborane (HBcat) have found increasing popularity in recent years. Pinacolborane, in particular, is cheap and easy to handle and almost always forms air-stable products. Pinacol boronic esters have also found other uses, such as Chan-Lam coupling.[6]

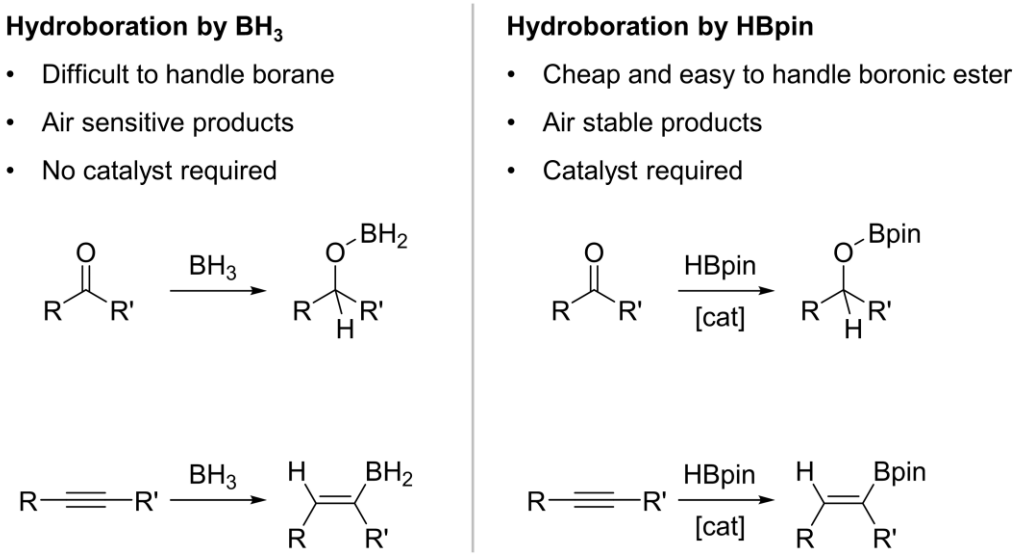

Scheme 4-2 *– Hydroboration by BH_3 or HBpin of ketones and alkynes. Hydroboration was originally report using BH_3[5] but boronic esters such as HBpin have increased in popularity due to their availability and the stability of the final product. Bpin is shown in Scheme 4-1.*

The major disadvantage to using HBpin is its lower reactivity in hydroboration. This means that a catalyst is required to achieve hydroboration of carbon-carbon multiple bonds, or sterically demanding polar multiple bonds such as ketones.

The hydroboration of alkenes and alkynes by boronic esters such as HBpin is usually catalysed by rhodium, iridium or palladium catalysts which are well explored.[7–11] More recently, there

has been a drive to replace such metals with more earth abundant and environmentally benign alternatives[12,13] such as aluminium,[14–16] copper,[17,18] and iron.[19]

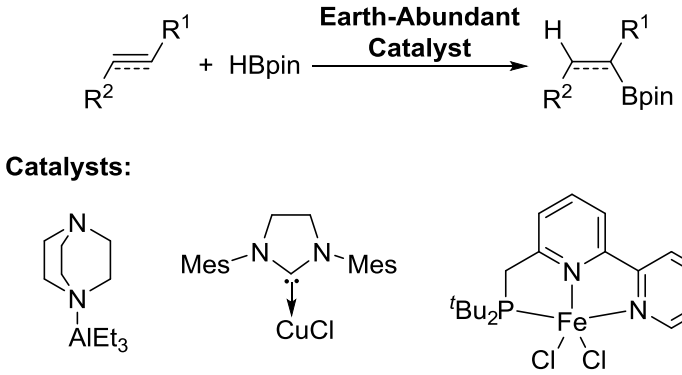

Scheme 4-3 *– Some examples of earth-abundant catalysts reported for the hydroboration of alkenes and alkynes.*[14,18,19]

4.1.2 Recent Advances in the Hydroboration of Carbonyl Compounds

Hydroboration is one method of reducing double bonds. Carbonyls are usually reduced to alcohols using stoichiometric amounts of metal hydrides, such as lithium aluminium hydride ($LiAlH_4$) or lithium triethylborohydride ($LiBEt_3H$). These reagents are often difficult to handle and are unselective. In contrast, the catalyst-promoted hydroboration of aldehydes, ketones and esters can be performed with a high degree of chemo- and stereo-selectivity.[20] Furthermore, the boric ester product provides the alcohol with a versatile protecting and directing group which can be particularly useful in organic synthesis.[21] A number of metal and main-group catalysts have already been reported to catalyse this process.[22]

A large number of studies have been carried out using titanium catalysts, many of which use a chiral ligand for stereoselectivity, such as catalyst **4.1**.[23–26] However, the vast majority of these reports make use of catecholborane, a less stable boronic ester compared with pinacolborane. The same is true of the selection of zinc compounds reported to catalyse this transformation.[27–30]

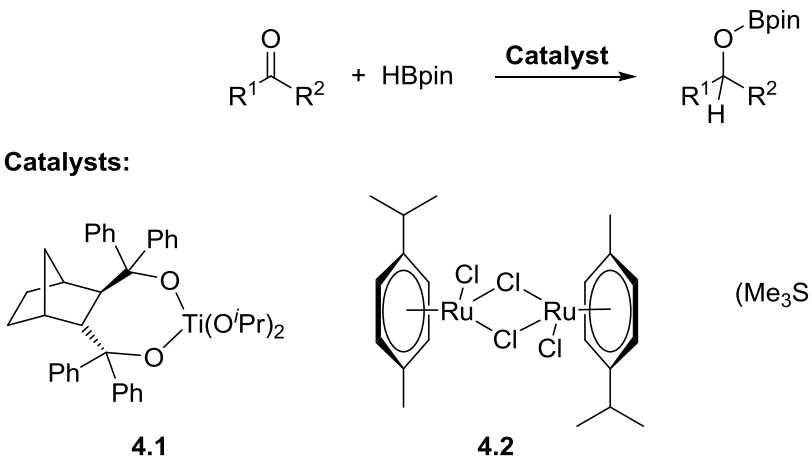

Scheme 4-4 *– Examples of metal catalysts used in the hydrboration of ketones.[26,31,32] R^1/R^2 = H, alkyl or aryl substituents.*

Some ruthenium complexes have been reported to carry out hydroboration using pinacolborane.[31,33] Interestingly, their activity is relatively low compared with some other catalysts. This is somewhat surprising as state-of-the-art systems often make use of metals such as ruthenium. For example, to give yields between 55% and 92%, catalyst **4.2** required heating to 60 °C for 15 hours at 0.1 mol% catalyst loading.[31]

The relatively cheap and commercially available lanthanum complex La(N(SiMe$_3$)$_2$)$_3$ (**4.3**), was shown to have exceptionally high reactivity towards ketones, requiring only 0.01 mol% catalyst loadings and 15 minutes at 25 °C for some substrates.[32] Remarkably, the hydroboration of ketones using **4.3** was faster than for aldehydes, opposite to what is observed for the vast majority of catalysts.[22,26,31,34,35] However, competition reactions between ketones and aldehydes always favoured the aldehyde for **4.3**. This suggests that the first intermediate in the hydroboration of aldehydes acts as a thermodynamic sink with a small kinetic barrier, while the turnover-limiting step must be rather slow. For ketones, the first step could be an equilibrium or a slow step, while the turnover-limiting step must be very fast.

4.1.3 The Move to Sustainable Catalysis

More recently, catalysis has seen a general drive towards sustainable alternatives to expensive and rare transition metals which was part of the rationale for the investigation of

the lanthanum complex **4.3**.[32] Lanthanum is estimated to be 39,000 times more abundant in the earth's crust than ruthenium (3.9×10^{1} mg/kg for La *vs* 1×10^{-3} mg/kg for Ru).[36]

Some main group elements are considerably more abundant than 2nd and 3rd row transition metals and in recent years a variety of main group species have been reported for the hydroboration of carbonyl complexes. Furthermore, there has been growing interest in the fundamental reactivity of main group species. In particular, how they compare with traditional transition metal catalysts.[37,38]

As early as 2000, Woodward *et al.* reported tetracoordinate gallium complex **4.4** for the enantioselective hydroboration of prochiral ketones.[39] The hydroboration of acetophenone catalyzed by **4.4** proceeds with 90% yield and 90% enantiomeric excess (*ee*) when using HBcat as the borane source, however when using HBpin the yield and *ee* were 41% and <2%, respectively. One example of the less reactive nature of pinacolborane.

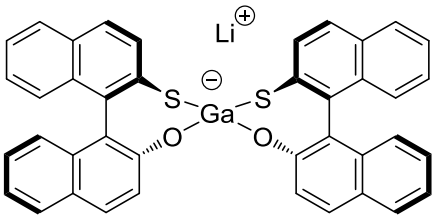

4.4

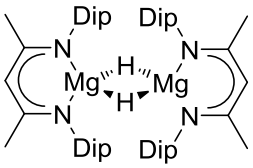

4.5

Scheme 4-5 *– Gallium catalyst **4.4** active in the stereoselective reduction of carbonyls by catacholborane[39] and magnesium catalyst **4.5** active in the reduction of carbonyls by pinacolborane. Dip – 2,6-di*isopropylphenyl.

More recently, in 2012 magnesium hydride **4.5** was reported to catalyse the hydroboration of carbonyls using HBpin.[34] Shortly afterwards, germanium(II) and tin(II) hydrides **4.6** and **4.7** (Scheme 4-6) were reported.[35] Catalysts **4.5**, **4.6**, and **4.7** were not stereoselective but their proposed mechanisms formed the basis for a number of future works studying the hydroboration of carbonyls, alkenes and alkynes. The proposed mechanism using **4.6** and **4.7** is shown in Scheme 4-6[35] and is virtually identical to that previously reported for **4.5**.[34] Until now, metallylenes **4.6** and **4.7** are the only low-oxidation-state main-group compounds reported to catalyse this transformation.

Both **4.6** and **4.7** are in equilibrium with their dimers but the monomers are the active species.[40,41] The first step in the mechanism was shown to be the hydrometallation of the

carbonyl by the M-H bond of the Ge(II) or Sn(II) hydride monomers. This reaction is rapid and the intermediates are isolable in stoichiometric reactions with 2,4-dimethyl-3-pentanone or *p*-anisaldehyde. This fundamental reaction has been reported for three coordinate germanium(II) and tin(II) hydrides but never with such high rates of reaction,[42–44] probably due to the low lying LUMOs of metallyenes **4.6** and **4.7**. Neither **4.6** nor **4.7** showed any stoichiometric reactivity with HBpin, strong evidence of hydrometallation as the first step. This was further supported by kinetic investigations which confirmed first order dependency on catalyst and HBpin and zero order dependency on ketone. This suggests the rate-determining step is σ-bond metathesis and therefore the hydrometallation product is the resting state in the cycle.

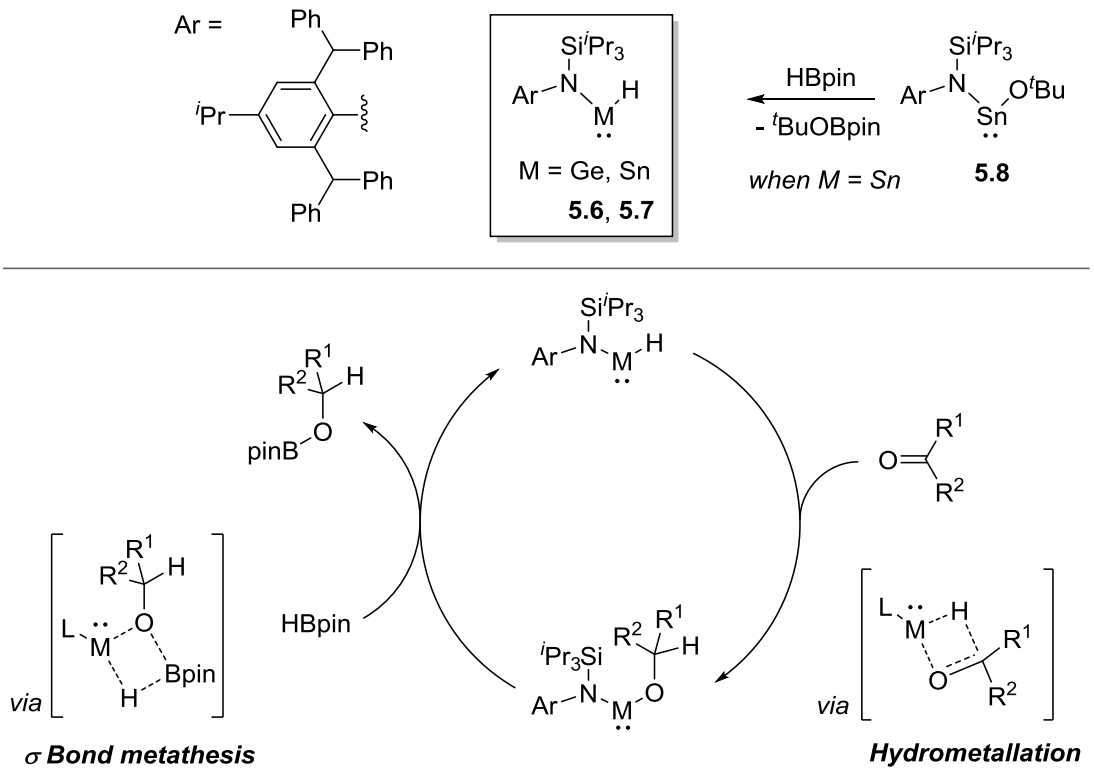

Scheme 4-6 *– Catalysts **4.6** and **4.7** for the hydroboration of ketones and aldehydes with pinacolborane and the proposed mechanism.[35] R^1/R^2 = H, alkyl or aryl.*

Stoichiometrically, the reaction of the hydrometallated product with HBpin forms the boric ester with clean regeneration of the metal hydrides. This unlikely sounding metal-oxygen bond cleavage was shown computationally to be exergonic by −3.4 kcal·mol^{-1} in the case of

4.7. A related study whereby a germanium hydride is generated *in situ* was reported this year.[45]

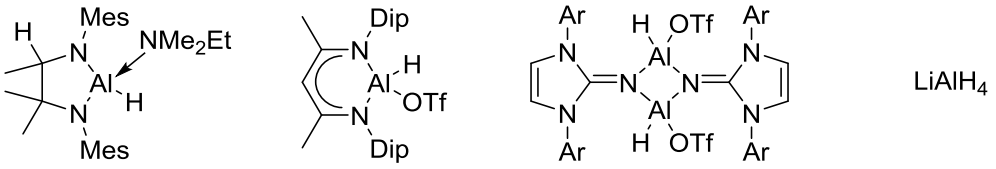

Scheme 4-7 *– Aluminium hydride catalysts for the hydroboration of carbonyls.[15,16,46,47] Mes = 2,4,6-trimethylphenyl. Dip = 2,6-di*iso*propylphenyl. Ar = Mes or Dip.*

This reactivity has since been extended to include aluminium hydrides (Scheme 4-7)[15,16,46] which culminated in a recent report from the Cowley group of the lithium aluminium hydride ($LiAlH_4$) promoted hydroboration of acetophenone.[47] Recently lithium borohydrides were also reported to initiate the hydroboration of carbonyls.[48,49] These examples are all proposed to follow mechanisms similar to that for **4.6** and **4.7** i.e. hydrometallation followed by metathesis. This method has also been used for the hydroboration of alkenes and alkynes with main group hydrides.[14,16,50]

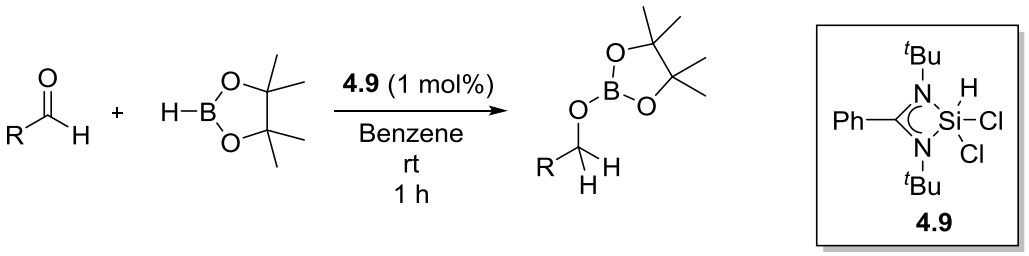

Scheme 4-8 *– The hydroboration of aldeyhydes catalysed by the neutral silicon(IV) species* ***4.9.***[51]

In 2017, the silicon hydride **4.9** was reported to catalyse the hydroboration of aldehydes by the same mechanism (Scheme 4-8).[51] However, the "hydride " of silane **4.9** is less hydridic than many main group hydrides. In fact, silane **4.9** can be deprotonated in a reductive dehydrochlorination to afford the corresponding silylene, as discussed in Chapter 1.[52] The weaker hydride character of **4.9** is reflected in its poor reactivity towards ketones and high selectivity for aldehydes.[51] Regardless, this is the first example of a silicon catalyst in hydroboration chemistry.

4.1.4 Base-Promoted Hydroboration of Carbonyls

Transition metal catalysts often make use of alkoxides as initiators.[53] Their primary role is to generate 16 electron species which are usually the active catalysts.

However, in 2011, the Clark group made the important discovery that alkoxides are able to catalyse the hydroboration of ketones with no additional transition metal catalyst. [54] Their procedure gave full conversion in 3 hours at ambient temperature using sodium *tert*-butoxide (NaO^{t}Bu) as an initiator.

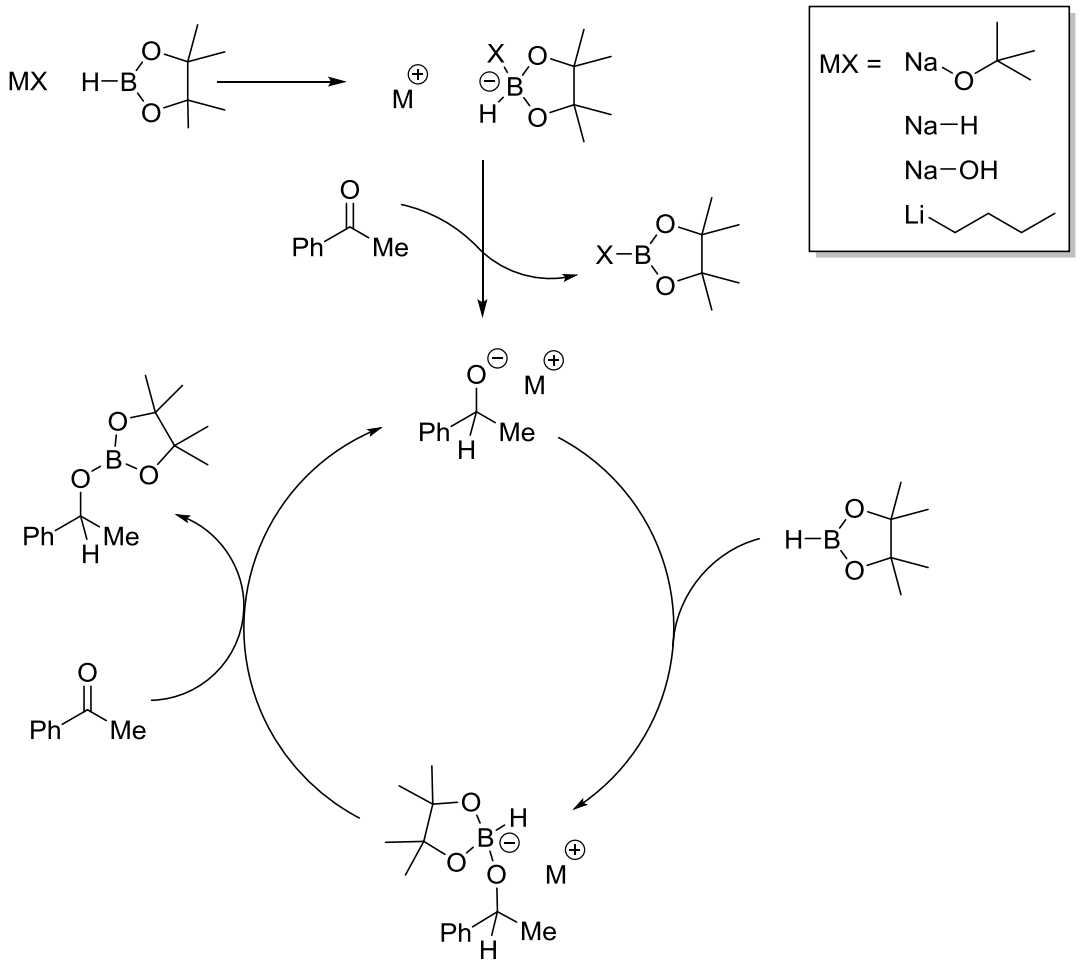

Scheme 4-9 *– The mechanism of base-catalysed hydroboration of acetophenone.[54–57] MX = NaO^{t}Bu, NaOH, NaH or Li^{n}Bu.*

The reaction proceeds *via* a different mechanism to the main-group hydrides discussed thus far. Scheme 4-9 shows the general mechanism of base-initiated hydroboration of carbonyls.

The key step is initial formation of a boronate intermediate by coordination of the base to pinacolborane. The boronate intermediate has increased hydridic character which allows it to undergo direct nucleophilic addition to the substrate. This generates the active alkoxide species. The active alkoxide species also coordinates HBpin to generate the strong hydride for delivery to a second equivalent of substrate, regenerating the alkoxide and allowing catalytic turnover.

Other alkali metal bases have since been reported to perform the hydroboration of carbonyls using the same mechanism, including NaOH,[55] NaH,[56] and ^{n}BuLi.[57] In each case the initial step is activation of the boron hydride by base coordination followed by direct delivery of the hydride to the substrate, as shown in Scheme 4-9.

4.2 Project Aims

The aim of this project was to discover new silicon compounds for the hydroboration of carbonyls and carbon-carbon multiple bonds.

Organosilanes with silicon hydride functionality are common reagents in organic, inorganic and materials chemistry. Novel silicon hydrides were investigated and compared with **4.9.**[51]

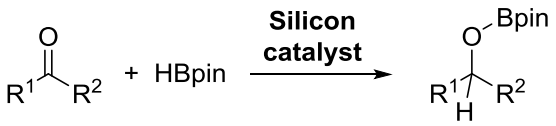

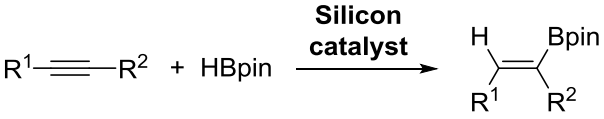

Silyl anions are also well-studied.[58] A common silyl anion was also investigated in the base-promoted hydroboration of carbonyls. The mechanism was explored, and the substrate scope developed and compared with reported catalysts. The hydroboration of carbon-carbon multiple bonds was also attempted.

4.3 Silicon Catalysts for the Hydroboration of Carbonyls

4.3.1 Si(IV) Catalysts for the Hydroboration of Benzaldehyde

Initially the hydroboration of aldehydes was carried out in the presence of silicon hydride **4.10**. There are some distinct similarities between **4.10** and previously reported **4.9.** They both have hydride and chloride functionalities. While **4.9** is five-coordinate, **4.10** has a pentamethylcyclopentadienyl (Cp*) group which is fluxional, as evidenced by the observation of one corresponding singlet resonance in the ^{1}H NMR spectrum which represents all 15 protons. However, the central silicon of **4.10** shows a signal at δ 20.2 in the ^{29}Si NMR spectrum. This is very different to the ^{29}Si resonance for **4.9 at** δ −96.8.[52] The 117.0 ppm difference in ppm highlights the different nature of the two silicon centres.

Table 4-1 *– The hydroboration of benzaldehyde in the presence of **4.10** and with no catalyst. Reaction conditions: 0.3 mmol benzaldehyde, 0.35 mmol pinacolborane, room temperature, 40 minutes.*

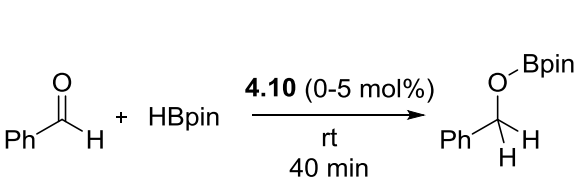

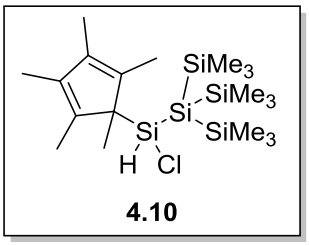

4.10

Entry	Solvent	Catalyst Loading (mol%)	Conversion (%)
1	Toluene	5	7.5
2	None	3	100
3	None	0	55

The reaction of 4,4,5,5-tetramethyl-1,3,2-dioxaborolane (pinacolborane, HBpin) with benzaldehyde was carried out in the presence of **4.10** (3-5 mol%), both in toluene and in the absence of solvent. Both reactions were carried out at room temperature. The reaction in toluene gave only 7.5% conversion after 40 minutes at room temperature (Table 4-1, entry 1). However, in the absence of solvent, the reaction reached full conversion in the same time, even when using a lower catalyst loading (Table 4-1, entry 2).

Despite multiple reports of catalysts for the hydroboration of aldehydes, the control reaction of benzaldehyde with pinacolborane proceeded with 55% conversion in 40 minutes in the absence of solvent or catalyst (Table 4-1, entry 3). Indeed, since these results were obtained, the catalyst- and solvent-free hydroboration of aldehydes was reported by the group of Hreczycho.[59] Their optimised procedure provides 95% conversion in one hour at room temperature or 99% conversion in 10 minutes at 60 °C.

This was a significant development to the field and future research should focus on the hydroboration of more sterically and electronically demanding ketones.

4.3.2 Si(IV) Catalysts for the Hydroboration of Acetophenone

The same paper by the group of Hreczycho showed that converting the ketone acetophenone to the corresponding boronic ester required prolonged heating.[59] In fact, after 24 hours at 80 °C they observed just 45% conversion, and at room temperature they saw no conversion, even after 24 hours. This is evidence of the requirement for a catalyst in this reaction. This reaction was repeated and is reported in Table 4-2, entry 1.

In the presence of **4.10**, 8% conversion of acetophenone is seen after only 20 minutes (Table 4-2, entry 2). In the presence of the related silane **4.11**, no conversion is seen under the same conditions. This could suggest that the tris(trimethylsilyl)silyl ($Si(SiMe_3)_3$) group plays a role, perhaps increasing the hydridic character of **4.10**. Using triethylsilane (Et_3SiH) as a catalyst gave only trace amounts of products (Table 4-2, entry 3). This rules out any involvement of the α-hydrides and also confirms that simple silanes are not efficient enough to deliver hydrides to deactivated carbonyls in the absence of a catalyst.

These results suggest that silicon(IV) hydrides may not be reactive enough to make use of the hydrometallation and sigma bond metathesis mechanism reported for other main group hydrides, although the correct substituents could alter this. Given the ability of inorganic bases to activate the hydride of HBpin, the reaction of acetophenone with pinacolborane was carried out in the presence of a silicon base, the silyl anion **4.12** (Table 4-2, entry 5). Indeed, anion **4.12** was found to be far more reactive than the silicon hydrides discussed thus far. Silyl anion **4.12** gave full conversion of acetophenone in 20 minutes at room temperature when using 3 mol% catalyst loading.

Table 4-2 *– The hydroboration of acetophenone in the presence of various catalysts. Reaction conditions: 0.3 mmol acetophenone, 0.35 mmol pinacolborane, room temperature, 20 min.*

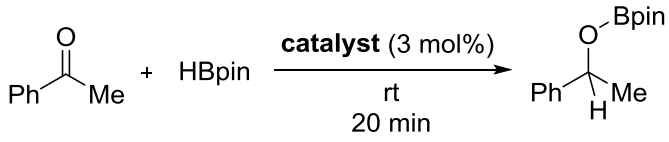

Catalysts:

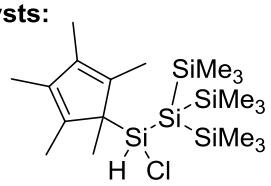

4.10

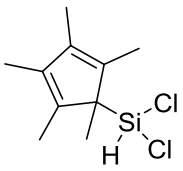

4.11

Et_3SiH

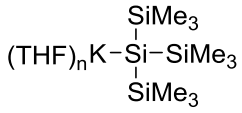

4.12

Entry	Catalyst	Conversion (%)
1	none	trace
2	**4.10**	8
3	**4.11**	trace
4	Et_3SiH	trace
5	**4.12**	100

4.3.3 A Silyl Anion Initiator for the Hydroboration of Acetophenone

Silyl Anion **4.12** is readily prepared by the reaction of commercially available tetrakis(trimethylsilyl)silane ($Si(SiMe_3)_4$) with KO^tBu[60] (Scheme 4-10). The corresponding lithium silyl anion can be prepared by the reaction of $Si(SiMe_3)_4$ with methyl lithium.[61] When using KO^tBu, the alkoxide base abstracts a trimethylsilyl group with formation of the silyl ether Me_3SiO^tBu. The reaction proceeds rapidly in THF and the anion can be generated *in situ* and used without further purification. It can also be crystallised from alkane solvents as the THF adduct. Unless otherwise stated, all reactions were carried out using purified **4.12** isolated as large, colourless single crystals. The amount of THF is quantified by integration of the ^1H NMR and was usually between 1.1 and 1.6 equivalents, consistent with previous reports.[60]

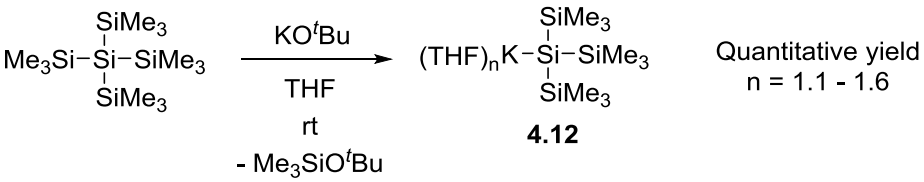

Scheme 4-10 *– The reaction of tetrakis(trimethylsiyl)silane ($Si(SiMe_3)_4$) with KO^tBu to give silyl anion* ***4.12.***

The hydroboration was carried out under the same conditions as when using **4.10** and **4.11**. The silyl anion catalysed hydroboration of acetophenone gave 100% conversion in just 20 minutes at room temperature and in the absence of solvent when using 3 mol% catalyst loading (Table 4-2, entry 5). This is in contrast to the alkoxide catalysed hydroboration which required three hours to reach completion when using 5 mol% catalyst loading in toluene.

Table 4-3 *– The hydroboration of acetophenone with HBpin catalysed by silyl anion* ***4.12*** *at various catalyst loadings. Reaction conditions: [a] 0.3 mmol acetophenone, 0.35 mmol HBpin, room temperature, no solvent; [b] 0.6 mmol acetophenone, 0.7 mmol HBpin, room temperature, no solvent; [c] 72 mmol acetophenone, 84 mmol HBpin, room temperature, no solvent.*

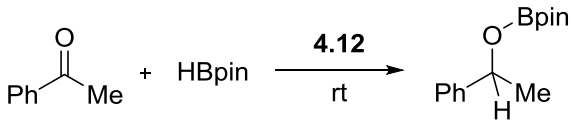

Entry	Catalyst loading (mol%)	Time	Conversion (%)
1	3	20 min	100[a]
2	1	20 min	67[b]
3	0.1	20 min	18[c]
4	0.1	1 h	31[c]
5	0.1	18 h	60[c]
6	0.1	48 h	75[c]

Importantly, the catalyst loading required when using **4.12** is significantly lower than for the alkoxide base which required 5 mol%. Reactions were carried out at catalyst loadings and reaction times (Table 4-3)**.** All reactions were carried out at room temperature in the absence of solvent and quenched after the stated time by exposure to air and addition of $CDCl_3$. The

results show that reducing the catalyst loading from 3 mol% to 1 mol% has a detrimental effect on the conversion, reducing it from 100% (Table 4-3, entry 1) to 67% (Table 4-3, entry 2) in the same length of time. However, even with extremely low catalyst loadings of 0.1 mol%, 75% conversion was achieved after 48 hours (Table 4-3, entry 6). This represents a turnover number of 750.

4.4 Optimisation of Conditions

4.4.1 Solvent

One key advantage of the silyl anion **4.12** over inorganic bases such as NaOH and NaO^{t}Bu is its solubility. The vast majority of potential substrates are soluble in organic solvents such as toluene, hexane or THF. Sodium hydroxide and sodium *tert*butoxide are only sparingly soluble in many common organic solvents.

On the other hand, **4.12** is readily soluble in polar and apolar organic solvents owing to the bulky trimethylsilyl substituents. This means that the silyl anion catalysed hydroboration reactions can be carried out with high conversions in a range of solvents unavailable to conventional inorganic bases.

Table 4-4 *– The silyl anion catalysed hydroboration of acetophenone with pinacolborane in various solvents. Yields calculated agains 1,3,5-trimethoxybenzene as an internal standard. Reaction conditions: 0.625 mmol acetophenone, 0.656 mmol HBpin, 3 mol% catalyst loading, 0.2 mL solvent, 20 minutes, room temperature.*

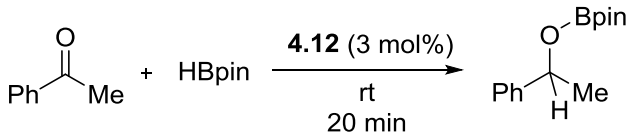

Entry	Solvent	Yield (%)
1	None	100
2	Toluene	97
3	THF	93
4	Hexane	89
5	DME	61

Therefore, the hydroboration of acetophenone catalysed by anion **4.12** was carried out in a variety of solvents. The reactions were carried out at 3 mol% catalyst loading and quenched after 20 minutes. NMR yields were measured against an internal standard of 1,3,5-trimethoxybenzene. The reaction was successful in all four solvents, evidence of the robustness of the procedure. The highest yield was obtained in toluene at 97%, while the lowest was from the reaction in dimethoxy ethane (DME) at 61%.

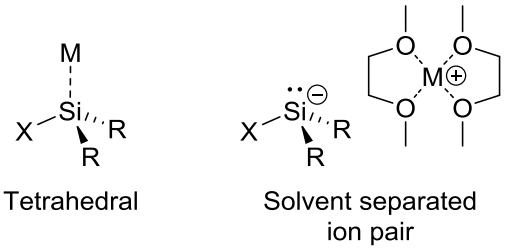

***Scheme 4-11** – The classical, tetrahedral silyl anion structure and a solvent separated ion pair in DME.*

DME is a highly coordinating solvent and can coordinate potassium ions well. This generates a solvent separated ion pair, as shown in Scheme 4-11. This is well evidenced by the ^{29}Si NMR chemical shift of the anionic silicon in **4.12** which is more shielded in DME than in any other solvent tested. The ^{29}Si chemical shift in DME is δ −196.[60] In C_6D_6, which should be similar to toluene, the ^{29}Si chemical shift is δ −188, while in THF it is found at an intermediate value of δ −194. Concurrently, anion **4.12** is a different colour in each solvent. In benzene and toluene it appears bright yellow, while in THF and DME it appears almost completely colourless.

The efficacy of toluene as a solvent was replicated at lower catalyst loadings (Table 4-5). When the catalyst loading is decreased to 0.5 mol% the yield in toluene is 81% after one hour and 75% in THF in the same time (Table 4-5, entry1). At even lower catalyst loadings THF appears more robust, showing 60% yield after one hour with just 0.1 mol% catalyst loading (Table 4-5, entry 2), a significant improvement on the solvent free protocol which gave 31% yield (Table 4-3, entry 4). Regardless, toluene was used as the primary solvent as it provides higher yields at reasonable catalyst loadings and is more compatible with frequent glovebox use.

Table 4-5 *– The hydroboration of acetophenone with HBpin catalysed by* ***4.12*** *at various catalysts loadings in toluene and THF. Reaction conditions: 1 h, room temperature; [a] 0.625 mmol acetophenone and HBpin, 0.1 mL solvent; [b] 1.25 mmol acetophenone and HBpin, 0.2 mL solvent.*

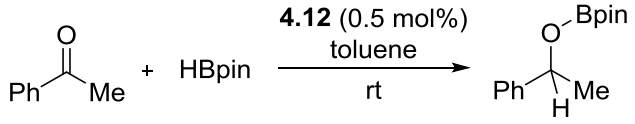

Entry	Catalyst Loading (mol%)	Yield (%)	
		THF	Toluene
1	0.5	75[a]	81[a]
2	0.1	60[a]	32[a]
3	0.05		29[b]

4.4.2 Stoichiometry

Catalysis reactions were carried out using either excess HBpin or excess acetophenone in order to determine if the yield could be improved.

When the catalysis was carried out using acetophenone as a model substrate, increasing the equivalents of HBpin to 1.2 decreased the yield to 72% (Table 4-6, entry 2). This suggests that HBpin or its decomposition products may be hindering the reaction progress. Consistently, increasing the amount of acetophenone to 1.2 equivalents increased the yield to 85% (Table 4-6, entry 3).

Table 4-6 *– The hydroboration of acetophenone catalysed by silyl anion* ***4.12*** *using excess HBpin or acetophenone. Reaction conditions: 0.625 mmol, room temperature, 40 µL toluene, 0.5 mol% catalyst loading, 1 hour.*

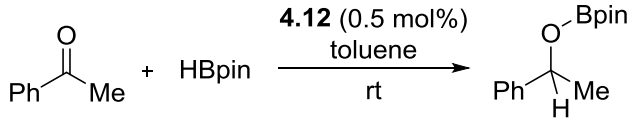

Entry	HBpin eq.	Acetophenone eq.	Yield (%)
1	1	1	81
2	1.2	1	71
3	1	1.2	85

4.4.3 Reaction Time

The silyl anion catalysed hydroboration of acetophenone was quenched after set time points in order to determine the evolution of product over time. The results are shown in Table 4-7. The results show that the reaction is complete in less than 15 minutes, after which point there is no improvement in the yield. This suggests an extremely rapid reaction followed by degradation of the catalyst, HBpin, or the final product. No HBpin was observed in the final reaction mixture by ^{1}H NMR spectroscopy. This supports the hypothesis that consumption of HBpin acts as the yield limiting process, either through reaction with substrate or through decomposition.

Table 4-7 *– The yield of the silyl anion catalysed hydrboration of acetophenone after given time periods. NMR yield measured against trimethoxybenzene as an internal standard. Reaction conditions: 0.625 mmol acetophenone and HBpin, 0.5 mol% catalyst loading, ambient temperature, 1 h.*

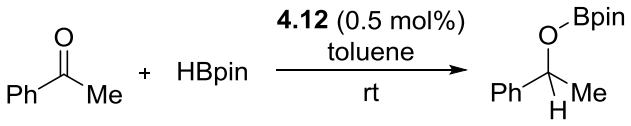

Entry	Time (min)	Yield (%)
1	15	80
2	30	83
3	45	81
4	60	81
5	90	83

4.5 Substrate Scope

In order to investigate the scope of the procedure and the functional group tolerance of the reaction a variety of substrates were subjected to the silyl anion catalysed hydroboration. The yield was determined by ^{1}H NMR spectroscopy using 1,3,5-trimethoxybenzene as an internal standard. Reactions were carried out using 0.5 mol% catalyst loading as standard. In general, reactions were performed on a 0.625 mmol scale in 40 µl solvent (15.6 M).

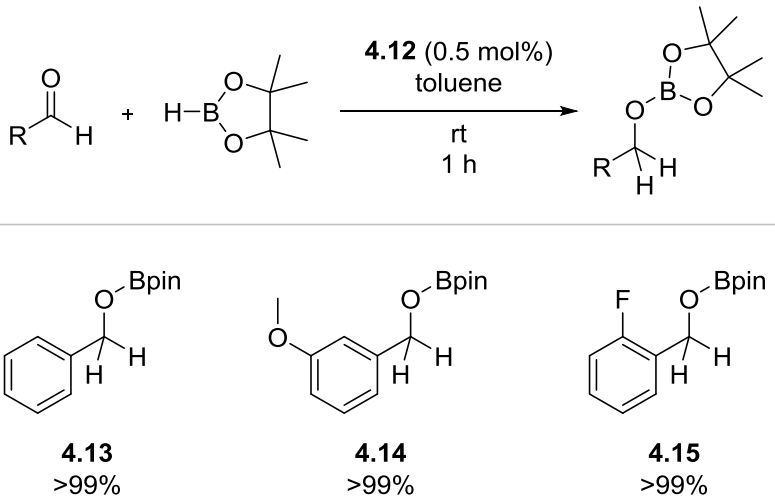

Scheme 4-12 *– Products from the hydroboration of aldehydes. Reaction conditions: 0.625 mmol substrate, 0.625 mmol HBpin, 0.5 mol%* ***4.12,*** *40 µL toluene, room temperature, one hour. NMR yield measured against trimethoxybenzene as an internal standard.*

Benzaldehyde, *m*-anisaldehyde and 2-fluorobenzaldhyde all underwent hydroboration in quantitative yields to give compounds **4.13**, **4.14** and **4.15**, respectively (Scheme 4-12). Aldehydes are generally more reactive than ketones for both steric and electronic reasons. They are considerably less sterically encumbered than ketones. Alkyl groups on ketones also offer inductive electronic stabilisation and stabilisation through hyperconjugation of the C-H σ bonding orbitals with the C=O π* antibonding orbitals. This has the overall effect of increasing the electron density on the carbon and reducing the electrophilicity of the C=O antibonding orbital and its tendency to undergo nucleophilic attack.

The electronic stabilisation afforded by alkyl groups is somewhat larger than that for aryl groups. The hydroboration of acetophenone derivatives should therefore be more accessible than dialkyl ketones.

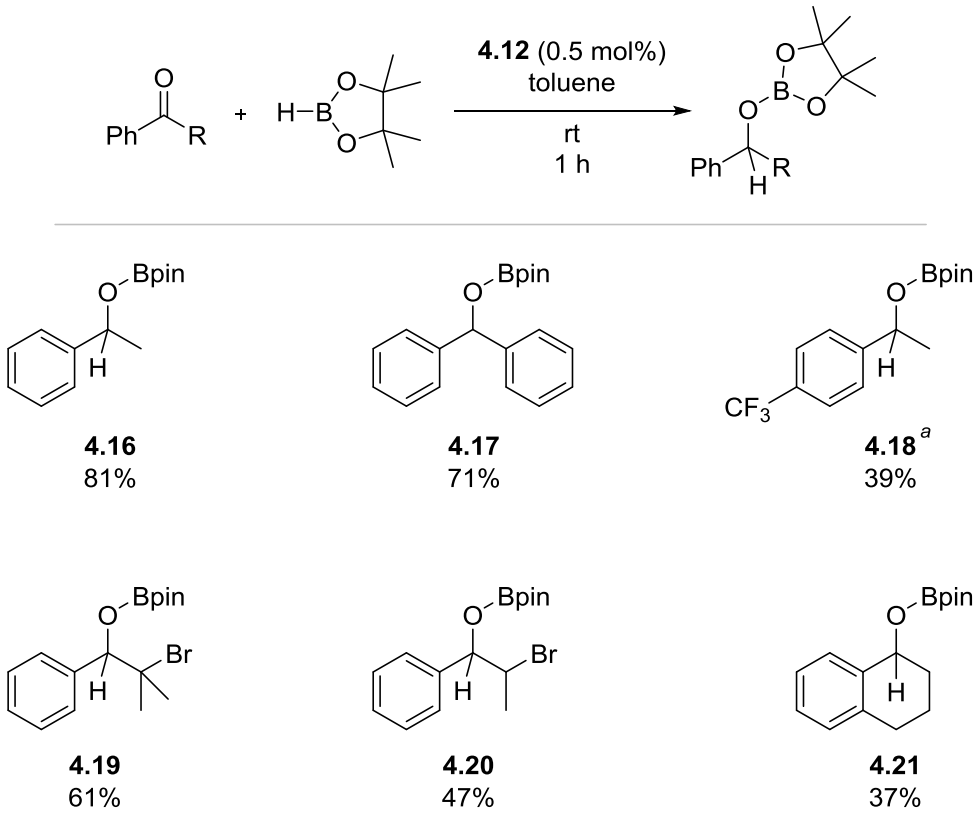

Scheme 4-13 *– Products from the hydroboration of acetophenone derived ketones. Reaction conditions: 0.625 mmol substrate, 0.625 mmol HBpin, 0.5 mol%* ***4.12,*** *40 µL toluene, room temperature, one hour. [a] 200 µL toluene added in order to dissolve the substrate. NMR yield measured against trimethoxybenzene as an internal standard.*

Indeed, all six acetophenone derivatives tested provided products in reasonable yields (Scheme 4-13). It should be noted that for lower yielding reactions the yield can be increased by increasing the catalyst loading. All reactions were carried out at 0.5 mol% catalyst loading which is on par with state-of-the-art main group catalysts for hydroboration.[34,35,47] Interestingly, 4'-(trifluoromethyl)acetophenone derivative **4.18** was only produced in 39% yield, despite the electron withdrawing nature of the CF_3 group which should make the substrate more susceptible to nucleophilic attack. This substrate is a solid which meant additional solvent was added in order to fully dissolve the substrate. This could decrease the rate due to the lower concentration. Equally, the reported yield of 71% for solid substrate benzophenone (product **4.17**) was achieved without additional solvent. When the substrate was fully dissolved the yield was decreased to 62%.

Silyl anion **4.12** is known to act as a nucleophile in nucleophilic substitution reactions.[58,62] However, the bromine leaving groups in 2-bromo*iso*butyrophenone (**4.19**, 61%) and 2-bromopropiophenone (**4.20**, 47%) were tolerated. The higher yield of **4.19** could reflect the greater steric bulk and therefore slower substitution reaction. The two diastereomers of product **4.20** were found in a ratio of 24:76.

The hydroboration of 2,4-dimethyl-3-pentanone proceeded in only trace yields (**4.22**, <3%). However, the structurally related ketone, 3-pentanone, underwent hydroboration in excellent yields (**4.23**, 77%). This suggests the low yield of **4.22** is largely due to steric effects.

It has also recently been shown that coordination of the aryl substituents to sodium plays an important role in the mechanism of the NaOH catalysed hydroboration of carbonyls with 9-BBN.[55] This effect should be increased when the counterion is potassium and explains why even bulky aryl ketones are susceptible to hydroboration under these conditions (e.g. **4.17**, **4.19** and **4.21**).

Vinyl and propargylic ketones were tolerated. Under these conditions, the hydroboration was shown to be completely selective for carbonyls over alkenes or alkynes. Furthemore, vinyl ketones were fully selective for 1,2 addition over 1,4 addition (**4.24** & **4.25**, Scheme 4-14). This shows that the mechanism does not involve the silyl anion acting as a base as this would likely lead to thermodynamic control of the reaction and 1,4-addition. Generation of the kinetic, 1,2-product suggests addition of a hard base such as a hydride. Vinyl ketones are also somewhat stabilised relative to aryl ketones but the effect is not strong enough to prevent hydroboration in this instance.

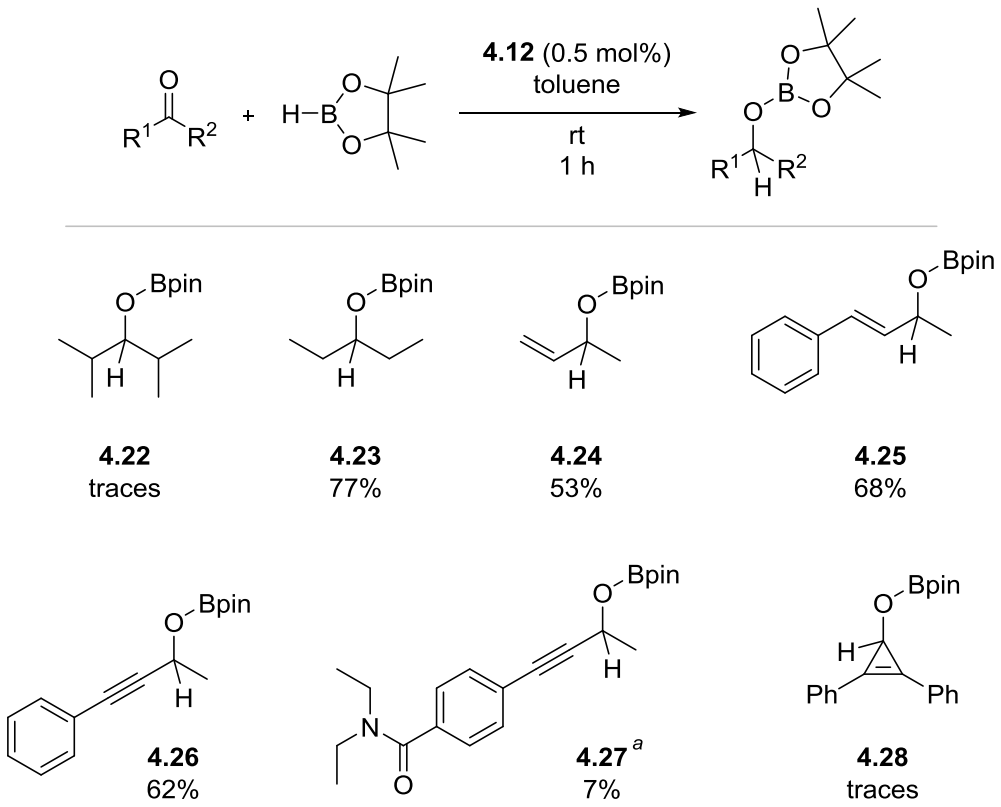

Scheme 4-14 *– Products from the hydrboration of various ketones. Reaction conditions: 0.625 mmol substrate, 0.625 mmol HBpin, 0.5 mol%* ***4.12,*** *40 µL toluene, room temperature, one hour. [a] 200 µL toluene added in order to dissolve the substrate. NMR yield measured against trimethoxybenzene as an internal standard.*

Propargyllic product **4.26** shows the same selectivity for 1,2 over 1,4 addition and no hydroboration of the triple bond under these conditions. However propargylic ketone **4.27** with an amide substituent was low yielding, perhaps in part due to addition of extra solvent. Furthermore, tertiary amides are known to undergo deoxygenation during hydrosilylation and hydroboration reactions to yield tertiary amines.[63,64] Indeed, the reaction mixture showed a complex mixture of products.

The hydroboration of diphenylcyclopropenone gave only trace yields (<3%) of product **4.28**. Diphenylcyclopropenone is characteristically aromatic with a partial positive charge on the cyclopropene ring and a partial negative charge on oxygen. Therefore, more forcing conditions may be required in order to hydrofunctionalise the ring. Indeed, the hydrofunctionalisation of a cyclopropenone has never been reported.

Finally, esters are the most deactivated class of carbonyl compounds due to the strong mesomeric donation from the adjacent oxygen lone pairs into the C=O antibonding orbital. This significantly reduces the possibility of nucleophilic attack. Indeed, three esters were shown to be resistant to hydroboration by HBpin catalysed by **4.12** (Scheme 4-15). Ethyl benzoate gave 0% yield even when heated to 80 °C for one hour (**4.29**). Reports of main-group catalysed hydroboration of esters usually use a strong main-group hydride such as $LiAlH_4$ or a three-coordinate magnesium hydride. This suggests that a much stronger hydride source is required to deliver a hydride to an ester.

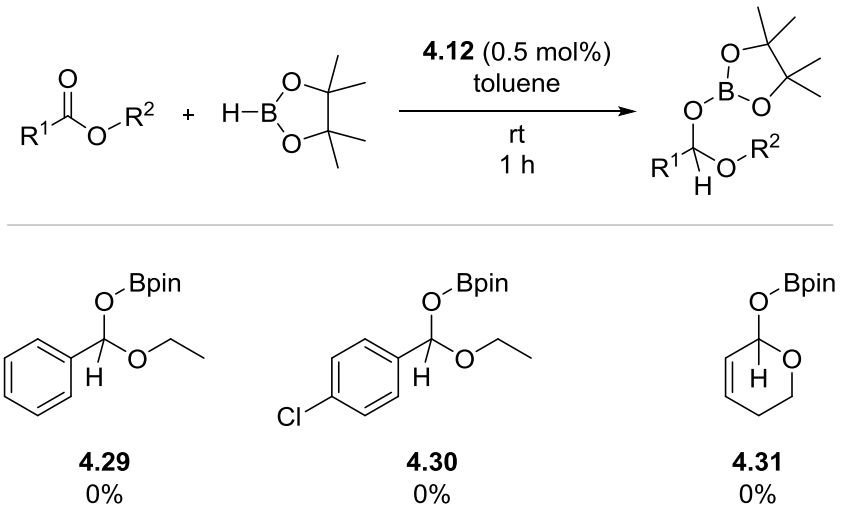

Scheme 4-15 *– Unobtained products from the hydroboration of esters. Reaction conditions: 0.625 mmol substrate, 0.625 mmol HBpin, 0.5 mol%* ***4.12,*** *40 µL toluene, room temperature, one hour. [a] 200 µL toluene added in order to dissolve the substrate. NMR yield measured against trimethoxybenzene as an internal standard.*

4.6 Mechanistic Investigation

The proposed mechanism for the silyl anion initiated hydroboration of carbonyls is shown in Scheme 4-16. The initiation step is addition of silyl anion **4.12** to pinacolborane to generate boron-ate complex **4.32**. The hydride of boron-ate **4.32** attacks the substrate to generate an alkoxide as the active species, eliminating silylboronic ester **4.33**. A series of stoichiometric reactions were carried out in order to gain evidence to support the proposed mechanism.

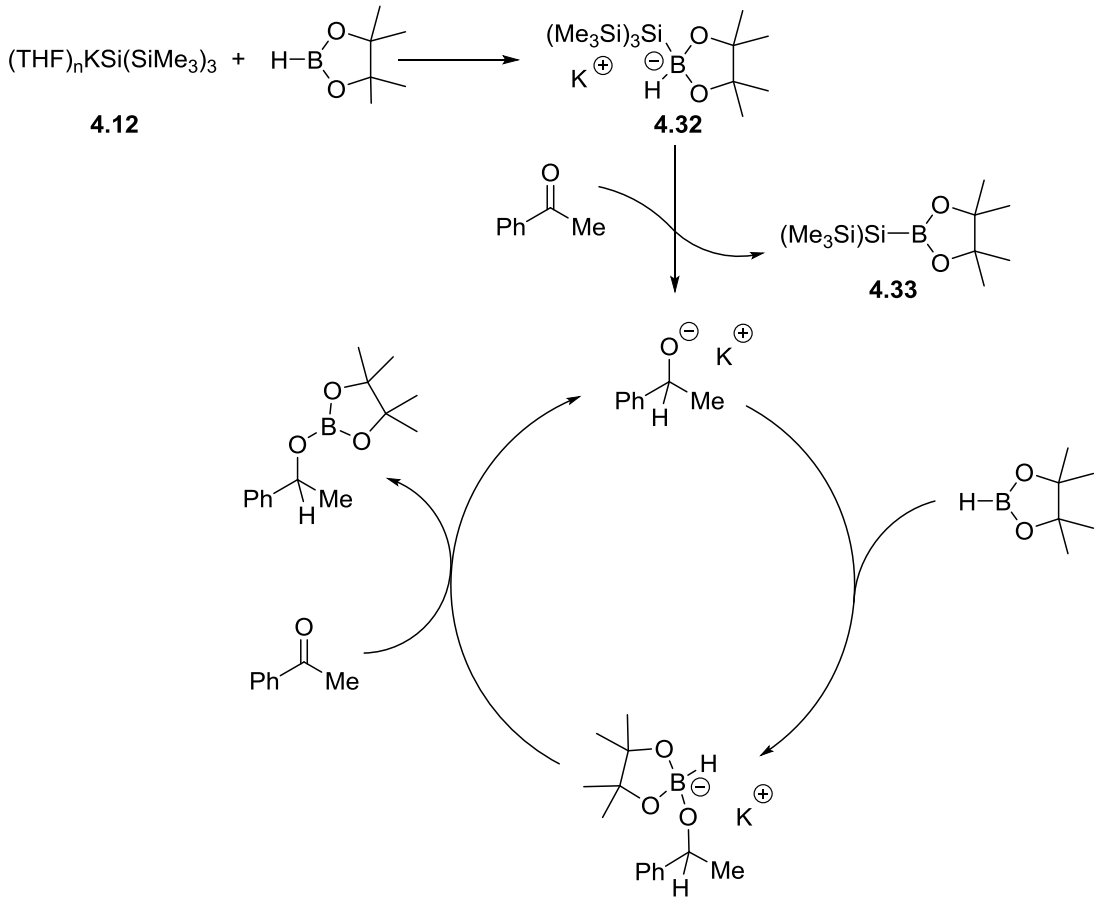

Scheme 4-16 *– Proposed mechanism for the silyl anion initiated hydroboration of acetophenone.*

4.6.1 Stoichiometric Reaction of Silyl Anion 4.12 with HBpin

The stoichiometric reaction of anion **4.12** with pinacolborane affords a gel-like solid when carried out in THF, benzene or in the absence of solvent.

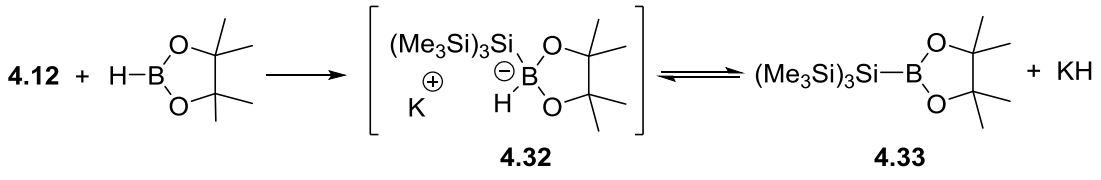

Poor solubility in C_6D_6

Scheme 4-17 *– The reaction of* ***4.12*** *with HBpin to give* ***4.33*** via *boron-ate* ***4.32****.*

When the reaction is carried out in C_6D_6, a sole broad singlet is observed in the ^{11}B NMR at δ 37.4 ($\nu_{½}$ = 230 Hz) which corresponds to silylboronic ester **4.33**, a reported compound

(Scheme 4-17).[65] This is downfield shifted relative to the sharp doublet observed for HBpin (δ 28.5, d, $^1J_{B\text{-}H}$ = 174 Hz, $\nu_{½}$ = 32 Hz). The observation of silylboronic ester **4.33** suggests boron-ate **4.32** as an intermediate.

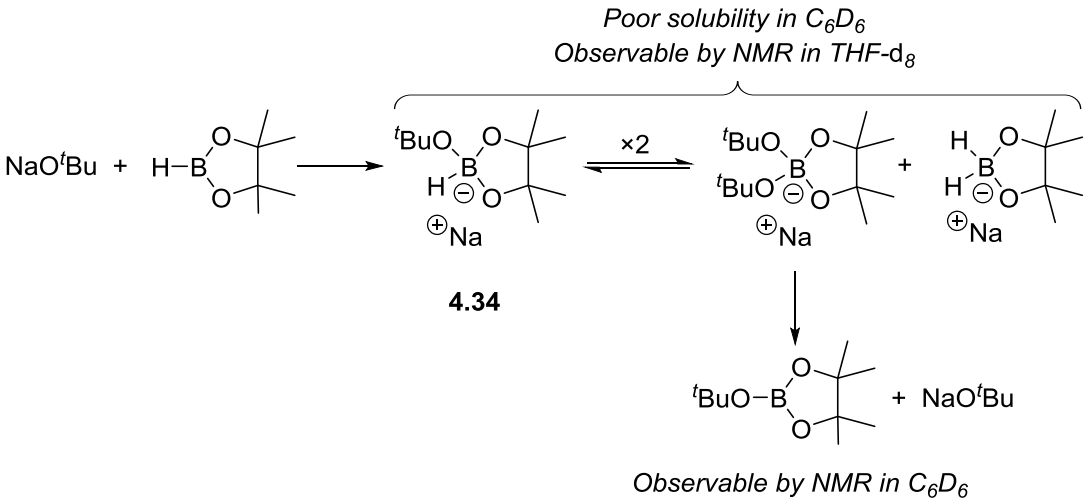

***Scheme 4-18** –The reaction of HBpin with NaO^{t}Bu gives a mixture of four coordinate boron-ate species in a ligand exchange equilibrium which are only observable in THF-d_8. Only the three coordinate boric ester is observable in apolar solvents such as C_6D_6.[54]*

The related reaction of NaO^{t}Bu with HBpin generates boron-ate complex **4.34**, which is in equilibrium with other boron-ate species in solution, as shown in Scheme 4-18.[54] However, only the three coordinate boric ester was observed in C_6D_6 due to poor solubility of the charged species.[54] This ligand exchange is less likely when substituting NaO^{t}Bu for **4.12** due to the massive steric bulk of the silyl anion but is still able to explain the observation of **4.33** as the sole product in C_6D_6.

However, in THF, the reaction of silyl anion **4.12** with HBpin shows three major products by ^{11}B NMR. Silylboronic ester **4.33** is the major product at δ 37.4. A sharp quartet at δ −45.4 ($^1J_{B\text{-}H}$ = 88 Hz) is indicative of BH_3·THF complex. A further sharp singlet is observed at δ 8.4 ($\nu_{½}$ = 32 Hz). The resonance at δ 8.4 is tentatively assigned to the silyl boron-ate complex **4.32** on the basis of its similarity with the boric ester **4.34** (δ 6.2) and the chemical shifts reported for trialkoxyborohydrides reported by Brown (δ 0.0 – 6.7).[66] While simple trialkoxyborohydrides give doublets in the ^{11}B NMR, the NaO^{t}Bu and KO^{i}Pr adducts of HBpin were reported as singlets. Silyl anion adduct **4.32** also appears as a singlet. BH_3 is a known

catalyst for hydroboration[67] and the presence of BH_3 in this reaction strongly suggests that when the catalysis is carried out in THF, BH_3 could play an active role.

Filtration of the reaction mixture through a silica plug allows isolation of silylboronic ester **4.33** as the pure product. This method of purification was first used to prepare boronic ester **4.33** by the reaction of anion **4.12** with ^{i}PrOBpin, as shown in Scheme 4-19.[65]

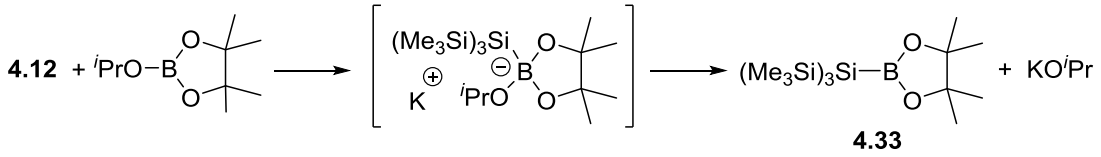

***Scheme 4-19** – The original synthesis of **4.33** from silyl anion **4.12** and* a boric ester.[65]

The formation of silylboronic ester **4.33** under the reaction conditions serves as evidence of **4.32** in the reaction mixture. This implies an analogous initial step to that reported for the alkoxide catalysed reaction shown in Scheme 4-9.[54] Given the large steric bulk and strong electron-donating ability of the silyl group, delivery of the hydride from **4.32** to acetophenone should be rapid, even compared with the analogous alkoxy borohydride. This is concordant with the lower catalyst loadings required for **4.12** compared with NaO^{t}Bu as the initiation step should be faster.[54]

BH_3 is a known catalyst for hydroboration chemistry.[67] The observation of BH_3 in the stoichiometric reaction of **4.12** with HBpin could suggest that BH_3 is the active catalyst. This is discussed further in section 4.7, however the hydroboration of alkenes and alkynes using **4.12** is not comparable to the BH_3 catalysed reduction, and BH_3 is not observed in C_6D_6 which is more similar to the reaction solvent, toluene. Therefore, BH_3 was ruled out as the active catalyst when the reaction is carried out in toluene.

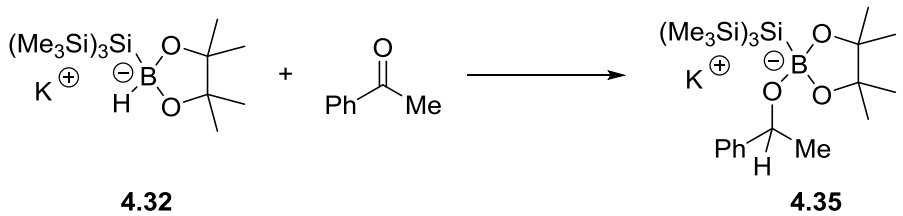

***Scheme 4-20** – The proposed reaction of boron-ate **4.32** to give complex **4.35**.*

The stoichiometric reaction of *in situ* generated boron-ate **4.32** with acetophenone gives a new boron-ate species with an ^{11}B NMR singlet resonance at δ 6.4 which is tentatively assigned to complex **4.35** based on similarity with other boron-ate compounds.[54,66] The ^{1}H and ^{29}Si NMR spectra show an intractable mixture of products.

4.6.2 Stoichiometric Reaction of Silyl Anion 4.12 with Acetophenone

The stoichiometric reaction of anion **4.12** with acetophenone was also investigated in order to determine any other possible initiation pathways. Given the propensity of **4.12** to act as a nucleophile in nucleophilic substitution reactions,[68,69] alkoxide **4.36** (Scheme 4-21) is a potential intermediate. Equally, **4.12** can act as a base so could lead to formation of enolate **4.37**. The reaction was carried out in benzene, THF and in the absence of solvent.

When the reaction is carried out without solvent, the reaction turns deep purple and a complex mixture of products is observed in the ^{1}H, ^{13}C and ^{29}Si NMR spectra. In particular, the ^{29}Si NMR spectrum shows resonances corresponding to tetrakis(trimethylsilyl)silane ($Si(SiMe_3)_4$) at δ −136 and tris(trimethylsilylsilane) ($HSi(SiMe_3)_3$) at δ −115. There is also evidence of remaining anion **4.12** at δ −190.

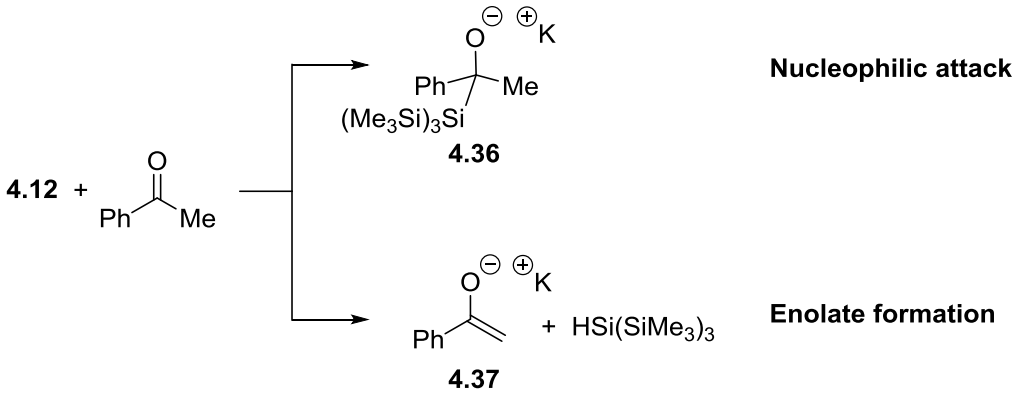

Scheme 4-21 *– Potential products of the reaction of* ***4.12*** *with acetophenone: nucleophilic attack to afford alkoxide* ***4.36*** *or deprotonation to afford enolate* ***4.37****.*

When the reaction is carried out in THF-d_8 the crude ^{1}H, ^{13}C and ^{29}Si spectra show a complex mixture of products. Some significant resonances are observed in the ^{13}C NMR spectrum at δ 68.2 and δ 73.2 which are in the region typical of alkoxides and could therefore correspond to alkoxide **4.36**.

When the reaction is carried out in C_6D_6 only one major product is observed which is assigned as alkoxde **4.36**. The ^{13}C NMR spectrum shows a sharp singlet at δ 75.1 which is in the region typical of alkoxides. Correlation spectroscopy shows long range coupling between the ^{13}C signal at δ 75.1 and multiplets in the aromatic region of the ^{1}H NMR between δ 7.40 and δ 7.38, assigned to the phenyl group of alkoxide **4.36**. The ^{13}C signal at δ 75.1 also shows long range correlation to a sharp singlet at δ 1.88 in the ^{1}H NMR which is assigned to the methyl group of alkoxide **4.36**. Enolate **4.37** should show no aliphatic signals and is therefore discounted.

Notably, a new, unidentified silane is observed as a minor product when the reaction is carried out in both C_6D_6 and THF. It was identified by an Si-H signal at δ 3.85 in the ^{1}H spectrum and δ −39 in the ^{29}Si spectrum with a $^{1}J_{HSi}$ coupling constant of 160 Hz. Correlation spectroscopy shows a related ^{29}Si signal at δ −16. The ^{1}J coupling constant of 160 Hz and the ^{1}H chemical shift of δ 3.85 likely indicate a four coordinate silicon(IV) compound.

The presence of **4.36** and **4.37** in solution could lead to a variety of rearrangement products. For example, alkoxide species are able to abstract $SiMe_3$ groups from polysilanes, as in the preparation of **4.12.**[60] The proposed mechanism for the base-catalysed reduction of ketones proceeds *via* alkoxide intermediates, therefore **4.36** and **4.37** will be both propagators of the reaction in the proposed mechanism shown in Scheme 4-16.

4.7 Attempted Hydroboration of Alkynes

Test reactions were carried out in order to determine the activity of silyl anion **4.12** in the hydroboration of alkynes. This reaction should be significantly more challenging due to the lack of an electrophilic centre. Indeed, for most main-group hydride catalysts, more forcing conditions are required in order to convert non-polar substrates.

For example $LiAlH_4$ is able to convert ketones to the boric ester in high yields at room temperature in 30 minutes with only 0.5 mol% catalyst loading. To convert alkenes to the corresponding boronic ester, four hours at 110 °C with 10 mol% catalyst loading is required[47] and phenylacetylene requires two hours at 60 °C.[70]

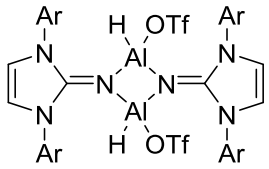

4.38

Scheme 4-22 *– Alluminium hydride* ***4.38****, a reported catalyst for the hydroboration of polar and apolar substrates.*[16]

Equally, the N-heterocyclicimino aluminium hydride **4.38** carries out the hydroboration of acetophenone at 60 °C in six hours, while phenylacetylene requires 40 hours at 80 °C.[16]

Given that anion **4.12** is able to generate a boron hydride labile enough to catalyse carbonyl reduction at room temperature in under one hour and at low catalyst loadings, the hydroboration of alkynes and alkenes should be achievable, even if prolonged heating is required.

As expected, the hydroboration of phenylacetylene did not occur at room temperature in the presence of **4.12.** However, when the reaction mixture was heated to 60 °C for two hours with 10 mol% catalyst loading, trace yields of the vinyl boronic ester were observed (Table 4-8, entry 2). Heating the reaction mixture to 110 °C gave 74% yield in two hours (entry 4), comparable activity to that reported for aluminium hydrides.[14–16]

Table 4-8 *– Conditions for the silyl anion catalysed hydroboration of phenylacetylene. Standard conditions: 0.5 mmol substrate, 0.55 mmol HBpin, neat.*

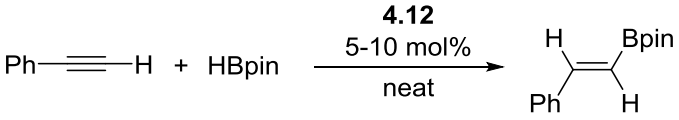

Entry	Catalyst Loading (mol%)	Temperature (°C)	Time (h)	Conversion (%)
1	10	rt	0.5	0
2	10	60	2	< 3
3	5	110	1	17
4	10	110	2	74

Initially the silyl anion catalyzed hydroboration of alkynes was tested with a small number of substrates (Scheme 4-23). The highest yield was found for phenylacetylene but all four substrates showed some conversion. Terminal alkynes were 100% selective for the linear product.

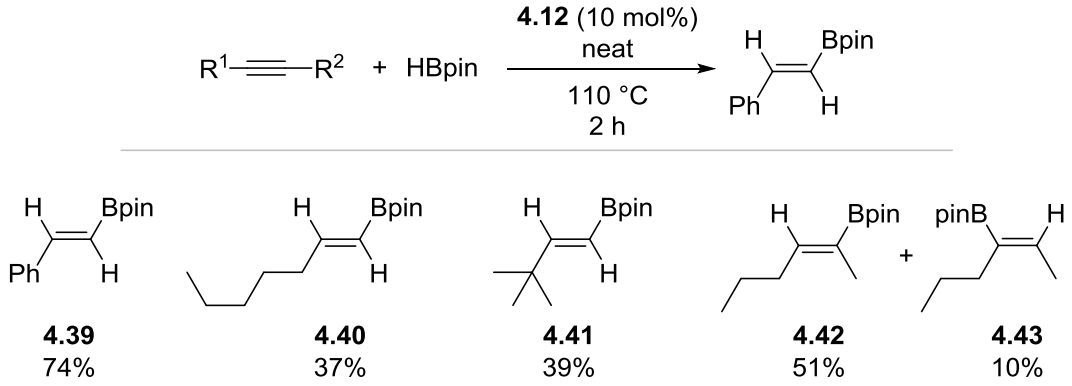

Scheme 4-23 *– Substrates in the silyl anion catalysed hydrboration of actylenes. Reaction conditions: 0.5 mmol substrate, 0.55 mmol HBpin, no solvent, 110 °C, 2 hours. NMR yield measured against trimethoxybenzene as an internal standard.*

Interestingly, **4.12** was able to catalyse the hydroboration of an internal alkyne, 2-hexyne (**4.42** and **4.43**). This proves that the mechanism cannot involve deprotonation of the alkyne which has been previously suggested for an aluminium hydride catalyst[15] and may be expected for a basic catalyst such as **4.12.** A recent report showed that sodium hydroxide is able to initiate the hydroboration of terminal alkynes but not internal alkynes.[55] Although the authors did not comment on the mechanism, the selectivity for terminal over internal alkynes could suggest acetylide coordination to HBpin to generate a boron-ate as shown in Scheme 4-24.

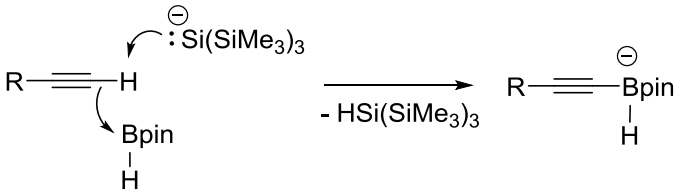

Scheme 4-24 *– Potential formation of an alkynyl boron-ate species.*

The hydroboration of an internal alkyne to give products **4.42** and **4.43** strongly suggests that deprotonation is not the main mechanism of alkyne hydroboration. Although silyl boron-ate

4.32 may be able to add directly to the alkyne, it is much more likely that the mechanism involves degradation of HBpin by anion **4.12** to give BH_3, which is reported to catalyse hydroboration reactions.[67]

The results for the hydroboration using **4.12** as a catalyst were largely unreliable, with yields varying from 20% to 80% under the same conditions for the same substrate. Furthermore, BH_3 was observed in the stoichiometric reaction between HBpin and **4.12** when it was carried out in THF. This is likely exacerbated by the high reaction temperatures and long reaction times.

The catalyst free hydroboration of alkynes by HBpin was actually reported with the initial publication of the preparation of HBpin,[71] presumably due to contamination by the BH_3 which was used to synthesise the HBpin.

Given the unreliable results and the likelihood that the catalysis is actually performed by BH_3, the hydroboration of alkynes was not pursued further.

4.8 Conclusions and Outlook

In conclusion, the silyl anion initiated hydroboration of aldehydes and ketones has been reported. This is an extremely rare example of a low-oxidation state silicon species acting as a catalyst and is the first example for hydroboration. The initiator, silyl anion **4.12**, is easy to prepare from commercially available reagents.

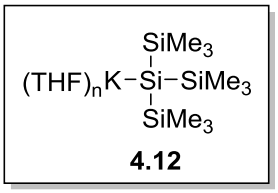

4.12

The mechanism was shown to proceed *via* coordination of the anion **4.12** to pinacolborane in order to generate a strong hydride which facilitates addition to the C=O bond.

The reported protocol was shown to tolerate a range of functionalities with strong selectivity for aldehydes and ketones over esters, alkenes and alkynes.

Furthermore, under more forcing conditions, **4.12** was shown to initiate the hydroboration of alkynes. However, it is likely that the active species is BH_3 produced *in situ*.

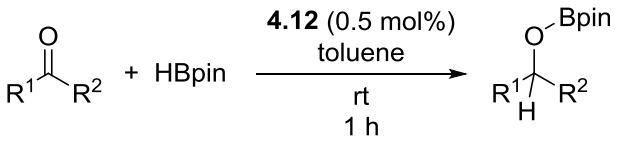

14 examples
Up up quantitative yields

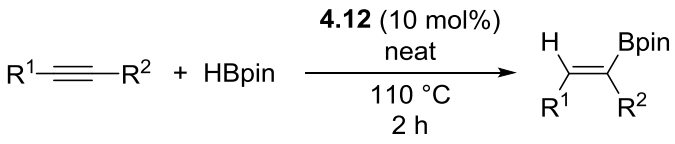

Preliminary studies
4 examples

4.9 References

[1] A. Suzuki, *Angew. Chem. Int. Ed.* **2011**, *50*, 6722–6737.

[2] N. Miyaura, A. Suzuki, *J. Chem. Soc. Chem. Commun.* **1979**, 866–867.

[3] Norio. Miyaura, Akira. Suzuki, *Chem. Rev.* **1995**, *95*, 2457–2483.

[4] A. J. J. Lennox, G. C. Lloyd-Jones, *Chem. Soc. Rev.* **2013**, *43*, 412–443.

[5] H. C. Brown, S. Krishnamurthy, *Tetrahedron* **1979**, *35*, 567–607.

[6] J. X. Qiao, P. Y. S. Lam, *Synthesis* **2011**, *2011*, 829–856.

[7] J. Huang, W. Yan, C. Tan, W. Wu, H. Jiang, *Chem. Commun.* **2018**, *54*, 1770–1773.

[8] D. M. Khramov, E. L. Rosen, J. A. V. Er, P. D. Vu, V. M. Lynch, C. W. Bielawski, *Tetrahedron* **2008**, *64*, 6853–6862.

[9] Y. Yamamoto, R. Fujikawa, T. Umemoto, N. Miyaura, *Tetrahedron* **2004**, *60*, 10695–10700.

[10] S. Pereira, M. Srebnik, *J. Am. Chem. Soc.* **1996**, *118*, 909–910.

[11] Kevin. Burgess, M. J. Ohlmeyer, *Chem. Rev.* **1991**, *91*, 1179–1191.

[12] P. Chirik, R. Morris, *Acc. Chem. Res.* **2015**, *48*, 2495–2495.

[13] L. L. Schafer, P. Mountford, W. E. Piers, *Dalton Trans.* **2015**, *44*, 12027–12028.

[14] A. Bismuto, S. P. Thomas, M. J. Cowley, *Angew. Chem. Int. Ed.* **2016**, *55*, 15356–15359.

[15] Z. Yang, M. Zhong, X. Ma, S. De, C. Anusha, P. Parameswaran, H. W. Roesky, *Angew. Chem. Int. Ed.* **2015**, *54*, 10225–10229.

[16] D. Franz, L. Sirtl, A. Pöthig, S. Inoue, *Z. Für Anorg. Allg. Chem.* **2016**, *642*, 1245–1250.

[17] H. R. Kim, I. G. Jung, K. Yoo, K. Jang, E. S. Lee, J. Yun, S. U. Son, *Chem. Commun.* **2010**, *46*, 758–760.

[18] Y. Lee, A. H. Hoveyda, *J. Am. Chem. Soc.* **2009**, *131*, 3160–3161.

[19] L. Zhang, D. Peng, X. Leng, Z. Huang, *Angew. Chem. Int. Ed.* **2013**, *52*, 3676–3680.

[20] B. T. Cho, *Chem. Soc. Rev.* **2009**, *38*, 443–452.

[21] U. K. Das, C. S. Higman, B. Gabidullin, J. E. Hein, R. T. Baker, *ACS Catal.* **2018**, *8*, 1076–1081.

[22] C. C. Chong, R. Kinjo, *ACS Catal.* **2015**, *5*, 3238–3259.

[23] I. Sarvary, F. Almqvist, T. Frejd, *Chem. – Eur. J.* **2001**, *7*, 2158–2166.

[24] F. Almqvist, L. Torstensson, A. Gudmundsson, T. Frejd, *Angew. Chem. Int. Ed. Engl.* **1997**, *36*, 376–377.

[25] C. W. Lindsley, M. DiMare, *Tetrahedron Lett.* **1994**, *35*, 5141–5144.

[26] G. Giffels, C. Dreisbach, U. Kragl, M. Weigerding, H. Waldmann, C. Wandrey, *Angew. Chem. Int. Ed. Engl.* **1995**, *34*, 2005–2006.

[27] S. G. Roh, J. U. Yoon, J. H. Jeong, *Polyhedron* **2004**, *23*, 2063–2067.

[28] M. Locatelli, P. G. Cozzi, *Angew. Chem. Int. Ed.* **2003**, *42*, 4928–4930.

[29] S.-G. Roh, Y.-C. Park, D.-K. Park, T.-J. Kim, J. H. Jeong, *Polyhedron* **2001**, *20*, 1961–1965.

[30] M. Bandini, P. G. Cozzi, M. de Angelis, A. Umani-Ronchi, *Tetrahedron Lett.* **2000**, *41*, 1601–1605.

[31] A. Kaithal, B. Chatterjee, C. Gunanathan, *Org. Lett.* **2015**, *17*, 4790–4793.

[32] V. L. Weidner, C. J. Barger, M. Delferro, T. L. Lohr, T. J. Marks, *ACS Catal.* **2017**, *7*, 1244–1247.

[33] L. Koren-Selfridge, H. N. Londino, J. K. Vellucci, B. J. Simmons, C. P. Casey, T. B. Clark, *Organometallics* **2009**, *28*, 2085–2090.

[34] M. Arrowsmith, T. J. Hadlington, M. S. Hill, G. Kociok-Köhn, *Chem. Commun.* **2012**, *48*, 4567–4569.

[35] T. J. Hadlington, M. Hermann, G. Frenking, C. Jones, *J. Am. Chem. Soc.* **2014**, *136*, 3028–3031.

[36] Thomas Jefferson National Accelerator Facility - Office of Science Education, "It's Elemental - The Periodic Table of Elements," can be found under https://education.jlab.org/itselemental/, **2019**.

[37] P. P. Power, *Nature* **2010**, *463*, 171–177.

[38] C. Weetman, S. Inoue, *ChemCatChem* **2018**, *10*, 4213–4228.

[39] A. J. Blake, A. Cunningham, A. Ford, S. J. Teat, S. Woodward, *Chem. – Eur. J.* **2000**, *6*, 3586–3594.

[40] T. J. Hadlington, C. Jones, *Chem. Commun.* **2014**, *50*, 2321–2323.

[41] T. J. Hadlington, M. Hermann, J. Li, G. Frenking, C. Jones, *Angew. Chem. Int. Ed.* **2013**, *52*, 10199–10203.

[42] A. Jana, H. W. Roesky, C. Schulzke, *Inorg. Chem.* **2009**, *48*, 9543–9548.

[43] A. Jana, H. W. Roesky, C. Schulzke, A. Döring, *Angew. Chem. Int. Ed.* **2009**, *48*, 1106–1109.

[44] A. Jana, H. W. Roesky, C. Schulzke, *Dalton Trans.* **2009**, *39*, 132–138.

[45] S. Sinhababu, D. Singh, M. K. Sharma, R. K. Siwatch, P. Mahawar, S. Nagendran, *Dalton Trans.* **2019**, *48*, 4094–4100.

[46] V. K. Jakhar, M. Kr. Barman, S. Nembenna, *Org. Lett.* **2016**, *18*, 4710–4713.

[47] A. Bismuto, M. J. Cowley, S. P. Thomas, *ACS Catal.* **2018**, *8*, 2001–2005.

[48] K. Kuciński, G. Hreczycho, *Green Chem.* **2019**, *21*, 1912–1915.

[49] D. Mukherjee, H. Osseili, T. P. Spaniol, J. Okuda, *J. Am. Chem. Soc.* **2016**, *138*, 10790–10793.

[50] Z. Yang, M. Zhong, X. Ma, K. Nijesh, S. De, P. Parameswaran, H. W. Roesky, *J. Am. Chem. Soc.* **2016**, *138*, 2548–2551.

[51] M. K. Bisai, S. Pahar, T. Das, K. Vanka, S. S. Sen, *Dalton Trans.* **2017**, *46*, 2420–2424.

[52] S. S. Sen, H. W. Roesky, D. Stern, J. Henn, D. Stalke, *J. Am. Chem. Soc.* **2010**, *132*, 1123–1126.

[53] K. Abdur-Rashid, S. E. Clapham, A. Hadzovic, J. N. Harvey, A. J. Lough, R. H. Morris, *J. Am. Chem. Soc.* **2002**, *124*, 15104–15118.

[54] I. P. Query, P. A. Squier, E. M. Larson, N. A. Isley, T. B. Clark, *J. Org. Chem.* **2011**, *76*, 6452–6456.

[55] Y. Wu, C. Shan, J. Ying, J. Su, J. Zhu, L. L. Liu, Y. Zhao, *Green Chem.* **2017**, *19*, 4169–4175.

[56] W. K. Shin, H. Kim, A. K. Jaladi, D. K. An, *Tetrahedron* **2018**, *74*, 6310–6315.

[57] Z. Zhu, X. Wu, X. Xu, Z. Wu, M. Xue, Y. Yao, Q. Shen, X. Bao, *J. Org. Chem.* **2018**, *83*, 10677–10683.

[58] C. Präsang, D. Scheschkewitz, in *Functional Molecular Silicon Compounds II* (Ed.: D. Scheschkewitz), Springer International Publishing, **2013**, pp. 1–47.

[59] H. Stachowiak, J. Kaźmierczak, K. Kuciński, G. Hreczycho, *Green Chem.* **2018**, *20*, 1738–1742.

[60] C. Marschner, *Eur. J. Inorg. Chem.* **1998**, *1998*, 221–226.

[61] H. Gilman, C. L. Smith, *J. Organomet. Chem.* **1968**, *14*, 91–101.

[62] K. Tamao, A. Kawachi, in *Adv. Organomet. Chem.* (Ed.: F. Gordon, A. Stone, and R. West), Academic Press, **1995**, pp. 1–58.

[63] J. A. Fernández-Salas, S. Manzini, S. P. Nolan, *Chem. Commun.* **2013**, *49*, 9758–9760.

[64] N. L. Lampland, M. Hovey, D. Mukherjee, A. D. Sadow, *ACS Catal.* **2015**, *5*, 4219–4226.

[65] E. Yamamoto, R. Shishido, T. Seki, H. Ito, *Organometallics* **2017**, *36*, 3019–3022.

[66] H. C. Brown, J. S. Cha, B. Nazer, *Inorg. Chem.* **1984**, *23*, 2929–2931.

[67] N. W. J. Ang, C. S. Buettner, S. Docherty, A. Bismuto, J. R. Carney, J. H. Docherty, M. J. Cowley, S. P. Thomas, *Synthesis* **2018**, *50*, 803–808.

[68] D. Wendel, T. Szilvási, C. Jandl, S. Inoue, B. Rieger, *J. Am. Chem. Soc.* **2017**, *139*, 9156–9159.

[69] A. V. Protchenko, A. D. Schwarz, M. P. Blake, C. Jones, N. Kaltsoyannis, P. Mountford, S. Aldridge, *Angew. Chem. Int. Ed.* **2013**, *52*, 568–571.

[70] A. Bismuto, *Unpubl. Work* **2018**.

[71] C. E. Tucker, J. Davidson, P. Knochel, *J. Org. Chem.* **1992**, *57*, 3482–3485.

Summary and Outlook

Summary and Outlook

This thesis has studied the fundamental chemistry of disilenes and silylenes and proven the potential of a silyl anion in nucleophile promoted hydroboration catalysis.

Chapter 2 reports a novel route to disilenes with small substituents, some of which can rearrange to their silylsilylene isomers. Several disilene and silylsilylene adducts were reported. Two disilene adducts, **2.28** and **2.50**, and one base-coordinated silylsilylene, **2.37**, were isolated and fully characterised. Through a base-coordination strategy, the disilene to silylsilylene rearrangement has been observed and controlled for the first time. Further work should focus on the reactivity of *in situ* generated, base-free disilenes and silylenes, for example with carbon monoxide or dinitrogen.

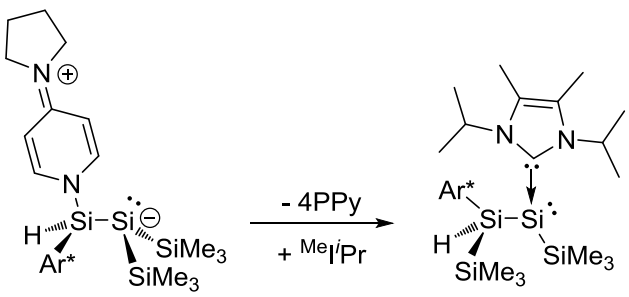

2.50 **2.37**

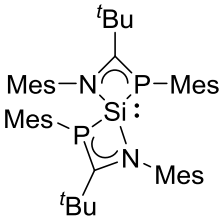

3.21

Chapter 3 studies three novel, bulky phospha-amidinate ligands. Coordination of the phosph-amidinate ligands to silicon gave phospha-amidinato silanes **3.10**, **3.13**, **3.14** and **3.15**. Reductions and reductive dehydrochlorinations of phospha-amidinato silanes led to the observation of some new silylenes, including four-coordinate silylene **3.21** which was isolated and fully characterised. The weak Si-P bonds in phospha-amidinato silylenes prevented onward study, however pohspha-amidinate ligands were found to be suitable for other main group elements, including aluminium and magnesium. Future work should focus on preparing different phosphorus substituents for silicon and other main group elements

Chapter 4 is the first report of low oxidation state silicon in hydroboration catalysis. The bulky hypersilyl anion, **4.12**, was found to be an active initiator for the hydroboration of aldehydes and ketones. The substrate scope and mechanism of the reaction were reported. It was found that the reaction proceeds through coordination of the silyl

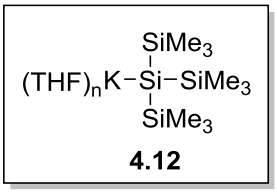

4.12

anion to pinacolborane to generate a reactive borohydride. Reaction of the borohydride with the carbonyl substrate generates an alkoxide species as the active catalyst. Furthermore, the silyl anion was found to initiate the hydroboration of alkynes. This was shown to most likely proceed through formation of BH_3 in the reaction mixture, a reported catalyst for hydroboration of alkynes. Future work should focus on preparing other silyl anions to compare their reactivity with **4.12**, for example in stereoselectivity.

Chapter 5
Experimental Methods

Chapter 5 Experimental Methods

5.1 General Considerations

All manipulations were carried out under an argon atmosphere using standard Schlenk or glovebox techniques. Solvents were either obtained from an Inert solvent purification system or distilled under argon prior to use. All solvents were stored over 4 Å molecular sieves. Dichloromethane and pyridine were distilled from calcium hydride, other solvents were distilled from sodium and benzophenone. Deuterated dichloromethane was distilled from calcium hydride and all other deuterated solvents were distilled from potassium and stored over 4 Å molecular sieves.

NMR spectra were recorded on Bruker PRO 500 MHz or AVA 500 MHz spectrometers. ^{1}H and ^{13}C NMR spectra were referenced to residual solvent signals.[1] ^{29}Si NMR spectra were referenced to an external standard of tetramethylsilane ($SiMe_4$). ^{31}P spectra were referenced to 85% H_3PO_4 in D_2O as an external standard. ^{11}B spectra were referenced to an external standard of trimethylborate ($B(OMe)_3$).

UV/Vis spectra were acquired under argon in hexane on a Varian Cary 300 UV-visible Spectrophotometer. Elemental analyses (EA) were performed by Stephen Boyer at London Metropolitan University. Mass spectrometry was performed by Alan Taylor at the University of Edinburgh.

The following compounds were prepared according to literature procedures: pentamethylcyclopentadiene (Cp*H),[2] 2,4,6-tri-tert-butylphenylphosphine (Mes^*PH_2),[3] 1,3,4,5-tetramethylimidazol-2-ylidene ($^{Me}I^iPr$),[4] 1,5-diisopropyl-3,4-dimethylimidazol-2-ylidene (^{Me}IMe),[4] bis-1,5-(2,6-diisopropylphenyl)imidazol-2-ylidene (IPr),[5] *N*-mesitylpivalamide,[6] (*N*-phenyl)(*tert*-butyl)carbonitrilium triflate,[6] Cp^*SiHCl_2,[7] Ar^*SiHCl_2,[8] $(THF)_nKSi(SiMe_3)_3$.[9]

Trichloro- and tetrachlorosilane were distilled from magnesium prior to use. Pinacolborane was distilled prior to use. All other regeants were obtained commercially and used without further purification.

5.2 Experimental Details for Chapter 2

5.2.1 Preparation of silane 2.23

Tris(trimethylsilyl)pentamethylcyclopentadienylchlorosilane [(Cp*)(Si(SiMe$_3$))SiHCl]

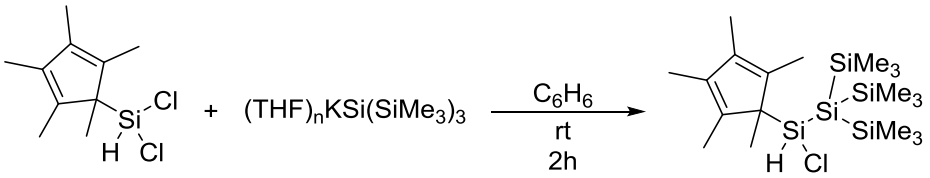

2.23

A solution of Cp*SiHCl$_2$ (1.15 g, 4.9 mmol) in C$_6$H$_6$ (10 mL) was added over 10 seconds to KSi(SiMe$_3$)$_3$·THF$_n$ (2.0 g, 4.9 mmol, n = 1.67) in C$_6$H$_6$ (40 mL) at room temperature giving a yellow/orange mixture which was stirred for 2 hours at room temperature. The volatiles were removed under reduced pressure and the resulting waxy solid was extracted with warm (45 °C) hexane (50 mL). The filtrate was concentrated and cooled to afford colourless, block-shaped crystals of silane **2.23** (1.35 g, 62%) of excellent purity for further synthetic work. Samples of higher purity could be obtained by dissolution of **2.23** in hexane, filtration through celite and multiple recrystallisations.

^{1}H NMR (500.2 MHz, C$_6$D$_6$, 300 K): δ (ppm) 5.43 (s, 1H, Si-*H*, $^1J_{H\text{-}Si}$ = 200 Hz, $^2J_{H\text{-}Si}$ = 13 Hz), 1.79 (br s, 15H, Cp*-C*H*$_3$), 0.27 (s, 27H, Si(Si*Me*$_3$)$_3$).

^{13}C{^{1}H} NMR (125.8 MHz, C$_6$D$_6$, 300 K): δ (ppm) 136.0 (br s, Cp* *C*-Me) 11.7 (br s, Cp* -*C*H$_3$), 2.4 (s, Si(Si*Me*$_3$)$_3$, $^1J_{C\text{-}Si}$ = 45 Hz).

^{29}Si{^{1}H} NMR (99.4 MHz, C$_6$D$_6$, 300 K): δ (ppm) 20.2 (s, Si-H), − 8.8 (s, Si(*Si*Me$_3$)$_3$), − 126.1 (s, *Si*(SiMe$_3$)$_3$)

Melting Point: 174-176 °C

Elemental Analysis: Despite repeated attempts compound **2.23** proved unsuitable for combustion analysis. Found (%): C, 50.95 H, 10.63. Calc. for C$_{19}$H$_{45}$Si$_5$: C, 51.00; H, 9.69.

Mass Peak Analysis: Calculated mass for C$_{19}$H$_{43}$ClSi$_5$ for most abundant isotope: 446.18942 Da; Observed mass peak: 446.18894 Da.

5.2.2 Generation of disilene 2.24 from silane 2.23

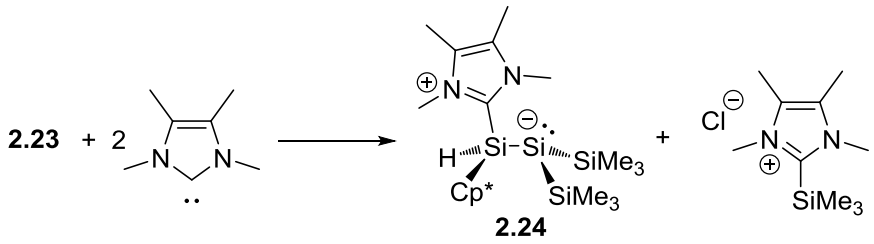

In a typical reaction, silane **2.23** (200 mg, 0.45 mmol) and ^{Me}IMe (111 mg, 0.90 mmol) were dissolved in benzene (5 mL) and stirred, giving a bright orange solution and a large amount of precipitate within the first hour. A reaction aliquot showed disilene **2.24** and ^{Me}IMe·SiMe$_3$Cl adduct as the major products by ^{1}H and ^{29}Si NMR but they could not be separated based on their solubility or by fractional crystallisation.

NMR data for **2.24** are assigned below.

^{1}H NMR (500.2 MHz, THF-d_8, 300 K): δ (ppm) 5.54 (s, 1H, Si-H, $^{1}J_{H\text{-}Si}$ = 166 Hz), 3.93 (s, 3H, ^{Me}IMe), 3.70 (s, 3H, ^{Me}IMe), 2.28 (br s, 3H, Cp*), 2.21 (s, 3H, ^{Me}IMe), 2.15 (s, 3H, ^{Me}IMe), 1.97 (br s, 3H, Cp*), 1.61 (br s, 3H, Cp*), 1.48 (br s, 3H, Cp*), 1.26 (br s, 3H, Cp*), 0.03 (s, 18H, SiMe$_3$ × 2).

^{29}Si{^{1}H} NMR (99.4 MHz, THF-d_8, 300 K): δ (ppm) − 5.3 (s, Si(*Si*Me$_3$)$_2$), – 10.3 (s, *Si*-H), − 216.5 (*Si*(SiMe$_3$)$_2$).

5.2.3 Preparation of disilene 2.28

Zwitterion [(⁺MeIiPr)(Cp*)SiH-Si⁻(SiMe₃)₂]

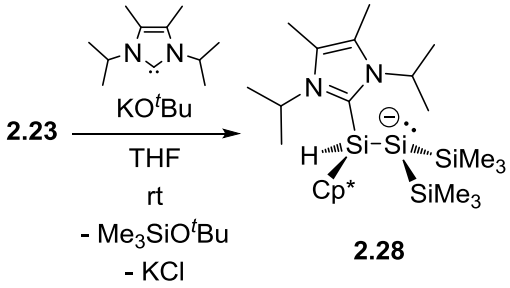

THF (40 mL) was added to a flask charged with **2.23** (1.44 g, 3.22 mmol), KO^{t}Bu (0.38 g, 3.37 mmol) and $^{Me}I^iPr$ (0.60 g, 3.33 mmol) and the resultant red/orange mixture was stirred for 16 hours. The volatiles were removed and the orange solid was extracted with benzene (1 × 50 mL, 2 × 10 mL). Removal of the volatiles and washing with diethyl ether (4 × 10 mL) gave pure disilene **2.28** as a bright orange powder (882 mg, 1.70 mmol, 53%). Orange, block-shaped single crystals suitable for X-ray diffraction could be grown from a concentrated solution in benzene at room temperature or diethyl ether at –20 °C.

^{1}H NMR (500.2 MHz, C_6D_6, 300 K): δ (ppm) 5.83 (sept, 1H, $^{Me}I^iPr$ C*H*Me$_2$, $^3J_{H\text{-}H}$ = 6.8 Hz), 5.71 (s, 1H, Si-H, $^1J_{H\text{-}Si}$ = 165 Hz), 5.06 (sept, 1H, $^{Me}I^iPr$ C*H*Me$_2$, $^3J_{H\text{-}H}$ = 6.8 Hz), 2.41 (s, 3H, Cp*), 1.95 (s, 3H, Cp*), 1.67 (s, 3H, Cp*), 1.60 (s, 3H, Cp*), 1.56 (d, 3H, $^{Me}I^iPr$ CH*Me*Me × 1, $^3J_{H\text{-}H}$ = 6.8 Hz) 1.54 (s, 3H, Cp*), 1.40 (s, 3H, $^{Me}I^iPr$ Me), 1.36 (s, 3H, $^{Me}I^iPr$ Me), 1.05 (d, 3H, $^{Me}I^iPr$ CH*Me*Me × 2, $^3J_{H\text{-}H}$ = 6.8 Hz), 0.95 (d, 3H, $^{Me}I^iPr$ CH*Me*Me × 1, $^3J_{H\text{-}H}$ = 6.8 Hz), 0.59 (s, 18H, SiMe$_3$ × 2).

^{13}C{^{1}H} NMR (125.8 MHz, C_6D_6, 300 K): δ (ppm) 156.1 (s, $^{Me}I^iPr$ C-Si), 141.4 (s, Cp* *C*-CH$_3$), 140.8 (s, Cp* *C*-CH$_3$), 132.6 (s, Cp* *C*-CH$_3$), 132.3 (s, Cp* *C*-CH$_3$), 127.1 (s, $^{Me}I^iPr$ *C*-CH$_3$), 126.9 (s, $^{Me}I^iPr$ *C*-CH$_3$), 56.4 (s, Cp* *C*-Si), 52.3 (s, $^{Me}I^iPr$ *C*(CH$_3$)$_2$), 51.2 (s, $^{Me}I^iPr$ *C*(CH$_3$)$_2$), 22.5 (s, $^{Me}I^iPr$ C(*C*H$_3$)$_2$), 21.9 (s, $^{Me}I^iPr$ C(*C*H$_3$)$_2$), 21.5 (s, $^{Me}I^iPr$ C(*C*H$_3$)$_2$), 20.5 (s, $^{Me}I^iPr$ C(*C*H$_3$)$_2$), 18.6 (s, Cp*-*C*H$_3$), 13.6 (s, Cp*-*C*H$_3$), 11.9 (s, Cp*-*C*H$_3$), 11.8 (s, Cp*-*C*H$_3$), 11.4 (s, Cp*-*C*H$_3$), 9.8 (s, $^{Me}I^iPr$ C*C*H$_3$), 9.7 (s, $^{Me}I^iPr$ C*C*H$_3$), 6.3 (s, Si(*C*H$_3$)$_3$).

^{29}Si{^{1}H} NMR (99.4 MHz, C_6D_6, 300 K): δ (ppm) – 5.1 (s, *Si*-H), − 13.0 (s, Si(*Si*Me$_3$)$_2$), − 202.2 (*Si*(SiMe$_3$)$_2$).

Melting point: 170 – 172 °C (dp)

Elemental Analysis: Found (%): C, 62.09; H, 10.27; N, 5.26. Calculated for $C_{27}H_{54}N_2Si_4$: C, 62.47; H, 10.49; N, 5.40.

Mass Peak Analysis: Calculated mass for $C_{27}H_{54}N_2Si_4$ for most abundant isotopes: 518.33587 Da; Observed mass peak: 518.33740 Da.

UV-vis: (λ_{max}, ε): 444 nm, 494 $dm^3\ mol^{-1}\ cm^{-1}$

5.2.4 Preparation of silane 2.35

Tris(trimethylsilyl)2,6-bis(2,4,6-trimethylphenyl)phenylchlorosilane [(Ar*)(Si(SiMe$_3$))SiHCl]

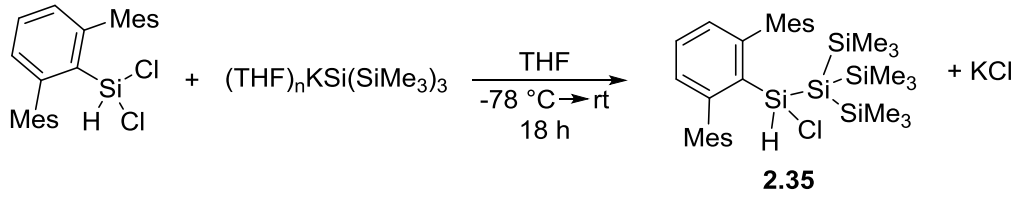

2.35

Potassium tris(trimethylsilyl)silyl was prepared *in situ* by the addition of THF (15 mL) to tetrakis(trimethylsilyl)silane (2 g, 6.23 mmol) and potassium *tert*-butoxide (0.76 g, 6.77 mmol). The reaction was stirred for 16 hours before removal of the volatiles and extraction with warm hexane (40 °C, 50 mL) to remove excess potassium *tert*-butoxide. The hexane was removed *in vacuo* and the anion was dissolved in THF (20 mL). The solution was added dropwise over 1 minute to a solution of terphenyldichlorosilane (2.6 g, 6.23 mmol) in THF (50 mL) at –78 °C. The reaction was allowed to warm to room temperature and stirred for a total of 18 hours.

The volatiles were removed *in vacuo* and the product was extracted with hot diethyl ether (3 × 90 mL). Concentration of the resultant solution afforded pure silane **2.35** as colourless, block-shaped crystals suitable for X-ray diffraction containing 0.33 equivalents of diethyl ether (confirmed by elemental analysis, ^{1}H and ^{13}C NMR) (1.92 g, 4.00 mmol, 64%).

^{1}H NMR (500.2 MHz, C_6D_6, 300 K): δ (ppm) 7.16 (t, $J_{H\text{-}H}$ = 7.5 Hz, 1H, *p*-*H*), 6.88 (s, 2H, Mes-*H*), 6.85 (s, 2H, Mes-*H*), 6.83 (d, $J_{H\text{-}H}$ = 7.5 Hz, 2H, *m*-*H*), 5.39 (s, $J_{H\text{-}Si}$ = 215,

13 Hz, 1H, Si-*H*), 2.24 (s, 6H, Mes-C*H*$_3$), 2.19 (s, 6H, Mes-C*H*$_3$), 2.14 (s, 6H, Mes-C*H*$_3$), 0.18 (s, 27H, Si(SiC*H*$_3$)$_3$).

^{13}C{^{1}H} NMR (125.8 MHz, C_6D_6, 300 K): δ (ppm) 149.8 (s, Ar *C*-Mes), 140.8 (s, Mes-*C*CH$_3$), 136.6 (s, Mes-*C*CH$_3$), 135.4 (br s, Mes-*C*CH$_3$), 133.4 (s, Ar *C*-Si) 131.0 (s, *p*-Ar), 129.4 (s *m*-Ar), 128.4 (s, Mes *m*-*C*H), 128.3 (s, Mes *m*-*C*H), 21.9 (s, Mes-*C*H$_3$), 21.9 (br s, Mes-*C*H$_3$), 20.8 (s, Mes-*C*H$_3$), 2.60 (s, Si*Me*$_3$, $^1J_{C\text{-}Si}$ = 45 Hz)

^{29}Si{^{1}H} NMR (99.4 MHz, C_6D_6, 300 K): δ (ppm) – 7.53 (s, *Si*-H), – 8.72 (s, *Si*Me$_3$), − 117.6 (s, *Si*(SiMe$_3$)$_3$).

Melting Point: 249-251 °C

Elemental Analysis: Found (%): C, 63.19; H, 8.62. Calc. for $C_{33}H_{53}ClSi_5 \cdot {}^1/_3C_4H_{10}O$: C, 63.35; H, 8.54.

Mass Peak Analysis: Calculated mass for $C_{33}H_{53}ClSi_5$ for most abundant isotopes: 624.26767 Da; Observed mass peak: 624.26739 Da.

5.2.5 Preparation of silylsilylene 2.37

NHC-stabilised silylsilylene

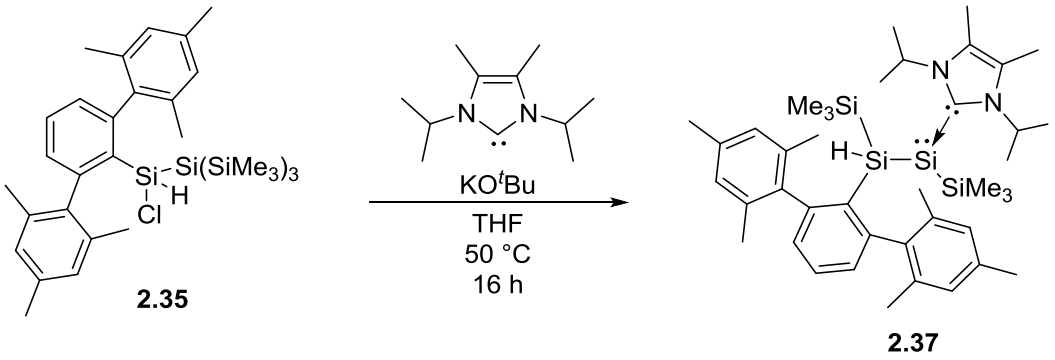

THF (50 mL) was added to a flask containing silane **2.35** (650 mg, 1.00 mmol), potassium *tert*-butoxide (131 mg, 1.17 mmol) and ^{Me}I^{i}Pr (180 mg, 1.00 mmol). The mixture was heated to 50 °C for 16 h at which point complete conversion was confirmed by ^{1}H NMR spectroscopy. Removal of the volatiles afforded a red oily solid which was extracted with pentane (2 × 30 mL) and concentrated to afford pure silylene **2.37** as red, block-shaped, extremely sensitive

crystals suitable for X-ray diffraction (283 mg, 0.41 mmol, 41%). An analytically pure sample was obtained by recrystallisation from pentane at − 20 °C.

^{1}H NMR (500.2 MHz, C_6D_6, 300 K): δ (ppm) 7.33 (br, 1H, MeIiPr, C*H*Me$_2$), 7.20 (t, 1H, *p*-Ar-*H*, $^{3}J_{H\text{-}H}$ = 7.5 Hz), 7.10 (s, 1H, Mes-*H*) 6.96 – 6.94 (m, 2H, Mes-*H* and *m*-Ar-*H*), 6.91 (d, 1H, *m*-Ar-*H*, $^{3}J_{H\text{-}H}$ = 7.5 Hz), 6.88 (s, 1H, Mes-*H*), 6.42 (s, 1H, Mes-*H*), 5.48 (br, 1H, MeIiPr, C*H*Me$_2$), 3.91 (s, 1H, Si-*H*, $^{1}J_{H\text{-}Si}$ = 155Hz), 2.81 (s, 3H, Mes-C*H*$_3$), 2.36 (s, 3H, Mes-C*H*$_3$), 2.28 (s, 3H, Mes-C*H*$_3$), 2.27 (s, 3H, Mes-C*H*$_3$), 2.22 (s, 3H, Mes-C*H*$_3$), 1.68 (br, 3H, ^{Me}I^{i}Pr C*H*$_3$), 1.61 (br, 3H, ^{Me}I^{i}Pr C*H*$_3$), 1.54 (s, 3H, Mes-C*H*$_3$), 1.06 (br, 6H, ^{Me}I^{i}Pr C*H*$_3$), 0.99 (br, 6H, ^{Me}I^{i}Pr C*H*$_3$), 0.35 (s, 9H, Si(C*H*$_3$)$_3$), 0.32 (s, 9H, Si(C*H*$_3$)$_3$).

^{13}C{^{1}H} NMR (125.8 MHz, C_6D_6, 300 K): δ (ppm) 172.2 (s, ^{Me}I^{i}Pr *C*-Si, $^{1}J_{C\text{-}Si}$ = 25 Hz), 149.9 (s, Ar *m*-*C*-Mes), 148.7 (s, Ar *m*-*C*-Mes), 143.8 (s, Mes *ipso*-*C*-Ar), 141.7 (s, Mes *ipso*-*C*-Ar), 141.1 (s, Ar *C*-Si), 137.9 (s, Mes *o*-*C*-CH$_3$), 136.0 (s, Mes *p*-*C*-CH$_3$), 135.5 (s, Mes *o*-*C*-CH$_3$), 135.2 (s, Mes *o*-*C*-CH$_3$), 135.1 (s, Mes *o*-*C*-CH$_3$), 134.3 (s, Mes *p*-*C*-CH$_3$), 129.6 (s Mes *C*-H), 128.9 (s, Ar *m*-*C*-H), 127.9 (s, Mes *C*-H), 127.8 (s, Mes *C*-H) 127.6 (s, Ar *p*-*C*-H), 127.5 (s, Ar *m*-*C*-H) 127.0 (s Mes *C*-H), 126.2 (br s, ^{Me}I^{i}Pr *C*-CH$_3$), 125.4 (br s, ^{Me}I^{i}Pr *C*-CH$_3$), 54.3 (s, ^{Me}I^{i}Pr *C*Me$_2$), 51.8 (s, ^{Me}I^{i}Pr *C*Me$_2$), 25.3 (s Mes-*C*H$_3$), 22.9 (br s, ^{Me}I^{i}Pr *C*H$_3$), 22.5 (s Mes-*C*H$_3$), 21.5 (br s, ^{Me}I^{i}Pr *C*H$_3$), 21.5 (s Mes-*C*H$_3$), 21.4 (s Mes-*C*H$_3$), 21.0 (s Mes-*C*H$_3$), 21.0 (br s, ^{Me}I^{i}Pr *C*H$_3$), 20.8 (s Mes-*C*H$_3$), 19.8 (br s, ^{Me}I^{i}Pr *C*H$_3$), 9.8 (s, ^{Me}I^{i}Pr *C*H$_3$ × 2), 5.0 (s, Si(*C*H$_3$)$_3$, $^{1}J_{C\text{-}Si}$ = 41 Hz, $^{2}J_{C\text{-}Si}$ = 10 Hz), 2.4 (s, Si(*C*H$_3$)$_3$, $^{1}J_{C\text{-}Si}$ = 43 Hz).

^{29}Si{^{1}H} NMR (99.4 MHz, C_6D_6, 300 K): δ (ppm) – 11.8 (s, *Si*Me$_3$), − 13.8 (s, *Si*Me$_3$), – 68.8 (s, *Si*-H), − 121.4 (*Si*(SiMe$_3$)(MeIiPr)).

Melting Point: 100-103 °C

Elemental Analysis: Found: C, 70.67; H, 9.18; N, 4.04. Calc. for: $C_{41}H_{64}N_2Si_4$ C, 70.62; H, 9.25; N, 4.02.

Mass Peak Analysis: Calculated mass for $C_{41}H_{64}N_2Si_4$ for most abundant isotopes: 696.41412 Da; Observed mass peak: 696.41267 Da.

UV-vis: (λ_{max}, ε): 470 nm, 862 dm^3 mol^{-1} cm^{-1}

5.2.6 Preparation of a mixture of 2.36 and 2.37 and conversion of 2.36 to 2.37

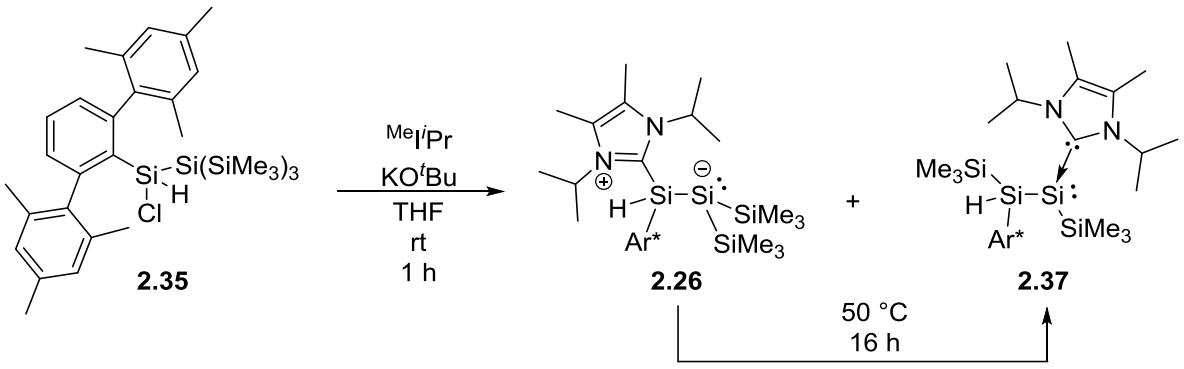

THF (15 mL) was added at ambient temperature to a flask containing silane **2.35** (230 mg, 0.35 mmol), $^{Me}I^{i}Pr$ (69 mg, 0.38 mmol) and KO^{t}Bu (39 mg, 0.35 mmol). After stirring for one hour, the volatiles were removed from a reaction aliquot (**Aq-1**, 0.5 mL) which was then redissolved in C_6D_6 for ^{1}H NMR measurement. The reaction mixture was then heated at 50 °C for 16 hours after which a second aliquot (**Aq-2**, 0.5 mL) was taken. The volatiles were removed from the aliquot and the sample was redissolved in C_6D_6 for ^{1}H NMR.

By ^{1}H NMR, a mixture of **2.36** and **2.37** is observed when the sample is kept at room temperature, but heating leads to complete consumption of **2.36**. The reaction is complete within 3 hours at 55 °C, Figure 5-1 shows the slower, cleaner conversion at 50 °C.

Figure 5-1 shows the ^{1}H NMR from 5.7 – 3.9 ppm of **Aq-1** and **Aq-2** which includes the Si-*H* resonances as well as some C*H*$(CH_3)_2$ resonances, and shows the complete consumption of **2.36** in this time.

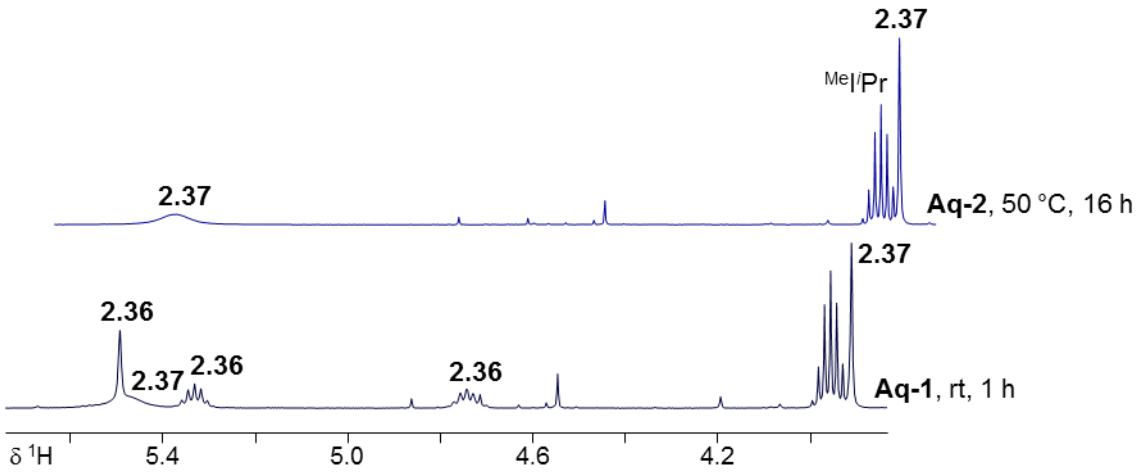

Figure 5-1 – *Expansion of ^{1}H NMR (500.2 MHz, C_6D_6, 300 K) showing the Si-H and some C<u>H</u>$(CH_3)_2$ resonances from a mixture of **2.36** and **2.37** after 1 hour at room temperature and after 16 hours at 50 °C.*

5.2.7 Generation of disilene 2.40 and silylsilylene 2.41

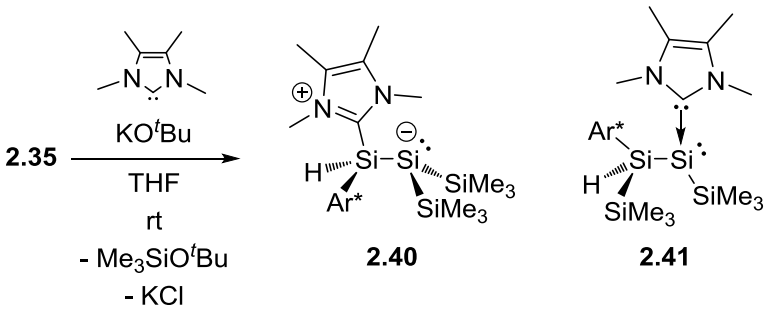

In a typical reaction, a solution of ^{Me}IMe (19 mg, 0.15 mmol) was cooled to −10 °C and added to a flask containing silane **2.35** (100 mg, 0.15 mmol) and KO^{t}Bu (18 mg, 0.16 mmol). The reaction mixture was stirred at −10 °C for one hour before being allowed to slowly warm to room temperature overnight. NMR spectroscopy revealed disilene **2.40** and silylsilylene **2.41** in solution which were not separated.

Some of the ^{1}H and ^{29}Si signals associated with disilene **2.40** are assigned below.

^{1}H NMR (500.2 MHz, C_6D_6, 300 K): δ (ppm) 5.28 (s, 1H, Si-<u>H</u>, $^{1}J_{H\text{-}Si}$ = 189 Hz).

^{29}Si{^{1}H} NMR (99.4 MHz, C_6D_6, 300 K): δ (ppm) −5.1 (s, Si(<u>Si</u>Me$_3$)$_2$) −41.6 (s, <u>Si</u>-H), −200.6 (s, <u>Si</u>(SiMe$_3$)$_2$).

The ^{29}Si signals associated with silylsilylene **2.41** are assigned below.

^{29}Si{^{1}H} NMR (99.4 MHz, C_6D_6, 300 K): δ (ppm) –7.1 (s, <u>*Si*</u>Me_3), −12.6 (s, <u>*Si*</u>Me_3), –67.2 (s, <u>*Si*</u>-H), −123.8 (<u>*Si*</u>($SiMe_3$)(^{Me}IMe)).

5.2.8 Generation of proposed disilene 2.48

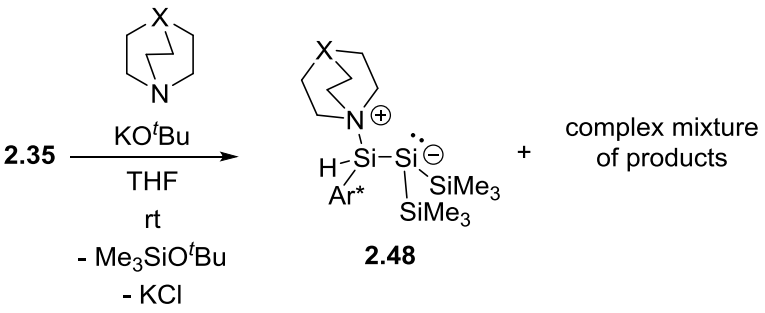

Disilene **2.48** was generated *in situ* using two base, quinuclidine (X = CH) and DABCo (X = N). In both cases, disilene **2.48** was only a minor product but was identified by comparison of specific NMR chemical shifts with other compounds.

5.2.8.1 Using DABCO as the base

Silane **2.35** (20 mg, 0.032 mmol), KO^{t}Bu (4 mg, 0.036 mmol) and DABCO (4 mg, 0.036 mmol) were dissolved in THF-d_8 in an NMR tube. A complex mixture of products were observed by ^{1}H and ^{29}Si NMR. The following signals are assigned to **2.48** (X = N).

^{1}H NMR (500.2 MHz, THF-d_8, 300 K): δ (ppm) 5.17 (s, 1H, Si-<u>*H*</u>).

^{29}Si{^{1}H} NMR (99.4 MHz, THF-d_8, 300 K): δ (ppm) −22.4 (s, <u>*Si*</u>-H), −183.4 (s, <u>*Si*</u>($SiMe_3$)$_2$).

5.2.8.2 Using quinuclidine as the base

Silane **2.35** (21 mg, 0.034 mmol), KO^{t}Bu (5 mg, 0.045 mmol) and quinuclidine (6 mg, 0.054 mmol) were dissolved in THF-d_8 in an NMR tube. A complex mixture of products were observed by ^{1}H and ^{29}Si NMR. A number of Si-H signals were observed in the ^{1}H-^{29}Si HMBC, none could be assigned to **2.48** (X = CH) with any degree of certainty.

5.2.9 Generation of DMAP coordinated disilene 2.49

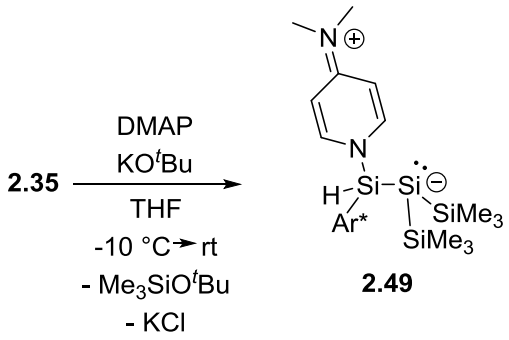

In a typical reaction, THF (12 mL) was added to a flask containing silane **2.28** (163 mg, 0.25 mmol), KO^{t}Bu (30 mg, 0.27 mmol) and DMAP (31 mg, 0.25 mmol) at −10 °C. The mixture turned orange and then deep red within 20 munites. The reaction was allowed to stir at room temperature for 90 minutes before the volatiles were removed under reduced pressure to afford a sticky red solid as the crude product. Disilene **2.49** was not isolated as a pure product but the ^{1}H and ^{29}Si NMR spectra are assigned below.

^{1}H NMR (500.2 MHz, THF-d_8, 300 K): δ (ppm) 7.91-7.89 (m, 2H, Py C-*H*), 7.37 (t, 1H, $^1J_{H\text{-}H}$ = 7.5 Hz, Ar *p*-C-*H*), 6.94 (s, 2H, Mes-*H*), 6.88 (d, 2H, $^1J_{H\text{-}H}$ = 7.5 Hz, Ar *m*-C-*H*), 6.70 (s, 2H, Mes-*H*), 6.51-6.49 (m, 2H, Py C-*H*), 5.43 (s, 1H, Si-*H*, $^1J_{H\text{-}Si}$ = 190 Hz), 3.17 (s, 6H, Mes-C*H*$_3$ × 2), 2.99 (s, 6H, Mes-C*H*$_3$ × 2), 2.34 (s, 6H, Mes-C*H*$_3$ × 2), 2.24 (s, 6H, N-C*H*$_3$ × 2), 1.76 (s, 6H, Mes-C*H*$_3$ × 2), −0.16 (s, 18H, Si(C*H*$_3$)$_3$ × 2).

^{29}Si{^{1}H} NMR (99.4 MHz, THF-d_8, 300 K): δ (ppm) 32.2 (s, *Si*-H), − 6.3 (s, Si(*Si*Me$_3$)$_2$), − 187.7 (*Si*(SiMe$_3$)$_2$).

5.2.10 Preparation of disilene 2.50

Ar* 4-Pyrrolidinopyridine Disilene

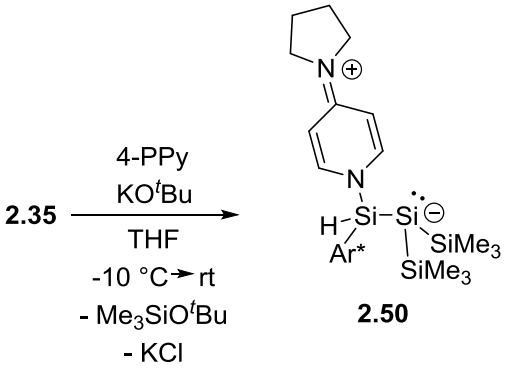

THF (50 mL) was added at – 70 °C to a flask containing silane **2.35** (1000 mg, 1.54 mmol), potassium *tert*-butoxide (215 mg, 1.91 mmol) and 4-pyrolidinopyridine (228 mg, 1.54 mmol). The resultant red mixture was warmed to –10 °C and then slowly warmed to ambient temperature over 4 hours at which point complete consumption of **2.35** was confirmed by ^{1}H NMR spectroscopy. Removal of the volatiles afforded a red solid which was extracted with toluene (2 × 80 mL) and concentrated to give disilene **2.50** as a deep red solid in > 90% (judged by NMR) purity (395 mg, 0.59 mmol, 39%). An analytically pure sample was obtained by recrystallisation from toluene at –20 °C.

^{1}H NMR (500.2 MHz, C_6D_6, 300 K): δ (ppm) 8.12-8.11 (m, 2H, Py C-*H*), 7.22 (t, 1H, $^1J_{H\text{-}H}$ = 7.6 Hz, Ar *p*-C-*H*), 7.06 (s, 2H, Mes-*H*), 6.92 (d, 2H, $^1J_{H\text{-}H}$ = 7.6 Hz, Ar *m*-C-*H*), 6.70 (s, 2H, Mes-*H*), 5.85 (s, 1H, Si-*H*, $^1J_{H\text{-}Si}$ = 189 Hz), 5.46-5.44 (m, 2H, Py C-*H*), 2.54 (s, 6H, Mes-C*H*$_3$ × 2), 2.32-2.20 (m, 4H, Py C-*H*$_2$), 2.26 (s, 6H, Mes-C*H*$_3$ × 2), 1.96 (s, 6H, Mes-C*H*$_3$ × 2), 1.07-1.02 (m, 4H, Py C-*H*$_2$ × 2), 0.41 (s, 18H, Si(C*H*$_3$)$_3$ × 2).

^{13}C{^{1}H} NMR (125.8 MHz, C_6D_6, 300 K): δ (ppm) 152.7 (s, Py-*C*-N(CH_2CH_2)$_2$), 148.5 (s, Ar *m*-*C*-Mes), 147.2 (s, Py-*C*-H), 140.9 (s, Mes *ipso*-*C*-Ar), 138.5 (s, Ar *C*-Si), 136.5 (s, Mes *o*-*C*-CH_3), 136.3 (s, Mes *p*-*C*-CH_3), 135.9 (s, Mes *o*-*C*-CH_3), 129.4 (s, Ar *p*-*C*-H), 128.9 (s, Ar *m*-*C*-H), 128.4 (s, Mes-*C*-H), 128.2 (s, Mes-*C*-H), 105.8 (s, Py-*C*-H), 46.7 (Py-*C*H_2 × 2), 24.2 (Py-*C*H_2 × 2), 22.9 (s, Mes-*C*H_3 × 2), 22.1 (s, Mes-*C*H_3 × 2), 20.9 (s, Mes-*C*H_3 × 2), 6.28 (s, Si(*C*H_3)$_3$, $^1J_{C\text{-}Si}$ = 40 Hz).

^{29}Si{^{1}H} NMR (99.4 MHz, C_6D_6, 300 K): δ (ppm) 34.6 (s, *Si*-H), − 5.92 (s, Si(*Si*Me_3)$_2$), − 184.0 (*Si*($SiMe_3$)$_2$).

Elemental Analysis: Found: C, 70.23; H, 8.63; N, 4.09. Calc. for: $C_{41}H_{64}N_2Si_4$ C, 70.42; H, 8.49; N, 4.21.

Mass Peak Analysis: Calculated mass for $C_{39}H_{56}N_2Si_4$ for most abundant isotopes: 664.35152 Da; Observed mass peak: 664.35346 Da.

5.2.11 Conversion of 2.50 to 2.36 and 2.37

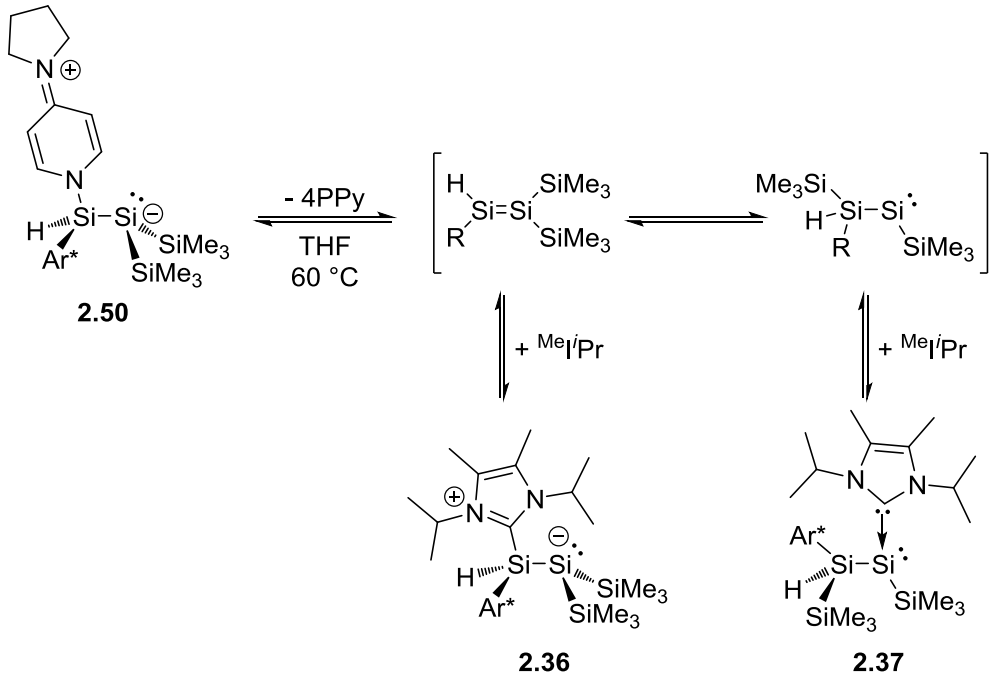

A sample of **2.50** (15 mg, 22 µmol) along with ^{Me}I^{i}Pr (7 mg, 38 µmol) and mesitylene (25 µL, 21.6 mg, 0.18 mmol) was dissolved in THF-d_8 in a Young's NMR tube. The sample was loaded into a preheated NMR spectrometer at 55 °C. The first ^{1}H spectrum was collected after 12 minutes. The sample was maintained at 55 °C in the spectrometer and further ^{1}H spectra were recorded every 5 minutes thereafter.

Figure 5-2 shows the three spectra and clear consumption of **2.50**. Initially, a mixture of **2.36** and **2.37** is obtained. Over time, **2.36** is consumed and the concentration of **2.37** increases.

Figure 5-3 shows a plot of the concentrations of **2.50**, **2.37** and **2.36** as calculated from integration against mesitylene as the internal standard.

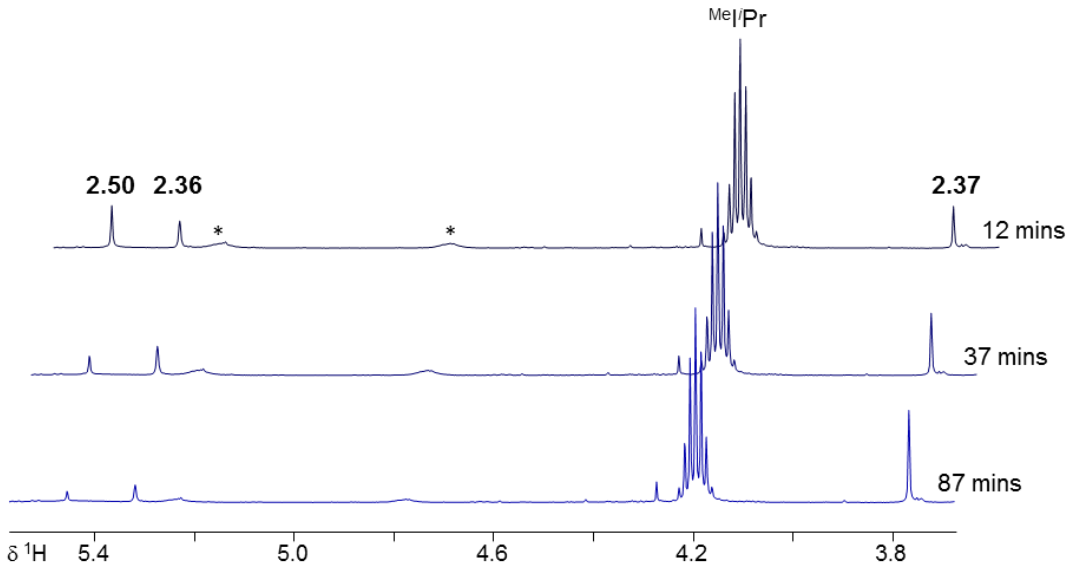

Figure 5-2 – *Expansion of the ^{1}H NMR (600.8 MHz, THF-d$_8$, 328 K) of a sample of* ***2.50*** *being heated in the presence of ^{Me}I^{i}Pr after 12, 37 and 87 minutes.*

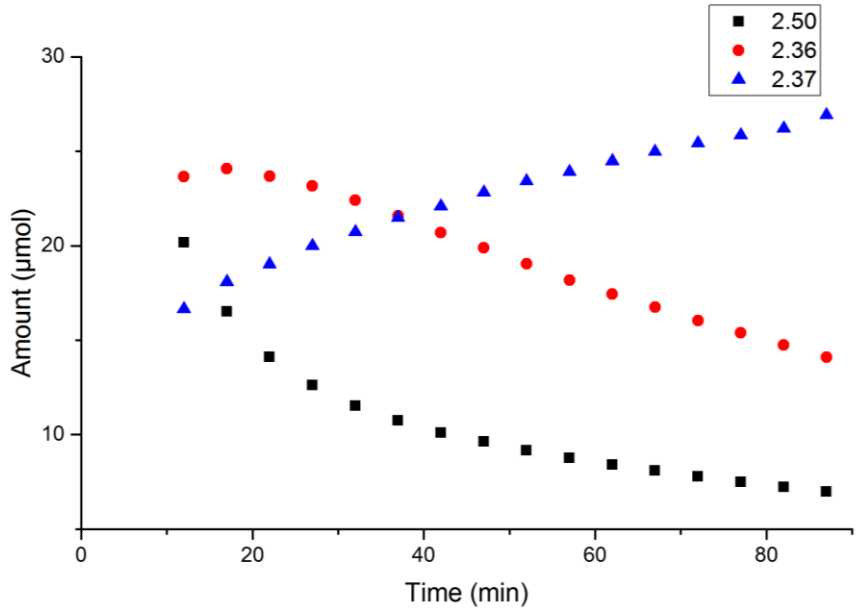

Figure 5-3 – *Plot of the concentration of* ***2.50****,* ***2.36*** *and* ***2.37*** *when* ***2.50*** *is heated to 55 °C in the presence of ^{Me}I^{i}Pr. Concentrations calculated from integration against mesitylene as an internal standard.*

5.2.12 Base dissociation from disilene 2.50

A sample of **2.50** was dissolved in THF-d_8 in an NMR tube along with mesitylene (20 µL, 0.14 mmol) as an internal standard. The sample was slowly heated in the NMR spectrometer and spectra were recorded at 278 K, 298 K, 318 K and 333 K. The sample was then cooled and spectra were recorded at the same temperatures.

Concentrations were calculated by calibrating integrals against the mesitylene internal standard.

Temp (K)	Mesitylene (mmol)	Uncoordinated 4-Ppy (µmol)	Coordinated 4-PPy (µmol)	Uncoordinated 4-Ppy (%)	Coordinated 4-Ppy (%)	
278	0.144	1.28	3.61	26.1	73.9	
298	0.144	1.30	3.79	25.5	74.5	Heating
318	0.144	1.52	3.50	30.3	69.7	
333	0.144	1.61	3.11	34.0	66.0	
318	0.144	1.55	3.73	29.4	70.6	Cooling
298	0.144	1.29	3.81	25.3	74.7	
278	0.144	1.27	3.62	26.0	74.0	

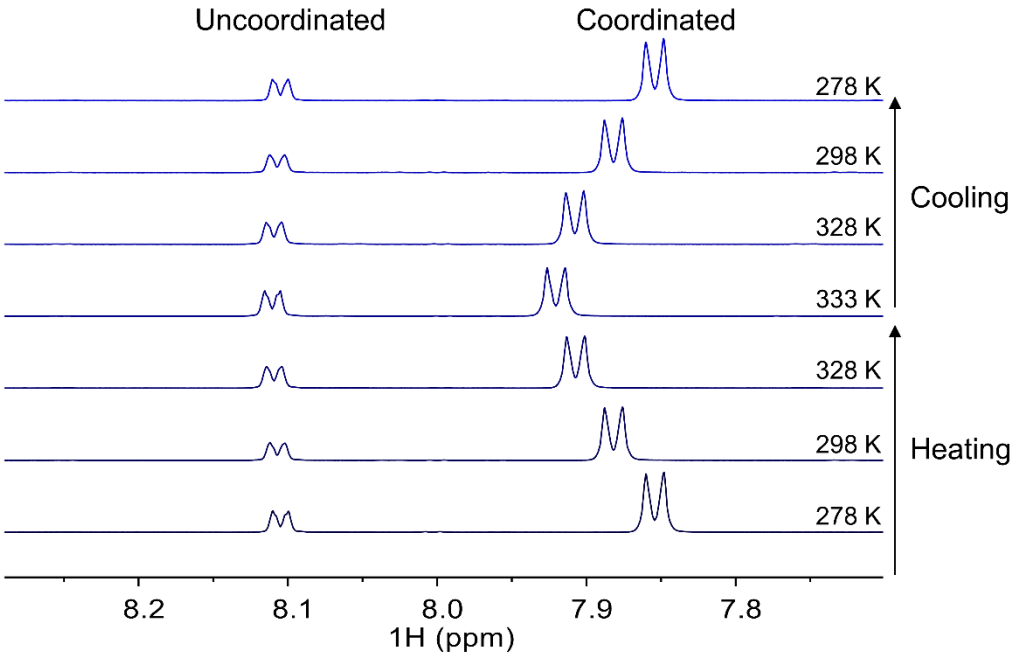

5.3 Experimental Details for Chapter 3

5.3.1 Preparation of 2-Bromomesitylene

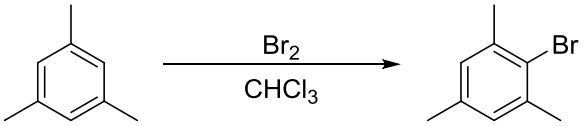

A solution of bromine (80 mL, 249.6 g, 1.56 mol) in chloroform (100 mL) was added dropwise to a solution of mesitylene (200 mL, 172.7 g, 1.43 mol) in chloroform (400 mL) at 0 °C over 2.5 h giving a pale yellow solution. The resulting HBr gas was vented through a bubbler containing aqueous sodium hydroxide solution (*ca.* 7.5 M, 200 mL, 1.5 mol). After the addition was completed the mixture was stirred for a further 1 h after which sodium thiosulfate (30 g) was added giving a yellow, lumpy mixture. The mixture was washed with aqueous sodium hydroxide solution (2 M, 200 mL) and distilled water (2 x 250 mL) and the organic fraction was dried over magnesium sulfate. Removal of the volatiles afforded the crude product as a pale yellow oil which was purified by vacuum distillation (8.2×10^{-2} mbar, 52 °C) to afford the pure product as a colourless oil (233.4 g, 1.17 mol, 82%).

^{1}H NMR (500 MHz, $CDCl_3$): δ (ppm) 2.35 (s, 3H), 2.49 (s, 6H), 6.99 (s, 2H)

5.3.2 Preparation of Dihalomesitylphosphine ($MesPX_2$, $X_2 = Cl_2$, BrCl, Br_2)[10]

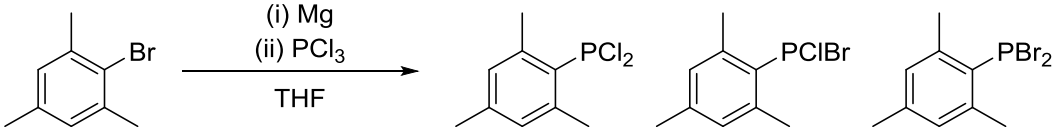

To a flask equipped with a reflux condenser and charged with magnesium (6.08 g, 250 mmol) was added enough THF to cover the magnesium (*ca.* 25 mL). 2-bromomesitylene (5 mL, 6.51 g, 32.7 mmol) was added slowly and the mixture was gently warmed until reflux began and the suspension turned grey. The remaining 2-bromomesitylene (10.4 mL, 13.5 g, 67.7 mmol) in THF (200 mL) was added dropwise at a rate that maintained reflux over 1 h. The resulting suspension was stirred at reflux for a further 1 h before cooling to RT.

The suspension was allowed to settle and the solution of 2-mesitylmagnesium bromide was carefully decanted to a dropping funnel without any solid being transferred. The solution was added dropwise to a solution of trichlorophosphine (26.3 mL, 41.3 g, 300 mmol) in THF (150 mL) at 0 °C and the solution was allowed to come to room temperature and stirred for 16 h. The volatiles were removed in vacuo and the product was extracted with hexane (300 mL). The remaining solid was washed with hexane (100 mL) and the volatiles were removed to afford the crude product which was purified by vacuum distillation (1.4×10^{-1} mbar, 82 °C) to afford the pure product (13.1 g, 56.7 mmol, 57 %) as a mixture of $MesPCl_2$ (78.4%), MesPClBr (20.3%) and $MesPBr_2$ (1.3%) (ratios determined by ^{31}P NMR signal integration). NMR data were in accordance with the literature.[10]

^{1}H NMR (500 MHz, C_6D_6): δ (ppm) 1.89-1.91 (m, 3H), 2.50-2.52 (m, 6H), 6.46-6.48 (m, 2H)

^{31}P{^{1}H} NMR (162 MHz, C_6D_6): δ (ppm) 168.8 (s, $MesPCl_2$), 163.0 (s, MesPClBr), 154.8 (s, $MesPBr_2$)

5.3.3 Preparation of Mesitylphosphine ($MesPH_2$)[10]

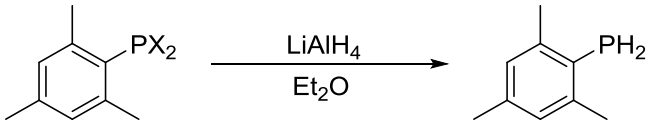

Dihalophosphine ($MesPX_2$, X_2 = Cl_2 (78.4%), BrCl (20.3%), Br_2 (1.3%)) (13.1g, 56.7 mmol) in diethyl ether (40 mL) was added very slowly over 1 h to a suspension of lithium aluminium hydride ($LiAlH_4$) (1.82 g, 47 mmol) in diethyl ether (75 mL) at −78 °C leading to the rapid production of white fumes. After addition was completed, the reaction was warmed to RT and stirred for 4 h before cooling to 0 °C for the careful, dropwise addition of degassed water (60 mL) resulting in the highly exothermic evolution of H_2 gas. After addition, the organic layer was separated and the aqueous layer was extracted with diethyl ether (3 × 50 mL) and the organic layers were combined. The volatiles were removed and the product was purified by vacuum distillation (1.7×10^{-1} mbar, 36 °C) to afford the pure product (9.36 g, 56.7 mmol, 61 %). NMR data were in accordance with the literature.[10]

^{1}H NMR (500 MHz, C_6D_6): δ (ppm) 2.08 (s, 3H), 2.20 (s, 6H), 3.60 (d, $^{1}J_{HP}$ = 203 Hz), 6.70 (s, 2H)

^{31}P NMR (162 MHz, C_6D_6): δ (ppm) –156.1 (t, $^{1}J_{PH}$ = 203 Hz)

5.3.4 Preparation of Dihalo(2,4,6-triisopropylphenylphosphine (TippPX$_2$, X$_2$ = Cl$_2$, BrCl, Br$_2$)[11]

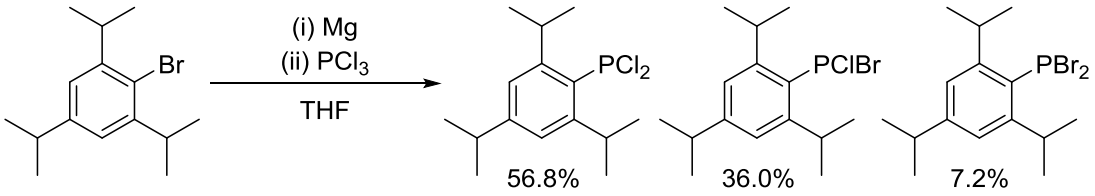

To a flask equipped with a reflux condenser and charged with magnesium (3.0 g, 123 mmol) was added enough THF to cover the magnesium (*ca.* 25 mL) and one iodine crystal. 2-bromomesitylene (5 mL, 5.59 g, 19.7 mmol) was added slowly and the mixture was gently warmed (*ca.* 70 °C) until reflux began and the suspension turned grey. The remaining 2-bromomesitylene (18 mL, 20.1 g, 71.0 mmol) in THF (120 mL) was added dropwise at a rate that maintained reflux over 40 mins with heating to 60 °C. The resulting suspension was stirred at reflux for a further 2 h before cooling to RT.

The suspension was allowed to settle and the solution of 2-mesitylmagnesium bromide was carefully decanted to a dropping funnel without any solid being transferred. The solution was added dropwise to a solution of trichlorophosphine (13.3 mL, 20.9 g, 152 mmol) in diethyl ether (150 mL) at − 78 °C over 40 minutes and the solution was allowed to come to room temperature and stirred for 16 h overnight. The following morning the solution was heated to 45 °C for 2 h to complete the reaction. The mixture was filtered and concentrated. After 12 h at –20 °C, off white crystals were isolated as a mixture of the products TippPCl$_2$ (56.8%), Tipp PClBr (36.0%), TippPBr$_2$ (7.2%) (ratios determined by ^{31}P NMR signal integration) (20.2 g, 61.7 mmol, 68%). NMR data were in accordance with the literature.[11]

^{1}H NMR (500 MHz, C_6D_6): δ (ppm) 7.06 – 7.04 (m, 2H, Tipp-*H*), 4.25 – 4.16 (m, 2H, *o*-C*H*Me$_2$), 2.66 – 2.57 (m, *p*-C*H*Me$_2$), 1.24 – 1.21 (m, 12H, *o*-CH(C*H*$_3$)$_2$), 1.09 – 1.07 (m, 6H, *p*-CH(C*H*$_3$)$_2$)

$^{31}P\{^{1}H\}$ NMR (162 MHz, C_6D_6): δ (ppm) 164.8 (s, $TippPCl_2$), 159.4 (s, TippPClBr), 151.9 (s, $TippPBr_2$)

5.3.5 Preparation of 2,4,6-tri*iso*propylphenylphosphine ($TippPH_2$)[12]

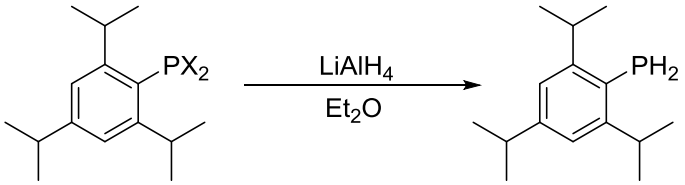

A suspension halophosphine ($TippPX_2$, X_2 = Cl_2 (56.8%), BrCl (36.0%), Br_2 (7.2%)) (20.2, 61.7 mmol) in diethyl ether (120 mL) was added slowly to a suspension of lithium aluminium hydride ($LiAlH_4$) (3.0 g, 79 mmol) in diethyl ether (100 mL) at 0 °C leading to the rapid production of white fumes. After addition was completed, the reaction was warmed to RT and stirred for 16 h. Degassed, distilled water (60 mL) was very carefully added resulting in the highly exothermic evolution of H_2 gas. After addition, the organic layer was separated and the aqueous layer was extracted with diethyl ether (2 × 50 mL) and the organic layers were combined. The volatiles were removed and the product was purified by vacuum distillation (3×10^{-1} mbar, 82 °C) to afford the pure product (10.2 g, 66%). NMR data were in accordance with the literature.[12]

^{1}H NMR (500 MHz, C_6D_6): δ (ppm) 1.20 (d, 12H $^{3}J_{HH}$ = 6.9 Hz, o-CH(C$\underline{H}_3$)$_2$), 1.21 (d, 6H $^{3}J_{HH}$ = 7 Hz, p-CH(C$\underline{H}_3$)$_2$), 2.77 (sept, 1H, $^{3}J_{HH}$ = 6.9 Hz, p-C$\underline{H}$(CH$_3$)$_2$), 2.77 (sept, 1H, $^{3}J_{HH}$ = 6.9 Hz, p-C$\underline{H}$(CH$_3$)$_2$), 3.44 (sept d, 2H, $^{3}J_{HH}$ = 6.8 Hz, $^{4}J_{HH}$ = 3.2 Hz, o-C$\underline{H}$(CH$_3$)$_2$), 3.83 (d, 1H, $^{1}J_{HP}$ = 203 Hz P-$\underline{H}$), 7.07 (d, 2H $^{3}J_{HH}$ = 2.3 Hz, Ar$\underline{H}$)

^{31}P NMR (162 MHz, C_6D_6): δ (ppm) –156.1 (t, $^{1}J_{PH}$ = 203 Hz)

5.3.6 Preparation of *N*-(2,2-dimethyl-1-(mesitylphosphino)propylidene)2,4,6-trimethylaniline (3.5)

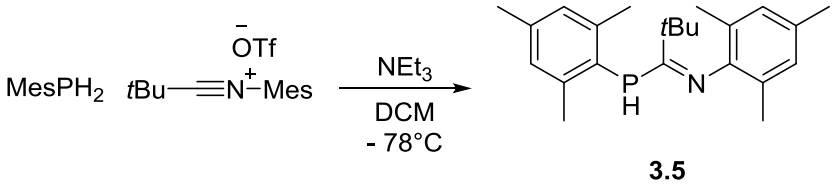

3.5

A solution of mesitylphosphine (9.36 g, 61.5 mmol) in dichloromethane (20 mL) was added dropwise *via* cannula over 5 minutes to a solution of (*N*-mesityl)(*tert*-butyl)carbonitrilium triflate (21.6 g, 61 mmol) in DCM (160 mL) at –78 °C. After stirring at this temperature for 10 minutes, triethylamine (8.57 mL, 6.22 g, 61.5 mmol) was added dropwise over 8 minutes and the reaction was stirred for a further 20 minutes. Subsequently, the cold bath was removed and the reaction was stirred for an additional 2 hours giving a yellow/orange mixture. After removal of the volatiles, the solid was extracted with pentane (100 mL), filtered through neutral alumina and washed through with pentane (2 x 100 mL). The resulting solution was concentrated and crystallised at –20 °C to afford yellow crystals of **3.5** (16.9 g, 47.8 mmol, 78 %).

^{1}H NMR (500.2 MHz, C_6D_6, 300 K): δ (ppm) 6.87 – 6.71 (m, 1H, NAr-*H*), 6.59 (d, *J* = 2.5 Hz, 2H, PAr-*H*), 6.53 (s, 1H, NAr-H), 4.97 (d, *J* = 245.3 Hz, 1H, P-*H*), 2.34 (s, 6H, PAr-*o*-Me-*H*), 2.25 (s, 3H, NAr-*o*-Me-*H*), 2.16 (s, 3H, NAr-*p*-Me-*H*), 2.01 (s, 3H, PAr-*p*-Me-*H*), 2.00 (s, 3H, NAr-*o*-Me-*H*), 1.33 (d, J_{HP} = 0.7 Hz, 9H, *t*-Bu-H).

^{13}C{^{1}H} NMR (125.8 MHz, C_6D_6, 300 K): δ (ppm) 182.6 (d, *J* = 59 Hz, P-*C*=N), 146.9 (d, *J* = 7.5 Hz, N-*ipso*-*C*(Ar)), 143.9 (d, *J* = 14 Hz, P-*ipso*-*C*(Ar)), 139.1 (d, *J* = 1.3 Hz, P-*p*-*C*(Ar)-Me), 131.2 (s, N-*p*-*C*(Ar)-Me), 129.0 (s, NAr*C*-H), 128.7 (d, *J* = 4.6 Hz, PAr*C*-H), 128.5 (s, NAr-*m*-C-H), 126.4 (d, *J* = 14 Hz, P-*o*-*C*(Ar)-Me), 125.4 (s, N-*o*-*C*(Ar)-Me), 123.5 (d, *J* = 1.3 Hz, N-*o*-*C*(Ar)-Me), 44.7 (d, *J* = 14 Hz, *C*Me_3), 29.3 (d, *J* = 3.5 Hz, C(*C*H_3)$_3$), 24.0 (d, *J* = 13 Hz, PAr-*o*-*C*H_3), 20.7 (s, NAr-*o*-*C*H_3), 20.5 (s, NAr-*p*-*C*H_3), 18.0 (d, *J* = 4.2 Hz, NAr-*o*-*C*H_3), 17.7 (d, *J* = 8 Hz, PAr-*p*-*C*H_3).

^{31}P NMR (202.5 MHz, C_6D_6, 300 K): δ (ppm) –80.6 (d, *J* = 244 Hz)

Melting Point: 76 –78 °C

Elemental Analysis: Found: C, 78.21; H, 9.23; N, 4.19. Calc. for $C_{23}H_{32}NP$: C, 78.15; H, 9.13; N, 3.96.

5.3.7 Preparation of *N*-(2,2-dimethyl-1-(tri*iso*propylphenylphosphino)propylidene)2,4,6-trimethylaniline (3.6)

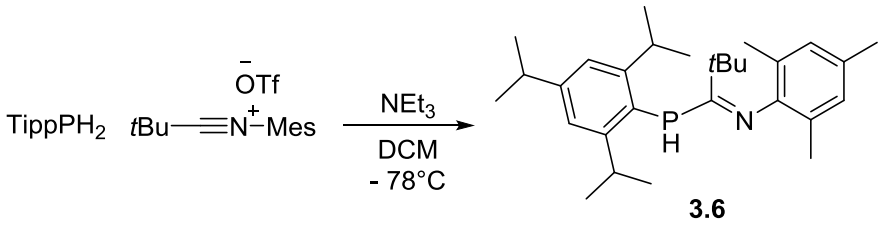

3.6

A solution of tri*iso*propylphenylphosphine (2.93 g, 12.4 mmol) in dichloromethane (15 mL) was added dropwise *via* cannula over 5 minutes to a solution of (*N*-mesityl)(*tert*-butyl)carbonitrilium triflate (4.36 g, 12.4 mmol) in DCM (75 mL) at –78 °C. After stirring at this temperature for 10 minutes, triethylamine (1.75 mL, 1.27 g, 12.5 mmol) was added dropwise over 2 minutes and the reaction was stirred for a further 10 minutes. Subsequently, the cold bath was removed and the reaction was stirred for an additional 2.5 hours giving a yellow/orange mixture. After removal of the volatiles, the solid was extracted with pentane (100 mL), filtered through neutral alumina and washed through with pentane (2 x 100 mL). The resultant solution was concentrated and crystallised at –20 °C to afford yellow crystals of **3.6** (3.09 g, 7.06 mmol, 57 %).

^{1}H NMR (500.2 MHz, C_6D_6, 300 K): δ (ppm) 7.06 (d, *J* = 2.4 Hz, 2H, PAr-*H*), 6.88 – 6.87 (m, 1H, NAr-*H*), 6.74 – 6.73 (m, 1H, NAr-*H*), 5.03 (d, *J* = 252 Hz, 1H, P-*H*), 3.48 (br s, 2H, *o*-C*H*Me$_2$), 2.67 (sept, *J* = 6.9 Hz, 1H, *p*-C*H*Me$_2$), 2.28 (s, 3H, NAr-*o*-C*H*$_3$), 2.23 (s, 3H, NAr-*o*-C*H*$_3$), 2.17 (s, 3H, NAr-*p*-C*H*$_3$), 1.29 (s, 9H, C(C*H*$_3$)$_3$), 1.26 (d, *J* = 6.8 Hz, 6H, *o*-CH(C*H*$_3$)$_2$), 1.15 (br d, *J* = 6.8 Hz, 6H, *o*-CH(C*H*$_3$)$_2$), 1.13 (dd, *J* = 6.9, 1.12 Hz, 6H, *p*-CH(C*H*$_3$)$_2$).

^{13}C{^{1}H} NMR (125.8 MHz, C_6D_6, 300 K): δ (ppm) 182.7 (d, *J* = 61 Hz, P-*C*=N), 154.5 (br s,P-*ipso*-*C*(Ar)), 151.5 (d, *J* = 1.2 Hz, PAr-*p*-*C*(Ar)-*i*Pr), 146.5 (d, *J* = 7.4 Hz, NAr-*ipso*-*C*(Ar)), 131.7 (s, NAr-*p*-*C*(Ar)-Me), 129.1 (s, NAr-*m*-*C*-H), 128.9 (s, NAr-*m*-*C*-H),

125.5 (d, *J* = 16 Hz, P-*o*-*C*(Ar)-*i*Pr), 124.9 (s, NAr-*o*-*C*(Ar)-Me), 124.7 (d, *J* = 2Hz, NAr-*o*-*C*(Ar)-Me), 121.5 (d, *J* = 4.6 Hz, PAr-*m*-*C*-H), 44.7 (d, *J* = 16 Hz, *C*Me$_3$), 34.3 (s, PAr-*p*-*C*Me$_2$), 33.0 (d, *J* = 15 Hz, PAr-*o*-*C*Me$_2$), 29.3 (d, *J* = 2.9 Hz, C(*C*H$_3$)$_3$), 24.3 (br s, PAr-*o*-C(*C*H$_3$)$_2$), 23.6 (br s, PAr-*o*-C(*C*H$_3$)$_2$), 23.6 (s, PAr-*p*-C(*C*H$_3$)$_2$), 20.5 (s, NAr-*p*-C(*C*H$_3$)$_2$), 18.1 (d, *J* = 13 Hz, NAr-*o*-C(*C*H$_3$)$_2$), 17.7 (d, *J* = 1.1 Hz, NAr-*o*-C(*C*H$_3$)$_2$).

^{31}P NMR (202.5 MHz, C_6D_6, 300 K): δ (ppm) –88.9 (d, *J* = 252 Hz)

Elemental Analysis: Found: C, 79.42; H, 10.18; N, 3.22. Calc. for $C_{23}H_{32}NP$: C, 79.59; H, 10.13; N, 3.20.

5.3.8 Preparation of *N*-(2,2-dimethyl-1-(tritertbutylphenylphosphino)propylidene)2,4,6-trimethylaniline (3.7)

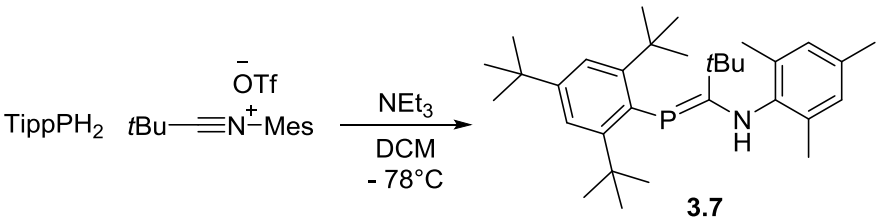

3.7

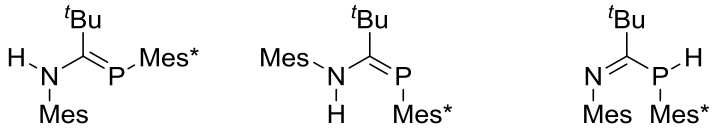

3.7a **3.7b** **3.7c**

A solution of tri*iso*propylphenylphosphine (1.5 g, 5.3 mmol) in dichloromethane (15 mL) was added dropwise *via* cannula over two minutes to a solution of (*N*-mesityl)(*tert*-butyl)carbonitrilium triflate (1.89 g, 5.3 mmol) in DCM (50 mL) at –78 °C. After stirring at this temperature for 15 minutes The mixture was a brown suspension. Triethylamine (0.75 mL, 0.54 g, 5.3 mmol) was added dropwise over one minute and the reaction was stirred for a further 15 minutes. Subsequently, the cold bath was removed and the reaction was stirred for an additional two hours giving an orange/brown mixture. After removal of the volatiles, the solid was extracted with pentane (100 mL), filtered through neutral alumina and washed

through with pentane (2 x 100 mL). The resulting solution was concentrated and crystallised at –20 °C to afford white crystals of **3.7** (0.81 g, 1.69 mmol, 32 %) which contained a small, inseparable amount of Mes*PH_2 (1.6 % by ^{31}P NMR signal integration).

^{1}H NMR An intractable mixture of **3.7a**, **3.7b**, and **3.7c** made assignment of the ^{1}H NMR impossible

^{31}P NMR (202.5 MHz, C_6D_6, 300 K): δ (ppm) 98.5 (d, $^{3}J_{PH}$ = 18 Hz, 52%, **3.7a**), 80.1 (s, **3.7b**, 17%), –53.6 ppm (d, $^{1}J_{PH}$ = 253 Hz, **3.7c**, 31%).

5.3.9 Preparation of Phospha-Amidinato Dichlorosilane 3.10

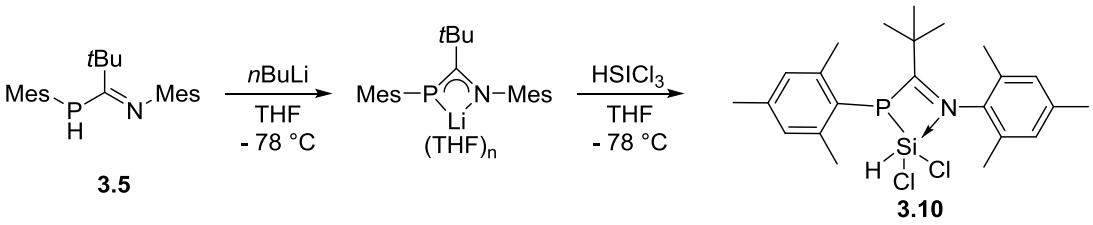

*n*BuLi (0.6 mL, 1.5 mmol, 2.5 M) in hexanes was added dropwise to a solution of phospha-amidine 3.5 (515 mg, 1.46 mmol) in THF (10 mL) at –78 °C. The cold bath was removed and the yellow mixture was stirred for 20 minutes as it came to room temperature. Lithiation was quantitative, as judged by ^{31}P NMR. The mixture was added dropwise over 3 minutes to a solution of trichlorosilane (0.3 mL, 3.03 mmol) in THF (10 mL) at –78 °C and the reaction was stirred for 3 h as it slowly came to ambient temperature. The volatiles were removed and the product was extracted with benzene (10 mL). Concentration of the filtrate and cooling to –20 °C afforded pale crystals of **3.10** as the pure product (540 mg, 82%)

^{1}H NMR (500.2 MHz, C_6D_6, 300 K): δ (ppm) 6.71 (d, 2H, *J* = 2.3 Hz, PAr-*H*), 6.60 (s, 2H, NAr-*H*), 6.52 (s, J_{HSi} = 340 Hz, Si-*H*), 2.69 (s, 6H, PMes-*o*-C*H*$_3$), 2.17 (s, 6H, NMes-*o*-C*H*$_3$), 2.05 (s, 3H, NMes-*p*-C*H*$_3$), 1.99 (s, 3H, PMes-*p*-C*H*$_3$), 0.78 (s, 9H, C(C*H*$_3$)$_3$).

^{13}C{^{1}H} NMR (125.8 MHz, C_6D_6, 300 K): δ (ppm) 206.4 (d, *J* = 28.5 Hz, P-*C*(*t*Bu)=N), 145.2 (d, *J* = 14.6 Hz, PMes-*C*(Ar)), 141.5 (d, *J* = 1.9 Hz, PMes-*C*(Ar)), 141.3 (d, *J* = 6.1 Hz, NMes-*C*(Ar)), 135.3 (s, PMes-*C*(Ar)), 129.8 (d, *J* = 5.2 Hz, P-*m*-*C*(Ar)-H), 129.2 (s, N-*m*-*C*(Ar)-H), 128.2 (s, N-*C*(Ar)), 42.3 (d, *J* = 16.0 Hz, *C*Me$_3$), 28.2 (d,

J = 2.6 Hz, C($\underline{C}$H$_3$)$_3$), 24.2 (d, J = 14.0 Hz, PMes-o-$\underline{C}$H$_3$), 20.8 (s, PMes-p-C$\underline{H}_3$), 20.5 (s, NMes-p-$\underline{C}$H$_3$), 19.1 (s, NMes-o-$\underline{C}$H$_3$).

^{29}Si{^{1}H} NMR (99.4 MHz, C_6D_6, 300 K): δ (ppm) –67.6 (d, $^1J_{SiP}$ = 59 Hz)

^{31}P{^{1}H} NMR (202.5 MHz, C_6D_6, 300 K): δ (ppm) –7.45 (s, $^1J_{PSi}$ = 54 Hz)

5.3.10 Preparation of Phospha-Amidinato Dichlorosilane 3.13

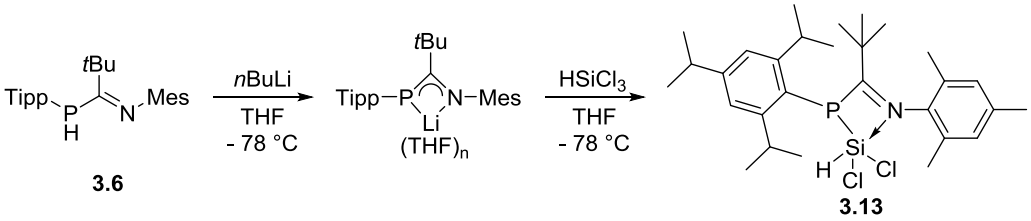

*n*BuLi (0.5 mL, 1.25 mmol, 2.5 M) in hexanes was added dropwise to a solution of phospha-amidine **3.6** (500 mg, 1.14 mmol) in THF (10 mL) at –78 °C. The cold bath was removed and the yellow mixture was stirred for 20 minutes as it came to room temperature. Lithiation was quantitative, as judged by ^{31}P NMR. The mixture was added dropwise over 3 minutes to a solution of trichlorosilane (0.25 mL, 2.47 mmol) in THF (mL) at –78 °C and the reaction was stirred for 3 h as it slowly came to ambient temperature. The volatiles were removed and the product was extracted with toluene (25 mL). Concentration of the filtrate and cooling to –20 °C afforded pale yellow crystals of **3.13** as the pure product (404 mg, 66%).

^{1}H NMR (500.2 MHz, C_6D_6, 300 K): δ (ppm) 7.18 (d, 2H, J = 2.7 Hz, PAr-$\underline{H}$), 6.63 (s, 2H NAr-$\underline{H}$), 6.34 (s, $^1J_{HSi}$ = 336 Hz, Si-$\underline{H}$), 4.22 – 4.12 (m, 2H, o-C$\underline{H}$Me$_2$), 2.71 (sept, 1H, J = 6.9 Hz, p-C$\underline{H}$Me$_2$), 2.18 (s, 6H, Mes-o-C$\underline{H}_3$), 2.06 (s, 3H, Mes-p-C$\underline{H}_3$), 1.50 (d, 6H, J = 6.8 Hz, o-CH(C$\underline{H}_3$)$_2$), 1.36 (d, 6H, J = 6.8 Hz, o-CH(C$\underline{H}_3$)$_2$), 1.13 (d, 6H, J = 6.9 Hz, p-CH(C$\underline{H}_3$)$_2$), 0.83 (s, 9H, C(C$\underline{H}_3$)$_3$).

^{13}C{^{1}H} NMR (125.8 MHz, C_6D_6, 300 K): δ (ppm) 206.6 (d, J = 29.6 Hz, TippP-C(tBu)=NMes), 155.8 (d, J = 13.2 Hz, P-*ipso*-$\underline{C}$(Ar)), 152.6 (d, J = 2.0 Hz, P-p-$\underline{C}$(Ar)-iPr), 141.3 (d, J = 6.0 Hz, N-o-$\underline{C}$(Ar)-Me), 135.3 (s, N-p-$\underline{C}$(Ar)-Me), 129.9 (d, J = 4.8 Hz), 129.3 (s, N-m-$\underline{C}$(Ar)-H), 124.4 (d, J = 27.5 Hz, P-o-$\underline{C}$(Ar)-iPr), 122.5 (d, J = 5.3 Hz, P-o-$\underline{C}$(Ar)-iPr), 41.6 (d, J = 16.7 Hz, $\underline{C}$Me$_3$), 34.2 (s, p-$\underline{C}$HMe$_2$), 33.9 (d, J =

16.0 Hz, *o*-<u>C</u>HMe$_2$), 28.5 (d, *J* = 2.6 Hz, C(<u>C</u>H$_3$)$_3$), 26.4 (s, *o*-CH(<u>C</u>H$_3$)$_2$), 23.7 (s, *o*-CH(<u>C</u>H$_3$)$_2$), 23.4 (s, *p*-CH(<u>C</u>H$_3$)$_2$), 20.4 (s, Mes-*p*-<u>C</u>H$_3$), 19.1 (s, Mes-*o*-<u>C</u>H$_3$).

^{29}Si{^{1}H} NMR (INEPT, 99.4 MHz, C_6D_6, 300 K, d_3 = 0.833 ms, d_4 = 1.25 ms): δ (ppm) – 65.6 (d, $^1J_{SiP}$ = 59 Hz)

^{31}P{^{1}H} NMR (202.5 MHz, C_6D_6, 300 K): δ (ppm) – 13.3 (s, $^1J_{PSi}$ = 58 Hz)

5.3.11 Preparation of Phospha-Amidinato Trichlorosilane 3.14

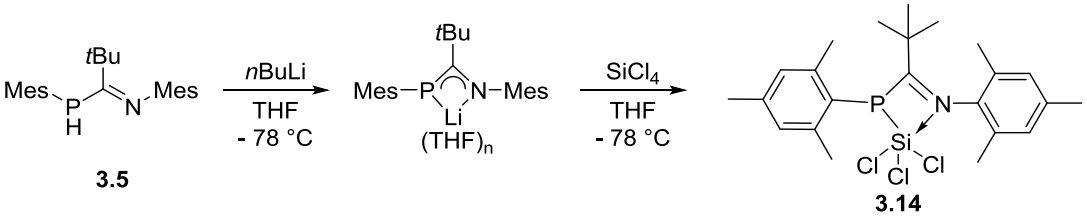

3.5 **3.14**

*n*BuLi (0.4 mL, 1 mmol, 2.5 M) in hexanes was added dropwise to a solution of phospha-amidine **3.5** (321 mg, 0.91 mmol) in THF (10 mL) at –78 °C. The cold bath was removed and the yellow mixture was stirred for 10 minutes as it came to room temperature. Lithiation was quantitative, as judged by ^{31}P NMR. Tetrachlorosilane (0.2 mL, 1.8 mmol) was added rapidly at –78 °C. The cold bath was removed and the mixture was allowed to come to room temperature over 45 minutes. The volatiles were removed and the product was extracted with toluene (25 mL). Concentration of the combined filtrates and cooling to –20 °C afforded yellow crystals of **3.14** as the pure product (214 mg, 48%).

^{1}H NMR (500.2 MHz, C_6D_6, 300 K): δ (ppm) 6.71 (d, 2H, *J* = 2.7 Hz, PAr-<u>H</u>), 6.64 (s, NAr-<u>H</u>), 2.73 (s, 6H, PMes-*o*-C<u>H</u>$_3$), 2.26 (s, 6H, NMes-*o*-C<u>H</u>$_3$), 2.07 (s, 3H, NMes-*p*-C<u>H</u>$_3$), 1.99 (s, 3H, PMes-*p*-C<u>H</u>$_3$), 0.84 (s, 9H, C(C<u>H</u>$_3$)$_3$).

^{13}C{^{1}H} NMR (125.8 MHz, C_6D_6, 300 K): δ (ppm) 200.8 (d, *J* = 22.2 Hz, P-<u>C</u>(*t*Bu)=N), 145.2 (d, *J* = 14.9 Hz, PMes-<u>C</u>(Ar)), 142.5 (d, *J* = 7.0 Hz, NMes-<u>C</u>(Ar)), 141.6 (d, *J* = 2.3 Hz, PMes-<u>C</u>(Ar)), 134.5 (s, PMes-<u>C</u>(Ar)), 129.8 (d, *J* = 5.6 Hz, P-*m*-<u>C</u>(Ar)-H), 129.2 (s, N-*m*-<u>C</u>(Ar)-H), 128.8 (d, *J* = 4.2 Hz, N-<u>C</u>(Ar)), 124.7 (d, *J* = 24.9 Hz, PMes-*o*-<u>C</u>(Ar)-Me), 42.6 (d, *J* = 20.8 Hz, <u>C</u>Me$_3$), 28.4 (d, *J* = 3.2 Hz, C(<u>C</u>H$_3$)$_3$), 24.6 (d, *J* = 14.3 Hz, PMes-*o*-<u>C</u>H$_3$), 20.8 (s, PMes-*p*-C<u>H</u>$_3$), 20.4 (s, NMes-*p*-<u>C</u>H$_3$), 19.8 (s, NMes-*o*-<u>C</u>H$_3$).

^{29}Si{^{1}H} NMR (99.4 MHz, C_6D_6, 300 K): δ (ppm) –37.2 (d, $^{1}J_{SiP}$ = 29 Hz)

^{31}P NMR (202.5 MHz, C_6D_6, 300 K): δ (ppm) 8.78 (s)

5.3.12 Preparation of Phospha-Amidinato Trichlorosilane 3.15

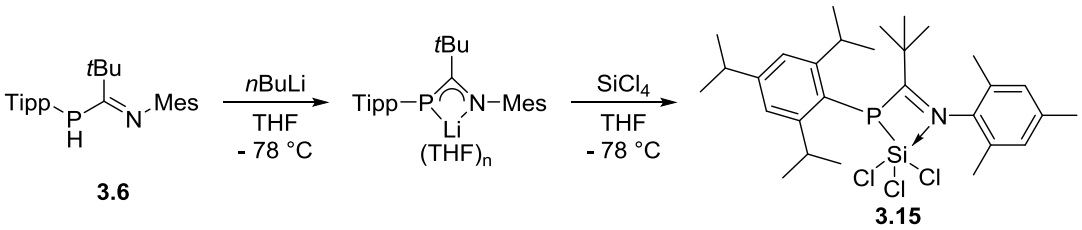

*n*BuLi (1.4 mL, 3.6 mmol, 2.5 M) in hexanes was added dropwise to a solution of phospha-amidine **3.6** (1.5 g, 3.43 mmol) in THF (25 mL) at –78 °C. The cold bath was removed and the yellow mixture was stirred for 20 minutes as it came to room temperature. Lithiation was quantitative, as judged by ^{31}P NMR. Tetrachlorosilane (0.8 mL, 6.97 mmol) was added rapidly at –78 °C and the reaction was stirred for 40 minutes. The cold bath was removed and the mixture was allowed to come to room temperature over 20 minutes. The volatiles were removed and the product was extracted with toluene (20 mL, 4 × 5 mL). Concentration of the combined filtrates to *ca*. 15 mL and cooling to –20 °C afforded yellow crystals of **3.15** as the pure product (1.22 g, 62%).

^{1}H NMR (500.2 MHz, C_6D_6, 300 K): δ (ppm) 7.18 (d, 2H, *J* = 3.1 Hz, PAr-*H*), 6.66 (s, NAr-*H*), 4.34 – 4.24 (m, 2H, *o*-C*H*Me$_2$), 2.70 (sept, 1H, *J* = 6.9 Hz, *p*-C*H*Me$_2$), 2.28 (s, 6H, Mes-*o*-C*H*$_3$), 2.07 (s, 3H, Mes-*p*-C*H*$_3$), 1.47 (d, 6H, *J* = 6.7 Hz, *o*-CH(C*H*$_3$)$_2$), 1.38 (d, 6H, *J* = 6.7 Hz, *o*-CH(C*H*$_3$)$_2$), 1.11 (d, 6H, *J* = 6.9 Hz, *p*-CH(C*H*$_3$)$_2$), 0.84 (s, 9H, C(C*H*$_3$)$_3$).

^{13}C{^{1}H} NMR (125.8 MHz, C_6D_6, 300 K): δ (ppm) 201.8 (d, *J* = 24 Hz, P-(*t*Bu)*C*=N), 156.4 (d, *J* = 14 Hz, P-*ipso*-*C*(Ar)), 153.3 (d, *J* = 2.0 Hz, P-*p*-*C*(Ar)-*i*Pr), 141.9 (d, *J* = 7.3 Hz, N-*o*-*C*(Ar)-Me), 134.8 (s, N-*p*-*C*(Ar)-Me), 129.3 (d, *J* = 4.6 Hz), 129.3 (s, N-*m*-*C*(Ar)-H), 123.5 (d, *J* = 24 Hz, P-*o*-*C*(Ar)-*i*Pr), 122.8 (d, *J* = 5.8 Hz, P-*o*-*C*(Ar)-*i*Pr), 42.2 (d, *J* = 20 Hz, *C*Me$_3$), 34.2 (d, *J* = 2.0 Hz, *p*-CHMe$_2$), 34.1 (s, *o*-CHMe$_2$), 28.9 (d, *J* = 3.0 Hz, C(*C*H$_3$)$_3$), 26.8 (s, *o*-CH(*C*H$_3$)$_2$), 23.6 (s, *o*-CH(*C*H$_3$)$_2$), 23.5 (s, *p*-CH(*C*H$_3$)$_2$), 20.4 (s, Mes-*p*-*C*H$_3$), 19.9 (s, Mes-*o*-*C*H$_3$).

^{29}Si{^{1}H} NMR (99.4 MHz, C_6D_6, 300 K): δ (ppm) –42.6 (d, $^{1}J_{SiP}$ = 33 Hz)

^{31}P{^{1}H} NMR (202.5 MHz, C_6D_6, 300 K): δ (ppm) –7.54 (s, $^{1}J_{PSi}$ = 34 Hz)

5.3.13 Generation of Phospha-Amidinato Silylene 3.18

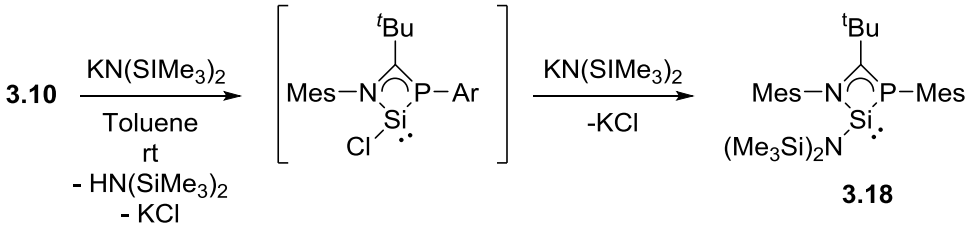

Toluene (20 mL) was added to silane **3.10** (50 mg, 0.11 mmol) and $KN(SiMe_3)_2$ (44 mg, 0.22 mmol) at room temperature. The reaction changed from colourless to orange and then red within five minutes. Removal of the volatiles and washing with hexane afforded crude **3.18** as a viscous red oil which could not be separated from up to 10-20% phospha-amidine **3.5** and other, unidentified impurities. Some of the ^{1}H resonances are assigned below.

^{1}H NMR (500.2 MHz, C_6D_6, 300 K): δ (ppm) 2.99 (s, 3H, Mes-C*H*$_3$), 2.63 (s, 6H, Mes-C*H*$_3$ ×2), 2.34 (s, 3H, Mes-C*H*$_3$), 2.19 (s, 3H, Mes-C*H*$_3$), 2.06 (s, 3H, Mes-C*H*$_3$), 2.05 (s, 3H, Mes-C*H*$_3$), 0.95 (s, 9H, ^{t}Bu), 0.30 (s, 18H, $SiMe_3$ ×2)

^{31}P{^{1}H} NMR (202.5 MHz, C_6D_6, 300 K): δ (ppm) –45.8 (s, $^{1}J_{PSi}$ = 69 Hz)

5.3.14 Preparation of Bis(Mesityl Phospha-Amidinato)Silylene 3.21

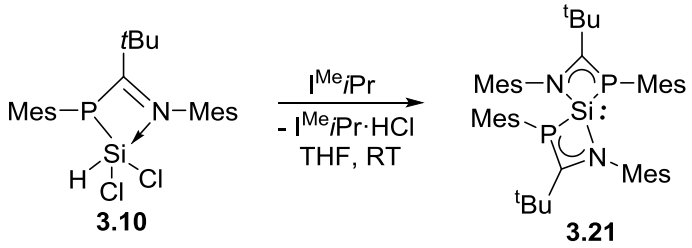

To a flask charged with phospha-amidine **3.5** (1.5 g, 4.24 mmol) in THF (45 ml) was added *n*BuLi (1.95 mL, 4.88 mmol, 2.5 M in hexanes) over 5 minutes at –78 °C. The resultant yellow mixture was stirred for 15 minutes as is came to room temperature. Lithiation was

quantitative, as judged by ^{31}P NMR. Trichlorosilane (862 mg, 0.64 mL, 6.36 mmol) was added dropwise at –78 °C and the reaction was warmed to room temperature and stirred for 2 h. Removal of the volatiles afforded a yellow foamy solid, to which solid 1,3-di*iso*propyl-4,5-dimethylimidazol-2-ylidene (I^{Me}*i*Pr) (765 mg, 4.24 mmol) was added followed by toluene (30 mL) at ambient temperature. The solution quickly turned deep red. After stirring for 1 h the solution was filtered and concentrated. Crystallisation and recrystallisation at –20 °C afforded the product as a deep red solid (461 mg, 30%).

^{1}H NMR (400.1 MHz, Tol-d_8, 223 K): δ (ppm) 6.78 (s, 1H, Ar-*H*), 6.73 (s, 1H, Ar-*H*), 6.67 (s, 1H, Ar-*H*), 6.44 (s, 1H, Ar-*H*), 2.95 (s, 3H, Me-*H*), 2.61 (s, 3H, Me-*H*), 2.45 (s, 3H, Me-*H*), 2.30 (s, 3H, Me-*H*), 2.17 (s, 3H, Me-*H*), 2.10 (s, 3H, Me-*H*), 1.03 (s, 9H, C(C*H*$_3$)$_3$).

^{31}P{^{1}H} NMR (162.0 MHz, Tol-d_8, 223 K): δ (ppm) –28.1 (s, $^{1}J_{PSi}$ = 79 Hz)

5.3.15 Generation of Gold Macrocycle 3.25

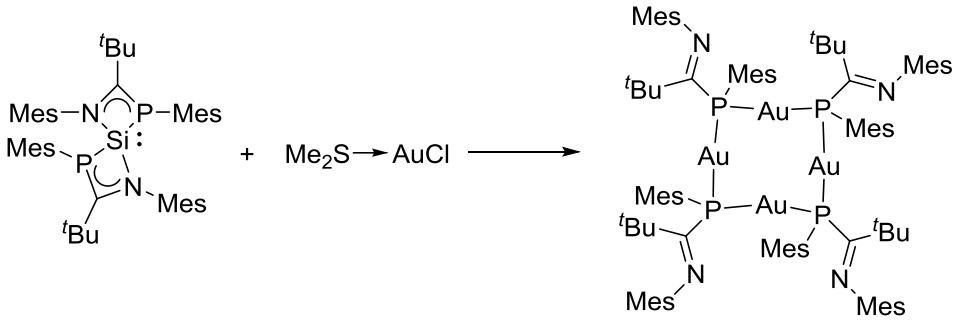

3.25

C_6D_6 was added to an NMR tube charged with silylene **3.21** (52 mg, 0.071 mmol) and Dimethylsulfide Gold Chloride Complex (21 mg, 0.71 mmol). After three hours at room temperature a complex mixture of products was observed by ^{1}H and ^{31}P NMR. Standing at room temperature afforded trace amounts of macrocycle **3.25** identified by single crystal X-ray diffraction.

5.3.16 Generation of Phospha-Amidinato Dimethyl Aluminium Complex 3.28

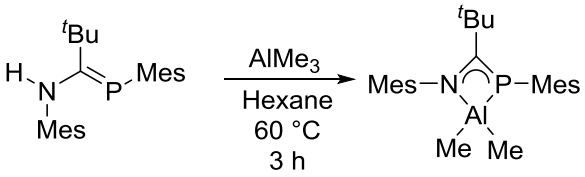

3.5 **3.28**

Trimethyl aluminium (72 mg, 96 µL, 1 mmol) was added to phospha-amidine **3.5** (353 mg, 1 mmol) in hexane (15 mL) at room temperature before heating to 60 °C for three hours to give aluminium complex **3.28** quantitatively. Single crystals of **3.28** suitable for X-ray diffraction were grown from hexane at −20 °C.

^{1}H NMR (500 MHz, C_6D_6, 300 K): δ (ppm) 6.81 (s, 2H, Ar-*H*), 6.60 (s, 2H, Ar-*H*), 2.72 (s, 6H, *o*-Me), 2.23 (s, 6H, *o*-Me), 2.09 (s, 3H, *p*-Me), 2.04 (s, 3H, *p*-Me), 0.95 (s, 9H, $C(CH_3)_3$), −0.16 (d, 6H, $AlMe_2$).

^{31}P{^{1}H} NMR (162.0 MHz, C_6D_6, 300 K): δ (ppm) –32.7 (s)

5.3.17 Generation of Phospha-Amidinato Dimethyl Aluminium Complex 3.29

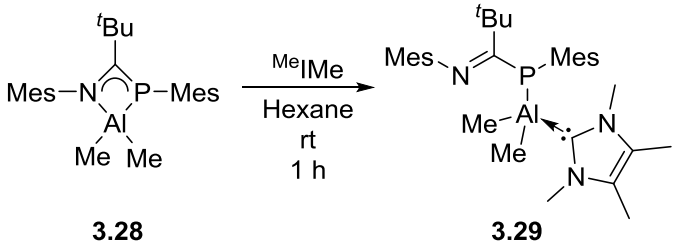

3.28 **3.29**

Aluminium complex **3.28** (140 mg, 0.24 mmol) and ^{Me}IMe (30 mg, 0.24 mmol) were dissolved in toluene with gentle warming. Stirring at room temperature for 1.5 h and cooling to −20 °C afforded small amounts of single crystals of **3.29**.

^{1}H NMR (500 MHz, C_6D_6, 300 K): δ (ppm) 6.53 (s, 2H, Ar-*H*), 6.44 (s, 2H, Ar-*H*), 2.79 (s, 6H, Mes *o*-Me), 2.32 (s, 6H, Mes *o*-Me), 2.28 (br s, 6H, NHC Me ×2), 2.16 (s,

3H, Mes *p*-Me), 2.05 (s, 3H, Mes *p*-Me), 1.74 (s, 9H, C(C$\underline{H}_3$)$_3$), 1.12 (br s, 6H, NHC Me ×2), −0.04 (br s, 6H, $AlMe_2$).

^{31}P NMR (162.0 MHz, C_6D_6, 300 K): δ (ppm) –65.9 (br s)

5.4 Experimental Details for Chapter 4

5.4.1 General Procedure for the Hydroboration of Aldehydes and Ketones

Pinacolborane (91 µL, 0.625 mmol) was added to a solution of anion **4.12** (1.24 mg, 0.0313 mmol) in toluene (20 µL) at room temperature resulting in a colour change from yellow to colourless. The substrate (0.625 mmol) was added and the reaction stirred for one hour at room temperature. After one hour a solution of trimethoxybenzene in $CDCl_3$ was added to the reaction mixture to quench the reaction. A ^1H NMR was recorded and *in situ* yield measured against triemethoxybenzene by intergration.

5.4.2 ^1H NMR Data for Ketone and Aldehyde Hydroboration Products

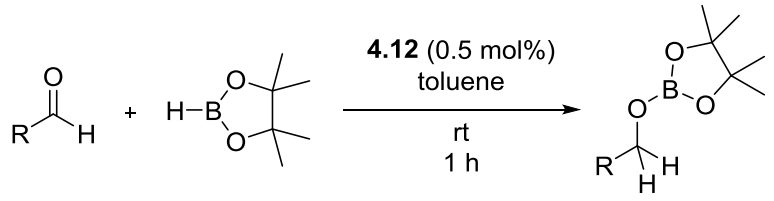

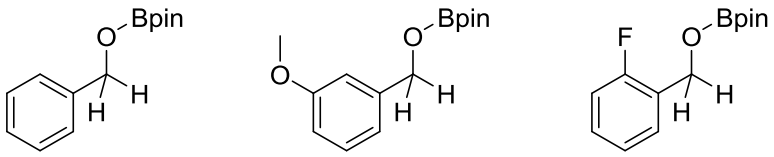

4.13 >99%

4.14 >99%

4.15 >99%

NMR data were in accordance with the literature.[13]

4.13 (400 MHz, $CDCl_3$, 300 K): δ (ppm) 7.27-7.22 (m, 4H), 7.19-7.15 (m, 1H) 4.84 (s, 2H), 1.18 (s, 12H).[13]

4.14 (400 MHz, $CDCl_3$, 300 K): δ (ppm) 7.28 (d, 2H, $^3J_{HH}$ = 8.6 Hz), 6.86 (d, 2H, $^3J_{HH}$ = 8.6 Hz), 4.85 (s, 2H), 3.79 (s, 3H), 1.26 (s, 12H).[13]

4.15 (400 MHz, $CDCl_3$, 300 K): δ (ppm) 7.50-7.43 (m, 1H), 7.30-7.01 (m, 3H), 5.03 (s, 2H), 1.30 (s, 12H).[13]

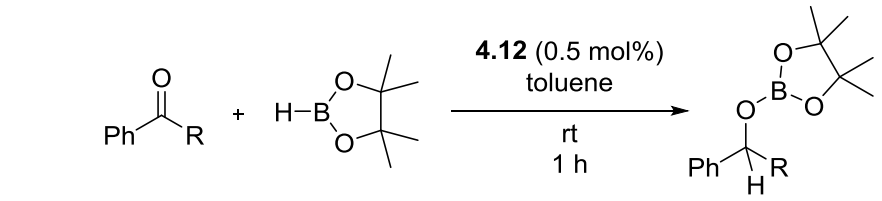

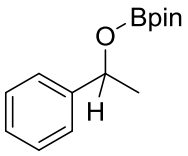

4.16
81%

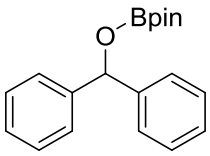

4.17
71%

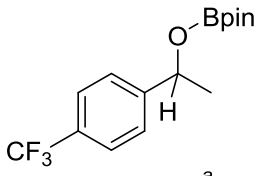

4.18[a]
39%

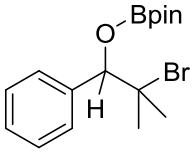

4.19
61%

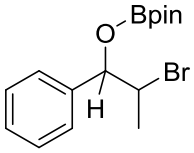

4.20
47%

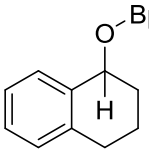

4.21
37%

*For **4.16**-**4.18** and **4.21** analytical data were in accordance with the literature.[14–16] Products **4.19** and **4.20** are previously unreported compounds.*

4.16 (400 MHz, $CDCl_3$, 300 K): δ (ppm) 7.39-7.37 (m, 2H, Ar-*H*), 7.34-7.31 (m, 2H, Ar-*H*), 7.26-7.23 (m, 1H, Ar-*H*), 5.27 (q, 1H, $^3J_{HH}$ = 6.5 Hz, C-*H*), 1.51 (d, 3H, $^3J_{HH}$ = 6.5 Hz, Me), 1.26 (s, 6H, Bpin-Me), 1.23 (2, 6H, Bpin-Me).[14]

4.17 (500 MHz, $CDCl_3$, 300 K): δ (ppm) 7.45-7.19 (m, 10H, Ar-*H*), 6.24 (s, 1H, C-*H*), 1.25 (s, 12H, Bpin-Me).[15]

4.18 (500 MHz, $CDCl_3$, 300 K): δ (ppm) 7.64 (d, 2H, $^3J_{HH}$ = 8.0 Hz, Ar-*H*), 7.54 (d, 2H, $^3J_{HH}$ = 8.0 Hz, Ar-*H*), 5.36 (q, 1H, $^3J_{HH}$ = 6.5 Hz, C-*H*), 1.56 (d, 3H, $^3J_{HH}$ = 6.5 Hz, Me), 1.31 (s, 6H, Bpin-Me), 1.28 (2, 6H, Bpin-Me).[14]

4.19 (400 MHz, $CDCl_3$, 300 K): δ (ppm) 7.49-7.17 (m, 5H, Ar-*H*), 5.28 (s, 1H, C-*H*), 1.77 (s, 3H, $C(C\underline{H}_3)_2$), 1.71 (s, 3H, $C(C\underline{H}_3)_2$), 1.27 (s, 6H, Bpin-Me), 1.22 (2, 6H, Bpin-Me).

4.20 Major diastereomer (500 MHz, $CDCl_3$, 300 K): δ (ppm) 7.42-7.14 (m, 5H, Ar-*H*), 5.12 (d, 1H, $^3J_{HH}$ = 7.4 Hz), 4.31-4.26 (m, 1H, C*H*Me), 1.54 (d, 3H, $^3J_{HH}$ = 6.9 Hz, C*H*$_3$), 1.27 (s, 6H, Bpin-Me), 1.24 (2, 6H, Bpin-Me).

Minor diasteromer (500 MHz, $CDCl_3$, 300 K): δ (ppm) 7.42-7.14 (m, 5H, Ar-*H*), 5.40 (d, 1H, $^3J_{HH}$ = 4.2 Hz), 4.33 (dp, 1H, $^3J_{HH}$ = 4.2, 6.8 Hz, C*H*Me), 1.60 (d, 3H, $^3J_{HH}$ = 6.8 Hz, C*H*$_3$), 1.29 (s, 6H, Bpin-Me), 1.25 (2, 6H, Bpin-Me).

4.21 (400 MHz, $CDCl_3$, 300 K): δ (ppm) 7.44-7.41 (m, 1H, Ar-*H*), 7.19-7.14 (m, 2H, Ar-*H*), 7.11-7.09 (m, 1H, Ar-*H*), 5.23 (t, $^3J_{HH}$ = 4.8 Hz, C-*H*), 2.85-2.82 (m, 1H, C*H*$_2$), 2.77-2.73 (m, 1H, C*H*$_2$), 2.11-2.04 (m, 1H, C*H*$_2$), 1.83-1.74 (m, 1H, C*H*$_2$), 1.33 (s, 6H, Bpin-Me), 1.32 (2, 6H, Bpin-Me).[16]

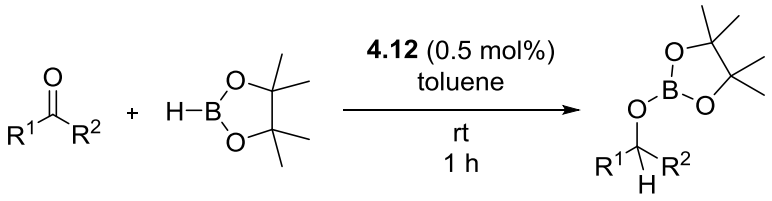

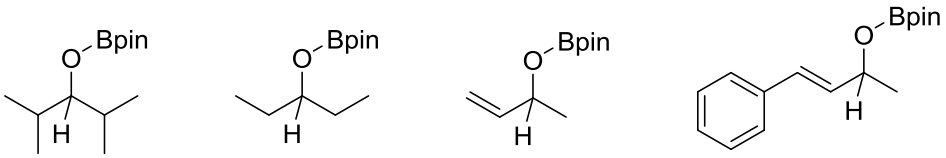

4.22 traces

4.23 77%

4.24 53%

4.25 68%

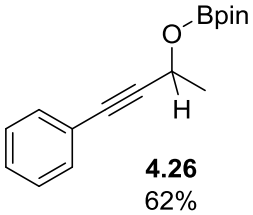

4.26 62%

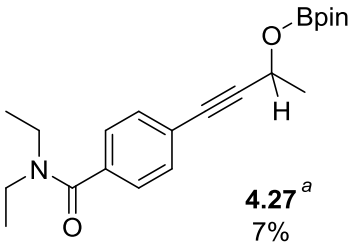

4.27 [a] 7%

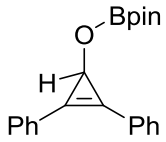

4.28 traces

*For **4.24** and **4.25** analytical data were in accordance with the literature.*[17,18] *Products **4.23**, **4.26** and **4.27** are previously unreported compounds.*

4.23 (400 MHz, $CDCl_3$, 300 K): δ (ppm) 3.90 (tt, $^3J_{HH}$ = 5.1, 7.2 Hz, C*H*^{i}Pr$_2$), 1.54-1.44 (m, 4H, C*H*$_2$ ×2), 0.92 (t, 6H, $^3J_{HH}$ = 7.4 Hz, C*H*$_3$ ×2), 1.27 (s, 12H, Bpin).

4.24 (600 MHz, $CDCl_3$, 300 K): δ (ppm) 5.93-5.87 (m, 1H, H_2C=C*H*), 5.25-5.21 (m, 1H, *H*$_2$C=CH), 5.07-5.04 (m, 1H, *H*$_2$C=CH), 4.74-4.69 (m, 1H C*H*O), 1.87-1.86 (m, 1H, C*H*$_3$).[18]

4.25 (600 MHz, $CDCl_3$, 300 K): δ (ppm) 6.63 (d, 1H, $^3J_{HH}$ = 16.0 Hz, PhC*H*=CH), 6.28 (dd, 1H, $^3J_{HH}$ = 5.8, 16.0 Hz, PhCH=C*H*), 4.91-4.87 (m, 1H, C-*H*), 1.42 (d, 3H, $^3J_{HH}$ = 6.5 Hz, Me), 1.31 (s, 6H, Bpin-Me), 1.30 (2, 6H, Bpin-Me).[17]

4.26 (400 MHz, $CDCl_3$, 300 K): δ (ppm) 7.46-7.42 (m, 5H, Ar-*H*), 5.10, (q, 1H, $^3J_{HH}$ = 6.7 Hz, C-*H*), 1.58 (d, 3H, $^3J_{HH}$ = 6.7 Hz, C*H*$_3$), 1.30 (s, 12H, Bpin).

4.27 The crude reaction mixture showed a complex mixture of products but small amounts of **4.27** were identified from characteristic resonances assigned below by comparison with product **4.26**.

(400 MHz, $CDCl_3$, 300 K): δ (ppm) 5.10, (q, 1H, $^3J_{HH}$ = 6.6 Hz, C-*H*), 1.59 (d, 3H, $^3J_{HH}$ = 6.6 Hz, C*H*$_3$), 1.30 (s, 12H, Bpin).

5.4.3 General Procedure for the Hydroboration of Alkynes

In a typical experiment, substrate (0.25 mmol) was added to anion **4.12** (10 mg, 0.025 mmol) in an NMR tube which gave an orange solution. HBpin was added and the reaction heated to 110 °C for two hours, at which point the reaction mixture had turned colourless. A solution of trimethoxybenzene in chloroform was added. A ^{1}H NMR was recorded and *in situ* yield measured against triemethoxybenzene by intergration.

5.4.4 ^{1}H NMR Data for Alkyne Hydroboration Products

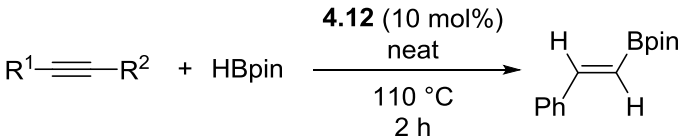

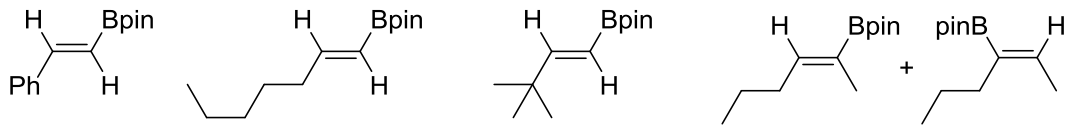

4.39 74% **4.40** 37% **4.41** 39% **4.42** 51% **4.43** 10%

NMR data were in accordance with the literature.[19,20]

4.39 (600 MHz, $CDCl_3$, 300 K): δ (ppm) 7.52 – 7.50 (m, 2H, Ar-*H*), 7.44 (d, 1H $^3J_{HH}$ = 18.4 Hz, C-*H*), 7.38 – 7.32 (m, 3H, Ar-*H*), 6.20 (d, 1H, $^3J_{HH}$ = 18.4 Hz, C-*H*), 1.35 (s, 12H, Bpin).[19]

4.40 (500 MHz, $CDCl_3$, 300 K): δ (ppm) 6.64 (dt, 1H, $^3J_{HH}$ = 18.0, 6.4 Hz, C-*H*), 5.4 (d, 1H, $^3J_{HH}$ = 18.0, C-*H*), 1.27 (s, 12H, Bpin).[20]

4.41 (500 MHz, $CDCl_3$, 300 K): δ (ppm) 6.65 (d, 1H, $^3J_{HH}$ = 18.3 Hz, C-*H*), 5.36 (d, 1H, $^3J_{HH}$ = 18.3 Hz, C-*H*), 1.28 (s, 12H), 1.03 (s, 9H).[19]

4.42 (500 MHz, $CDCl_3$, 300 K): δ (ppm) 6.31 (t, 1H, $^3J_{HH}$ = 7.1 Hz, C-*H*) 2.11 (q, 4H, $^3J_{HH}$ = 7.3), 1.72 (d, 3H, $^3J_{HH}$ = 7.0 Hz), 1.69 (s, 3H), 1.48-1.40 (m, 2H), 1.27 (s, 12H), 0.93 (t, 3H $^3J_{HH}$ = 7.3Hz).[19]

4.43 (500 MHz, $CDCl_3$, 300 K): δ (ppm) 6.43 (q, 1H, $^3J_{HH}$ = 6.7 Hz), 1.74 (d, 3H, $^3J_{HH}$ = 6.7 Hz), 1.40-1.35 (m, 2H), 1.24 (s, 12H), 0.91 (t, 3H, $^3J_{HH}$ = 7.6 Hz).[19]

5.4.5 Stoichiometric Reactions of Acetophenone and Silyl Anion 4.12

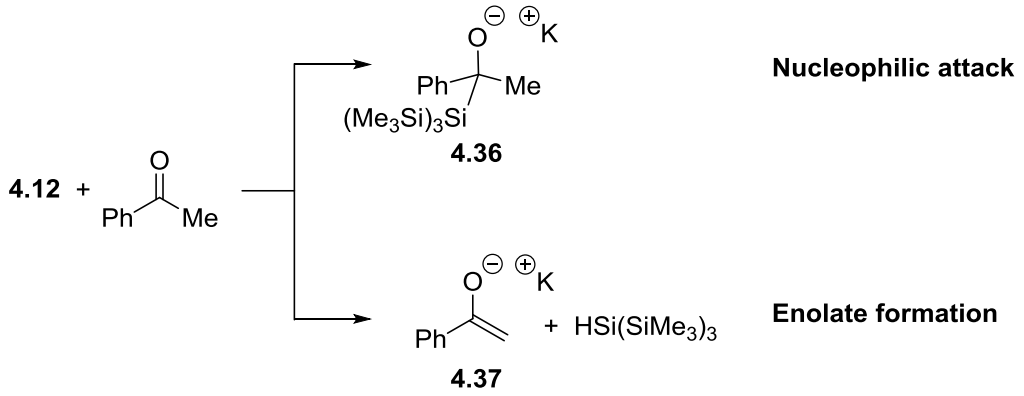

In a typical reaction anion **4.12** (20 mg, 0.05 mmol) was dissolved inTHF-d_8 or C_6D_6 (0.6 mL). Acetophenone (6 µL, 0.05 mmol) was added at room temperature which resulted in a colour change from yellow to colourless.

In THF-d_8 a complex mixture was observed. Some significant ^{13}C resonances are provided below.

^{13}C NMR (126 MHz, THF-d_8, 300 K): δ (ppm) 73.2 (s), 68.2(s).

When carried out in C_6D_6 only one major product is observed which is assigned to alkoxide **4.36**, as shown above, through the following NMR signals.

^{1}H NMR (500 MHz, C_6D_6, 300 K): δ (ppm) 7.40-7.38 (m, 5H, Ar-*H*), 1.88 (s, 3H, C*H*$_3$).

^{13}C NMR (126 MHz, C_6D_6, 300 K): δ (ppm) 75.1 (s, *C*-O$^-$)

5.4.6 Stoichiometric Reaction of HBpin and Silyl Anion 4.12

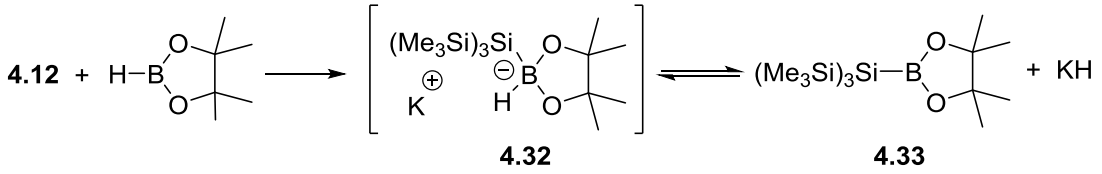

Poor solubility in C_6D_6

In a typical reaction anion **4.12** (14 mg, 0.07 mmol) was dissolved inTHF-d_8 or C_6D_6 (0.6 mL). Pinacolborane (9 µL, 0.07 mmol) was added at room temperature which resulted in the formation of a gel like solid.

In both solvents the ^{1}H NMR gave broad, intractable signals. In C_6D_6 a single ^{11}B resonance was observed which is assigned to silyl boronic ester **4.33**, in accordance with the literature.[21]

^{11}B NMR (160 MHz, C_6D_6, 300 K): δ (ppm) 37.3.

In THF-d_8 a mixture of boronic ester **4.33**[21] and THF·BH_3 were observed, along with a new resonance which is tentatively assigned to boron-ate complex **4.32**.

^{11}B NMR (160 MHz, C_6D_6, 300 K): δ (ppm) 37.3 (**4.33**), 8.4 (**4.32**), −45.4 (BH_3·THF).

5.4.7 Generation of Silyl Boronic Ester 4.33 *via* Boron-ate 4.32

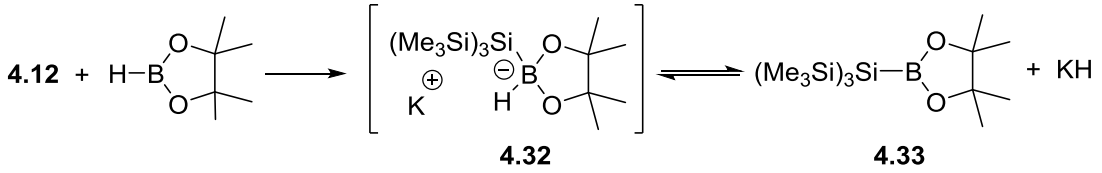

Poor solubility in C_6D_6

Silyl anion **4.12** (99 mg, 0.25 mmol) was dissolved in hexane and HBpin (36 µL, 0.25 mmol) was added dropwise at room temperature giving a colourless solution with a gel-like

suspension which was stirred at room temperature for 16 hours. Filtration of the reaction mixture through a silica plug afforded crude silyl boronic ester **4.33** quantitatively. NMR data were in accordance with the literature.[21]

^{1}H NMR (500 MHz, C_6D_6, 300 K): δ (ppm) 1.19 (s, 12H, Bpin), 0.18 (s, 12H, $Si(SiMe_3)_3$).

^{11}B NMR (160 MHz, C_6D_6, 300 K): δ (ppm) 37.3.

5.5 Crystallographic Data

Crystallography was performed by Dr Gary Nichol at the University of Edinburgh.

Full crystallographic data is available and the end of this section.

5.5.1 Silane 2.23

Experimental

Single colourless block-shaped crystals of **2.23** were recrystallised from hexane by slow cooling. A suitable crystal (0.52×0.29×0.23) mm^3 was selected and mounted on a MITIGEN holder in Paratone oil on a Rigaku Oxford Diffraction SuperNova diffractometer. The crystal was kept at T = 120.0 K during data collection. Using **Olex2**[22], the structure was solved with the **ShelXS**[23] structure solution program, using the Direct Methods solution method. The model was refined with version 2014/7 of **ShelXL**[24] using Least Squares minimisation.

Crystal Data

$C_{57}H_{129}Cl_3Si_{15}$, M_r = 1342.29, orthorhombic, $Cmc2_1$ (No. 36), a = 44.9370(12) Å, b = 12.5333(2) Å, c = 14.5469(3) Å, $\alpha = \beta = \gamma = 90^{\circ}$, V = 8193.0(3) $Å^3$, T = 120.0 K, Z = 4, Z' = 0.5, $\mu(MoK_\alpha)$ = 0.362, 73400 reflections measured, 10189 unique (R_{int} = 0.0811) which were used in all calculations. The final wR_2 was 0.1746 (all data) and R_1 was 0.0816 (I > 2(I)).

Plot

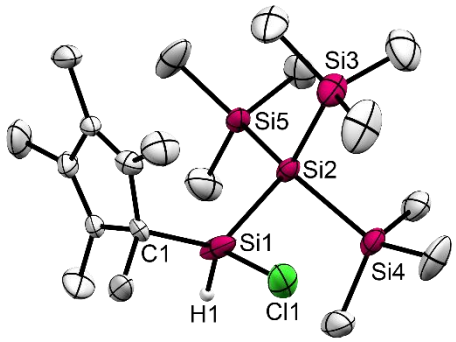

Hydrogen atoms (other than H1), disorder and second independent molecule omitted for clarity. Thermal ellipsoids set to 50%.

5.5.2 Disilene Adduct 2.28

Experimental

Single pale orange block-shaped crystals of **2.28** were recrystallised from diethyl ether by slow cooling. A suitable crystal (0.20×0.07×0.04) mm^3 was selected and mounted on a MITIGEN holder in Paratone oil on a Rigaku Oxford Diffraction SuperNova diffractometer. The crystal was kept at T = 120.0 K during data collection. Using **Olex2**[22], the structure was solved with the **ShelXS**[23] structure solution program, using the Direct Methods solution method. The model was refined with version 2014/7 of **ShelXL**[24] using Least Squares minimisation.

Crystal Data

$C_{27}H_{54}N_2Si_4$, M_r = 519.08, monoclinic, $P2_1/c$ (No. 14), a = 11.32508(20) Å, b = 16.0662(3) Å, c = 18.3367(3) Å, β = 103.2283(16)°, α = γ = 90°, V = 3247.86(10) $Å^3$, T = 120.0 K, Z = 4, Z' = 1, μ(CuK_α) = 1.809, 26957 reflections measured, 6729 unique (R_{int} = 0.0889) which were used in all calculations. The final wR_2 was 0.1551 (all data) and R_1 was 0.0558 (I > 2(I)).

Plot

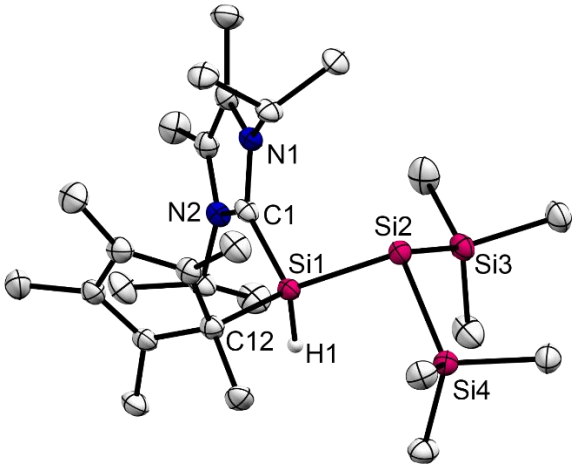

Hydrogen atoms (other than H1) and disorder omitted for clarity. Thermal ellipsoids set to 50%.

5.5.3 Silane 2.35

Experimental

Single colourless block-shaped crystals of **2.35** were recrystallised from hexane by slow cooling. A suitable crystal (0.17×0.13×0.08) mm^3 was selected and mounted on a MITIGEN holder in Paratone oil on a Rigaku Oxford Diffraction SuperNova diffractometer. The crystal was kept at a steady T = 120.0 K during data collection. The structure was solved with the **ShelXT**[23] structure solution program using the Intrinsic Phasing solution method and by using **Olex2**[22] as the graphical interface. The model was refined with version 2018/3 of **ShelXL**[24] using Least Squares minimisation.

Crystal Data

$C_{33}H_{53}ClSi_5$, M_r = 625.65, monoclinic, $P2_1/c$ (No. 14), a = 16.7147(2) Å, b = 11.49900(10) Å, c = 19.04910(10) Å, β = 90.0000(10)˚, α = γ = 90˚, V = 3661.28(6) $Å^3$, T = 120.0 K, Z = 4, Z' = 1, μ(CuK_α) = 2.632, 57789 reflections measured, 7613 unique (R_{int} = 0.0735) which were used in all calculations. The final wR_2 was 0.2024 (all data) and R_1 was 0.0807 (I > 2(I)).

Plot

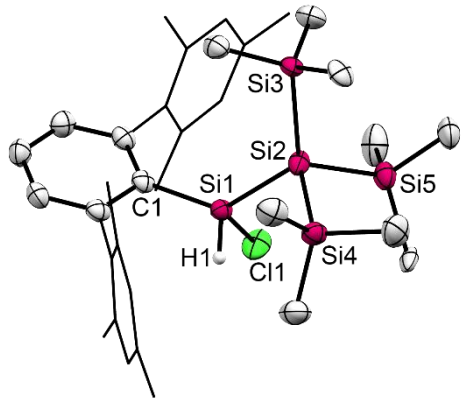

Hydrogen atoms (other than H1) and disorder omitted for clarity. Thermal ellipsoids set to 50%.

5.5.4 Silylsilylene 2.37

Experimental

Single dark orange block-shaped crystals of **2.37** were recrystallised from pentane by slow cooling. A suitable crystal (0.42×0.36×0.24) mm^3 was selected and mounted on a MITIGEN holder in Paratone oil on a Rigaku Oxford Diffraction SuperNova diffractometer. The crystal was kept at T = 120.0 K during data collection. Using **Olex2**,[22] the structure was solved with the **ShelXS**[23] structure solution program, using the Direct Methods solution method. The model was refined with version 2017/1 of **ShelXL**[24] using Least Squares minimisation.

Crystal Data

$C_{41}H_{64}N_2Si_4$, M_r = 697.30, monoclinic, $P2_1/n$ (No. 14), a = 12.3461(4) Å, b = 18.7939(8) Å, c = 18.9399(6) Å, β = 104.669(3)°, $\alpha = \gamma = 90°$, V = 4251.4(3) $Å^3$, T = 120.0 K, Z = 4, Z' = 1, μ(MoK_α) = 0.168, 52088 reflections measured, 21719 unique (R_{int} = 0.0642) which were used in all calculations. The final wR_2 was 0.1466 (all data) and R_1 was 0.0608 (I > 2(I)).

Plot

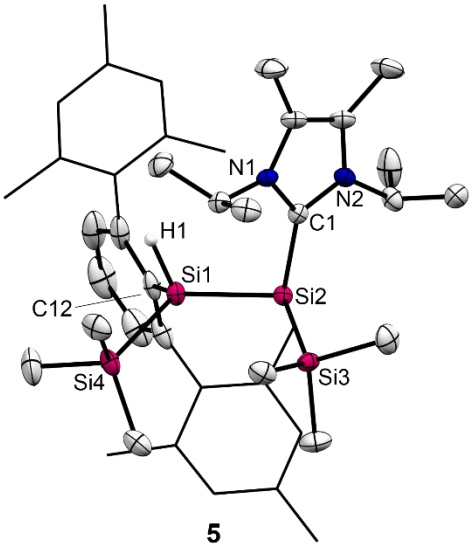

5

Hydrogen atoms (other than H1) and disorder omitted for clarity. Thermal ellipsoids set to 50%.

5.5.5 Disilene Adduct 2.50

Experimental

Single dark red block-shaped crystals of **2.50** were recrystallised from toluene by slow evaporation. A suitable crystal (0.16×0.09×0.07) mm^3 was selected and mounted on a MITIGEN holder in Paratone oil on a Rigaku Oxford Diffraction SuperNova diffractometer. The crystal was kept at a steady T = 120.0 K during data collection. The structure was solved with the **ShelXS**[23] structure solution program using the Direct Methods solution method and by using **Olex2**[22] as the graphical interface. The model was refined with version 2018/3 of **ShelXL**[24] using Least Squares minimisation.

Crystal Data

$C_{39}H_{56}N_2Si_4$, M_r = 665.21, monoclinic, $P2_1/c$ (No. 14), a = 15.89104(14) Å, b = 16.29426(12) Å, c = 15.02549(12) Å, β = 95.5918(8)°, $\alpha = \gamma$ = 90°, V = 3872.08(5) $Å^3$, T = 120.0 K, Z = 4, Z' = 1, μ(CuK_α) = 1.629, 41474 reflections measured, 8017 unique (R_{int} = 0.0750) which were used in all calculations. The final wR_2 was 0.1363 (all data) and R_1 was 0.0489 (I > 2(I)).

Plot

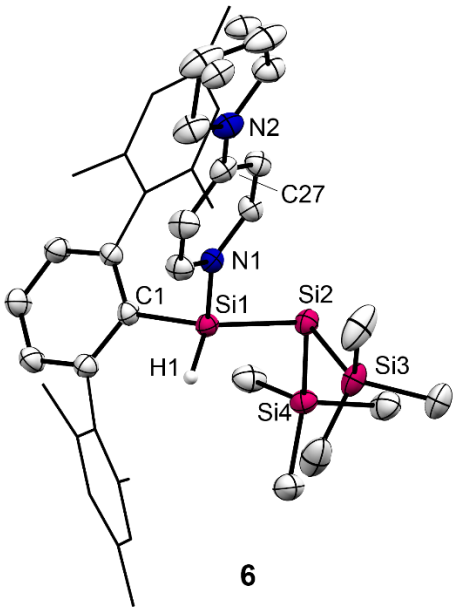

Hydrogen atoms (other than H1) and disorder omitted for clarity. Thermal ellipsoids set to 50%.

5.5.6 Phospha-Amidine 3.7

Experimental.

Single colourless block-shaped crystals of **3.7** were recrystallised from pentane by slow evaporation. A suitable crystal (0.29×0.08×0.07) mm^3 was selected and mounted on a MITIGEN holder in Paratone oil on a Rigaku Oxford Diffraction SuperNova diffractometer. The crystal was kept at T = 120.0 K during data collection. Using **Olex2**[22] the structure was solved with the **ShelXS**[23] structure solution program, using the Direct Methods solution method. The model was refined with version 2014/7 of **ShelXL**[24] using Least Squares minimisation.

Crystal Data.

$C_{69}H_{112}N_2P_2$, M_r = 1031.54, monoclinic, $P2_1/c$ (No. 14), a = 10.26764(11) Å, b = 9.95168(15) Å, c = 31.7681(4) Å, β = 90.6629(9)°, $\alpha = \gamma$ = 90°, V = 3245.86(7) $Å^3$, T = 120.0 K, Z = 2, Z' = 0.5, μ(CuK_α) = 0.886, 27126 reflections measured, 6732 unique (R_{int} = 0.0632) which were used in all calculations. The final wR_2 was 0.1594 (all data) and R_1 was 0.0580 (I > 2(I)).

Plot

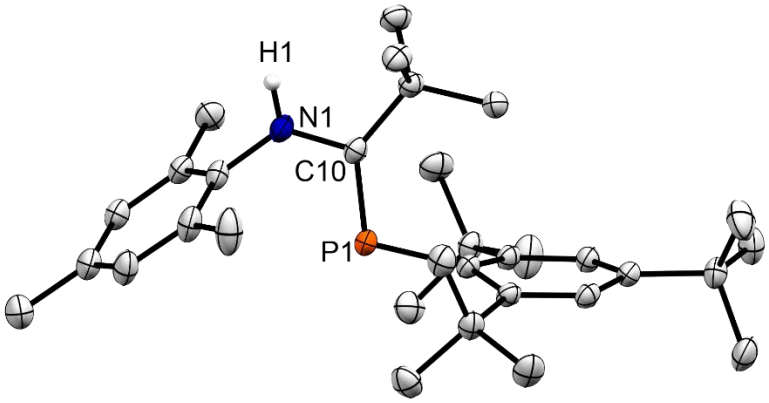

Hydrogen atoms (other than H1) omitted for clarity. Thermal ellipsoids set to 50%.

5.5.7 Silane 3.10

Experimental.

Single colourless block-shaped crystals of **3.10** were recrystallised from benzene by slow evaporation. A suitable crystal (0.26×0.18×0.07) mm^3 was selected and mounted on a MITIGEN holder in Paratone oil on a Rigaku Oxford Diffraction SuperNova diffractometer. The crystal was kept at T = 120.0 K during data collection. Using **Olex2**[22] the structure was solved with the **ShelXT**[23] structure solution program, using the Direct Methods solution method. The model was refined with version of **ShelXL**[24] using Least Squares minimisation.

Crystal Data.

$C_{23}H_{32}Cl_2NPSi$, M_r = 452.45, monoclinic, $P2_1/c$ (No. 14), a = 8.8740(4) Å, b = 13.4389(6) Å, c = 20.2034(9) Å, β = 98.304(4)°, α = γ = 90°, V = 2384.12(18) $Å^3$, T = 120.0 K, Z = 4, Z' = 1, $\mu(MoK_\alpha)$ = 0.399, 21709 reflections measured, 6022 unique (R_{int} = 0.0550) which were used in all calculations. The final wR_2 was 0.1544 (all data) and R_1 was 0.0634 (I > 2(I)).

Plot

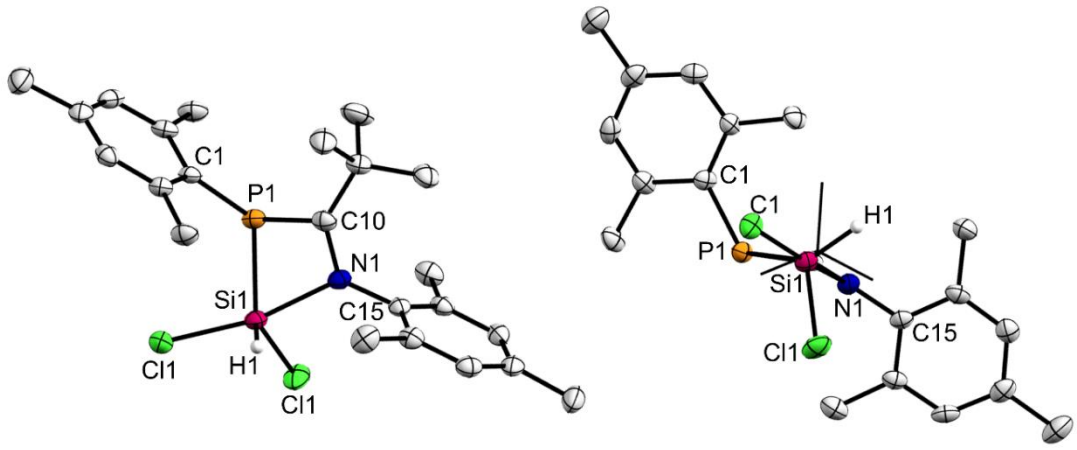

Hydrogen atoms (other than H1) omitted for clarity. Thermal ellipsoids set to 50%.

5.5.8 Silane 3.15

Experimental.

Single colourless plate-shaped crystals of **3.15** were recrystallised from THF by slow cooling. A suitable crystal (0.10×0.04×0.03) mm^3 was selected and mounted on a MITIGEN holder in Paratone oil on a Rigaku Oxford Diffraction SuperNova diffractometer. The crystal was kept at T = 120.0 K during data collection. Using **Olex2**,[22] the structure was solved with the **ShelXS**[23] structure solution program, using the Direct Methods solution method. The model was refined with version 2014/7 of **ShelXL**[24] using Least Squares minimisation.

Crystal Data.

$C_{29}H_{43}NSiPCl_3$, M_r = 571.05, monoclinic, $P2_1/n$ (No. 14), a = 9.76651(16) Å, b = 17.0908(3) Å, c = 18.3754(4) Å, β = 92.1764(16)°, $\alpha = \gamma$ = 90°, V = 3064.96(10) $Å^3$, T = 120.0 K, Z = 4, Z' = 1, $\mu(CuK_\alpha)$ = 3.704, 46223 reflections measured, 6359 unique (R_{int} = 0.1023) which were used in all calculations. The final wR_2 was 0.1745 (all data) and R_1 was 0.0628 (I > 2(I)).

Plot

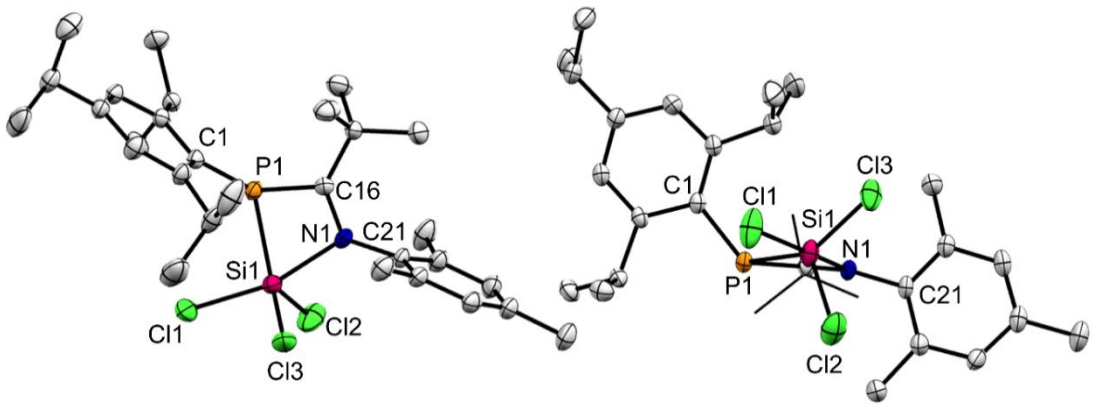

Hydrogen atoms (other than H1) omitted for clarity. Thermal ellipsoids set to 50%.

5.5.9 Silylene 3.21

Experimental.

Single red prism-shaped crystals of **3.21** were recrystallised from a mixture of benzene and toluene by slow evaporation. A suitable crystal (0.43×0.15×0.15) mm^3 was selected and mounted on a MITIGEN holder in Paratone oil on a Rigaku Oxford Diffraction SuperNova diffractometer. The crystal was kept at T = 120.0 K during data collection. Using **Olex2**[22] the structure was solved with the **ShelXT**[23] structure solution program, using the Direct Methods solution method. The model was refined with version of **ShelXL**[24] using Least Squares minimisation.

Crystal Data. $C_{46}H_{62}N_2P_2Si$, M_r = 733.00, monoclinic, P2/n (No. 13), a = 13.0222(4) Å, b = 8.1872(3) Å, c = 19.7562(7) Å, β = 93.500(3)°, $\alpha = \gamma$ = 90°, V = 2102.38(12) $Å^3$, T = 120.0 K, Z = 2, Z' = 0.5, μ(MoKα) = 0.165, 36326 reflections measured, 5577 unique (R_{int} = 0.0514) which were used in all calculations. The final wR_2 was 0.1145 (all data) and R_1 was 0.0473 (I > 2(I)).

Plot

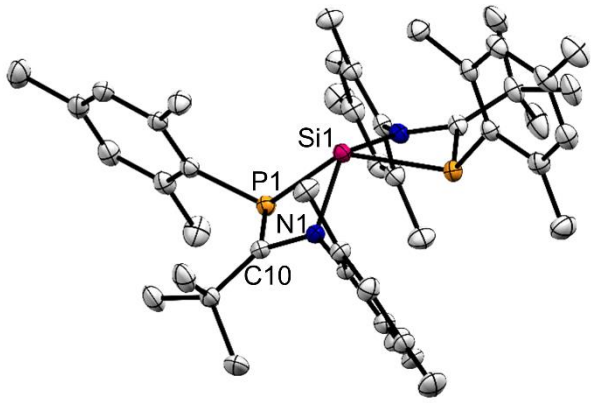

Hydrogen atoms (other than H1) omitted for clarity. Thermal ellipsoids set to 50%.

5.5.10 Gold Macrocycle 3.25

Experimental.

Single colourless prism-shaped crystals of **3.25** were recrystallised from d6-benzene by slow evaporation. A suitable crystal (0.17×0.12×0.10) mm^3 was selected and mounted on a MITIGEN holder in Paratone oil on a Rigaku Oxford Diffraction SuperNova diffractometer. The crystal was kept at T = 120.0 K during data collection. Using **Olex2**,[22] the structure was solved with the **ShelXS**[23] structure solution program, using the Patterson Method solution method. The model was refined with version 2014/7 of **ShelXL**[24] using Least Squares minimisation.

Crystal Data.

$C_{116}D_{24}Au_4H_{124}N_4P_4$, M_r = 2534.27, tetragonal, P-42$_1$c (No. 114), a = 17.9615(3) Å, b = 17.9615(3) Å, c = 16.6151(6) Å, $\alpha = \beta = \gamma = 90^{\circ}$, V = 5360.3(3) Å^3, T = 120.0 K, Z = 2, Z' = 0.25, μ(MoK$_\alpha$) = 5.565, 42160 reflections measured, 4915 unique (R_{int} = 0.0824) which were used in all calculations. The final wR_2 was 0.0787 (all data) and R_1 was 0.0380 (I > 2(I)).

Plot

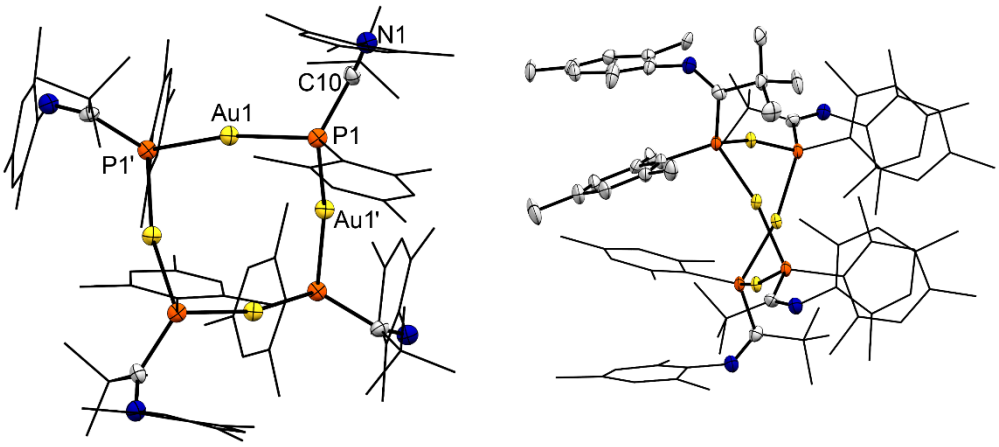

Hydrogen atoms omitted for clarity. Thermal ellipsoids set to 50%.

5.5.11 Dimethyl Aluminium Complex 3.28

Experimental.

Single light yellow prism-shaped crystals of **3.28** were recrystallised from hexane by cooling. A suitable crystal (0.36×0.19×0.15) mm^3 was selected and mounted on a MITIGEN holder in Paratone oil on a Rigaku Oxford Diffraction SuperNova diffractometer. The crystal was kept at T = 120.0 K during data collection. Using **Olex2**,[22] the structure was solved with the **ShelXS**[23] structure solution program, using the Direct Methods solution method. The model was refined with **ShelXL**,[24] using Least Squares minimisation.

Crystal Data. $C_{25}H_{37}AlNP$, M_r = 409.50, orthorhombic, Pbca (No. 61), a = 15.8059(5) Å, b = 15.6324(4) Å, c = 19.8891(6) Å, $\alpha = \beta = \gamma = 90^{\circ}$, V = 4914.3(3) $Å^3$, T = 120.0 K, Z = 8, Z' = 1, $\mu(MoK_\alpha)$ = 0.158, 44472 reflections measured, 6477 unique (R_{int} = 0.0687) which were used in all calculations. The final wR_2 was 0.1377 (all data) and R_1 was 0.0643 (I > 2(I)).

Plot

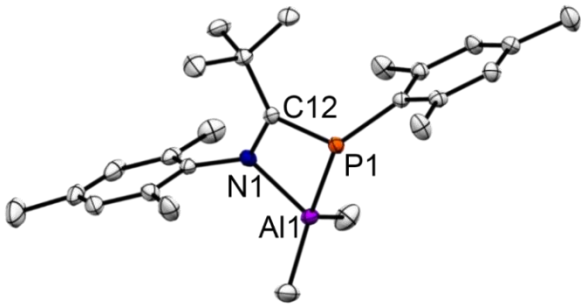

4x21

Hydrogen atoms omitted for clarity. Thermal ellipsoids set to 50%.

5.5.12 Dimethyl Aluminium Complex 3.29

Experimental.

Single colourless block-shaped crystals of **3.29** were recrystallised from hexane by slow evaporation. A suitable crystal (0.22×0.17×0.08) mm^3 was selected and mounted on a MITIGEN holder in Paratone oil on a Rigaku Oxford Diffraction SuperNova diffractometer. The crystal was kept at T = 120.0 K during data collection. Using **Olex2**,[22] the structure was solved with the **ShelXS**[23] structure solution program, using the direct solution method. The model was refined with version 2014/7 of **ShelXL**[24] using Least Squares minimisation.

Crystal Data. $C_{32}H_{49}AlN_3P$, M_r = 533.69, monoclinic, $P2_1/c$ (No. 14), a = 8.6530(3) Å, b = 19.9776(7) Å, c = 18.7067(6) Å, β = 97.860(3)°, $\alpha = \gamma$ = 90°, V = 3203.36(19) $Å^3$, T = 120.0 K, Z = 4, Z' = 1, μ(MoK_α) = 0.137, 53722 reflections measured, 6527 unique (R_{int} = 0.0714) which were used in all calculations. The final wR_2 was 0.1204 (all data) and R_1 was 0.0653 (I > 2(I)).

Plot

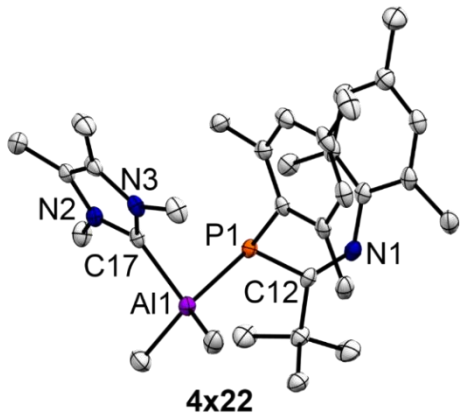

Hydrogen atoms omitted for clarity. Thermal ellipsoids set to 50% probability.

5.5.13 Aluminium Hydride 3.30

Experimental.

Single colourless plate-shaped crystals of **3.30** were recrystallised from toluene by cooling. A suitable crystal (0.10×0.09×0.04) mm^3 was selected and mounted on a MITIGEN holder in Paratone oil on a Rigaku Oxford Diffraction SuperNova diffractometer. The crystal was kept at T = 120.0 K during data collection. Using **Olex2**,[22] the structure was solved with the **ShelXS**[23] structure solution program, using the Direct Methods solution method. The model was refined with version 2014/7 of **ShelXL**[24] using Least Squares minimisation.

Crystal Data.

$C_{46}H_{63}AlN_2P_2$, M_r = 732.90, monoclinic, P2/n (No. 13), a = 13.1018(2) Å, b = 8.10353(13) Å, c = 20.1040(3) Å, β = 92.4888(14)°, α = γ = 90°, V = 2132.45(6) $Å^3$, T = 120.0 K, Z = 2, Z' = 0.5, $\mu(CuK_\alpha)$ = 1.360, 31922 reflections measured, 4430 unique (R_{int} = 0.0866) which were used in all calculations. The final wR_2 was 0.1449 (all data) and R_1 was 0.0526 (I > 2(I)).

Plot

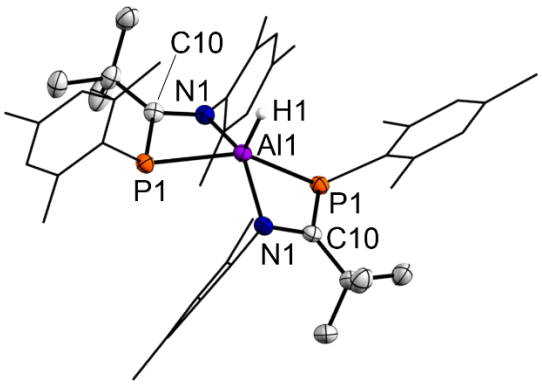

Hydrogen atoms (other than H1) omitted for clarity. Thermal ellipsoids set to 50% probability.

5.5.14 Full Crystallographic Data for All Crystal Structures

Compound	**2.23**	**2.28**	**2.35**
Formula	$C_{57}H_{129}Cl_3Si_{15}$	$C_{27}H_{54}N_2Si_4$	$C_{33}H_{53}ClSi_5$
$D_{calc.}$/ g cm^{-3}	1.088	1.062	1.135
μ/mm^{-1}	0.362	1.809	2.632
Formula Weight	1342.29	519.08	625.65
Colour	colourless	pale orange	colourless
Shape	block	block	block
Size/mm^3	0.52×0.29×0.23	0.20×0.07×0.04	0.17×0.13×0.08
T/K	120.0	120.0	120.0
Crystal System	orthorhombic	monoclinic	monoclinic
Space Group	$Cmc2_1$	$P2_1/c$	$P2_1/c$
a/Å	44.9370(12)	11.32508(20)	16.7147(2)
b/Å	12.5333(2)	16.0662(3)	11.49900(10)
c/Å	14.5469(3)	18.3367(3)	19.04910(10)
α/°	90	90	90
β/°	90	103.2283(16)	90.0000(10)
γ/°	90	90	90
V/Å^3	8193.0(3)	3247.86(10)	3661.28(6)
Z	4	4	4
Z'	0.5	1	1
Wavelength/Å	0.71073	1.54184	1.54184
Radiation type	MoK_α	CuK_α	CuK_α
Θ_{min}/°	3.121	3.701	4.491
Θ_{max}/°	29.686	76.052	76.070
Measured Refl.	73400	26957	57789
Independent Refl.	10189	6729	7613
Reflections Used	9272	5415	7338
R_{int}	0.0811	0.0889	0.0735
Parameters	540	319	508
Restraints	263	0	4
Largest Peak	0.606	0.502	0.458
Deepest Hole	-0.693	-0.581	-0.553
GooF	1.120	1.038	1.232
wR_2 (all data)	0.1746	0.1551	0.2024
wR_2	0.1706	0.1430	0.2013
R_1 (all data)	0.0887	0.0710	0.0825
R_1	0.0816	0.0558	0.0807

Compound	**2.37**	**2.50**	**3.7**
Formula	$C_{41}H_{64}N_2Si_4$	$C_{39}H_{56}N_2Si_4$	$C_{69}H_{112}N_2P_2$
$D_{calc.}$/ g cm^{-3}	1.089	1.141	1.055
μ/mm^{-1}	0.168	1.629	0.886
Formula Weight	697.30	665.21	1031.54
Colour	dark orange	dark red	colourless
Shape	block	block	block
Size/mm^3	0.42×0.36×0.24	0.16×0.09×0.07	0.29×0.08×0.07
T/K	120.0	120.0	120.0
Crystal System	monoclinic	monoclinic	monoclinic
Space Group	$P2_1/n$	$P2_1/c$	$P2_1/c$
a/Å	12.3461(4)	15.89104(14)	10.26764(11)
b/Å	18.7939(8)	16.29426(12)	9.95168(15)
c/Å	18.9399(6)	15.02549(12)	31.7681(4)
α/°	90	90	90
β/°	104.669(3)	95.5918(8)	90.6629(9)
γ/°	90	90	90
V/Å^3	4251.4(3)	3872.08(5)	3245.86(7)
Z	4	4	2
Z'	1	1	0.5
Wavelength/Å	0.71073	1.54178	1.54184
Radiation type	MoK_α	CuK_α	CuK_α
Θ_{min}/°	2.808	3.895	4.306
Θ_{max}/°	29.725	76.331	76.225
Measured Refl.	52088	41474	27126
Independent Refl.	21719	8017	6732
Reflections Used	12023	6815	6152
R_{int}	0.0642	0.0750	0.0632
Parameters	447	441	356
Restraints	0	35	0
Largest Peak	0.465	0.302	0.657
Deepest Hole	-0.594	-0.399	-0.365
GooF	0.919	1.056	1.056
wR_2 (all data)	0.1466	0.1363	0.1594
wR_2	0.1360	0.1320	0.1546
R_1 (all data)	0.1169	0.0564	0.0626
R_1	0.0608	0.0489	0.0580

Compound	**3.7**	**3.10**	**3.15**	**3.21**
Formula	$C_{69}H_{112}N_2P_2$	$C_{23}H_{32}Cl_2NPSi$	$C_{29}H_{43}NSiPCl_3$	$C_{46}H_{62}N_2P_2Si$
$D_{calc.}$/ g cm^{-3}	1.055	1.261	1.238	1.158
μ/mm^{-1}	0.886	0.399	3.704	0.165
Formula Weight	1031.54	452.45	571.05	733.00
Colour	colourless	colourless	colourless	red
Shape	block	block	plate	prism
Size/mm^3	0.29×0.08×0.07	0.26×0.18×0.07	0.10×0.04×0.03	0.43×0.15×0.15
T/K	120.0	120.0	120.0	120.0
Crystal System	monoclinic	monoclinic	monoclinic	monoclinic
Space Group	$P2_1/c$	$P2_1/c$	$P2_1/n$	P2/n
a/Å	10.26764(11)	8.8740(4)	9.76651(16)	13.0222(4)
b/Å	9.95168(15)	13.4389(6)	17.0908(3)	8.1872(3)
c/Å	31.7681(4)	20.2034(9)	18.3754(4)	19.7562(7)
α/°	90	90	90	90
β/°	90.6629(9)	98.304(4)	92.1764(16)	93.500(3)
γ/°	90	90	90	90
V/Å^3	3245.86(7)	2384.12(18)	3064.96(10)	2102.38(12)
Z	2	4	4	2
Z'	0.5	1	1	0.5
Wavelength/Å	1.54184	0.71073	1.54178	0.71073
Radiation type	CuK_α	MoK_α	CuK_α	MoK_α
Θ_{min}/°	4.306	2.771	3.533	3.085
Θ_{max}/°	76.225	29.688	76.297	29.688
Measured Refl.	27126	21709	46223	36326
Independent Refl.	6732	6022	6359	5577
Reflections Used	6152	4844	4894	4681
R_{int}	0.0632	0.0550	0.1023	0.0514
Parameters	356	266	328	240
Restraints	0	0	0	0
Largest Peak	0.657	1.307	0.679	0.366
Deepest Hole	-0.365	-0.476	-0.524	-0.342
GooF	1.056	1.063	1.056	1.056
wR_2 (all data)	0.1594	0.1544	0.1745	0.1145
wR_2	0.1546	0.1441	0.1606	0.1077
R_1 (all data)	0.0626	0.0809	0.0830	0.0596
R_1	0.0580	0.0634	0.0628	0.0473

Compound	**3.21**	**3.25**	**3.28**
Formula	$C_{46}H_{62}N_2P_2Si$	$C_{116}D_{24}Au_4H_{124}N_4P_4$	$C_{25}H_{37}AlNP$
$D_{calc.}$/ g cm^{-3}	1.158	1.570	1.107
μ/mm^{-1}	0.165	5.565	0.158
Formula Weight	733.00	2534.27	409.50
Colour	red	colourless	light yellow
Shape	prism	prism	prism
Size/mm^3	0.43×0.15×0.15	0.17×0.12×0.10	0..36×0.19×0.15
T/K	120.0	120.0	120
Crystal System	monoclinic	tetragonal	orthorhombic
Space Group	P2/n	P-42$_1$c	Pbca
a/Å	13.0222(4)	17.9615(3)	15.8059(5)
b/Å	8.1872(3)	17.9615(3)	15.6324(4)
c/Å	19.7562(7)	16.6151(6)	19.8891(6)
α/°	90	90	90
β/°	93.500(3)	90	90
γ/°	90	90	90
V/Å^3	2102.38(12)	5360.3(3)	4914.3(3)
Z	2	2	8
Z'	0.5	0.25	1
Wavelength/Å	0.71073	0.71073	0.71073
Radiation type	MoK$_\alpha$	MoK$_\alpha$	MoK$_\alpha$
Θ_{min}/°	3.085	2.930	2.800
Θ_{max}/°	29.688	25.346	29.782
Measured Refl.	36326	42160	44472
Independent Refl.	5577	4915	6477
Reflections Used	4681	4323	5091
R_{int}	0.0514	0.0824	0.0687
Parameters	240	299	264
Restraints	0	0	0
Largest Peak	0.366	1.042	0.374
Deepest Hole	-0.342	-1.507	-0.318
GooF	1.056	1.052	1.105
wR_2 (all data)	0.1145	0.0787	0.1377
wR_2	0.1077	0.0754	0.1271
R_1 (all data)	0.0596	0.0477	0.0904
R_1	0.0473	0.0380	0.0643

Compound	**3.29**	**3.30**
Formula	$C_{32}H_{49}AlN_3P$	$C_{46}H_{63}AlN_2P_2$
$D_{calc.}$/ g cm^{-3}	1.107	1.141
μ/mm^{-1}	0.137	1.360
Formula Weight	533.69	732.90
Colour	colourless	colourless
Shape	block	plate
Size/mm^3	0.22×0.17×0.08	0.10×0.09×0.04
T/K	120.0	120.0
Crystal System	monoclinic	monoclinic
Space Group	$P2_1/c$	P2/n
a/Å	8.6530(3)	13.1018(2)
b/Å	19.9776(7)	8.10353(13)
c/Å	18.7067(6)	20.1040(3)
α/°	90	90
β/°	97.860(3)	92.4888(14)
γ/°	90	90
V/Å^3	3203.36(19)	2132.45(6)
Z	4	2
Z'	1	0.5
Wavelength/Å	0.71073	1.54184
Radiation type	MoK_α	CuK_α
Θ_{min}/°	2.934	3.950
Θ_{max}/°	26.371	76.049
Measured Refl.	53722	31922
Independent Refl.	6527	4430
Reflections Used	5765	3862
R_{int}	0.0714	0.0866
Parameters	349	242
Restraints	0	0
Largest Peak	0.401	0.449
Deepest Hole	-0.239	-0.386
GooF	1.195	1.048
wR_2 (all data)	0.1204	0.1449
wR_2	0.1159	0.1377
R_1 (all data)	0.0780	0.0603
R_1	0.0653	0.0526

5.6 Computational Details for Chapter 2

All computations in this section were carried out by Julia I. Schweizer, Maximillian Menche and Max C. Holthausen at the Institut für Anorganische Chemie, Goethe-Universität, Max-von-Laue-Straße 7, 60438 Frankfurt/Main, Germany.

Geometry optimizations and harmonic frequency calculations were performed using the Gaussian16 program package[25] employing the M06-L density functional[26] and the 'fine' grid option in combination with the 6-31+G(d,p) basis set.[27] For improved computational efficiency the density fitting approximation was used for these calculations (the 'auto' keyword was used for the automatic generation of a fitting basis set). Stationary points were characterized as minima or first order saddle points by eigenvalue analysis of the computed Hessians. Connectivities between minima and transition states implied in Figures and Schemes were validated either by intrinsic-reaction-coordinate (IRC) following calculations[28] or by displacing the transition state geometries along both directions of the transition mode, followed by unconstrained optimizations to the respective minima. Single-point calculations were conducted on the optimized geometries using the M06-2X functional[29] in combination with the 6-311++G(2d,2p) basis set[30], and the 'ultrafine' grid option.[31] The SMD polarizable continuum model[32] was employed to account for solvent effects (THF), SMD-M06-2X/6-311++G(2d,2p)//RI-M06-L/6-31+G(d,p). The wave functions used for bonding analysis were obtained at the M06-2X/6-311++G(2d,2p)//RI-M06-L/6-31+G(d,p) level of theory. Natural bond orbital (NBO) calculations were performed using the NBO 6.0.18 program[33] interfaced with Gaussian09.[34] The AIMAll[35] and multiwfn[36] programs were used for QTAIM analyses.[37] Unscaled zero-point vibrational, thermal and entropic corrections were obtained from computed Hessian matrices computed at the RI-M06-L/6-31+G(d,p) level using standard procedures as implemented in Gaussian16 to obtain free energy values at standard conditions (T = 298.15 K, p = 1 atm). Pictures of molecular structures were generated with the Cylview[38] and ChemCraft[39] programs.

5.6.1 Structural metrics of the computed and the X-RAY structure of 2.28

Table 5-1 *– Selected metrics of the computed and the X-RAY structure of* ***2.28****. Hydrogen atoms and NHC methyl/iso-propyl groups are omitted in the computed structure.*

	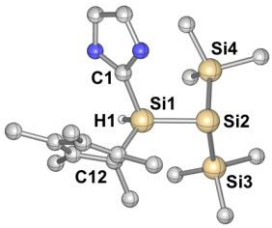 computed structure	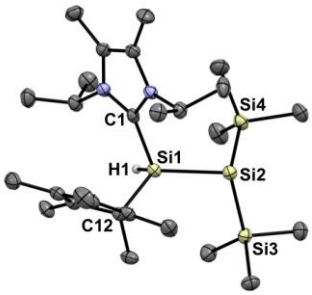 exp. X-RAY
Si1–Si2	2.31 Å	2.36 Å
Si1–H1	1.50 Å	1.48 Å
Si1–C1	1.95 Å	1.95 Å
Si1–C12	1.97 Å	1.95 Å
Si2–Si3	2.36 Å	2.36 Å
Si2–Si4	2.37 Å	2.36 Å
C1–Si1–Si2	111°	110°
C1–Si1–Si2–Si3	–160°	–170°
Σ∢(Si2)	286°	297°

5.6.2 Structural metrics of the computed and the X-RAY structure of 2.37

Table 5-2 *– Selected metrics of the computed and the X-RAY structure of* ***2.37****. Hydrogen atoms and NHC methyl/iso-propyl groups are omitted in the computed structure.*

	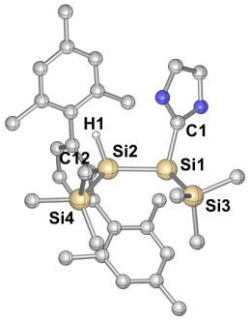 computed structure	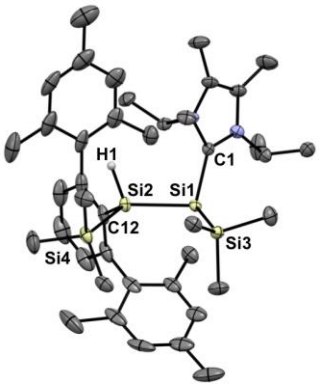 exp. X-RAY
Si1–Si2	2.36 Å	2.39 Å
Si1–Si3	2.33 Å	2.34 Å
Si1–C1	1.96 Å	1.98 Å
Si2–Si4	2.35 Å	2.36 Å
Si2–H1	1.49 Å	1.39 Å
Si2–C12	1.92 Å	1.93 Å
C1–Si1–Si2	102°	102°
C1–Si1–Si2–Si4	–116°	–117°
Σ∢(Si1)	319°	317°

5.6.3 Structural metrics of the computed and the X-RAY structure of 2.50

Table 5-3 *– Selected metrics of the computed and the X-RAY structure of* ***2.50****. Hydrogen atoms are omitted in the computed structure.*

	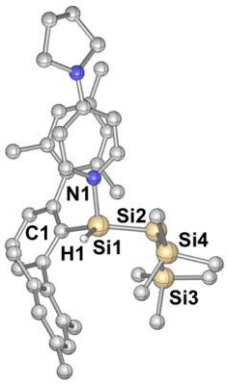 computed structure	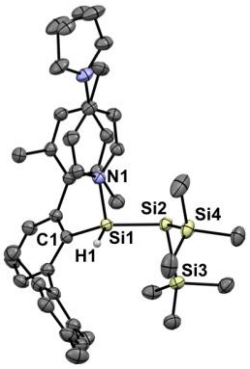 exp. X-RAY
Si1–Si2	2.29 Å	2.32 Å
Si1–H1	1.49 Å	1.44 Å
Si1–N1	1.94 Å	1.88 Å
Si1–C1	1.91 Å	1.91 Å
Si2–Si3	2.34 Å	2.35 Å
Si2–Si4	2.35 Å	2.36 Å
N1–Si1–Si2	103°	104°
N1–Si1–Si2–Si4	94°	79°
Σ∢(Si2)	303°	298°

5.6.4 QTAIM analysis of 2.28

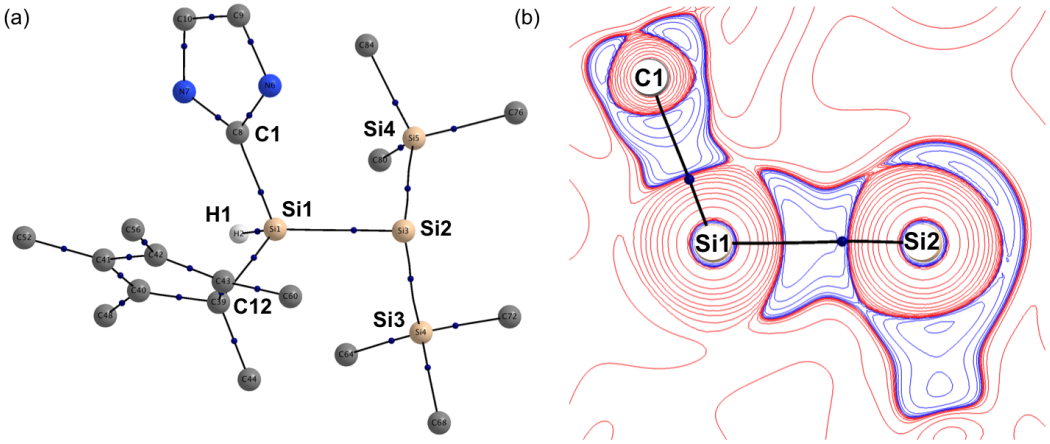

Figure 5-4 *– QTAIM analysis of* ***2.28****. (a) Molecular graph; (b) 2D plot of* $\nabla^2\rho(r)$*; charge concentration (blue) and depletion (red), bond paths (black lines), and bcps (blue dots).*

Table 5-4 *– Selected properties of the electron density distribution in* ***2.28****; atom numbering as displayed in [crossref]. The electron density* ρ_{bcp} *is given in* $e\text{Å}^{-3}$*, the Laplacian of the electron density* $\nabla^2\rho_{bcp}$ *in* $e\text{Å}^{-5}$*, the total energy density* H_{bcp} *in* $E_h\text{Å}^{-3}$*.* $\varepsilon_{bcp} = \lambda_1/\lambda_2 - 1$ *is the bond ellipticity derived from the two negative eigenvalues of the Hessian matrix of the electron density at the bcp, with* $\lambda_1 \geq \lambda_2$*. The delocalization index* $\delta_{A,B}$ *represents the number of electrons shared between two atoms A and B.*

	ρ_{bcp}	$\nabla^2\rho_{bcp}$	H_{bcp}	ε_{bcp}	$\delta_{A,B}$
Si1–Si2	0.54	–1.69	–0.05	0.11	0.85
Si1–H1	0.79	3.01	–0.08	0.04	0.55
Si1–C1	0.64	3.89	–0.05	0.05	0.46
Si1–C12	0.68	1.12	–0.07	0.07	0.51
Si2–Si3	0.55	–2.43	–0.04	0.05	0.80
Si2–Si4	0.54	–2.29	–0.04	0.06	0.81

5.6.5 NBO analysis of 2.28

Table 5-5 – *Selected results of the NBO analysis of* ***2.28****; wave functions computed at the M06-2X/6-311++G(2d,2p)//RI-M06-L/6-31+G(d,p) level of DFT.*

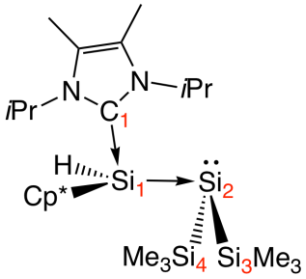

Bond	NBO analysis (NLMOs)[a]		
	pol. [%]	hybr.	WBI
C1–Si1	76% (C1)	$sp^{1.35}$(C1)	0.66
	22% (Si1)	$sp^{3.08}$(Si1)	
Si1–Si2	55% (Si1)	$sp^{1.07}$(Si1)	1.04
	41% (Si2)	$sp^{4.47}$(Si2)	
Si2–Si3	47% (Si2)	$sp^{4.69}$(Si2)	0.95
	48% (Si3)	$sp^{1.53}$(Si3)	
Si2–Si4	45% (Si2)	$sp^{5.55}$(Si2)	0.96
	50% (Si4)	$sp^{1.43}$(Si4)	
LP(Si2)	91% (Si2)	$sp^{0.79}$(Si2)	
	2% (Si1)	$sp^{22.8}$(Si1)	

[a] pol. = polarization, hybr. = hybridization, WBI = Wiberg bond index.

Table 5-6 – *Fragment charges obtained from NPA analysis of* ***2.28****; wave functions computed at the M06-2X/6-311++G(2d,2p)//RI-M06-L/6-31+G(d,p) level of DFT.*

Fragment	NPA charge/e
NHC	0.38
NHC→Si(H)Cp*	0.66
$Si(SiMe_3)_2$	–0.66

5.6.6 Evaluation of Haaland's Definition of Dative Bonds

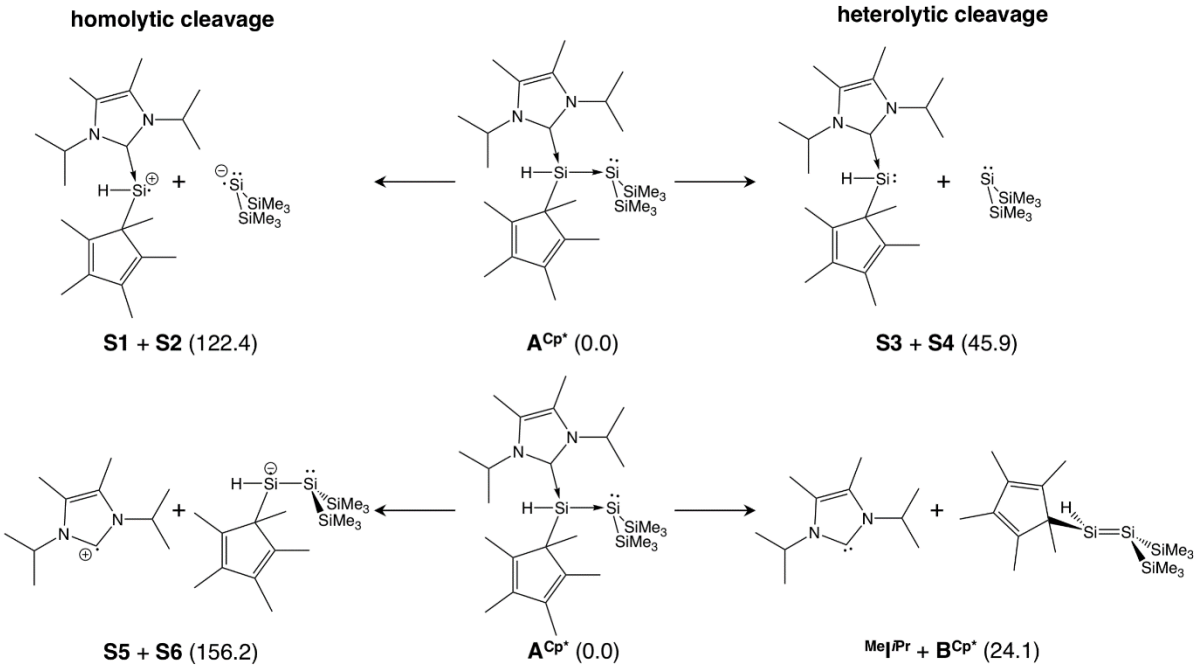

Figure 5-5 *– Computed homolysis and heterolysis of bonds in* $\mathbf{A}^{\mathbf{Cp^*}}$ *(cf.* ***2.28****);* ΔG^{298} *in kcal mol*$^{-1}$ *(M06-2X/6-311++G(2d,2p)//RI-M06-L/6-31+G(d,p)).*

5.6.7 QTAIM analysis of 2.36

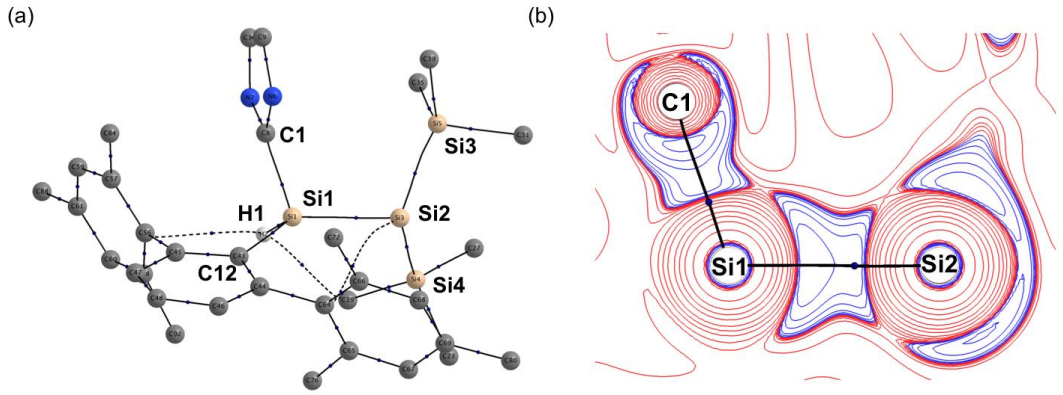

Figure 5-6 – *QTAIM analysis of **2.36**. (a) Molecular graph; (b) 2D plot of $\nabla^2\rho(r)$; charge concentration (blue) and depletion (red), bond paths (black lines), and bcps (blue dots).*

Table 5-7 – *Selected properties of the electron density distribution in **2.36**; atom numbering as displayed in Figure S7. The electron density ρ_{bcp} is given in $e\text{Å}^{-3}$, the Laplacian of the electron density $\nabla^2\rho_{bcp}$ in $e\text{Å}^{-5}$, the total energy density H_{bcp} in $E_h\text{Å}^{-3}$. $\varepsilon_{bcp} = \lambda_1/\lambda_2 - 1$ is the bond ellipticity derived from the two negative eigenvalues of the Hessian matrix of the electron density at the bcp, with $\lambda_1 \geq \lambda_2$. The delocalization index $\delta_{A,B}$ represents the number of electrons shared between two atoms A and B.*

	ρ_{bcp}	$\nabla^2\rho_{bcp}$	H_{bcp}	ε_{bcp}	$\delta_{A,B}$
Si1–Si2	0.53	–1.85	–0.05	0.15	0.86
Si1–H1	0.80	3.27	–0.08	0.04	0.55
Si1–C1	0.66	4.58	–0.06	0.10	0.47
Si1–C12	0.72	2.66	–0.07	0.03	0.52
Si2–Si3	0.54	–2.32	–0.04	0.10	0.82
Si2–Si4	0.55	–2.39	–0.04	0.06	0.81

5.6.8 NBO analysis of 2.36

Table 5-8 *– Selected results of the NBO analysis of* ***2.36****; wave functions computed at the M06-2X/6-311++G(2d,2p)//RI-M06-L/6-31+G(d,p) level of DFT.*

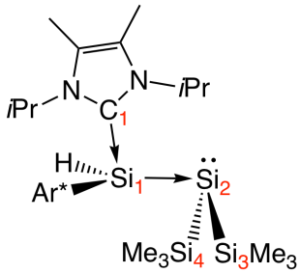

Bond	NBO analysis (NLMOs)[a]		
	pol. [%]	hybr.	WBI
C1–Si1	75% (C1)	$sp^{1.32}$(C1)	0.68
	23% (Si1)	$sp^{3.42}$(Si1)	
Si1–Si2	55% (Si1)	$sp^{1.20}$(Si1)	1.04
	41% (Si2)	$sp^{4.47}$(Si2)	
Si2–Si3	47% (Si2)	$sp^{4.67}$(Si2)	0.97
	49% (Si3)	$sp^{1.51}$(Si3)	
Si2–Si4	45% (Si2)	$sp^{5.37}$(Si2)	0.98
	50% (Si4)	$sp^{1.43}$(Si4)	
LP(Si2)	90% (Si2)	$sp^{0.79}$(Si2)	
	2% (Si1)	p (Si1)	

[a] pol. = polarization, hybr. = hybridization, WBI = Wiberg bond index.

Table 5-9 – *Fragment charges obtained from NPA analysis of* ***2.36****; wave functions computed at the M06-2X/6-311++G(2d,2p)//RI-M06-L/6-31+G(d,p) level of DFT.*

Fragment	NPA charge/e
NHC	0.38
NHC→Si(H)Cp*	0.65
$Si(SiMe_3)_2$	–0.65

5.6.9 QTAIM analysis of 2.50

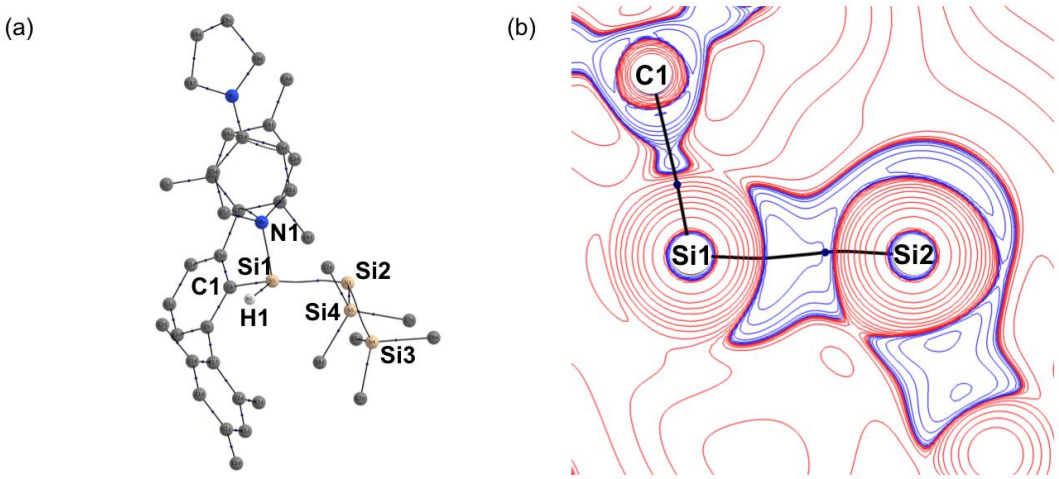

Figure 5-7 *– QTAIM analysis of* ***2.50****. (a) Molecular graph; (b) 2D plot of* $\nabla^2\rho(r)$*; charge concentration (blue) and depletion (red), bond paths (black lines), and bcps (blue dots).*

Table 5-10 *– Selected properties of the electron density distribution in* ***2.50****; atom numbering as displayed in Figure S8. The electron density* ρ_{bcp} *is given in* $e\text{Å}^{-3}$*, the Laplacian of the electron density* $\nabla^2\rho_{bcp}$ *in* $e\text{Å}^{-5}$*, the total energy density* H_{bcp} *in* $E_h\text{Å}^{-3}$*.* $\varepsilon_{bcp} = \lambda_1/\lambda_2 - 1$ *is the bond ellipticity derived from the two negative eigenvalues of the Hessian matrix of the electron density at the bcp, with* $\lambda_1 \geq \lambda_2$*. The delocalization index* $\delta_{A,B}$ *represents the number of electrons shared between two atoms A and B.*

	ρ_{bcp}	$\nabla^2\rho_{bcp}$	H_{bcp}	ε_{bcp}	$\delta_{A,B}$
Si1–Si2	0.55	–1.67	–0.05	0.21	0.93
Si1–H1	0.81	3.02	–0.08	0.05	0.54
Si1–N1	0.55	5.56	–0.03	0.06	0.37
Si1–C1	0.76	2.89	–0.07	0.10	0.55
Si2–Si3	0.58	–2.69	–0.04	0.07	0.82
Si2–Si4	0.57	–2.52	–0.04	0.06	0.81

5.6.10 NBO analysis of 6

Table 5-11 *– Selected results of the NBO analysis of* ***2.50****; wave functions computed at the M06-2X/6-311++G(2d,2p)//RI-M06-L/6-31+G(d,p) level of DFT.*

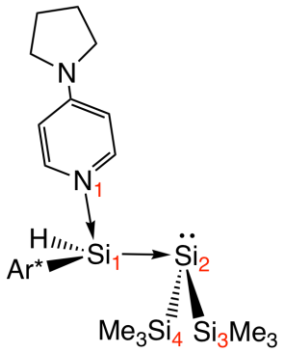

Bond	NBO analysis (NLMOs)[a]		
	pol. [%]	hybr.	WBI
N1–Si1	86% (N1)	$sp^{2.38}$(N1)	0.38
	12% (Si1)	$sp^{3.69}$(Si1)	
Si1–Si2	54% (Si1)	$sp^{0.98}$(Si1)	1.15
	43% (Si2)	$sp^{4.72}$(Si2)	
Si2–Si3	48% (Si2)	$sp^{4.41}$(Si2)	0.96
	47% (Si3)	$sp^{1.59}$(Si3)	
Si2–Si4	49% (Si2)	$sp^{3.76}$(Si2)	0.97
	47% (Si4)	$sp^{1.62}$(Si4)	
LP(Si2)	87% (Si2)	$sp^{0.97}$(Si2)	
	5% (Si1)	p (Si1)	

[a] pol. = polarization, hybr. = hybridization, WBI = Wiberg bond index.

Table 5-12 *– Fragment charges obtained from NPA analysis of* ***2.50****; wave functions computed at the M06-2X/6-311++G(2d,2p)//RI-M06-L/6-31+G(d,p) level of DFT.*

Fragment	NPA charge/e
4-PPy	0.20
4-PPY→Si(H)Ar*	0.63

$Si(SiMe_3)_2$	–0.63

5.6.11 Additional Information on the Reaction Mechanism

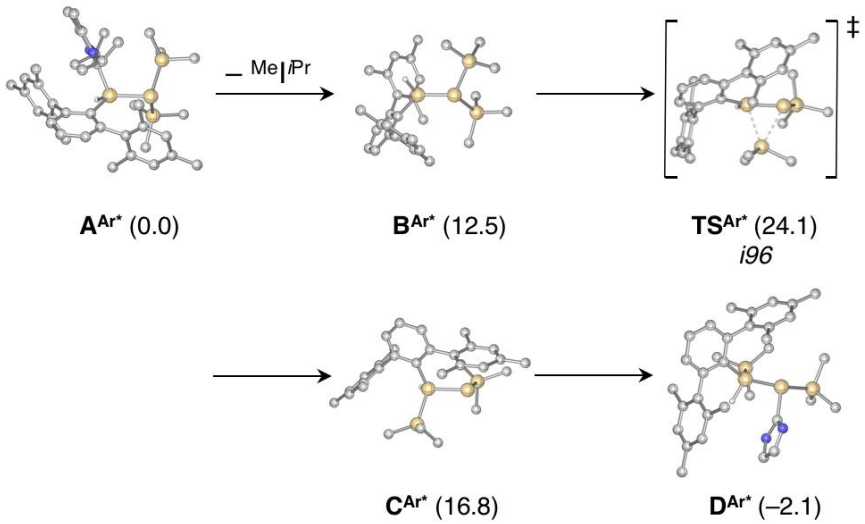

Scheme 5-1 *– Computed reaction path for the disilene/silylsilylene isomerization of* $\boldsymbol{A^{Ar*}}$ *to* $\boldsymbol{D^{Ar*}}$*;* ΔG^{298} *in kcal* mol^{-1} *(SMD-M06-2X/6-311++G(2d,2p)//RI-M06-L/6-31+G(d,p)).*

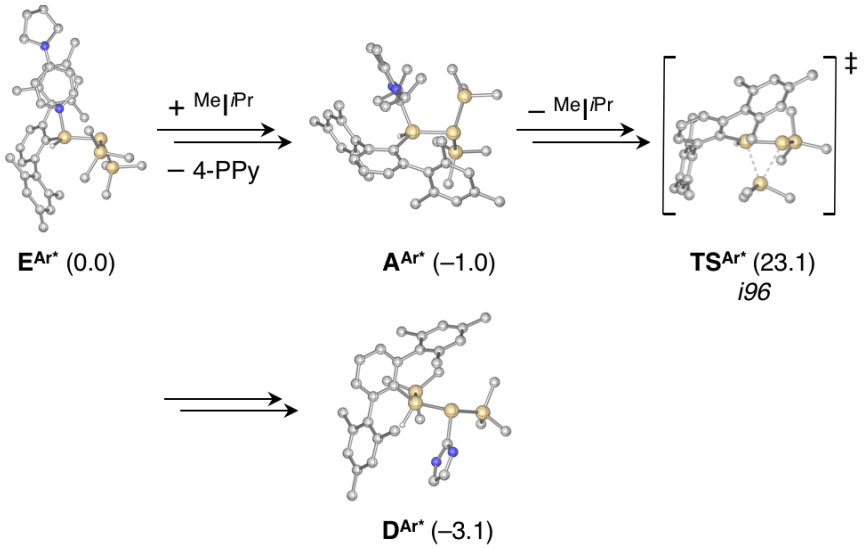

Scheme 5-2 *– Computed reaction path for the disilene/silylsilylene isomerization of* E^{Ar*} *to* D^{Ar*}*;* ΔG^{298} *in kcal* mol^{-1} *(SMD-M06-2X/6-311++G(2d,2p)//RI-M06-L/6-31+G(d,p)).*

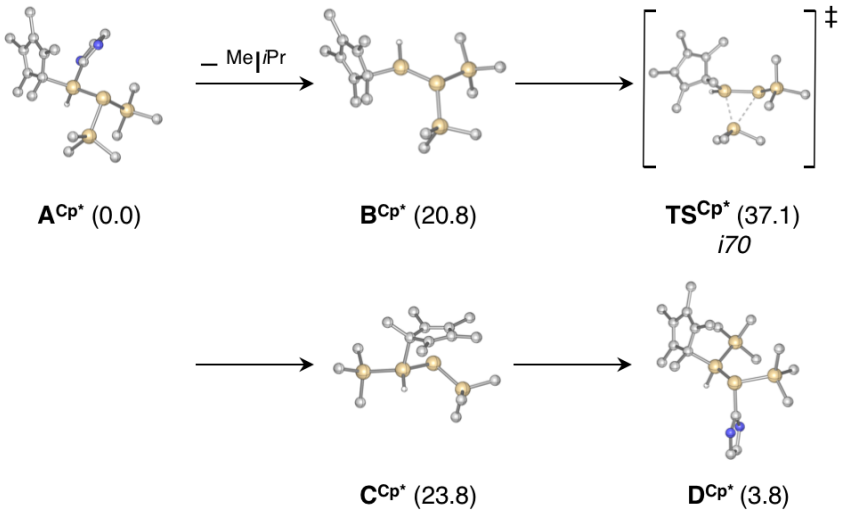

Scheme 5-3 *– Computed reaction path for the disilene/silylsilylene isomerization of* A^{Cp*} *to* D^{Cp*}*;* ΔG^{298} *in kcal* mol^{-1} *(SMD-M06-2X/6-311++G(2d,2p)//RI-M06-L/6-31+G(d,p)).*

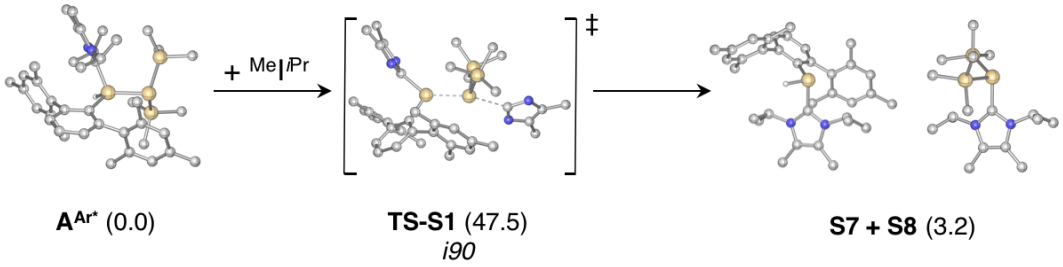

Scheme 5-4 *– Computed reaction path for the NHC-assisted Si–Si bond cleavage in* ***A^Ar**; ΔG^298 in kcal mol^–1 (SMD-M06-2X/6-311++G(2d,2p)//RI-M06-L/6-31+G(d,p)).*

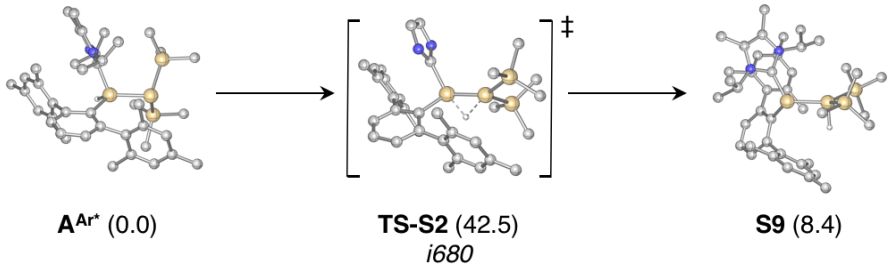

Scheme 5-5 *– Computed reaction path for the hydride migration in* ***A^Ar**; ΔG^298 in kcal mol^–1 (SMD-M06-2X/6-311++G(2d,2p)//RI-M06-L/6-31+G(d,p)).*

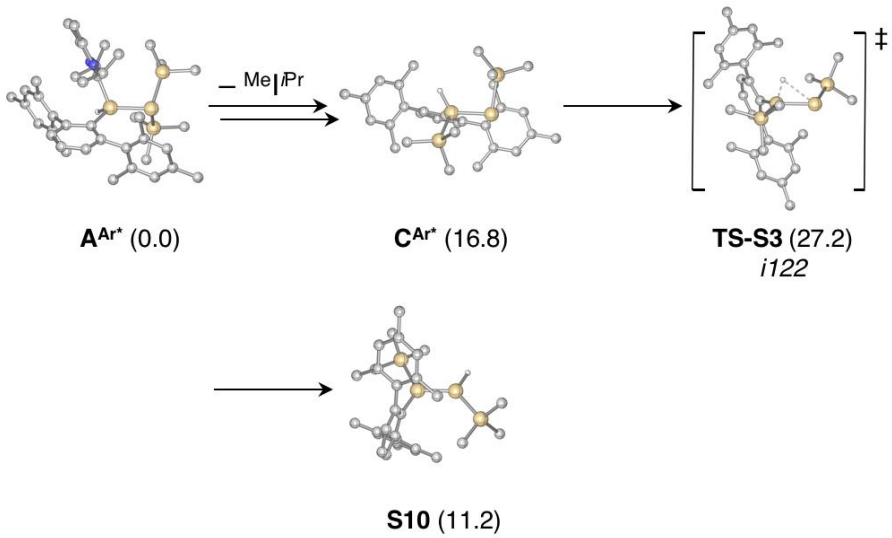

Scheme 5-6 *– Computed reaction path for the hydride migration in* ***C^Ar**; ΔG^298 in kcal mol^–1 (SMD-M06-2X/6-311++G(2d,2p)//RI-M06-L/6-31+G(d,p)).*

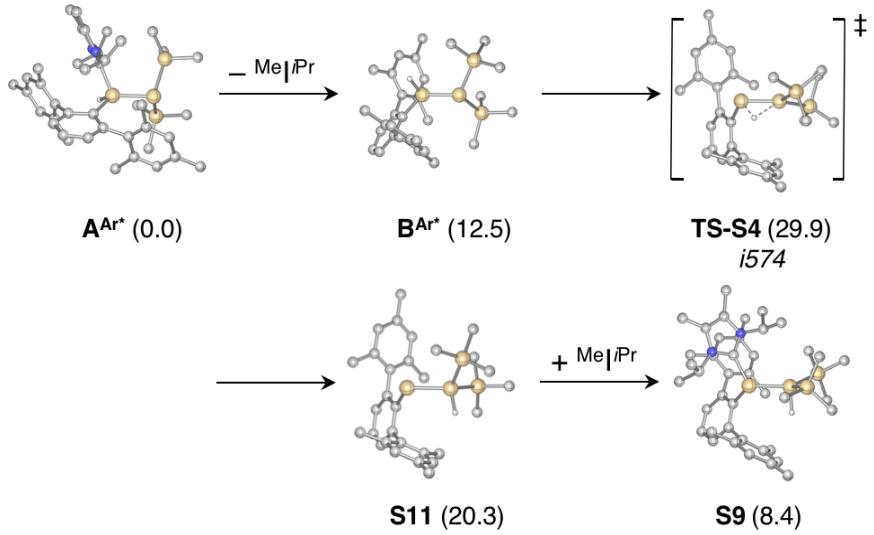

Scheme 5-7 *– Computed reaction path for the hydride migration in* $\mathbf{B^{Ar*}}$*;* ΔG^{298} *in kcal mol*$^{-1}$ *(SMD-M06-2X/6-311++G(2d,2p)//RI-M06-L/6-31+G(d,p)).*

5.7 References

[1] G. R. Fulmer, A. J. M. Miller, N. H. Sherden, H. E. Gottlieb, A. Nudelman, B. M. Stoltz, J. E. Bercaw, K. I. Goldberg, *Organometallics* **2010**, *29*, 2176–2179.

[2] P. Dupau, L. Bonomo, *1,4-Hydrogenation of Dienes with Ru Complexes*, **2008**, WO2008/120175 (A1).

[3] A. H. Cowley, N. C. Norman, M. Pakulski, G. Becker, M. Layh, E. Kirchner, M. Schmidt, in *Inorg. Synth.* (Ed.: A.P. Ginsberg), John Wiley & Sons, Inc., **1990**, pp. 235–240.

[4] N. Kuhn, T. Kratz, *Synthesis* **1993**, *1993*, 561–562.

[5] X. Bantreil, S. P. Nolan, *Nat. Protoc.* **2011**, *6*, 69–77.

[6] T. van Dijk, S. Burck, M. K. Rong, A. J. Rosenthal, M. Nieger, J. C. Slootweg, K. Lammertsma, *Angew. Chem. Int. Ed.* **2014**, *53*, 9068–9071.

[7] P. Jutzi, D. Kanne, M. Hursthouse, A. J. Howes, *Chem. Ber.* **1988**, *121*, 1299–1305.

[8] C. Gerdes, W. Saak, D. Haase, T. Müller, *J. Am. Chem. Soc.* **2013**, *135*, 10353–10361.

[9] C. Marschner, *Eur. J. Inorg. Chem.* **1998**, *1998*, 221–226.

[10] Y. Takeda, T. Nishida, S. Minakata, *Chem. – Eur. J.* **2014**, *20*, 10266–10270.

[11] J. Möbus, Q. Bonnin, K. Ueda, R. Fröhlich, K. Itami, G. Kehr, G. Erker, *Angew. Chem. Int. Ed.* **2012**, *51*, 1954–1957.

[12] Y. van den Winkel, H. M. M. Bastiaans, F. Bickelhaupt, *J. Organomet. Chem.* **1991**, *405*, 183–194.

[13] H. Stachowiak, J. Kaźmierczak, K. Kuciński, G. Hreczycho, *Green Chem.* **2018**, *20*, 1738–1742.

[14] S. Khoo, J. Cao, F. Ng, C.-W. So, *Inorg. Chem.* **2018**, *57*, 12452–12455.

[15] P. K. Verma, S. A. S., K. Geetharani, *Org. Lett.* **2018**, *20*, 7840–7845.

[16] S. Chen, D. Yan, M. Xue, Y. Hong, Y. Yao, Q. Shen, *Org. Lett.* **2017**, *19*, 3382–3385.

[17] V. L. Weidner, C. J. Barger, M. Delferro, T. L. Lohr, T. J. Marks, *ACS Catal.* **2017**, *7*, 1244–1247.

[18] M. Ma, J. Li, Q. Xiao, M. Luo, *Asymmetric Diimine Monovalent Magnesium Compound, and Preparation Method and Application Thereof in Epoxy Silane Hydroboration*, **2018**, CN108569984 (A).

[19] A. Bismuto, S. P. Thomas, M. J. Cowley, *Angew. Chem. Int. Ed.* **2016**, *55*, 15356–15359.

[20] D. P. Ojha, K. R. Prabhu, *Org. Lett.* **2016**, *18*, 432–435.

[21] E. Yamamoto, R. Shishido, T. Seki, H. Ito, *Organometallics* **2017**, *36*, 3019–3022.

[22] O. V. Dolomanov, L. J. Bourhis, R. J. Gildea, J. A. K. Howard, H. Puschmann, *J. Appl. Crystallogr.* **2009**, *42*, 339–341.

[23] G. M. Sheldrick, *Acta Crystallogr. Sect. Found. Adv.* **2015**, *71*, 3–8.

[24] G. M. Sheldrick, *Acta Crystallogr. A* **2008**, *64*, 112–122.

[25] M. J. Frisch, G. W. Trucks, H. B. Schlegel, G. E. Scuseria, M. A. Robb, J. R. Cheeseman, G. Scalmani, V. Barone, G. A. Petersson, H. Nakatsuji, X. Li, M. Caricato, A. V. Marenich, J. Bloino, B. G. Janesko, R. Gomperts, B. Mennucci, H. P. Hratchian, J. V. Ortiz, A. F. Izmaylov, J. L. Sonnenberg, D. Williams-Young, F. Ding, F. Lipparini, F. Egidi, J. Goings, B. Peng, A. Petrone, T. Henderson, D. Ranasinghe, V. G. Zakrzewski, J. Gao, N. Rega, G. Zheng, W. Liang, M. Hada, M. Ehara, K. Toyota, R. Fukuda, J. Hasegawa, M. Ishida, T. Nakajima, Y. Honda, O. Kitao, H. Nakai, T. Vreven, K. Throssell, J. A. Montgomery, Jr., J. E. Peralta, F. Ogliaro, M. J. Bearpark, J. J. Heyd, E. N. Brothers, K. N. Kudin, V. N. Staroverov, T. A. Keith, R. Kobayashi, J. Normand, K. Raghavachari, A. P. Rendell, J. C. Burant, S. S. Iyengar, J. Tomasi, M. Cossi, J. M. Millam, M. Klene, C. Adamo, R. Cammi, J. W. Ochterski, R. L. Martin, K. Morokuma, O. Farkas, J. B. Foresman, D. J. Fox, Gaussian 16, Revision B.01 Gaussian, Inc., Wallingford CT, **2016**.

[26] Y. Zhao, D. G. Truhlar, *J. Chem. Phys.* **2006**, *125*, 194101.

[27] a) R. Ditchfield, W. J. Hehre, J. A. Pople, *J. Chem. Phys.* **1971**, *54*, 724-728; b) W. J. Hehre, R. Ditchfield, J. A. Pople, *J. Chem. Phys.* **1972**, *56*, 2257-2261; c) M. M. Francl, W. J. Pietro, W. J. Hehre, J. S. Binkley, M. S. Gordon, D. J. DeFrees, J. A. Pople, *J. Chem. Phys.* **1982**, *77*, 3654-3665; d) M. S. Gordon, *Chem. Phys. Lett.* **1980**, *76*, 163-168; e) P. C. Hariharan, J. A. Pople, *Theor. Chim. Acta* **1973**, *28*, 213-222; f) T. Clark, J. Chandrasekhar, G. W. Spitznagel, P. V. R. Schleyer, *J. Comput. Chem.* **1983**, *4*, 294-301;

g) G. W. Spitznagel, T. Clark, P. v. R. Schleyer, W. J. Hehre, *J. Comput. Chem.* **1987**, *8*, 1109-1116.

[28] K. Fukui, *Acc. Chem. Res.* **1981**, *14*, 363-368.

[29] Y. Zhao, D. Truhlar, *Theor. Chem. Acc.* **2008**, *120*, 215-241.

[30] a) A. D. McLean, G. S. Chandler, *J. Chem. Phys.* **1980**, *72*, 5639-5648; b) R. Krishnan, J. S. Binkley, R. Seeger, J. A. Pople, *J. Chem. Phys.* **1980**, *72*, 650-654.

[31] S. E. Wheeler, K. N. Houk, *J. Chem. Theory Comput.* **2010**, *6*, 395-404.

[32] A. V. Marenich, C. J. Cramer, D. G. Truhlar, *J. Chem. Phys. B* **2009**, *113*, 6378-6396.

[33] E. D. Glendening, J. K. Badenhoop, A. E. Reed, J. E. Carpenter, J. A. Bohmann, C. M. Morales, C. R. Landis, F. Weinhold, NBO 6.0 Theoretical Chemistry Institute, University of Wisconsin, Madison, http://nbo6.chem.wisc.edu, **2013**.

[34] a) M. J. Frisch, G. W. Trucks, H. B. Schlegel, G. E. Scuseria, M. A. Robb, J. R. Cheeseman, G. Scalmani, V. Barone, B. Mennucci, G. A. Petersson, H. Nakatsuji, M. Caricato, X. Li, H. P. Hratchian, A. F. Izmaylov, J. Bloino, G. Zheng, J. L. Sonnenberg, M. Hada, M. Ehara, K. Toyota, R. Fukuda, J. Hasegawa, M. Ishida, T. Nakajima, Y. Honda, O. Kitao, H. Nakai, T. Vreven, J. A. Montgomery, Jr., J. E. Peralta, F. Ogliaro, M. Bearpark, J. J. Heyd, E. Brothers, K. N. Kudin, V. N. Staroverov, R. Kobayashi, J. Normand, K. Raghavachari, A. Rendell, J. C. Burant, S. S. Iyengar, J. Tomasi, M. Cossi, N. Rega, J. M. Millam, M. Klene, J. E. Knox, J. B. Cross, V. Bakken, C. Adamo, J. Jaramillo, R. Gomperts, R. E. Stratmann, O. Yazyev, A. J. Austin, R. Cammi, C. Pomelli, J. W. Ochterski, R. L. Martin, K. Morokuma, V. G. Zakrzewski, G. A. Voth, P. Salvador, J. J. Dannenberg, S. Dapprich, A. D. Daniels, O. Farkas, J. B. Foresman, J. V. Ortiz, J. Cioslowski, D. J. Fox, Gaussian 09, Revision D.01 Gaussian, Inc., Wallingford CT, **2013**; b) E. D. Glendening, C. R. Landis, F. Weinhold, *WIREs Comput. Mol. Sci.* **2012**, *2*, 1-42; c) E. D. Glendening, C. R. Landis, F. Weinhold, *J. Comput. Chem.* **2013**, *34*, 1429-1437.

[35] T. A. Keith, AIMAll 16.01.09, TK Gristmill Software, Overlad Park KS, USA, http://aim.tkgristmill.com, **2016**.

[36] a) T. Lu, Multiwfn 3.3.7 - A Multifunctional Wavefunction Analyzer School of Chemical and Biological Engineering, University of Science and Technology, Beijing, China, **2013**; b) T. Lu, F. Chen, *J. Comput. Chem.* **2012**, *33*, 580-592.

[37] a) R. F. W. Bader, *Atoms in Molecules: A Quantum Theory*, Oxford University Press, Oxford, **1990**; b) C. F. Matta, R. J. Boyd, *The Quantum Theory of Atoms in Molecules*, Wiley-VCH, Weinheim, **2007**.

[38] C. Y. Legault, Cylview 1.0b Université de Sherbrooke, http://www.cylview.org, **2009**.

[39] G. A. Andrienko, ChemCraft http://www.chemcraftprog.com, **2015**.